Kent Academic Repository

van Ewyk, Robert L (1978) *The effect of gases on the electrical properties of some organic semiconductors.* **Doctor of Philosophy (PhD) thesis, University of Kent.**

THE EFFECT OF GASES

ON THE

ELECTRICAL PROPERTIES

OF

SOME ORGANIC SEMICONDUCTORS

Doctor of Philosophy
Thesis.

Chemical Physics.

January, 1978

Robert L. van Ewyk,
University of Kent,
Canterbury.

TO

MY MOTHER AND FATHER,

JIM, ROD AND TINA

Acknowledgements

The author sincerely thanks: Drs. A.V. Chadwick and J.D. Wright for their guidance, encouragement and optimism through 'thick and thin';

Drs. Alan Jones and Alwyn Jones for their discussions and help with the research carried out at the Safety in Mines Research Establishment (Sheffield);

the Science Research Council and the Safety in Mines Research Establishment for providing a research studentship.

Thanks are also expressed to the technical staff at the university's chemical laboratory, especially V. Bush, D.A. Pugh and P.R.J. Smith.

In addition, the author is indebted to Miss T. Smyke, who typed this thesis, and to Mr. A. Fassam for the preparation of the photographs.

The author also wishes to remember numerous friends who helped him keep his sanity during the three years of research!

Abstract

Effects of gases (primarily N_2O_4, BF_3, O_2 and NH_3) on the electrical properties of molecular single crystals of donors (phthalocyanine and its Mn(II), Co(II), Ni(II), Cu(II), Zn(II) and Pb(II) complexes, anthracene, perylene and the bis(8-hydroxyquinoline) complexes of Cu(II) and Pd(II)), electron acceptor (7,7,8,8 tetracyanoquinodimethane) and an electron donor-acceptor complex (perylene/7,7,8,8 tetracyanoquinodimethane) have been studied. Apparatus was constructed permitting measurement of semiconduction and photoconduction in vacuo and in various gas pressures, over a temperature range of 290-500K.

The conductivity of electron donor and acceptor crystals was only enhanced by electron acceptor and donor gases, respectively, whereas the donor-acceptor complexes were enhanced slightly by both types of gases. Gas effects were confined to the crystal surfaces, except for oxygen on phthalocyanines. The rate and magnitude of conductivity changes on varying the gas pressure were consistent with chemisorption involving electron transfer. Electron transfer between π delocalised orbitals (e.g. N_2O_4 on phthalocyanines) gave reversible adsorption and gas pressures above 10^3Pa resulted in complete surface coverage, each adsorbed molecule producing one surface charge carrier. The more localised σ orbitals (e.g. BF_3 on phthalocyanines) resulted in stronger adsorption. Exceptionally, irreversible chemical reaction follows electron transfer (e.g. N_2O_4 on anthracene). Enhanced semiconduction is accompanied by significant reductions in the activation energy, to values comparable with the photoconduction activation energy. Photoconduction is more sensitive than semiconduction to low gas pressures. Changes in the photoconduction spectral response reflect the influence of adsorbed gases on the exciton dissociation process. Adsorbed N_2O_4 inhibits the singlet photoconduction in tetracyanoquinodimethane and perylene, but smaller low energy response, with fine structure, possibly triplet bulk photoconduction, persists. Increased surface ionized state density reduces the carrier mobility, resulting in reduced dependence of photocurrent on incident light intensity.

The implications of these findings for the design of organic semiconductor gas detectors are discussed.

CONTENTS

iv

v

Chapter 1 - Introduction

Both the semiconductive and photoconductive properties
of a wide variety of organic solids have been previously
reported (e.g. F. Gutmann and L.E. Lyons, 1967). In some
cases it was noted that the presence of a gas, usually oxygen,
influenced the conductivity properties. However, very few
studies have been specifically designed to study the effect
of a range of different gases on the electrical properties
of a variety of organic semiconductors.

Initial studies were started by an interest in the
mechanism of olfactory transduction. A number of workers
(e.g. N.A. Milas, W.M. Bostman and R. Heggie, 1939 and
M.H. Briggs and R.B. Duncan, 1961) found that both α- and
β-carotene were present in steer noses. This discovery
resulted in a number of studies of the semiconductive
properties of β-carotene and their dependence on the nature
of the gaseous environment. One of the first comprehensive
studies was carried out by B. Rosenberg(1961) and it was
found that in the presence of adsorbed oxygen the magnitude
of both the surface conduction and the photoconduction were
enhanced (by factors of 10^3 and 25 respectively) with respect
to their values in an argon ambient. Further work was carried
out (B. Rosenberg, T.N. Mistra and R. Switzer, 1968) using a
wide variety of gases (e.g. O_2, SO_2, NH_3, H_2S, N_2O_4, NO, CH_3OH,
C_2H_5OH, H_2O, CO_2, N_2, A and He). It was established that both
electron acceptor and electron donor gases enhanced the conduc-
tivity (by values of up to 10^4-10^6 for N_2O_4, NH_3, H_2S and
CH_3OH) coupled with a decrease in the activation energy for
conduction. Other studies were carried out (e.g. R.J. Cherry

1

and D. Chapman, 1967 and G.J. van Oirschot, D. van Leeuwen and J. Medema, 1972) and similar effects were observed. In all of these studies the samples were in the form of either compressed pellets or thin films.

The semiconductivity of other organic materials, especially anthracene and phthalocyanine, has been studied in various gaseous environments. It was reported by A.T. Vartanyan, 1950, that oxygen enhanced the photoconduction of anthracene films. This effect was confirmed by A.C. Chynoweth, 1954, for single crystals and has been observed by a number of other workers (e.g. A. Bree, D.J. Carswell and L.E. Lyons, 1955 and A. Bree and L.E. Lyons, 1960). Also, it has been noted by several workers (e.g. T.C. Waddington and W.G. Schneider, 1956 and 1958; A. Bree and L.E. Lyons, 1956 and D.M.J. Compton and W.G. Schneider, 1956) that electron acceptor gases (BF_3, HCl, SO_2, N_2O_4, O_2, NO and Cl_2) enhanced the photocurrent whereas electron donor gases (NH_3, $(CH_3)_3N$, $(C_2H_5)_2O$, C_2H_5OH, H_2O and $(CH_3)_2CO$) decreased the photocurrent.

The phthalocyanines and their metal complexes have been extensively studied. In 1948 A.T. Vartanyan reported that the conductivity of metal free, copper and magnesium phthalocyanines were enhanced by the presence of oxygen. It was concluded by J.A. Bomman (1958) that both the photoconductivity and the dark conductivity of copper, cobalt, lead and metal free phthalocyanines were enhanced on exposure to oxygen. Other studies have reached similar conclusions (e.g. F. Gutmann and L.E. Lyons, "Organic Semiconductors" Chapter 3, 1967).

An extensive study of the effect of various gases on a series of phthalocyanines was undertaken by J. Kaufhold and K. Hauffe (1965) using an elevated temperature ($\sim$ 430K). In this study metal free, iron, cobalt, nickel, copper and zinc phthalocyanines were used, in the form of sublimed films. It was concluded that the dark conductivity was enhanced and the activation energy decreased to 10% of its vacuo value by nitrous oxide and dinitrogen tetroxide. The effect caused by these gases could be reversed by ammonia. In the cases of zinc and iron phthalocyanines it was noted that an irreversible conductivity change occurred on exposure to nitrous oxide or dinitrogen tetroxide. An attempt was made to study the effects of gases on the photocurrent; however, it was found that above certain gas pressures the more marked enhancement of semiconduction obscured effects on the photocurrent.

G.J. van Oirschot, D. van Leeuwen and J. Medema (1972) carried out a major study of the effects of a wide variety of gases (O_2, NH_3, SO_2, CO_2, N_2O_4, CO, H_2, H_2S, N_2, Cl_2 and air) on the conductivity of metal free phthalocyanine films. Again it was found that dinitrogen tetroxide increased the dark conductivity approximately 10^6 fold. However, unlike Kaufhold and Hauffe, they found that ammonia increased the conductivity substantially (approximately 10^4-10^5 fold). Other gases also increased the conductivity (O_2, Cl_2 and SO_2). Some attempt was made to study the effect of altering the gas pressure on conductivity; however, only a few measurements were made and it is possible that these contained substantial errors due to the conductivity of the substrate (quartz). It was noted that ammonia and water vapour greatly

enhanced the conductivity of quartz.

Although previous studies have revealed that some gases could produce significant effects on the electrical properties of organic solids, the effects could not be interpreted clearly. This was partly due to the uncertainty about the nature of the semiconductor surfaces (in most cases films were used) and partly because of the lack of sufficient data on which of the parameters of semiconduction and photoconduction were being affected by the gases. The work to be described in this thesis is a development of these earlier studies, using single crystals with well defined faces to simplify the problems concerning the nature of the sample surfaces.

The initial objectives of this thesis are listed below.

1) To determine the type of chemical properties dominating the adsorption of gases onto the surfaces of organic crystals.

2) To test if photoconductivity is more sensitive than semiconduction and more informative about the gas-semiconductor interaction.

3) To examine a wide range of materials to test the following hypothesis: That only electron donor gases on electron acceptor crystals or electron acceptor gases on electron donor crystals enhance the conductivity significantly.

4) To obtain reproducible results for a series of metal phthalocyanine single crystals to establish whether gases affect the activation energy or pre-exponential factor, or both.

4

Chapter 2 - Theories

2·1 Dark conductivity: Introduction

Electrical conduction can only occur if free charge carriers are present in the materials. In organic materials the charge carriers can be electrons, holes or, rarely, protons. One of the main observables is the conductivity (σ); this is defined as the amount of charge transported through unit cross-sectional area in unit time per unit electric field gradient. Consider a cubic metre of the material containing n charge carriers of valence Z and charge e. Then the total charge in the cube is

$$Zen \quad \text{coulombs.}$$

The mobility of the carriers is defined as the velocity per unit electric field gradient (1 volt per metre). Hence the conductivity can be expressed as

$$\sigma = Zen\mu \quad (\Omega m)^{-1}. \qquad ...(2·1)$$

When several species of charge carriers are present equation (2·1) becomes

$$\sigma = \sum_i (Z_i en_i \mu_i) \qquad ...(2·2)$$

where i = the number of species present. This equation is only valid if the interaction between the charge carriers is negligible. This is commonly referred to as the 'law of independent migration'.

Charge carrier movement through crystal lattices has been described by several theories, namely the band model, the hopping model, the polaron model and the tunnelling model. These will be described below.

2·2 Dark conductivity: Band model

This model was first developed by F. Bloch in 1928 to describe the energy states of an electron in a crystal. He proposed that the potential energy function (U) of the electron should be invariant under a crystal lattice translation (a), i.e.

$$U(x) = U(x+a). \qquad \ldots(2\cdot3)$$

This assumes that the crystal field potential is periodic and that the periodicity is the same as the lattice spacing. Hence a Hamiltonian can be set up to give solutions to the Schrödinger wave equation and the solutions have the following general form:

$$\psi_k(r) = \exp(ik\cdot r) \, U_k(r) \qquad \ldots(2\cdot4)$$

The potential energy term ($U_k(r)$) is a function of both the wave vector (k) and the displacement vector (r); it also obeys the condition given in equation (2·3). For real values of k the solutions are well behaved and these constitute an energy band. However, for imaginary values of k the solutions of equation (2·4) are unacceptable and these result in a forbidden energy band. Therefore the electrons can only exist in the allowed energy band and to move from one band to an adjacent band they must cross a potential barrier (the forbidden band or band gap), as shown in figure (2·1). The band width, distribution of energy levels within the band and magnitude of the energy gap are dependent on the symmetry of the crystal field. This in turn depends on the lattice symmetry, molecular spacings and the nature of the molecules in the crystal lattice.

FIGURE (2·1)
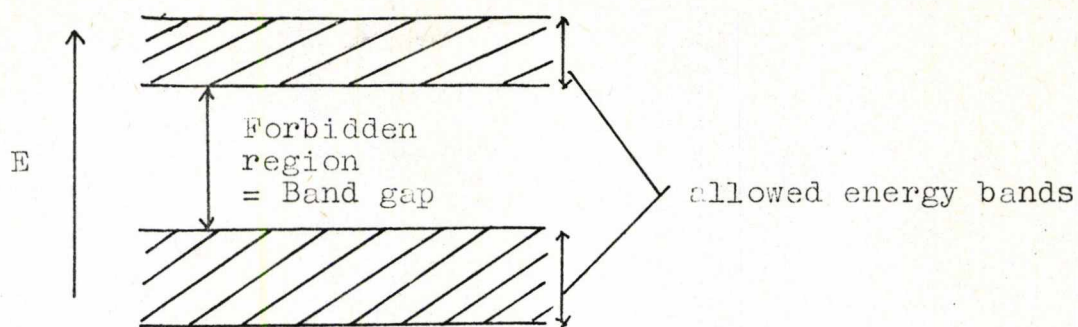
The binding forces encountered in molecular crystals are generally smaller than those found in metals and most other inorganic crystals. This results in a larger inter-molecular separation (a) and consequently the extent of molecular overlap is reduced. In the Bloch band theory the band width (J) is determined by the resonance integral (C. Kittel, 1971),

$$J = \frac{h^2}{8a^2 m^*} \, ,$$

where m^* is the effective mass of the charge carriers. Hence in molecular crystals the reduction in the degree of molec-ular overlap is reflected in a narrowing of the band width. In the case of anthracene the band width has been calculated at 0·11 eV (J.L. Katz, J. Jortner, S.I. Choi and S.A. Rice, 1963; R. Silbey, J. Jortner, S.A. Rice and M.T. Vala, 1965). This corresponds to an effective mass of about forty times that of a free electron, assuming that m^* is not dependent on k, which is not true for very narrow bands. A large effective mass corresponds to low effective mobility and for low mobilities the mean free path (λ) is less than the lattice spacing (A.F. Ioffé, 1959). Since the energy and

7

the position of the charge carrier are well-defined, using the Bloch band theory, the Uncertainty Principle is violated. Therefore the band theory is not applicable to narrow band conductors (i.e. molecular crystals). Furthermore, the predicted temperature dependence for mobility is

$$T^{-m} \quad \text{where } m \geqslant 1,$$

for a narrow band conductor (band width less than kT). This prediction is inconsistent with experimental measurements (L.B. Schein, 1977 and N. Karl, 1974) of mobility, many of which include examples of temperature dependences of T^{-m} with $m < 1$. L.B. Schein (1977) found that the drift mobility appeared to be temperature independent over a large temperature range (300K) for anthracene and arsenic sulphide (As_2S_3).

2·3 Dark conductivity: Hopping model

In this case the charge carrier is considered to be localized on a molecular site. Conduction is achieved by the carriers hopping from one site to the next. However, to do this an energy barrier must be overcome and consequently this is an activated process. This model assumes that the charge carriers can be considered as particles, whereas in the Bloch band theory the carriers are described in terms of waves.

One of the more successful hopping models was developed by T. Holstein in 1959. In this case it was assumed that the energy required to hop was derived from the molecular vibrations. It was then concluded that the mobility (μ) was related to the hopping energy (E(hop)) and to the temperature by the following equation.

8

$$\mu = T^{-3/2} \exp\left(\frac{-E(hop)}{kT}\right).$$

At high temperatures this reduces to a $T^{-3/2}$ dependence. This model has been found to fit naphthalene data (W. Mey and A.M. Hermann, 1973) approximately. It has also been found that the simple activated model (i.e. $\mu \propto \exp\left(\frac{-E(hop)}{kT}\right)$) is obeyed in a few cases (e.g. F.J. Martin, 1954).

Other more sophisticated models have also been developed (e.g. R.W. Munn and S.W. Siebrand, 1969 and 1970) to explain various sets of data. However in each case, at low temperatures the dominating term becomes $\exp\left(\frac{-E(hop)}{kT}\right)$. This is inevitable due to the initial assumptions in setting up the model (i.e. that the carriers must pass over an energy barrier in order to move from one site to another). Recently L.B. Schein (1977) carried out mobility measurements on several materials over a large temperature range (exceeding 300K). He found that mobility changed very little over the entire range. This clearly demonstrated that an activated process was not present. Therefore it was concluded that the hopping model does not effectively explain the conduction mechanism in organic semiconductors.

2·4 Dark conductivity: Polaron model

The polaron is defined as the combination of an electron or hole and its strain field. The most important effect of the lattice deformation is the increase in the effective mass of the charge carrier. If such a carrier is treated by the Bloch band theory approach of a periodic lattice potential, the results are similar to those obtained with a simple hopping model. However, since the theory is very

9

complex and little is known about polarons, there is little
to be gained in using them in preference to the simpler
hopping model.

2.5 Dark conductivity: Tunnelling model

In the hopping model the charge carriers had to pass
over an energy barrier in order to move from one molecular
site to another. If the energy barrier is sufficiently
narrow then the carrier, an electron or hole but not a
heavier carrier, could quantum-mechanically tunnel through
the barrier. If there are many such barriers then the
result of this quantum mechanical treatment would be a
quasi-band structure for the energy levels in the crystal.
However, in a real crystal the barriers are of different
energies and widths. As a result the mobility of the charge
carriers is determined by the 'transparency' of the largest
barrier present. This model has been principally suggested
by D.D. Eley, G.D. Parfitt, M.J. Perry and D.H. Taysum, 1953;
D.D. Eley and G.D. Parfitt, 1955 and D.D. Eley and D.J. Spivey,
1962.

One of the main conclusions obtained from this model
is that a correlation between the pre-exponential factor and
activation energy should exist. Although such a correlation
is often found (F. Gutmann and L.E. Lyons, 1967), it is not
conclusive evidence for the tunnelling model. Even the
interpretation of such evidence is subject to some controversy
(G.R. Johnston, 1971).

In conclusion, none of the four models discussed is
able to describe the motion of carriers through a molecular
crystal adequately. The Bloch band theory breaks down when

the band widths are very small, as is the case for molecular crystals. Also, it predicts a temperature dependence for mobility that is not observed experimentally. Similarly the conceptually simple hopping model predicts an incorrect mobility temperature dependence. The polaron model is mathematically complex and does not offer any great advantages over the much more simple hopping model. And finally the application of the tunnelling model to organic systems is open to controversy.

2·6 Dark conductivity: carrier generation and loss

When a conductor is in a steady state then the following condition is met by the system:

rate of carrier generation = rate of carrier loss.

Also, there are two distinct regions of conductivity, one where Ohms law is obeyed and one where it is not, i.e. $I \propto v^n$, Ohms law only applies if $n = 1$. In the work presented in this thesis the conductivity was always Ohmic. Therefore the electrodes did not influence the conductivity mechanism; they merely removed and replenished the charge carriers.

The charge carrier generation process can either be an intrinsic or an extrinsic mechanism. In the former case thermal excitation produces an electron and a hole charge carrier. If one uses the band model then this process simply excites an electron from the valence band into the conduction band, leaving a 'hole' in the valence band (see figure (2·2)). In the case of the hopping model a molecule is excited so that it loses an electron, forming a hole. Both the hole and the electron are free to move through the conductor. For the extrinsic conduction mechanism impurities must be

11

FIGURE (2·2)

Electron ther-
mally excited
into the con-
duction band

empty conduction band

Band gap

filled valence band
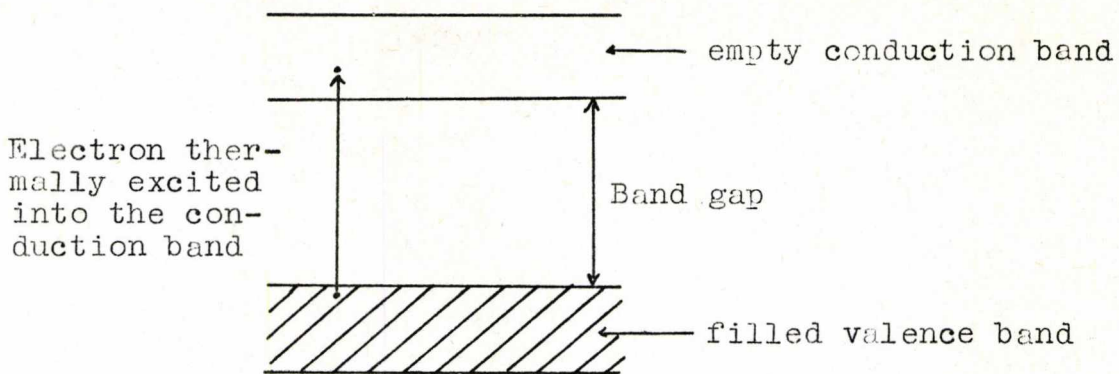
present. These can be donor (donate electrons) or acceptor
(accept electrons) types. Thermal excitation then merely
produces a single carrier, an electron or hole depending on
the type of impurity present. To maintain charge neutrality
the impurity centre becomes charged, positive if it is a
donor impurity and negative if it is an acceptor type impurity,
as shown in figure (2·3).

FIGURE (2·3)

Impurity
(donor type)

Donor states

conduction
band

electron
excited into
the conduction
band

Free
electron

electron
excited into
the acceptor
band leaving
a 'hole' in
the valence
band

valence
band

Acceptor states

HOPPING MODEL

BAND MODEL
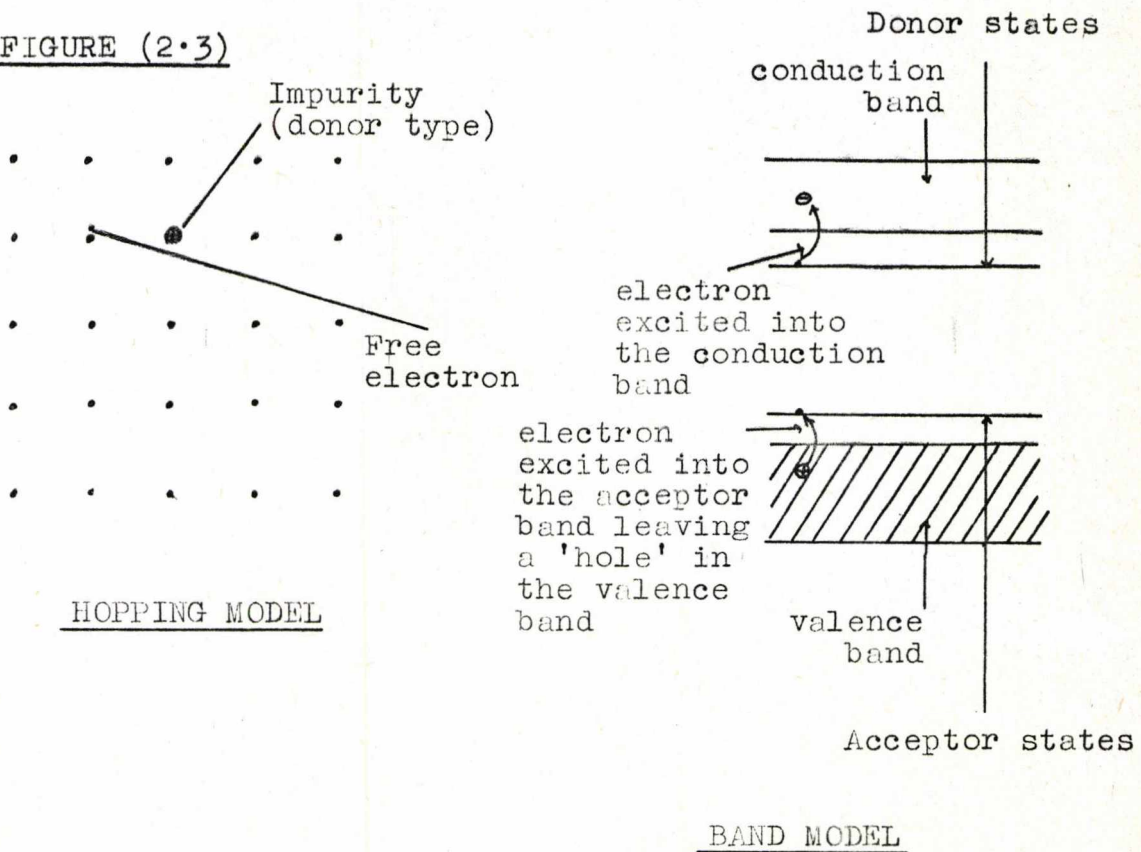
The number of carriers thermally excited is governed by Boltzmann's statistics, i.e.

$$n \propto \exp\left(\frac{-\Delta E}{2kT}\right) \quad \text{for intrinsic conduction}$$

$$n \propto \exp\left(\frac{-\Delta E}{kT}\right) \quad \text{for extrinsic conduction}$$

where ΔE is the excitation energy. Hence the generation process can either produce a hole and an electron as free carriers (intrinsic conduction) or, either one as a carrier and the other in a bound state (extrinsic conduction). From the band model (figure (2·3)) it can be seen that extrinsic conduction requires less energy and therefore dominates at low temperatures. Using the Boltzmann equation an expression for the temperature dependence of conductivity may be derived:

$$n = n_o \exp\left(\frac{-\Delta E}{(2)kT}\right)$$

substituting into equation (2·1)

$$\sigma = Ze\mu n_o \exp\left(\frac{-\Delta E}{(2)kT}\right)$$

$$= Z\sigma_o \exp\left(\frac{-\Delta E}{(2)kT}\right).$$

However, the valence term is unity for electrons, holes and protons. Therefore the conductivity expression becomes

$$\sigma = \sigma_o \exp\left(\frac{-\Delta E}{(2)kT}\right) \qquad \ldots(2\cdot5)$$

or in terms of resistivity (ρ)

$$\rho = \frac{1}{\sigma} = \rho_0 \exp \left(\frac{\Delta E}{(2)kT} \right) \qquad \ldots (2 \cdot 6)$$

Carrier loss may occur via three main processes.

a) Electrode loss

In this case the carrier is lost at the electrode if it is not simultaneously replaced by a similar carrier at the other electrode.

b) Trapping loss

The carrier falls into a trap. It is then no longer free and therefore does not contribute to the conduction. However, thermal re-excitation is possible; the ease with which this happens depends on the trap depth. Therefore the effect of trapping is to reduce the effective mobility of the charge carriers.

c) Recombination loss

The simple case is when an electron and hole collide and therefore recombine. However, more probably, this effect occurs at recombination centres. In this case one of the charge carriers is trapped in a deep trap, making thermal re-excitation very unlikely. Recombination then occurs when a carrier of opposite sign collides with the trapped carrier. It can be seen from figure $(2 \cdot 4)$ that at a certain energy the probabilities of recombination or trapping are equal; this energy is defined as the demarcation energy. The trapping and recombination bands arise due to the distribution of trap depths.

FIGURE (2·4)
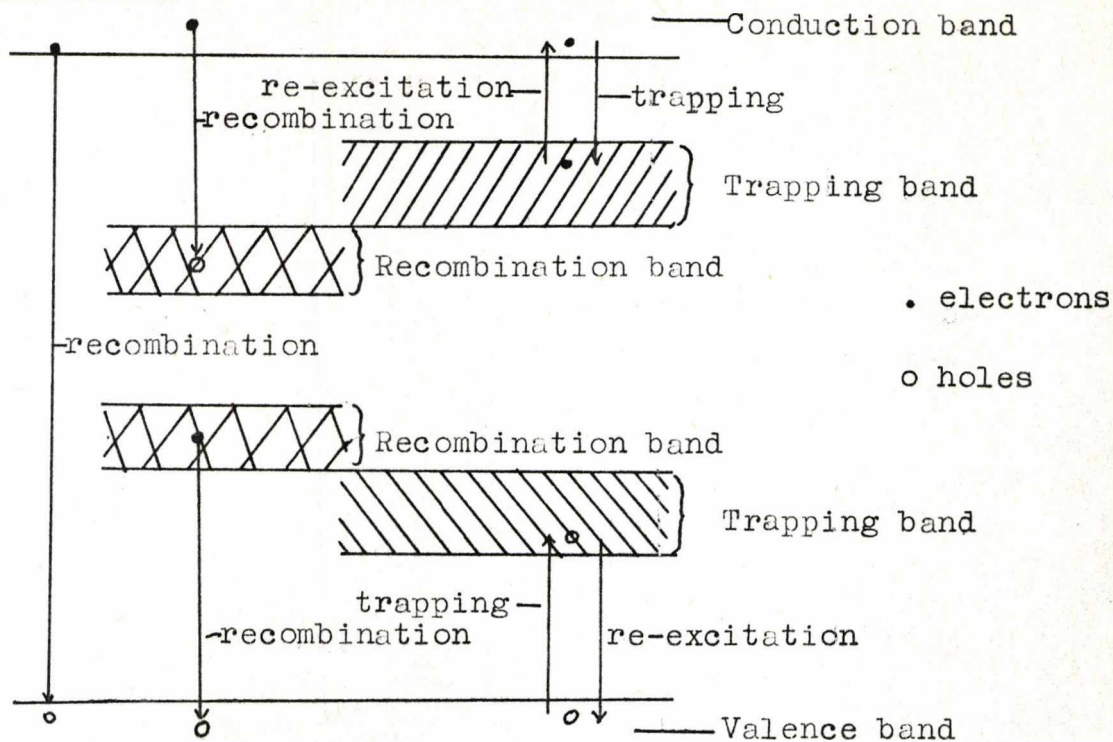
2·7   Dark conductivity: Charge carrier formation energies

In the generation of free charge carriers in a crystal
there are four main energy changes that must be considered.
These are the ionization potential (IP), the electron affinity
(EA), the polarization energies (P^+ and P^-) and finally the
formation energy (ΔW). When these are considered the follow-
ing expression for the activation energy (E) will result:

$$E = IP - EA - (P^+ + P^-) + \Delta W \qquad \qquad \dots(2\cdot7)$$

It should be noted that all of these terms relate to the
pure material and consequently the derived activation energy
is for intrinsic conduction (i.e. the production of both
an electron and hole charge carriers). The formation energy
is very small (J.L. Lippert, M.W. Hanna and P.J. Trotter,
1969) in comparison with the other energies and may there-
fore be neglected. By comparison of the calculated activation

15

energy (equation (2·7)) and measured activation energy, it is possible to ascertain if intrinsic or extrinsic conduction is being observed.

2·8 Steady state photoconductivity: Introduction

After a charge carrier has been generated in the conductor it becomes indistinguishable from all the other carriers. Consequently all the arguments relating to the loss and movement of carriers apply to 'photo'-carriers. Measurement of the spectral response and magnitude of photoconduction can yield valuable information about the generation process, especially when these data are correlated with other spectroscopic measurements.

In the steady state the rate of carrier generation is equal to the rate of carrier loss (cf. section (2·6)). It has already been stated that carrier loss may occur via three main processes, namely

1) electrode loss
2) trapping loss
3) recombination loss.

Since the extinction coefficients of the compounds studied were very high ($\sim 10^5$, cf. Chapter 5) in the wavelength region studied and all the crystals were relatively thick (typically 0·01 mm) it is assumed that all the incident photons were absorbed. Furthermore, it is assumed that each absorbed photon gave rise to an exciton. However, not every exciton gives rise to a charge carrier. The proportionality factor between charge carrier generation rate and rate of absorption of photons is the quantum yield parameter and this will be discussed in section (2·9). Excitons may decay by one of the following processes:

1) A radiationless transition to the ground state.

2) Fluorescence emission to the ground state.

3) Dissociation into two charge carriers by interaction with a phonon (thermal process).

4) Dissociation into two charge carriers by collision with another exciton. One exciton reverts to the ground state and the energy liberated is used to dissociate the other one.

5) Dissociation into two charge carriers by absorption of a photon (photoionization).

6) Dissociation into two charge carriers by the effect of an electric field (the Poole-Frenkel effect).

7) Dissociation into two charge carriers at the electrodes.

8) Dissociation into two charge carriers at surface or impurity sites.

Some of the above processes generate charge carriers via a single photon process (3,6,7 and 8), whereas the others require two photons (processes 4 and 5). It should be possible to differentiate between these two groups by altering the concentration profile (the change in concentration with respect to penetration depth) of the photons. In the first group the number of charge carriers generated is only dependent on the total number of absorbed photons. However, the double excitation and photoionization processes (numbers 4 and 5 respectively) are dependent on the photon concentration. It is known that in many molecular crystals the absorption of photons is strongly polarized in the direction of the molecular stacking axis. Hence by altering the polarization angle of the incident photons, the penetration depth and consequently the concentration profile are altered.

This offers an easy means of testing which photogeneration process dominates.

2·9 Steady state photoconductivity: quantum yield parameter

The quantum yield parameter, Q, is defined as follows:

$$Q = \frac{\text{carrier generation rate}}{\text{photon flux X illumination area}}$$

Furthermore, under steady state conditions the carrier generation rate is equal to the carrier loss rate. The processes by which carriers are lost have already been mentioned (cf. section (2·8)). Carrier loss to the electrodes is given by the current divided by the electronic charge. Trapping does not affect the loss rate under steady state conditions, it only reduces the carrier mobility. Hence the only other process by which carriers may be lost is recombination. This loss rate has been calculated using a gas phase collision model by V.M. Vincent in 1972 and it was shown,

$$\text{loss rate} = \frac{2^{\frac{1}{2}} \pi d^2 l^2}{2e^2 \, V\mu wt} \, (Id^2 + 2IdIp)$$

where l = electrode separation

  w = sample width

  t = sample thickness

  e = electronic charge

  V = applied voltage

  μ = mobility of the majority carrier

Id = dark current

Ip = photo current

  d = approach distance for recombination.

18

It should be noted that it is assumed that the dark and
photo majority carriers are the same, otherwise no photo
current would be observed due to rapid recombination of the
dark and photogenerated carriers. Therefore the total loss
rate is given by:

$$\text{total loss rate} = \text{carrier generation rate}$$

$$= \frac{2^{\frac{1}{2}} \pi \, d^2 l^2}{2e^2 \, V\mu wt} \, (Id^2 + 2IdIp) + \left(\frac{Id + Ip}{e}\right) \qquad \ldots (2 \cdot 8)$$

$$= R$$

Hence the quantum yield parameter is given by:

$$Q = \frac{R}{LA} \qquad \text{where A = illumination area.}$$

From equation $(2 \cdot 8)$ it can be seen that if recombination
predominates, a bimolecular process, then the observed current
would be proportional to the square root of photon flux.
However, if the electrode loss term dominates then the current
would be directly proportional to the photon flux. Hence
in general it is found that

$$I \propto L^n \qquad \qquad \text{I = observed current}$$

$$0 \cdot 5 \leqslant n \leqslant 1 = \text{intensity dependence.}$$

It should be noted that this argument has been for a single
photon excitation process. If two photons were required
to create excitons then it would be found that

$$I \propto L^n \qquad \qquad \text{where } 1 \leqslant n \leqslant 2.$$

However, in this and many other studies intensity dependences
of less than $0 \cdot 5$ have been measured. This cannot be explained
using the equation $(2 \cdot 8)$; a possible explanation is given in
the following section.

A simplification of the quantum yield parameter term is possible if the recombination and electrode loss rates are approximately equal. This will be the case if the intensity dependence is approximately $0\cdot75$. Using this assumption the loss rate simply becomes twice the loss rate at the electrodes, i.e.

$$2 \; X\left(\frac{I}{e}\right)$$

$$\therefore \; Q = \frac{2I}{LeA} \qquad \qquad \ldots (2\cdot9)$$

$2\cdot10$ Steady state photoconductivity: Intensity dependence

It has already been shown that the intensity dependences can vary between $0\cdot5$ and $1\cdot0$ for a single photon excitation process. However, intensity dependences lower than $0\cdot5$ have been measured in this (cf. Chapter 5) and other work. G.H. Heilmeier and S.E. Harrison (1963) demonstrated that in a diffusion limited case the intensity dependence became $1/3$ (i.e. $I \propto L^{1/3}$). These workers concluded that as the carrier density increased, the lifetime and hence the diffusion length decreased. The overall effect is that the carrier's lifetime is decreased with respect to the transit time and consequently fewer carriers are able to reach the electrodes.

$2\cdot11$ The Elovich equation

In the study of activated adsorption, it was found by S.Yu Elovich and G.M. Zhabrova in 1939 that in most cases the variation in velocity with the amount adsorbed, q, obeyed the following equation:

$$\frac{dq}{dt} = a \exp (-bq) \qquad \text{where a and b are constants.}$$

This is known as the Elovich equation. It can be derived for both uniform and non-uniform surfaces; however, to do this it is necessary to first consider the adsorption process from first principles.

Consider a surface of uniform area placed in a gas at a pressure p. Then the number (n) of gas molecules striking the surface per second is given by:

$$n = \frac{p}{\sqrt{2\pi mkT}}$$

where m = mass of the gas molecule
k = Boltzmann's constant
T = absolute temperature.

However, not every collision necessarily results in adsorption; therefore, the rate of adsorption onto the surface is defined by:

$$U = \frac{sp}{\sqrt{2\pi mkT}} \qquad \qquad \ldots (2 \cdot 10)$$

where s is the sticking probability and is defined as

$$\frac{1}{s} = \frac{\text{number of surface collisions}}{\text{number of adsorbed molecules}} .$$

When a gas molecule collides with the surface there are several conditions that must be fulfilled before adsorption can take place. If the adsorption process is activated the gas molecule must possess sufficient energy to overcome this barrier. However, not every molecule possessing the required activation energy will necessarily be adsorbed; it must also pass through the correct activated complex configuration. When the gas molecule has sufficient energy and passes through the correct configuration it must also

lose an amount of energy exceeding the original thermal energy. Furthermore, this energy transfer must occur rapidly, otherwise it will remain in the excited state for the duration of one vibration and then desorb. These last three factors, activation energy, correct configuration and energy transfer, have all been associated with the chemisorption mechanism. However, there are two other physical factors that must be taken into account. Firstly, surface heterogeneity alters the activity of chemisorption for the various sites. This is reflected as a change in the sticking probability. Secondly, some collisions inevitably occur with occupied sites. The probability of this occurring will, obviously, increase with increasing surface coverage. A collision with an occupied site need not imply that adsorption will not occur. It is known that molecules can be adsorbed weakly to form a second layer. The molecules will then be able to migrate until a vacant site is found. However, some of the molecules will desorb before finding a vacant site. All of these five factors will act to decrease the sticking probability and consequently the rate of adsorption.

Taking the above factors into consideration, an expression for the sticking probability may be written as

$$s = \sigma f(\theta) \exp\left(\frac{-E}{RT}\right) \qquad \dots(2\cdot11)$$

where σ = condensation coefficient

$f(\theta)$ = function of the surface coverage

E = activation energy

R = gas constant.

The condensation coefficient is the probability that a molecule will be adsorbed, providing it has sufficient energy. The probability that a collision will take place in a vacant site is dealt with by the surface coverage function $(f(\theta))$. In this expression no account is taken of the variation of both the activation energy $(E(\theta))$ and the condensation coefficient with surface coverage. Therefore equation (2·11) must be rewritten as

$$s(\theta) = \sigma(\theta) \; f(\theta) \; \exp\left(\frac{-E(\theta)}{kT}\right) \qquad \ldots(2\cdot12)$$

Now if this function, $s(\theta)$, is replaced for the sticking probability (s) in equation (2·10) the resultant adsorption velocity equation becomes

$$U = \frac{\sigma(\theta)p}{\sqrt{2\pi mkT}} \quad f(\theta) \; \exp\left(\frac{-E(\theta)}{kT}\right) \qquad \ldots(2\cdot13)$$

However, this has neglected any effect due to surface heterogeneity. To take this into account the surface must be divided into small elements of area ds, each of which is uniform. Then the velocity equation will be obtained by integration.

$$U = \frac{p}{\sqrt{2\pi mkT}} \int_{0}^{\prime} \sigma_s \; f(\theta_s) \; \exp\left(\frac{-E_s}{RT}\right) \cdot ds \qquad \ldots(2\cdot14)$$

Using the preceding equations the Elovich equation may be derived for both uniform and non-uniform surfaces. Taking the simpler uniform surface case first, the activation energy for adsorption is assumed to increase linearly with increasing surface coverage, i.e.

$$E = Eo + \propto \theta$$

Substituting this value into the velocity equation (equation (2·13)) it becomes

$$U = \frac{\sigma p}{\sqrt{2\pi mkt}} f(\theta) \exp\left[\frac{-(E_O + \alpha\theta)}{RT}\right]$$

Then, assuming that σ is not too dependent on θ,

$$U \propto f(\theta) \exp\left(\frac{-\alpha\theta}{RT}\right) \qquad \qquad \ldots(2·15)$$

This can be simplified still further since the fractional number of vacant sites is given by $(1-\theta)$. Then the chance of a gas molecule colliding with a vacant site will be equal to $(1-\theta)$.

$$\therefore f(\theta) = (1-\theta)$$

Substituting this result into equation (2·15),

$$U \propto (1-\theta) \exp\left(\frac{-\alpha\theta}{RT}\right)$$

Then, providing the surface is not near full coverage the variation of $(1-\theta)$ with respect to the exponential term may be neglected.

$$\therefore U \propto \exp\left(\frac{-\alpha\theta}{RT}\right) \qquad \qquad \ldots(2·16)$$

This is an Elovich type equation.

The inhomogeneous surface may be treated in a similar manner. The surface is divided into a number of elements each of area ds. In these small elements the activation energy increases linearly with s.

$$\therefore E_s = E_o + \alpha s.$$

Substituting this value into equation (2·14) and assuming that σ is independent of Θ the following equation results.

$$U = \frac{\sigma p}{\sqrt{2\pi mkT}} \int_o^1 (1 - \Theta s)\ \exp\left[\frac{-(E_o + \alpha s)}{RT}\right] \cdot ds \quad \ldots(2\cdot17)$$

To carry out this integral an approximation is made. At very low coverage the activation energy will be a minimum and sites will therefore be rapidly occupied. When the surface coverage nears completion the activation energy will be a maximum, and hence the rate of filling the sites will become slow. Hence the surface may be considered to consist of an almost covered part, low activation energy, and an almost bare part, high activation energy. Using this simplification integration need only be carried from Θ, the fraction of the surface covered at the moment being considered, to total coverage (s = 1). Then equation (2·17) becomes

$$U = \frac{\sigma p}{\sqrt{2\pi mkt}} \int_\Theta^1 \exp\left[\frac{-(E_o + \alpha s)}{RT}\right] \cdot ds$$

$$= \frac{\sigma p}{\sqrt{2\pi mkt}}\ \frac{RT}{\alpha}\ \exp\left(\frac{-E_o}{RT}\right)\ \left[\exp\left(\frac{-\alpha\Theta}{RT}\right) - \exp\left(\frac{-\alpha}{RT}\right)\right]$$

$$\ldots(2\cdot18)$$

Then if Θ does not approach unity (i.e. the surface is not totally covered),

$$\exp\left(\frac{-\alpha\Theta}{RT}\right) > \exp\left(\frac{-\alpha}{RT}\right) \ .$$

Hence equation (2·9) becomes

$$U = \frac{\sigma p}{\sqrt{2\pi mkT}} \; \frac{RT}{\alpha} \; \exp\left(\frac{-E_0}{RT}\right) \exp\left(\frac{-\alpha\theta}{RT}\right)$$

i.e. $U \propto \exp\left(\dfrac{-\alpha\theta}{RT}\right)$ (cf. equation (2·16)).

This is again a form of the Elovich equation.

To test if the Elovich equation is applicable to a set of results a plot of ln (time) versus volume adsorbed, or surface coverage, should yield a straight line.

Chapter 3 - Materials

3.1 Introduction

The selection of appropriate materials was of vital importance to the objectives of this work, and involved an attempt to fulfil three sets of criteria simultaneously. Firstly, since electrical properties of molecular crystals are sensitive to very small traces of impurities of certain types, chemical purity and stability were required. Absolute purity and freedom from chemical reactions are in practice unattainable ideals in a molecular crystal which must simultaneously fulfil the electrical requirements discussed below, and the aim was therefore to select materials which could be reproducibly purified by available techniques to a high and readily characterised purity level, and which were also stable to moisture, air and many common gases in the absence of light. Secondly, the materials were required to fulfil several physical criteria, notably that they should form good quality single crystals. Well-formed single crystals greatly simplify the interpretation of electrical data obtained for the materials, since effects due to anisotropy of structure may be readily characterised, and grain-boundary and related effects of physical discontinuities within the solid are minimised. Since the electrical characteristics of the compounds were to be studied in high vacuum, non-volatility was required; or at least the sublimation rate had to be too small, over the temperature range studied, to be of any significance. Other physical criteria were reasonable mechanical strength and the possibility of attaching electrical contacts. Since many of the

materials only formed small crystals, contact had to
be made to very small areas (typically ·1 X ·3mm)
and electrically conducting silver paint was found to be
the only convenient contact material. The main requirement
for satisfactory contacts was then that the material of the
crystal should not react with the silver paint nor be
excessively soluble in the solvents used in the paint. The
third and most important set of criteria concerned electri-
cal properties. Since the project aimed to study the effects
of gases on electrical conductivity of molecular crystals
it was essential to use systems where the interaction between
gas and solid led to changes in the electronic states of the
bulk or surface of the solid. The main type of interaction
likely to satisfy this criterion appeared to be that between
electron donor and electron acceptor species, and the solids
and gases used were chosen with this in mind, although
some more neutral species were used for comparison purposes.
Since many of the gases used were polar molecules, it was
felt that the interaction would be strongest with solids
containing polarizable atoms or metal atoms capable of
extending their coordination sphere to include the gas mole-
cule. Hence some molecular crystals studied were chosen
to include molecules where the presence or absence of a
polarizable or metal atom, as well as the ionization potential
or electron affinity, could be systematically varied without
unduly changing the general shape of the molecule or its
crystal structure. Finally, it was important to choose
materials with appropriate magnitude of semiconduction and
photoconduction in vacuo. The resistivity of the sample
had to be low enough to measure reproducibly, yet not so

low that changes produced by the influence of gases were negligible compared to the vacuum conduction of the material. In practice the optimum resistivity for small crystals of the type studied proved to be approximately $10^{10}\Omega m$. Measurable photoconduction was also considered a valuable characteristic since, for solids with intense optical absorption, this could potentially provide a more sensitive probe for surface effects than semiconduction data.

It was found that phthalocyanine and its metal complexes met all the above criteria to a reasonable degree. The phthalocyanines studied were manganese, cobalt, copper, nickel, lead, zinc and metal free; these are all electron donors. Other donors studied were: perylene, phenanthrene, anthracene, copper oxinate and palladium oxinate. Difficulty was encountered with both anthracene and phenanthrene due to their volatility. Several other materials were also studied. These were: benzidine-TCNQ (7,7,8,8 tetracyanoquinodimethane), perylene-TCNQ, and bis[cis-3,4-bis(trifluoromethyl)-1,2-dithiete]nickel^{O}. It was found that benzidine-TCNQ formed very brittle crystals and the nickel complex suffered very badly from sublimation. The chemical structures of all the materials are shown in table (3.1).

3.2 Preparation of phthalocyanines

Lead, copper, zinc, manganese and metal free phthalocyanines were prepared by the technique developed by Linstead et al (1938). The first stage of this reaction was to prepare dilithium phthalocyanine. This was accomplished by reacting phthalonitrile with lithium amyloxide; an excess of the latter had to be used to ensure that dilithium phthalocyanine

29

TABLE (3·1)

COMPOUND (DONORS)	STRUCTURE	IONIZATION POTENTIAL	
		GASEOUS	SURFACE
Phthalocyanines (Pc)	M = Mn,Co,Cu,Ni,Pb,Zn,H_2	MFPC 7·36[1] Zn 7·37[1] Cu 7·37[1] Ni 7·45[1] Co 7·46[1] Mn 7·26[1] Pb	5·20[2] 5·00[2] 4·95[3] 5·00[4]
Perylene		7·22[5]	5·39[3]
Anthracene		7·40[6]	5·5[8] 5·65[9]
Phenanthrene		7·85[6]	6·45[9]
Benzidine	H_2N—⟨⟩—⟨⟩—NH_2	6·80[7]	
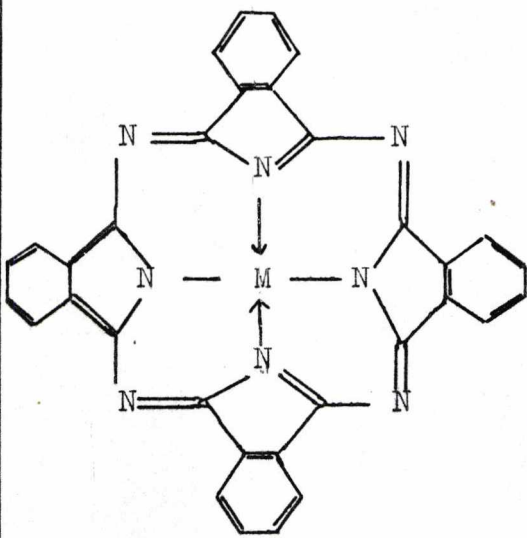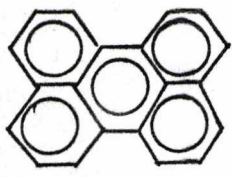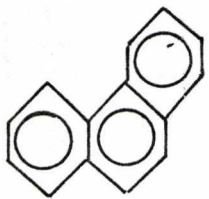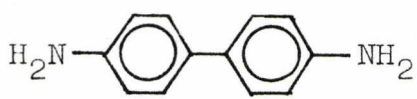
TABLE (3·1)
(continued)

COMPOUND (DONORS)	STRUCTURE	IONIZATION POTENTIAL
Copper and palladium oxinates	 M = Pd(II) or Cu(II)	
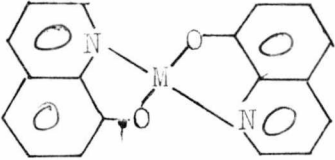
COMPOUND (ACCEPTORS)	STRUCTURE	ELECTRON AFFINITY
TCNQ		$2·88^{10}$
Bis[cis-1,2-(trifluoromethyl) 1,2-ethienedithiolato]nickel		
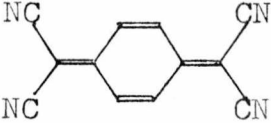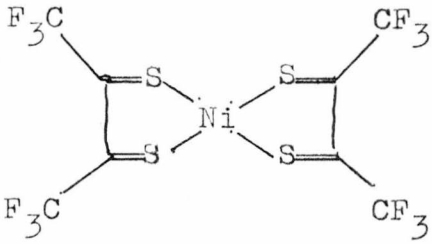
1) D.D. Eley, D.J. Hazeldine and T.F. Palmer, 1973

2) M. Pope, 1962

3) M. Calvin and D.R. Kearns, 1961

4) P. King and L.E. Lyons, unpublished work

5) J. Briegleb, 1961

6) J. Briegleb and J. Czekalla, 1959

7) H. Kusakawa and S. Nishizaki, 1965

8) M. Voler, 1931

9) L.E. Lyons and G.C. Morris, 1960

10) L.E. Lyons and L.D. Palmer, 1976

was formed and not lithium hydrogen phthalocyanine. The
experimental procedure was as follows. Phthalonitrile was
added to a solution of amyl alcohol containing lithium.
On addition the solution turned from colourless to green.
When the solution was slowly heated to boiling a vigorous
exothermic reaction took place. After about thirty minutes
the solution was allowed to cool down to room temperature
before diluting it with benzene. After filtration a dark
blue residue of dilithium phthalocyanine and basic lithium
compounds was obtained. Soxhlet extraction, using dry ace-
tone, removed the dilithium phthalocyanine from the basic
lithium impurities.

The second stage of this reaction consisted of a double
decomposition reaction. Two solutions were prepared using
dry alcohol. One solution contained anhydrous metal chlor-
ide (or lead acetate when preparing lead phthalocyanine);
the other solution contained dilithium phthalocyanine.
Both solutions were mixed together and left to stand for
a few hours, forming a precipitate of metal phthalocyanine.
This precipitate was filtered off and then washed with dry
alcohol to remove any excess dilithium phthalocyanine
or metal chloride. Further purification was carried out
by dissolving the metal phthalocyanine in concentrated
sulphuric acid. After filtration the compound was precipi-
tated out by adding distilled water. Metal free phthalo-
cyanine was prepared by adding the dilithium phthalocyanine
to sulphuric acid. Apart from preparing some of the phthalo-
cyanines by using the above technique, the bulk of material
was purchased from Eastman Kodak Limited, including cobalt
and nickel derivatives.

Reaction for zinc phthalocyanine:

$$4(C_8H_4N_2) + 2Li \xrightarrow[\text{amyl alcohol}]{} (C_8H_4N_2)_4Li_2$$

$$(C_8H_4N_2)_4Li_2 + ZnCl_2 + \xrightarrow[\text{ethyl alcohol}]{} (C_8H_4N_2)_4Zn + 2LiCl$$
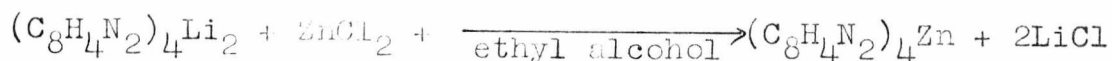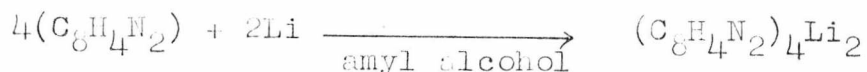
3.3 Preparation of 3,4-Bis(trifluoromethyl)-1,2-dithiete

Since this preparation required the rather severe conditions of refluxing sulphur (C. G. Krespan, 1961), the apparatus had to be designed to be capable of attaining high temperatures without detrimental results. From figure (3.1) it can be seen that a fluidized sand bath was used as a heat source. The bath was capable of keeping the apparatus at a temperature between 370K up to 1100K in a controlled manner(to within a few K) by using a 'zero voltage crossing proportional' temperature controller in conjunction with a chromel-alumel thermocouple. After setting up the apparatus as shown in figure (3.1), with the exception of the solid carbon dioxide baths, the system was thoroughly flushed with nitrogen. While maintaining a small nitrogen flow (monitored on the bubbler) the sulphur was heated until it refluxed. To prevent the refluxing column from becoming clogged with solid sulphur it was kept at about 470K with an electrical heating tape. After placing the solid carbon dioxide baths into position, the hexafluorobut-2-yne was slowly passed into the refluxing sulphur. The first cold trap was specifically designed to allow observation of the rate of product collection, thus enabling an estimation of the reaction rate to be made. By controlling the rate of hexafluorobut-2-yne addition (monitored by the bubbler) the product formation rate could be kept low.

FIG: (3.1) APPARATUS FOR THE PREPARATION OF THE DITHIETE

HEATING TAPE

AIR REFLUX COLUMN

2 NECKED FLASK

SULPHUR

BUBBLER

N₂

HEXAFLUORO-
BUT-2-YNE

PRODUCT

COLD TRAPS

BUBBLER

FLUIDIZED SAND BATH
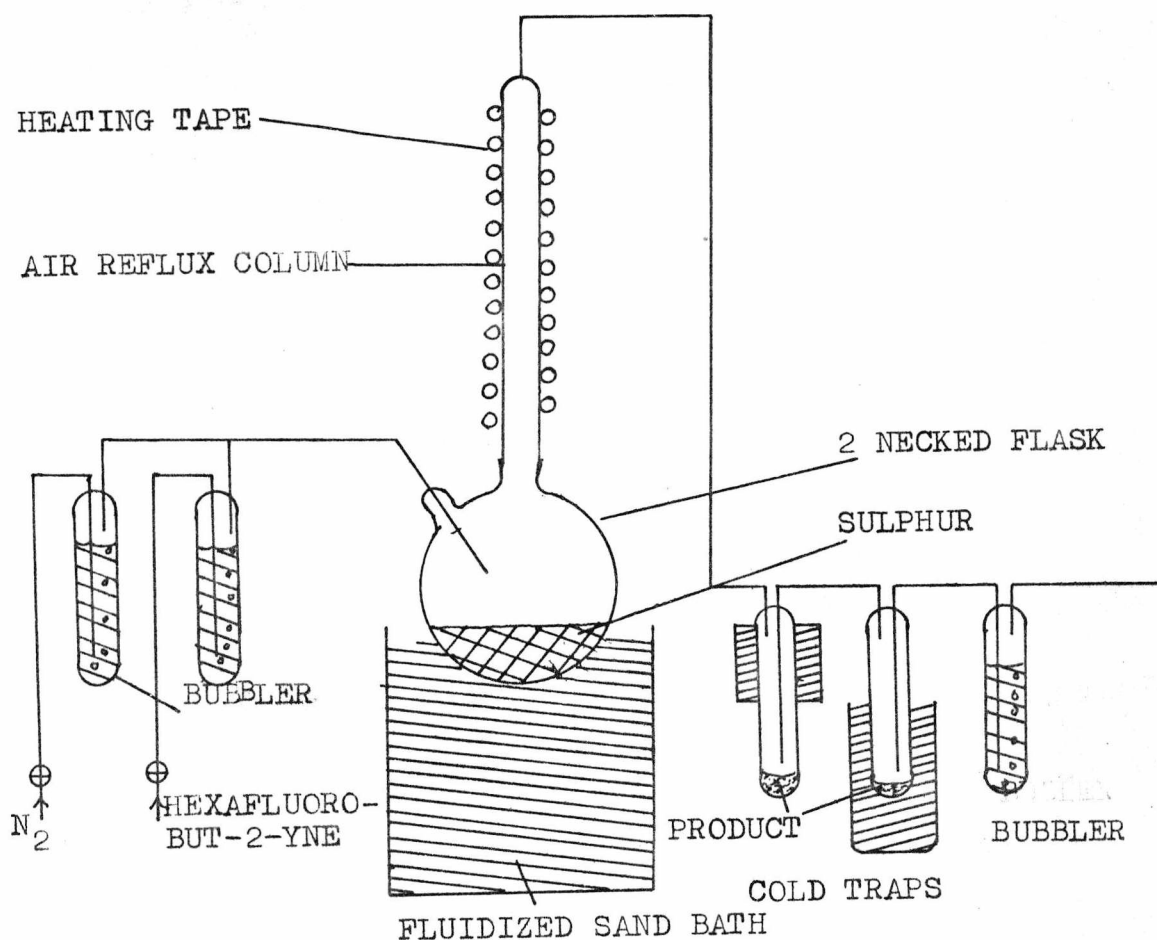
FIG: (3.2) APPARATUS FOR THE PREPARATION OF THE NICKEL COMPLEX

COPPER
SPIRAL

1L. FLASK

TAP '2'

BUNSENS

TAP '5'

N₂

TAP '1'

BUBBLER

TAP '4'

TAP '3'

COLD TRAP
AND ROTARY
PUMP

Ni(CO)₄

ENCLOSED MANOMETER

3,4 BIS TRI(FLUORO)METHYL-
1,2 DITHIETE IN DRY PENTANE

34
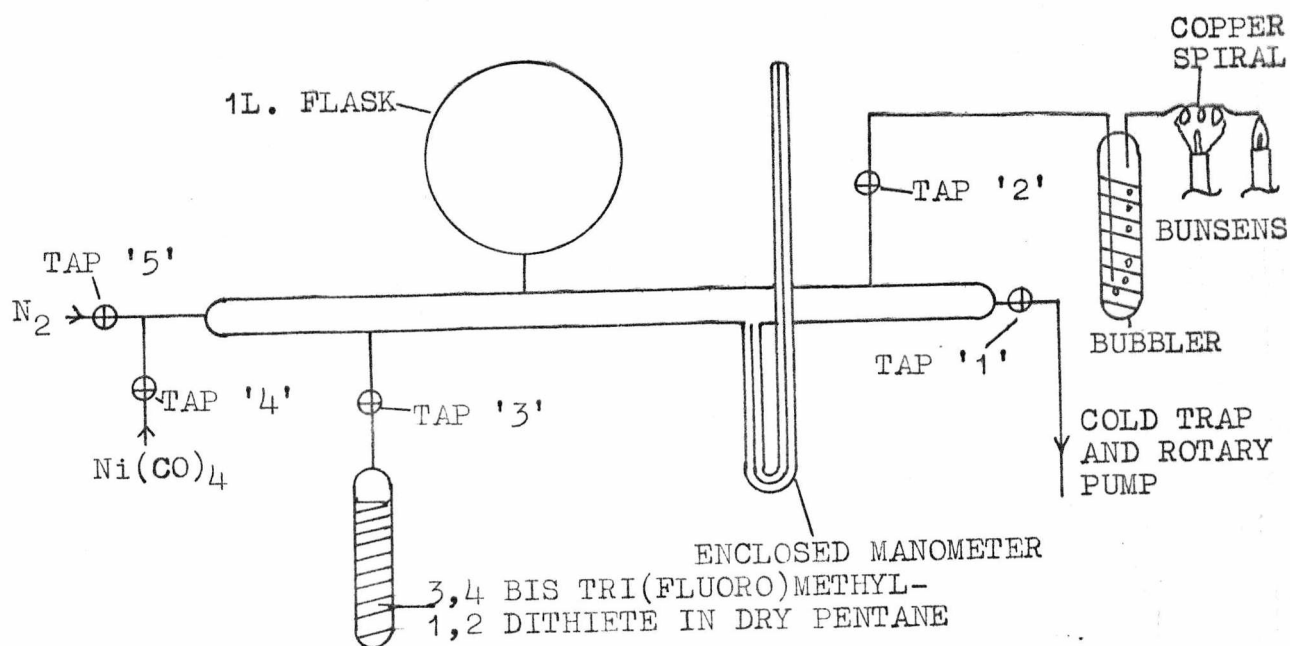
Purification of the dark red malodorous liquid was carried out by repeated distillation (10 times), and resulted in a malodorous straw yellow liquid. It was found that after purification the 3,4bis(trifluoromethyl)-1,2-dithiete readily dimerised (in a few hours) and it was found that this dimer could not be reacted with nickel carbonyl to form bis[cis-3,4bis(trifluoromethyl)-1,2-dithiete]nickel^0, hence the 3,4bis(trifluoromethyl)-1,2-dithiete was only purified immediately before use.

Reaction:

$$CF_3 - C = C - CF_3 + S_2 \longrightarrow \begin{array}{c} S - C \diagup^{CF_3} \\ | \quad \parallel \\ S - C \diagdown_{CF_3} \end{array}$$
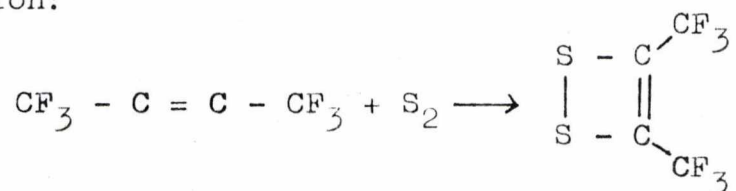
3.4 Preparation of Bis[cis-3,4-bis(trifluoromethyl)-1,2-dithiete]nickel^0

Preparation of this compound was reported as being straightforward (Davison, Edelstein, Holm & Maki, 1963; and Davison & Holm, 1967). The two reactants, bis(trifluoromethyl)-1,2-dithiete and nickel carbonyl, were simply mixed together in dry n-pentane at 263K. However, in practice, this preparation proved difficult to perform because of the extremely high toxicity of the nickel carbonyl. The TLV limit for this chemical is 0·001 p.p.m. Unfortunately the detection of the musty odour could not be relied upon to give adequate warning. Exposure even to very low levels could be lethal and carcinogenic and the onset of any symptoms could be delayed by up to 36 hours. Hence a completely closed reaction system had to be designed. As a further precaution, the apparatus was made to fit into a fume cupboard; the resulting design is shown in figure (3.2).

Special attention was given to using a reaction procedure whereby adequate precautions were taken in handling the nickel carbonyl. Bis(trifluoromethyl)-1,2-dithiete was dissolved in some dry n-pentane and placed in the apparatus as shown in figure (3.2). By opening taps '5' and '4' the entire apparatus was flushed with nitrogen. After this had been completed a dewar of liquid nitrogen was placed around the n-pentane solution. When this had frozen solid, taps '2', '4' and '5' were closed and the apparatus was then evacuated using a rotary pump. Two liquid nitrogen cold traps were placed in between the apparatus and pump, to ensure adequate trapping of any contaminants. After a vacuum of about 1 Pa had been attained tap '1' was closed and the dewar of liquid nitrogen removed from the n-pentane solution. The system was then allowed to slowly reach room temperature. This degassing procedure was carried out four times.

After evacuating the system, as before, taps '1' and '3' were closed. Then by opening tap '4' a small amount of nickel carbonyl was allowed into the apparatus, measured by means of the enclosed mercury manometer. The actual amount added was carefully calculated so that when the reaction had reached completion the pressure inside the apparatus would be slightly less than atmospheric. In this calculation the vapour pressure of n-pentane (at 293K) and the fact that 4 molecules of carbon monoxide were produced for each nickel carbonyl molecule, had to be taken into consideration. After addition of the reactant, tap '4' was closed and tap '3' was slowly opened. The dewar of liquid nitrogen was then removed and replaced with a solid

36

carbon dioxide bath; by lowering this bath the solution
was allowed to warm up very slowly. While the reaction was
proceeding the n-pentane solution changed from a yellow-
orange colour to very deep violet; also, the pressure in-
creased inside the apparatus. These changes provided two
means by which the reaction rate could be observed, and
if it became too fast, tap '3' could be closed to slow it
down. After reaching room temperature the solution was
left for one hour.

When the reaction had reached completion it was
necessary to remove any excess nickel carbonyl. This was
accomplished by opening tap '5' and building up the pressure
inside the apparatus to slightly greater than atmospheric.
Tap '5' was then closed and tap '2' opened slowly, after
igniting the bunsen burners. By opening tap '5' a little,
a slow flow of nitrogen was passed through the apparatus.
The flow rate was monitored by the bubbler. Nickel carbonyl
was destroyed by the action of the water bubbler, hot copper
tube and naked flame. The first only destroyed some of the
gas; the primary function of the bubbler was to monitor the
flow rate. All the nickel carbonyl was dissociated by passing
it through a hot copper tube (about 900K). For safety the
effluent gas was passsed into a bunsen flame; any nickel
carbonyl would then be burned. Since nickel carbonyl burns
with a green flame, the latter process also served as a
check to see if the hot copper tube was working satisfac-
torily.

The system was flushed for about twelve hours, after
which the n-pentane solution was transferred to a conical
flask. Nitrogen was then bubbled through the solution to

remove some of the dissolved nickel carbonyl. The solution
was then heated slowly, and the bulk reduced to one half.
By crystallisation a product of shiny purple black crystals
was obtained. Further purification was carried out by re-
crystallisation from dry n-pentane and entrainer sublimation
(cf. section 3.7).

Reaction:

$$2\left(\begin{array}{c} F_3C\diagdown C\diagdown S \\ \| | \\ F_3C\diagup C\diagdown S \end{array}\right) + Ni(CO)_4 \xrightarrow[263K]{\text{in n-pentane}} \begin{array}{c} F_3C\diagdown C=S \diagdown \diagup S=C\diagup CF_3 \\ | Ni | \\ F_3C\diagup C=S \diagup \diagdown S=C\diagdown CF_3 \end{array}$$

$$+\ 4\ CO$$

3.5 Preparation of Copper and Palladium oxinates

a) Copper oxinate

Analar 8-hydroxyquinoline was dissolved in warm ethyl
alcohol. This was added to a second solution containing
copper acetate dissolved in hot distilled water. The solid,
copper oxinate, was collected, washed with distilled water
and dried.

b) Palladium oxinate

Bis(ammonia)bis(chloro)palladium(II) $(Pd(NH_3)_2Cl_2)$ was
dissolved in hot distilled water. The solution was
filtered into a solution of analar 8-hydroxyquinoline
dissolved in acetic acid. The precipitate, a yellow
solid, was collected, washed with distilled water and dried.

Crystals of both oxinates were grown by slow evap-
oration of solutions in chloroform.

3.6 Preparation of the benzidine-TCNQ complex

Before this complex could be prepared the chemicals had to be purified. Benzidine was obtained from Koch-Light Laboratories and had an estimated impurity level of 2%. Since this chemical is very carcinogenic great care had to be taken to avoid any physical contact. Purification was accomplished by using repeated zone refining. TCNQ was purified by repeated crystallisation from acetonitrile.

To make the complex two solutions containing the equal molar weights of benzidine and TCNQ were made using the same dry solvent. In this study the solvents used were: acetone, dichloromethane and chloroform. The two solutions were added together in a conical flask and crystallisation was then carried out in the dark (to prevent any photoinitiated reaction from occurring) with a flow of cool nitrogen over the solvent. Small dark green needle shaped crystals were obtained.

3.7 Purification and crystal growth

Two techniques were employed for purification and crystal growth, namely entrainer sublimation and crystallisation. The former technique is discussed in chapter 4 and was used for: anthracene, perylene, TCNQ, bis[cis-3,4-bis(trifluoromethyl)-1,2-dithiete] nickel^{o} and all the phthalocyanines. The crucial factor for obtaining good, high purity, single crystals was the control of the hot and cool zone temperatures. This was especially found to be true for the phthalocyanines (Fielding et al,1973); if the hot zone was too hot then decomposition occurred and if the zone was too cool the separation between various phthalocyanines was poor. Before any crystals were grown the material was

PHTHALOCYANINES	FORMULA	PREDICTED				ANALYSED			ESTIMATED
		C	H	N	OTHERS	C	H	N	
Metal free	$C_{32}H_{18}N_8$	74·70	3·50	21·80	0	74·32	3·32	2·73	0
Manganese	$C_{32}H_{16}N_8Mn$	67·73	2·82	19·76	Mn 9·69	68·51	2·33	19·83	Mn:9·33
Cobalt	$C_{32}H_{16}N_8Co$	67·26	2·80	19·62	Co 10·32	67·26	2·90	19·54	Co:10·30
Nickel	$C_{32}H_{16}N_8Ni$	67·28	2·80	19·63	Ni 10·29	66·61	2·35	19·26	Ni:11·78
Copper	$C_{32}H_{16}N_8Cu$	66·72	2·78	19·46	Cu 11·04	66·63	2·60	19·30	Cu:11·47
Zinc	$C_{32}H_{16}N_8Zn$	66·51	2·77	19·40	Zn 11·32	66·61	2·61	10·44	Zn:11·34
Lead	$C_{32}H_{16}N_8Pb$	53·39	2·23	15·57	Pb 28·81	53·62	2·60	15·51	Pb:28·47

TABLE (3.2)   PURITY ESTIMATES OF THE PHTHALOCYANINES

41

COMPOUNDS	FORMULA	PERCENTAGE COMPOSITION									ESTIMATED
		PREDICTED				ANALYSED					
		C	H	N	OTHERS	C	H	N	S		
Perylene	$C_{18}H_{12}$	94·74	5·26	0	–	94·7	5·3	0	–		–
Phenanthrene	$C_{14}H_{10}$	94·38	5·62	0	–	94·4	5·6	0	–		–
Anthracene	$C_{14}H_{10}$	94·38	5·62	0	–	94·3	5·7	0	–		–
Benzidine	$C_{12}H_{12}N_2$	78·26	6·52	15·22	–	78·3	6·6	15·1	–		–
TCNQ	$C_{12}H_4N_4$	70·59	1·96	27·45	–	70·6	1·9	27·5	–		–
Perylene-TCNQ	$C_{18}H_{12}-C_{12}H_4N_4$	84·25	3·5	12·25	–	84·3	3·5	12·2	–		–
Bis[cis-3,4-(trifluoro-methyl)-1,2-dithiete]nickel	$F_{12}C_8S_4Ni$	18·79	0	0	F-44·62 S-25·10 Ni-1149	18·8	0	0	25·1		Ni + F 56·1

TABLE (3·3) PURITY ESTIMATES OF COMPOUNDS

entrainer sublimed at least twice. Crystals obtained using this technique were needle-like for all the materials except anthracene, which gave platelets.

Crystallisation was used for benzidine-TCNQ, copper and palladium oxinate, phenanthrene, TCNQ, and bis[cis-3,4-bis-(trifluoromethyl)-1,2-dithiete]nickel$^\circ$. This process was always carried out in the dark with a flow of cool nitrogen over the solvent.

Purity of these materials and crystals was estimated using Carbon, Hydrogen and Nitrogen analysis. This was performed by Mr. G.M.J. Powell using a modified Hewlett-Packard F+M185-C,H,N analyser. The results are presented in tables (3·2) and (3·3).

3·8 Preparation of lead phthalocyanine films

Before any films were grown onto a strontium fluoride substrate, the material was purified by repeated entrainer sublimations. After cleaning the substrate in acetone and allowing it to dry, two silver electrodes were vacuum deposited onto it; the electrode pattern is shown in figure (3·3). A stainless steel mask was used for this purpose and could be arranged to give an electrode separation of 0·25mm, 0·37mm or 0·50mm. By measuring the surface area of the film and the weight difference of the substrate before and after film deposition, the film thickness was estimated to be about 200nm.

The lead phthalocyanine was placed in a tungsten boat and placed inside the vacuum chamber. When the system had been under a vacuum of 10^{-3} Torr for thirty minutes the boat was slowly heated (to allow the sample to degas) until

the phthalocyanine slowly sublimed. After a suitable film had been deposited the boat and substrate were allowed to cool down before the vacuum chamber was opened. In some cases the lead phthalocyanine film was deposited first. The arrangement of electrode, film and substrate can be seen in figure (3·3).
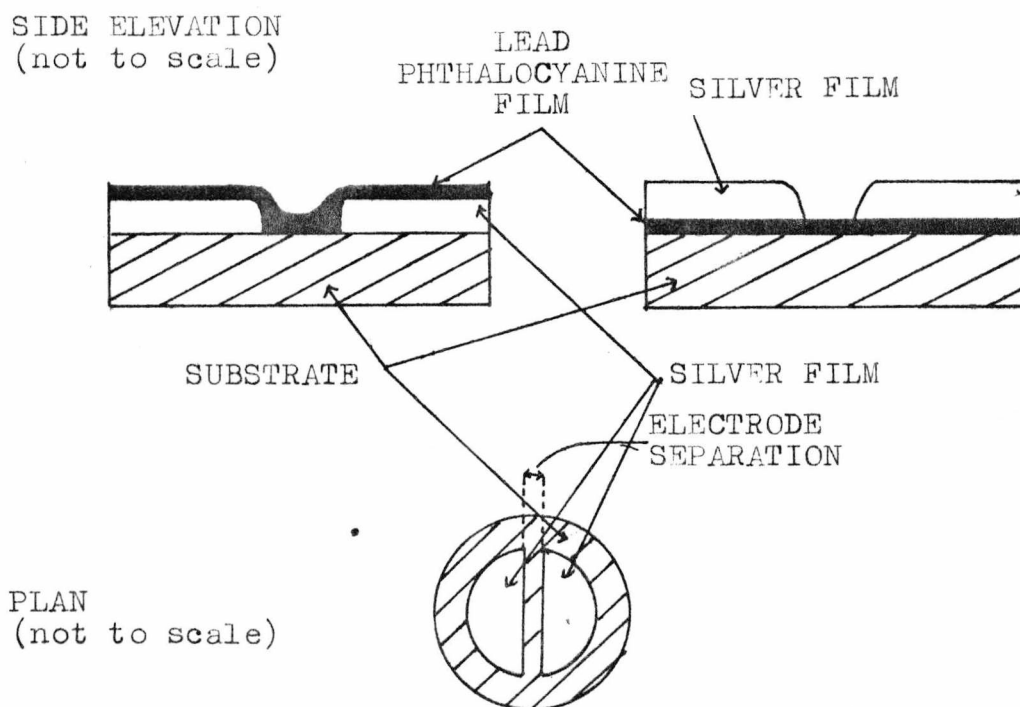
The estimation of lead phthalocyanine film thickness proved to be difficult. Three techniques were tried, namely weight difference, electron microscopy and optical absorption. Weight difference failed because of the very small differences (less than $\frac{1}{2}$mg) and electron microscopy failed because the film became charged by the electron beam (due to the high resistivity of the phthalocyanines). Optical absorption was moderately successful and the films were estimated to be about 200nm thick. In this technique the lead phthalocyanine film was dissolved in a known amount of αchloronaphthalene.

The optical absorbance of this solution at 642 nm was then accurately measured and compared with the absorbance of solutions containing known concentrations of lead phthalocyanine. Hence by extrapolation an estimate of the weight of the film was made; then, knowing the area, the thickness was calculated.

To obtain good organic films the growth rate must be kept low and the substrate temperature should be about one third of the material's boiling point (G. Roberts, 1977). If the substrate temperature is too low then small crystallites are obtained and if the temperature is too high re-evaporation of the film can lead to surface roughness. The theoretical basis of this argument assumes that the film is a mixture of amorphous and crystalline^material and is as follows. From the Clausius - Clapeyron equation the following expression may be obtained:

$$\frac{d\ln P}{dT} = \frac{L}{RT^2} \quad ,$$

where L is the latent heat of evaporation of the material and R is the gas constant. On integration, with respect to temperature, the following equation is obtained:

$$\ln P = \frac{-L}{RT} \quad .$$

If Tb is the boiling point of the material and Te is the substrate temperature, then on substitution into the above equation,

$$\ln\left(\frac{P_a}{P_s}\right) = \frac{L}{RT_b}\left(\frac{T_b}{T_e} - 1\right) \quad \ldots(3\cdot 1),$$

where Pa and Ps are respectively atmospheric and sublimation pressures. For vacuum sublimation $P_s \simeq 10^{-5}$ Torr, and from

Trouton's constant a value of 10·5 is obtained for $\dfrac{L}{RTb}$
(assuming that the amorphous material behaves like a
liquid). Substituting these values into equation (3·1)
(Te/Tb) is found to be 0·35. If this condition is maintained,
the amorphous component of the film is in equilibrium with
the vapour of the material. Te thus represents the highest
substrate temperature attainable without loss of amorphous
material by sublimation and consequent roughening of the film.

3·9 Gas purification

The gases and vapours used in this study were: dinitrogen
tetroxide, boron trifluoride, oxygen, air, ethylene, carbon
monoxide, ammonia, tetracyanoethylene (TCNE) and a series
of substituted pyridines. The latter series consisted of
2,4,6 collidine, 2,6 lutidine, and α,β, and γ picolines
and these were purified by spinning band distillation and
by using vapour phase chromatography. The purity was esti-
mated to be better than 99·9%. With the exception of air
and TCNE all the other gases were obtained in cylinders
from B.D.H. Chemicals. These gases were not purified any
further but they were thoroughly dried by using molecular
sieves. Using this type of drying agent and the apparatus
described in Chapter 4 the water content of the dried gases
was estimated to be below 1 ppm.

Chapter 4 - Apparatus

4·1a General requirements - electrical

In this work it was necessary to be able to measure resistances from 10^5 up to 10^{16} Ohms. This then required that the insulation resistance of the apparatus should be at least 10^{18} Ohms. Also, due to the high resistances encountered, long stabilization times (τ) were met $(\tau = RC,$ C was of the order of 10^{-13} F, hence τ in the worst case was 10^3s); as a consequence only a D.C. measuring technique could be employed. Furthermore, in order to prevent electrical breakdown in the crystals only relatively low potentials could be employed (100's of volts). Hence the electrical equipment had to be capable of detecting currents as little as 10^{-14}A. This then posed a problem of minimizing electrical noise and pickup, and of providing a stable power supply.

The resistances of the compounds studied were strongly temperature dependent. In order to be able to measure this dependence the crystal had to be capable of being heated up to reasonably high temperatures (500K in the case of phthalocyanines) in a controlled manner. Also, it was necessary for the crystal to be maintained at a constant temperature (within $\frac{1}{2}$K) over long periods to ensure that it was in a steady state. Obviously the temperature of the crystal needed to be monitored accurately.

4·1b General requirements - vacuum and gases

For the measurement of gas effects on the conductivity of crystals to have any meaning, it must be possible to measure the electrical characteristics of the compound in a

46

gas-free environment. Ideally vacua of the order of 10^{-8} Pa
should be used (the time for a monolayer of gas to form on
the crystal would then be $\sim$ hrs, assuming 100% sticking
probability). Another approach is to study the pressure
dependence of the gas effect; in this case it is easy
to see at which pressure the gas does not have any effect.
The latter method was used in this study.

The apparatus was designed so that it was simple and
gave a good repeatable vacuum. Special emphasis was put on
pressure measurement. Another important criterion was that
the system should be as leak-free as possible. This was
required since the system had to be kept at fixed pressures
for relatively long periods, while the crystal reached an
equilibrium condition. Since the crystals themselves were
prepared as chemically pure as possible the gases also had
to be both dry and pure.

4.2 Current measurement

Two electrometers were available for measuring very
small currents: a Keithley 610C and an Electronic Industries
Limited Vibron model 62A. The former employs a 'MOSFET'
(metal oxide, semiconductor, field effect transistor) input
stage to give its very high input resistance of 10^{14} Ohms;
a very sensitive D.C. amplifier then amplifies the signal
and displays it on a large mirror backed meter. The
Vibron's operation is based on the changing position of a
vibrating reed (600 Hz.) relative to a charged electrometer
plate. This induces a 600 Hz A.C. signal, the amplitude
being modulated by the potential of the electrometer plate.
This signal is then amplified by a 600 Hz tuned amplifier,

again displaying the result on a large mirror backed meter.
It was found that the Keithley was by far the easier to use
since the standard resistances were switched internally,
and consequently it was used extensively in this work.

The technique employed to measure the resistance of
the crystal (R_c) was to apply an accurately known potential,
Vapp, across the crystal in series with a standard resistor
(R_s); see figure (4.1).

<div align="center">
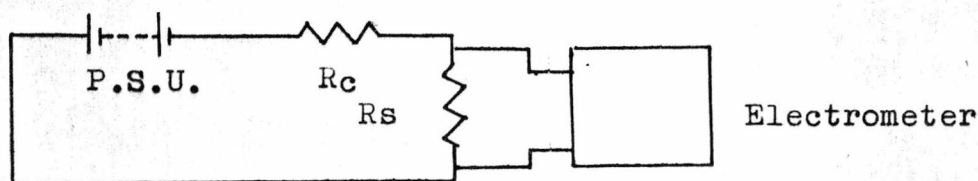
Figure (4.1)

</div>

The current flowing through the circuit is given by:

$$I = V_s/R_s \qquad \text{(Ohms Law)}$$

where V_s is the measured potential drop across R_s. Now the
resistance of the crystal may be found from

$$R_c = (V_{app} - V_s)/I$$

By keeping V_s less than 1% of Vapp, it may be ignored and then

$$R_c = V_{app}/I$$

Since very small currents were being measured (typically
10^{-12} A) all the wiring and resistances were screened and
earthed through a central point, thereby overcoming the
possibility of any 'hum' loops. A good earth was provided
by a large copper plate buried in the ground beneath the
water table; connection between plate and equipment was
accomplished by a thick copper strip. Further, to avoid
mains transients interfering with the measuring equipment,
the instruments were powered via an inductive filtering unit.

4.3 Power supply

One of the essential requirements for accurate conductivity measurements is the provision of a stable noise-free power supply. The output should preferably be switchable and reversible. In these studies a potential range of 1V up to 2kV was required. It was found that a Harwell 1359A power supply used in conjunction with two Harwell 1007B potential dividers admirably fulfilled all the criteria. The power supply gives a D.C. potential from 200V up to 4900V in switched steps of 100V. Both of the Harwell 1007B units divide the input potential into twenty equal steps; there is also an overlapping fine control between each step. The specification of the final set up was:

```
1V-10V      in switched steps of   0.5V
10V-200V    in switched steps of    10V
200V-4900V  in switched steps of   100V
```

The equipment was checked at regular intervals with a Bradley digital voltmeter and it was found that the real potential was never more than 2% different from the indicated value. Ripple noise and drift were monitored over a 60 hr. period with an Oxford series 3000 chart recorder. The following values were obtained:

ripple and noise - 2mV peak to peak, maximum
drift - $\pm 0.1\%$ (after a 12 hr. warm up period)

4.4 Temperature measurement

It has already been noted that it is desirable to be able to measure the crystal's temperature to within 1/2K. Furthermore, this accuracy must be maintained over the entire temperature range, in this case 273K up to 500K (the upper limit is the maximum temperature to which phthalocyanines may be heated in vacuum without sublimation

becoming a problem; for the other organics this limit was lower). The method employed for measuring temperature was to use a platinum resistance thermometer in conjunction with two copper-constantan thermocouples.

The platinum resistance thermometer provided a known reference junction for one of the thermocouples, the other thermocouple being placed near the crystal. Hence the crystal's temperature could easily be found by calculating the platinum resistance temperature and either subtracting or adding the temperature difference indicated by the thermocouples. By using this arrangement not only was an accurate measurement of the temperature of the crystal possible (to about 1/4K) but an indication of the temperature differential within the heating block was also obtained. This in turn gave some idea of when the heating block and crystal were in thermal equilibrium (the differential thermocouple would then indicate a small temperature). A diagrammatic representation of the system is shown in figure (4.2)
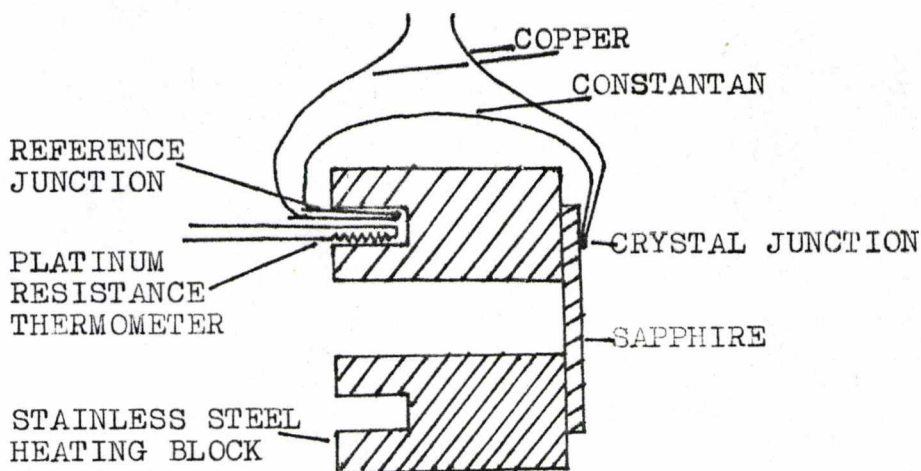

Figure (4.2)

Both the platinum resistance and the reference thermo-couple were placed in a very tightly fitting hole in the heating block, thereby ensuring that they were in very good thermal contact. The other thermocouple was attached onto the sapphire substrate using Acheson DAG 915 silver paste, to ensure good thermal contact. A stainless steel clip held the substrate onto the heating block. The copper leads from the differential thermocouple were attached to glass/metal seals; these were in close proximity to each other thereby ensuring that they were at the same temperature and cancelling out any unwanted thermal emfs. A similar arrange-ment was used for the platinum resistance leads. Insulation between the leads inside the cell was accomplished by covering them with thin glass tubes.

The thermal emf. produced by the differential thermo-couple was measured with a Comark microvoltmeter. This instrument has a very high input resistance of $10^9 \Omega$ per volt and hence draws negligible current. By using the programme given in the appendix, the thermal emf. was related to temperature.

The platinum resistance was used to measure the tempera-ture by placing it in a bridge circuit and measuring the 'out of balance' potential. This potential was kept below 200mV so that the heating effect of the platinum resistance would be negligible (at 573K this potential is about 120mV, and the thermometer has a resistance of 214Ω hence the heating effect $= \frac{V^2}{R} \approx 10^{-4}W$). Since the 'out of balance' signal was small it had to be amplified up to a reasonable level; an operational amplifier was used for this purpose. The full circuit diagram is given in figure (4.3),

__PLATINUM RESISTANCE THERMOMETER AMPLIFIER__
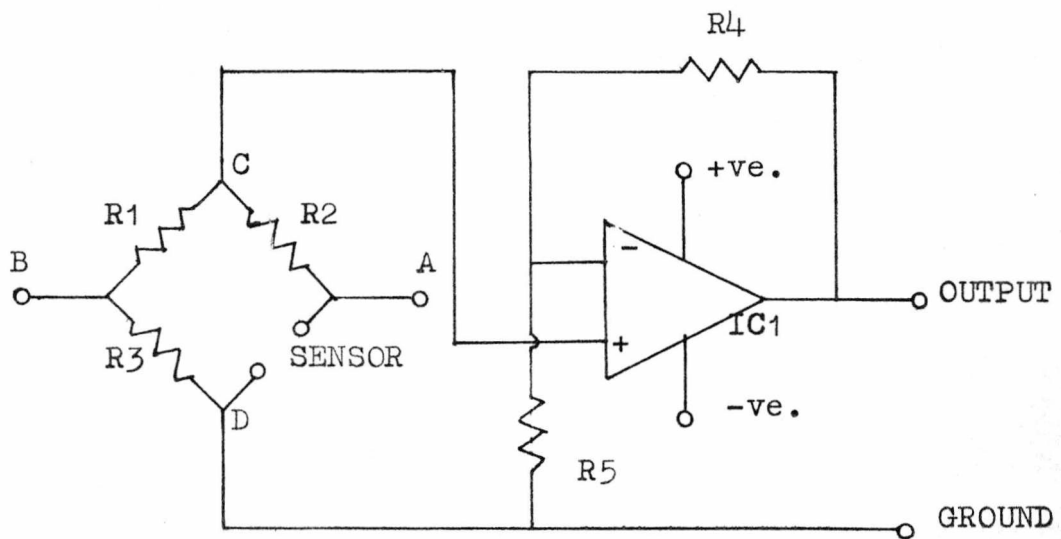
__BRIDGE AND AMPLIFIER__
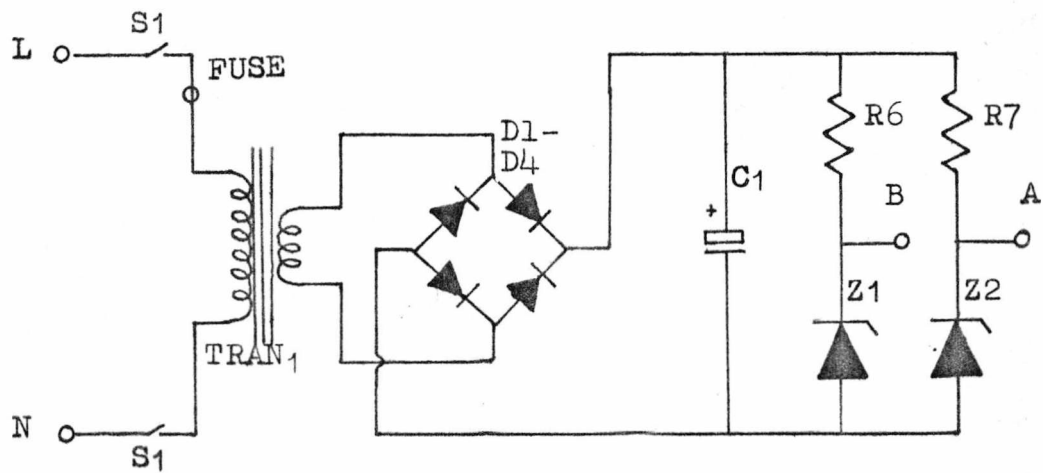
__BRIDGE POWER SUPPLY__

__AMPLIFIER POWER SUPPLY__

52
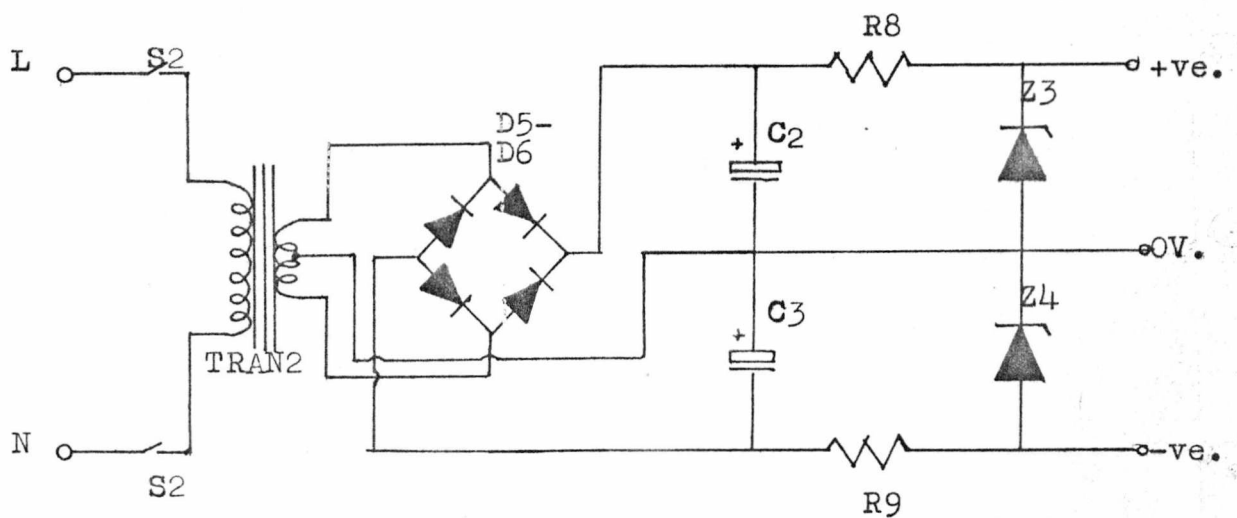
and the operation was as follows. An accurate reference potential (about 1V) was applied across the bridge at points 'A' and 'B'. If R1 = R2 and sensor = 100Ω = R3 (which corresponds to 273K) then the bridge would be in balance and the 'out of balance' signal across points 'C' and 'D' was zero. Since the platinum resistance had a positive temperature coefficient, increasing temperature resulted in an increasing resistance. Hence the bridge became unbalanced and a current flowed. The higher the sensor's resistance the higher the current flow and consequently a greater potential was developed across 'C' and 'D'.

The reference potential was derived from two Zener diodes (Z1 and Z2). Using this type of arrangement the temperature coefficient of both Zener diodes acted in the same way, thereby keeping the potential difference between them constant. Since the temperature fluctuation was never more than a few degrees K, the reference potential hardly varied at all (it was found that this fluctuation was less than 10µV for a 3K change in temperature). The bridge rectifier (D1-D4) supplied fully rectified D.C. which was smoothed by capacitor C1. The Zener diodes were reverse biased, hence they only conducted when the potential applied to them was greater than their Zener voltage, the higher the excess potential the greater the current carried by Z1 and Z2. Thus the potential drop across the Zener diodes remained constant. Current flow through Z1 and Z2 was limited by resistors R6 and R7. For the amplifier power supply a similar arrangement was used; however, in this case the current demand of the amplifier had to be taken into consideration when calculating the series resistances R8 and R9.

An operational amplifier was chosen because it could easily be made to amplify signals, with very high accuracy. This device could be made to amplify signals in excess of 10^4 times; however, in this case an amplification factor of a modest 25 (approximately) was required. The amplification factor depends on the extent of negative feedback (100% negative feedback gives the amplifier a gain of unity), which was programmed by the potential divider R4 and R5. The amplifier's gain was simply given by: $G = (R4 + R5)/R5$. With increasing gain the amplifier's bandwidth is decreased, but in this case only D.C. signals were being amplified so this was of no consequence.

To set up the platinum resistance thermometer and amplifier the sensor was put in position in the heating block; the output from the amplifier was then noted for different temperatures. The block heater was used for heating and the differential thermocouple was used to measure the block temperature, by placing the crystal junction in an ice-water bath (reference 273K). This was carried out for a temperature range of 273K up to 600K in steps of 5K. A polynomial of degree 5 was then fitted to the data using a standard curve fitting programme ('PLOFIT') on the university's computer. From the resulting equation a table was drawn up of amplifier output voltage versus temperature in 0·1K steps; the programme used may be found in the appendix. As a further check the heating block was placed in a carbon tetrachloride bath (CCl_4 was used because of its very low conductivity, and therefore did not interfere with the measurement of the platinum resistance). Bath temperature was monitored using a copper-constantan thermocouple with a

273K reference junction and a large mercury in glass thermo-
meter. Extremely good agreement was achieved so it was
concluded that the temperature measuring equipment func-
tioned according to specification (i.e. better than 1/4K).

4.5 Temperature control

This section falls neatly into two parts, the heating
system and the power controller. The former basically
consisted of an electrical heating element wound around
a stainless steel block. Apart from acting as a heat sink
the block also provided a means of attaching the substrate,
temperature measuring devices and a sensor. One of the
main difficulties in employing electrical heating is to
reduce electrical interference to a minimum in the sensitive
current measuring equipment from the heater. This was
achieved by using a bylar (non-inductively) wound heater
placed in, and insulated from, an earthed stainless steel
sheath. This device was obtained from Pyrotenax Limited.
A major advantage gained in using electrical heating was
the ease with which it could be effectively sealed into the
vacuum system; temperature control also became a minor
problem. The installation of block, heater and sensor may
be seen in figure (4.6).

Construction of a controller for the heater was rela-
tively straightforward. It was decided that D.C. should
be used to power the heater, thereby minimizing any electrical
noise reaching the current detecting equipment. A platinum
resistance placed in the heating block acted as a sensor
for the controller. The circuit diagram of the controller
can be seen in figure (4.4); since the bridge and amplifier

55

FIG: (4.4) HEATER CONTROLLER
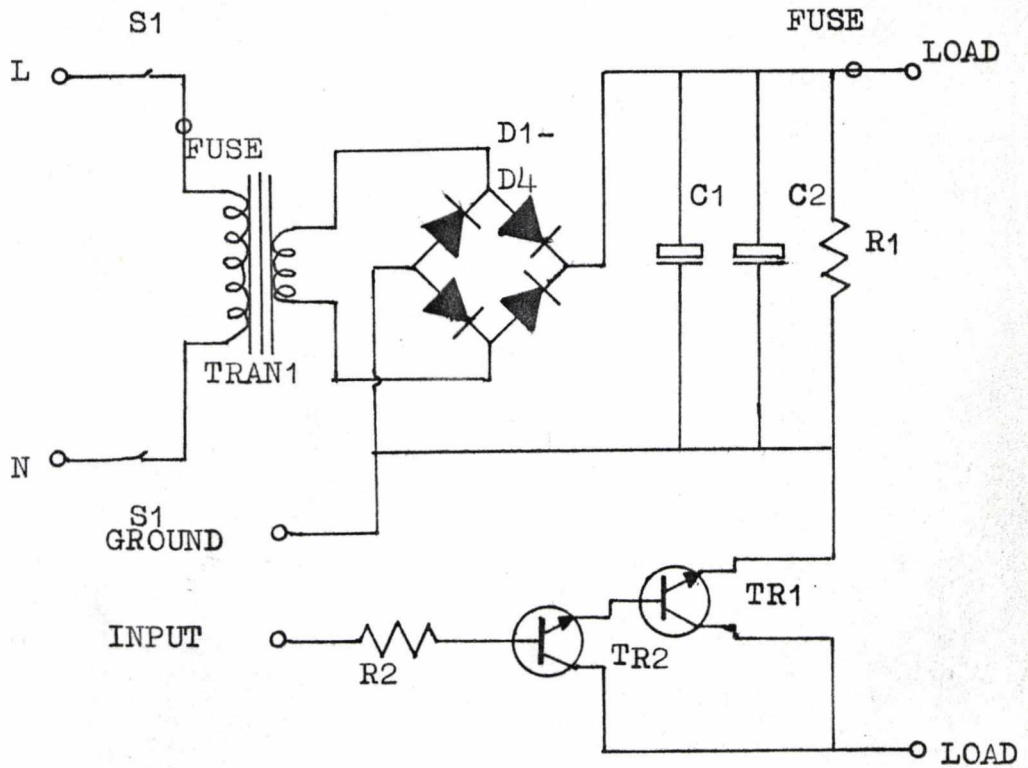
D.C. POWER CONTROLLER

BRIDGE AND AMPLIFIER

56
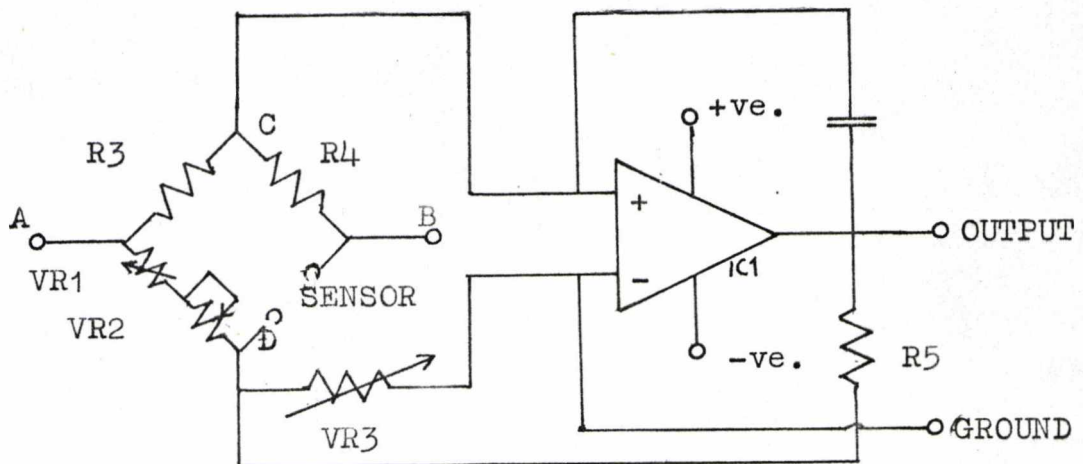
power supplies were identical to those used in the platinum resistance thermometer amplifier, they are omitted. In this case the bridge had preset and variable resistances (VR1 and VR2) in the arm balancing the sensor. This was so that the bridge could be made to balance at various values of sensor resistance (i.e. temperature). As before a reference potential was placed across the bridge at points 'A' and 'B'; the 'out of balance' signal appeared across points 'C' and 'D'. This potential was influenced by the sensor and the setting of VR1 and VR2. When balance was attained it implied that the heating block was at the required temperature. If the bridge's 'out of balance' signal was positive the block was too hot and if the block was too cold the signal would be negative. The colder the block was with respect to the required temperature, the larger the 'out of balance' signal would be; this small signal was amplified by the operational amplifier (IC1). In this case the gain was variable (VR3).

From the output of the amplifier it was easy to ascertain how much power should be supplied to the heater. When the output was positive or zero then no power was required; however, when the output was negative the power supplied should be related to the amplifier output. This then gave the controller proportionality which in turn lead to better temperature control. A simple series regulator was constructed to fulfil these requirements. The circuit diagram is shown in figure (4.4). The bridge rectifier (D1-D4) provided fully rectified D.C., which was fully smoothed by capacitors C1 and C2 (resistor R1 ensured that these capacitors were discharged when the controller was switched off). Transistor TR1 was placed in series with

57

the load. The potential of the base determined the extent of conduction and hence the amount of power supplied to the load. (TR1 would only conduct when its base was negative, i.e. a P.N.P. transistor.) Since the operational amplifier's output was insufficient to drive TR1 it had to be buffered by TR2, current flow from the amplifier being limited by resistor R2.

With this controller the block could be maintained at temperatures from 293K up to 600K with an accuracy of 1/4K. The current induced in the current measuring equipment when the heater was supplied with full power was 10^{-11} A. However, in normal operation the heater was never switched on and off rapidly with full power, so the induced current was far less, typically 10^{-13} A. When the system was operated under vacuum it was noted that the temperature swing of the block was very large (about 10K). This was because the heater was too powerful for its purpose since very little heat was escaping from the block. This problem was overcome by introducing a ballast, consisting of three 100W light bulbs, connected in parallel with the heater.

4.6 The optical system

In order to measure photoconduction spectra a system capable of providing uniform monochromatic light of measurable intensity was required. The range under study was 400nm up to 800nm. A Grubb Parsons M2 grating monochromator with two optical benches on which the lamp and suitable mirrors could be mounted, was used. The light source consisted of a 55 Watt, 12V quartz halogen bulb powered from the mains via a transformer and a Variac. Once the light had been monochromated it was focussed onto the sample, via suitable

CRYSTAL

MICROVOLTMETER

GRATING

SOLENOID
OPERATED
MIRROR

LIGHT
SOURCE

THERMOPILE
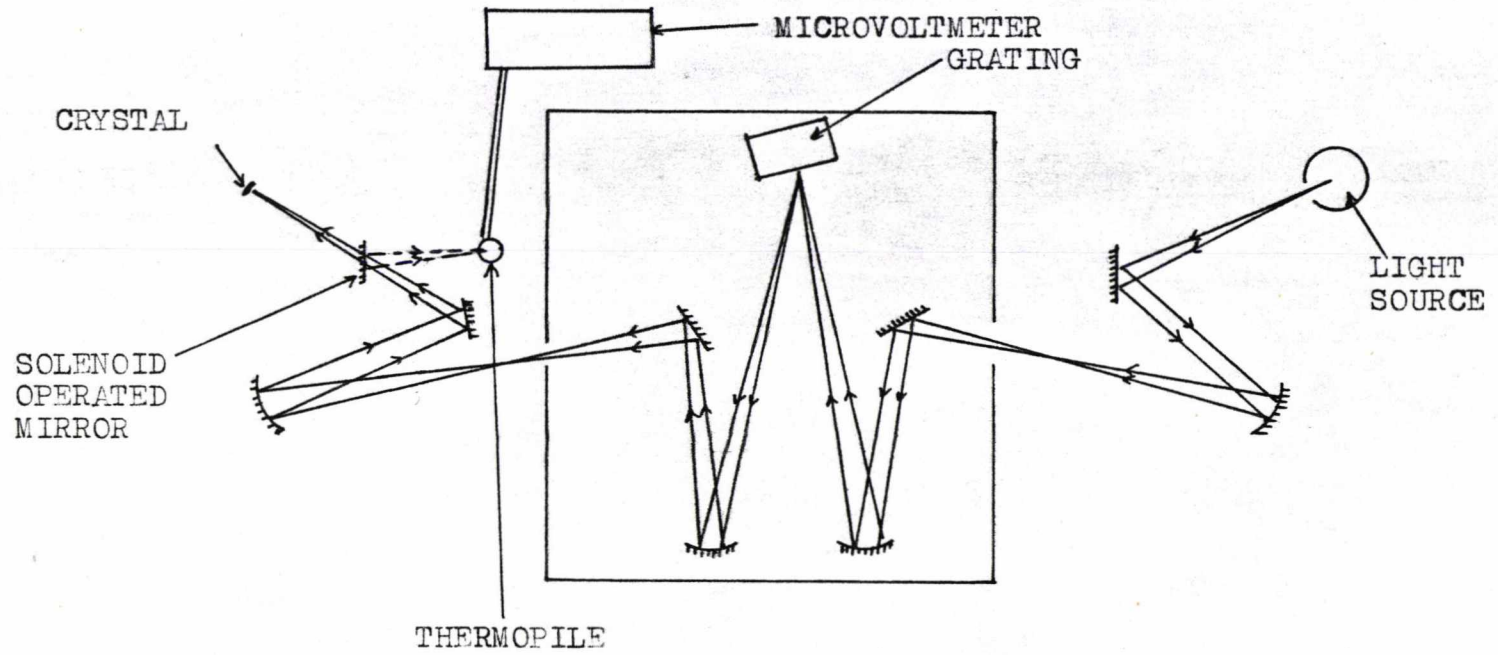
FIG: (4·5) GRATING MONOCHROMATOR

mirrors, through a 1" glass window in the cell (as may be seen from the schematic diagram in figure (4.5)). All the mirrors and the light source were placed inside light tight covers.

Light intensity was measured by means of a room temperature compensated Hilger Schwartz thermopile. A Comark microvoltmeter was used to monitor the output of this device. The monochromated beam was redirected onto the thermopile by means of a solenoid operated mirror. Intensity variation of the beam was accomplished by adjusting the power supplied to the lamp with the Variac, since the monochromator was used at constant slit width. To prevent any interference from second order diffraction suitable filters could be placed in between the light source and the diffraction grating.

4.7 The Chart recorder

Extensive use was made of an Oxford Instruments series 3000 twin channel chart recorder, for both steady state and dynamic measurements. One pen normally monitored temperature and the other current, via the electrometer chart recorder output. Using this technique it was easy to establish when the crystal had reached both electrical and thermal equilibrium. It was also possible to study the dynamic response of the crystal to a small perturbation. This was especially useful in studying the effect of gases. By means of the calibrated offset control, very small signals could be accurately studied in the presence of large signals. This was very useful in measuring photoconduction spectra.

4.8 The cell

The main design criterion was that the cell should be capable of holding a high vacuum. With this in mind a stainless steel system was designed and built (figure (4.6)). It can be seen that the cell consisted of two parts, the main body and the top 4 1/2" flange containing all the connections into the cell. Detail of the latter can be seen in figure (4.7). The body was made from a 2" diameter stainless steel tube. A 5" 'O' ring sealing flange was argon arc welded onto one end of this. The other end had a 4 1/2" copper gasket sealing flange attached in a similar manner. The former sealed the high vacuum valve onto the cell and the latter was used for bolting on the top flange. Two 1" diameter stainless steel tubes were welded into the main body; the other end of the small tubes had 1 3/4" copper gasket sealing flanges welded onto them. One of the side arms was used to bolt on a 1" glass port and the other arm used to mount the ionization gauge head (Vacuum Generators type VIG 20). Since the gauge was mounted in a narrow tube it had to have its tungsten filament replaced by a thorium coated irridium one. This was to cut down the heat generated (the tungsten filament operates at about 1500K and the thorium coated irridium filament operates at about 1000K), thereby reducing the temperature of the steel tube and preventing an erroneous pressure reading due to excessive outgassing from the tube.

To obtain a high vacuum in any stainless steel system it must be possible to heat the steel up to about 500K. This is known as 'baking out' and effectively speeds up the desorption of gases from the steel. A heating element similar

FIG: (4.6) <u>H.V. CELL</u>

6 WAY SOCKET

HIGH RESISTANCE LEAD THROUGH

SCREENED 6 WAY CABLE

TUNGSTEN/QUARTZ SEAL

HEATER SOCKET

QUARTZ TUBE

AIR COOLING INLET

6 WAY LEAD THROUGH

QUARTZ/STAINLESS STEEL GRADED SEAL

$4\frac{1}{2}''$ FLANGE

STAINLESS STEEL ROD

REFERENCE THERMO- COUPLE

'BAKE OUT' HEATER COIL

'HOT JUNCTION' PLATINUM RESISTANCE THERMOMETER

$1\frac{3}{4}''$ FLANGE

CRYSTAL THERMOCOUPLE

1" GLASS WINDOW

IONIZATION GAUGE HEAD

STAINLESS STEEL CLIP

SAPPHIRE SUBSTRATE

PLATINUM RESISTANCE SENSOR

HEATER COIL

$5''$ FLANGE

Not shown, for reasons of clarity:

second ultra high resistance lead through.

air cooling exit tube

electrical connections between Pt. resistances and thermocouples to 6 way lead through.

to that used to heat the block (cf section 4.5) was used, with the power supply controlled by a **Variac**. This arrangement minimized electrical interference and eliminated the problem of electrical shorting to the cell body, which was a problem when electrical heating tape was used.

All the electrical and mechanical connections for the mounting block were made through one 4 1/2" flange. This was in order to facilitate easy removal of the cell block and associated devices. In all, six connections were made through this flange: two ultra high insulation resistance (U.H.I.R.) lead throughs, one six way electrical lead through, an air cooling inlet and outlet, and finally the heater connection. All of these components were silver soldered into suitable holes. It was at this point that a major problem arose. At first standard silver solder was used but on evacuation it was found that the cell was contaminated by metals evaporated out of the solder. On investigation it was found that some metals have relatively high vapour pressures and are therefore unsuitable for use in vacuum systems. Table (4.1) lists the vapour pressure at various temperatures, for metals found in common solders. It was found that only metals like lead, silver, copper and tin were suitable (these have vapour pressures well below 10^{-4} Pa at 373K). Hence to overcome this problem some silver solder was specially made up by melting together silver and copper in a graphite crucible (60% silver and 40% copper, by weight).

The U.H.I.R. lead throughs were made by using: a quartz tube, a tungsten to quartz seal, a quartz to pyrex graded seal, and a pyrex to metal graded seal, as shown in

64

METAL	TEMPERATURE (K)		
	373	473	573
Cadmium	$2 \cdot 3 \times 10^{-5}$	$4 \cdot 0 \times 10^{-2}$	$6 \cdot 1$
Zinc	$9 \cdot 6 \times 10^{-14}$	$6 \cdot 4 \times 10^{-4}$	$0 \cdot 2$
Lead	$1 \cdot 2 \times 10^{-16}$	$3 \cdot 3 \times 10^{-11}$	$1 \cdot 1 \times 10^{-7}$
Silver — Vapour Pressure (Pa)	$3 \cdot 9 \times 10^{-11}$	$1 \cdot 0 \times 10^{-12}$	$3 \cdot 1 \times 10^{-15}$
Copper	$3 \cdot 3 \times 10^{-37}$	$5 \cdot 6 \times 10^{-24}$	$2 \cdot 5 \times 10^{-17}$
Tin	$8 \cdot 8 \times 10^{-27}$	$2 \cdot 4 \times 10^{-16}$	$1 \cdot 6 \times 10^{-11}$
Iron	$1 \cdot 3 \times 10^{-42}$	$2 \cdot 9 \times 10^{-31}$	$7 \cdot 1 \times 10^{-24}$

TABLE (4·1) VAPOUR PRESSURES OF VARIOUS METALS
(Smithsonian Physical Tables, p. 363)

figure (4.6). Two such lead throughs were used, one to supply the potential to the crystal and the other to connect the current measuring equipment. Connection between stainless steel rods and crystal was by means of a very thin copper wire. This damped out any vibrations from the rods to the crystal and reduced possible heat losses.

Electrical connections for thermocouples, platinum resistance thermometer and sensor were all made into a single pyrex to metal seal, as shown in figure (4.6). Connections between lead throughs and devices were made by using thin copper wires, soft soldering them into position. Care was again taken in using a solder containing only metals with low vapour pressures (it was found that ordinary 60/40 tin/lead solder was good enough). The mounting block was held securely in position by a stainless steel tube, fitting tightly into a groove around the block, which also provided a means of cooling (by blowing cool air through it).

The cell body was earthed to the central earth point with a stout copper wire. This then effectively screened all the electrical wiring inside the cell. As may be seen in figure (4.6) the lead throughs outside the cell were electrically screened by a thick aluminium cover which also provided a means of mounting all the electrical connectors. The two U.H.I.R. lead throughs were connected to U.H.F. sockets. Since these sockets have P.T.F.E. inserts they have a very high insulation resistance (approximately $10^{18}\Omega$). The six way lead through was connected to a six way socket; this provided easy connection to all the thermocouples and platinum resistances. Since the heater sometimes carried a high current its connecting lead and socket were kept as

far away as possible from all the other leads and sockets. The
aluminium can gave electrical screening and also provided mech-
anical protection for the rather delicate U.H.I.R. lead
throughs. The can itself was securely fastened to the top
flange with bolts; the whole screening assembly could be
very easily demounted for cleaning.

Tests were carried out to check the vacuum and electrical
performance of the whole system. For the vacuum check the
cell was baked for 14 hours at 470K. After cooling, the
final vacuum attained was 6×10^{-5}Pa. It was found that in
practice a vacuum of 10^{-4}Pa could be readily attained. The
leak rate of the cell was checked by closing the main valve
and studying the rate of pressure increase; it was found to
be of the order of 10^{-9}Pa m^3 s^{-1}.

For electrical performance tests the sapphire substrate
had two parallel strips (10^{-2}m long and $2 \cdot 5 \times 10^{-3}$m separation)
painted on it with Acheson DAG 915 silver paste. Insulation
resistance was then measured in various ambients. The results
are shown in table (4·2).

<div align="center">TABLE (4·2)</div>

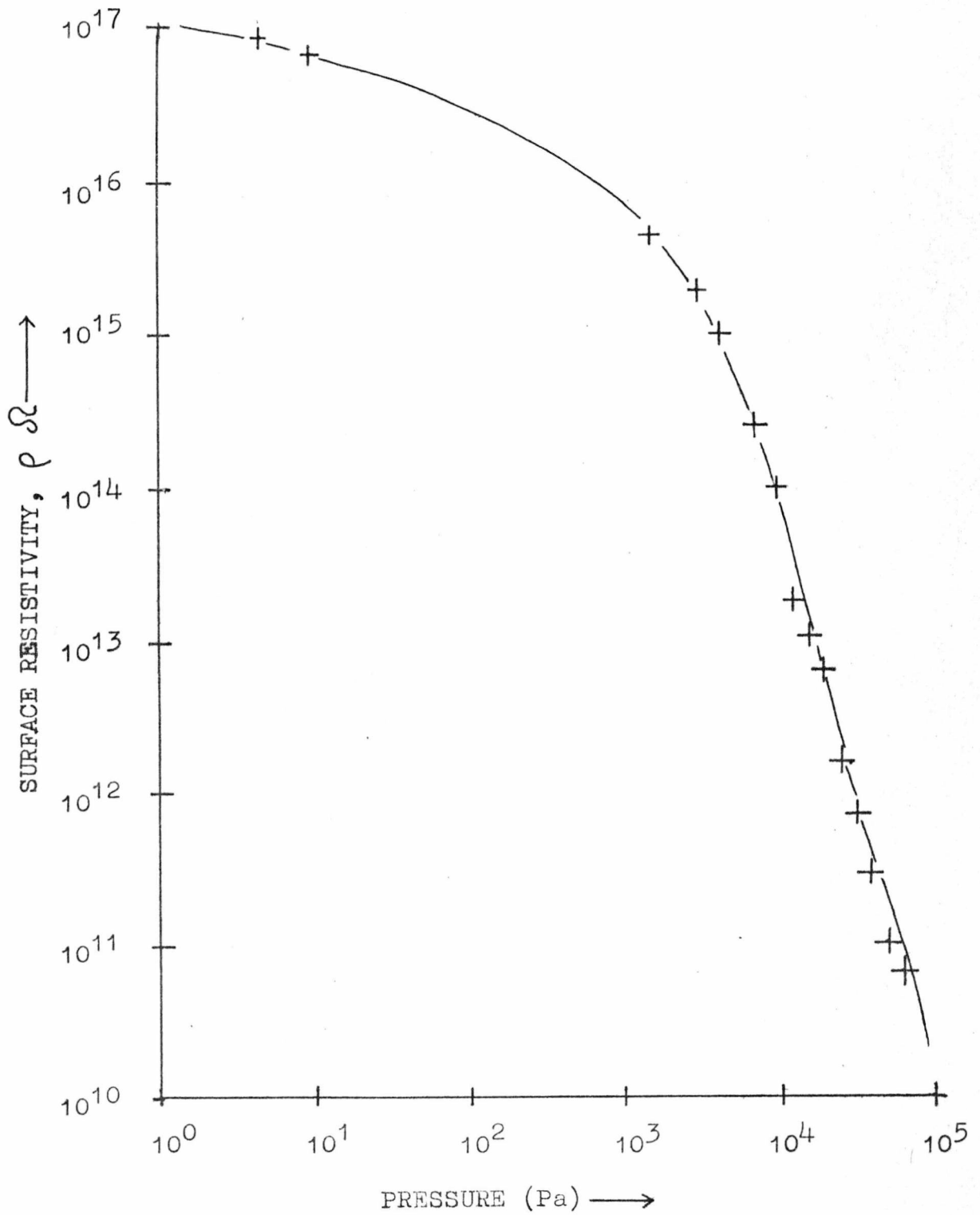| Ambient	Insulation resistance Ω	Apparent sapphire sur-face resistivity Ω/sq
10^{-2} Pa vacuum, 295K	10^{17}	4×10^{17}
10^{-2} Pa vacuum, 400K	5×10^{15}	2×10^{16}
1×10^5 Pa dry air, 295K	10^{16}	2×10^{17}
2×10^4 Pa dry N_2O_4, 295K	5×10^{16}	2×10^{17}
4×10^4 Pa dry BF_3, 295K	5×10^{16}	2×10^{17}
5×10^4 Pa dry NH_3, 295K	5×10^{10}	2×10^{11}

Since ammonia had a dramatic effect on the substrate, the pressure dependence of this effect was studied. The results are shown in figure(4.8); a similar result has been noted by other workers (G.J. van Oirschot, D. van Leeuwen & J. Medema; 1972). A check on the photoconductivity was also made in each gas environment; however, none could be observed.

4.9 The H.V. system

The schematic of the H.V. line is shown in figure (4.9). With the exception of a few obvious components, the system was constructed from glass. A three stage mercury diffusion pump was used to attain the very high vacuum. To prevent any loss in pumping speed and consequently in the ultimate vacuum, all glassware above the pump was kept free from bends (each 90° bend lowers the pumping speed by a factor of ~ 2). Directly above the pump a high conductivity liquid nitrogen cold trap was used to prevent mercury reaching the cell. The main design criteria for this trap were to keep the effective bore as wide as that of the pump, and to get very good trapping with a minimal loss in pumping efficiency. The resulting design is shown in figure (4.10) and is commonly known as a 'gold fish bowl' trap .

To back the diffusion pump a complete Edwards 2" oil diffusion pumping system was used. This unit was kindly lent to us by the Safety in Mines Research Establishment (Sheffield). Between the backing and diffusion pumps a large liquid nitrogen cold trap was placed together with a Pirani gauge. The latter was used to check that the backing pressure was sufficiently low (1 Pa) to allow the mercury diffusion pump to be switched on. To prevent vibration

FIG: (4.8) EFFECT OF AMMONIA ON SAPPHIRE

PIRANI GAUGE

CELL

BALL & SOCKET
JOINT

H.V. VALVE

BALL & SOCKET
JOINT

H.V. TAPS

½

2 STAGE OIL
DIFFUSION PUMP

PIRANI GAUGE

COLD TRAP

'GOLD FISH
BOWL' COLD
TRAP

BALL & SOCKET
JOINT

AIR VENT

ROTARY PUMP

EDWARDS 2" OIL
DIFFUSION PUMP UNIT

3 STAGE MERCURY
DIFFUSION PUMP

FIG: (4.9) H.V. LINE

BALL & SOCKET JOINT

DEWAR TUBES

INSULATION FOAM

CELL

LIQUID
NITROGEN
LEVEL
SENSOR

FUNNEL

DEWAR VENT

LIQUID
NITROGEN

'GOLD FISH BOWL'
COLD TRAP

BALL & SOCKET
JOINT
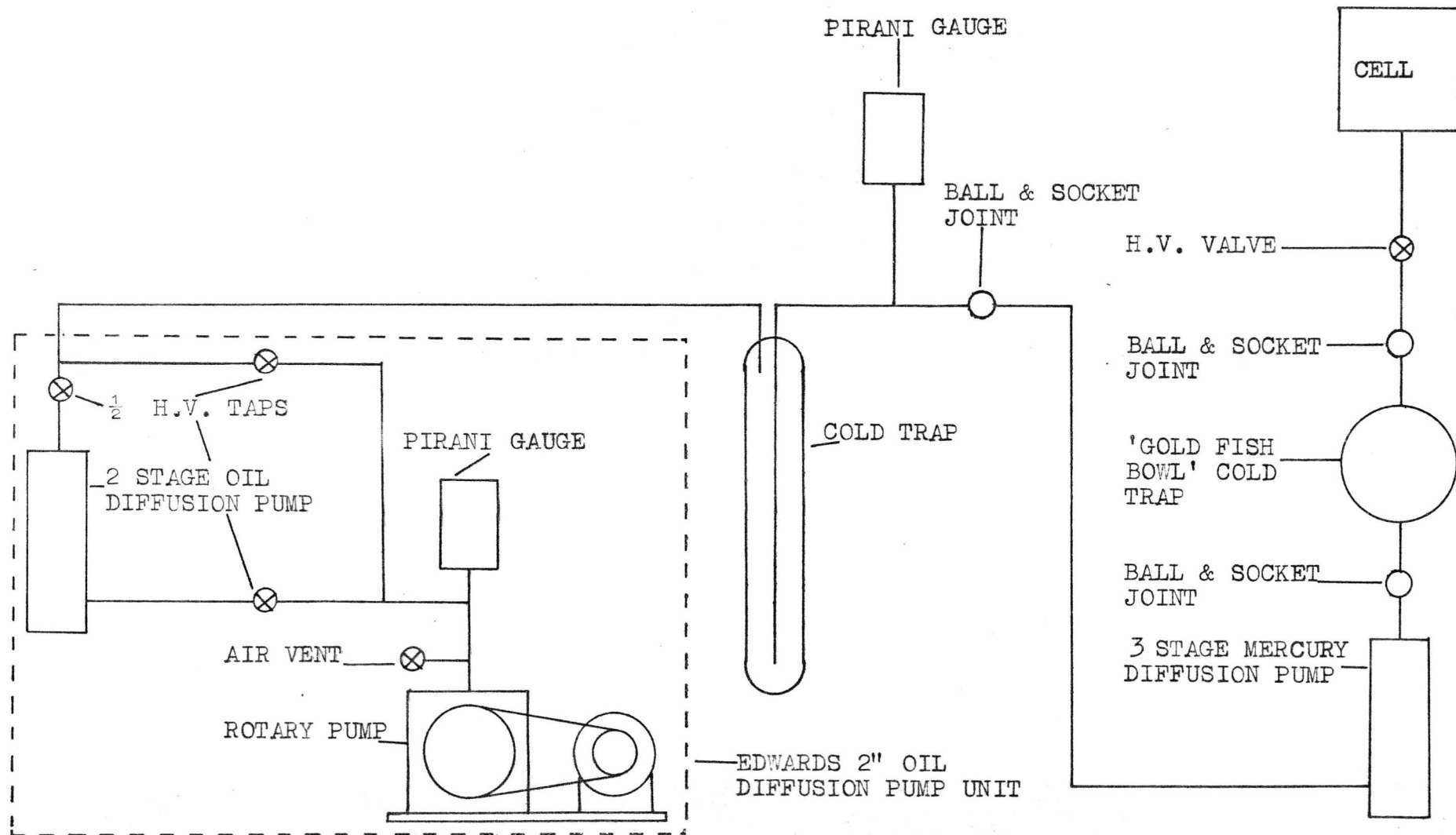
SOLENOID
OPERATED
VALVE
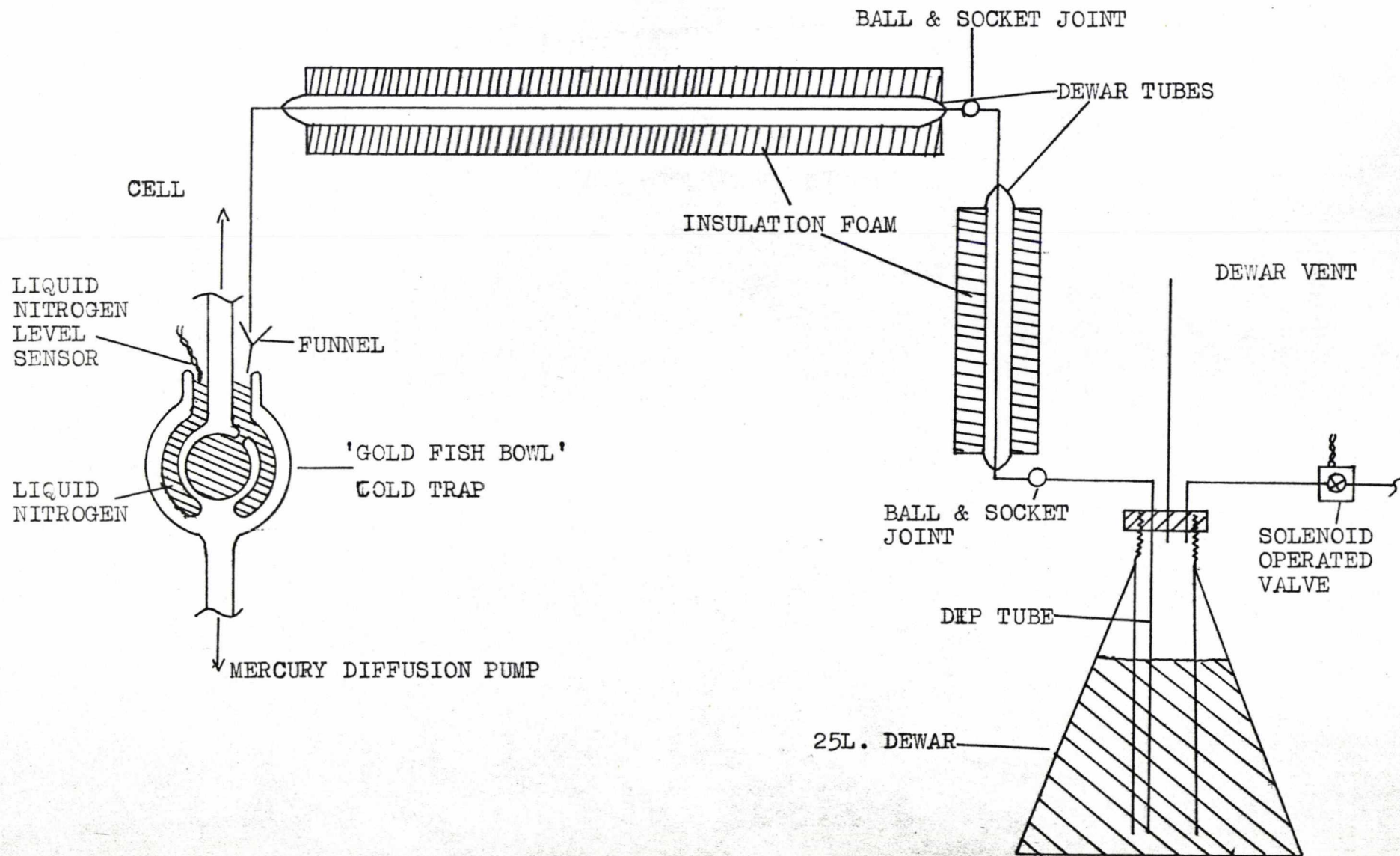
DIP TUBE

MERCURY DIFFUSION PUMP

25L. DEWAR

70

FIG: (4.10) AUTOMATIC LIQUID NITROGEN FILLER

from the backing pump reaching the H.V. line, and consequently the cell, a thick rubber vacuum hose was used. Large bore greased ball and socket joints were used to connect the diffusion pump and 'gold fish bowl' trap into the line. This was to allow for easy removal and cleaning. Finally, the connection between the glass vacuum line and stainless steel system was accomplished with a 2" graded glass to metal seal.

It was found that the 'gold fish bowl' trap needed filling with liquid nitrogen every few hours. Since the vacuum system was used continuously for long periods an automatic liquid nitrogen filler was designed and constructed. The complete system is shown in figure (4.10). Operation of the system was as follows: the level sensing device switched on the solenoid operated valve when the liquid nitrogen level became too low. When the solenoid was on, compressed air was fed into the large (0.025 m^3) dewar; this then forced out liquid nitrogen through the dip and dewar tubes and into the trap. As soon as the trap was full the solenoid was switched off. A vent in the dewar allowed for the liquid nitrogen to boil off without excess pressure being built up. While the filling system cooled down to liquid nitrogen temperature, cold nitrogen gas was blown through the dewar tubes. To prevent this from blowing liquid nitrogen out of the trap, a funnel with a small polystyrene ball was placed between trap and tube.

The electronic circuit used to sense the liquid nitrogen level and control the solenoid is shown in figure (4.11). Two diodes (D2 and D3) were used as the sensing element. They were reverse biased so that their resistances were very

FIG: (4.11) LIQUID NITROGEN LEVEL SENSOR
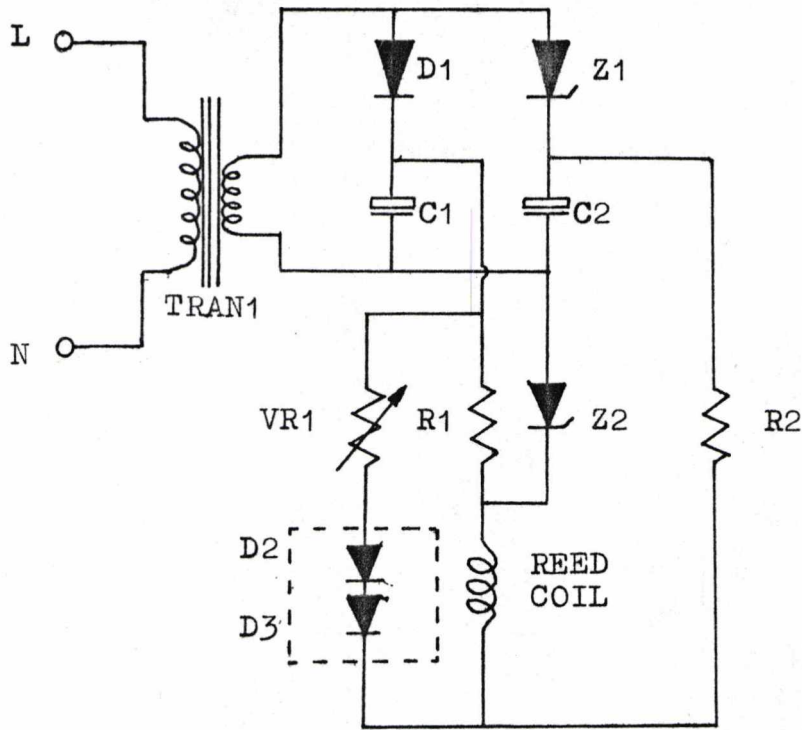
SENSOR ELECTRONICS
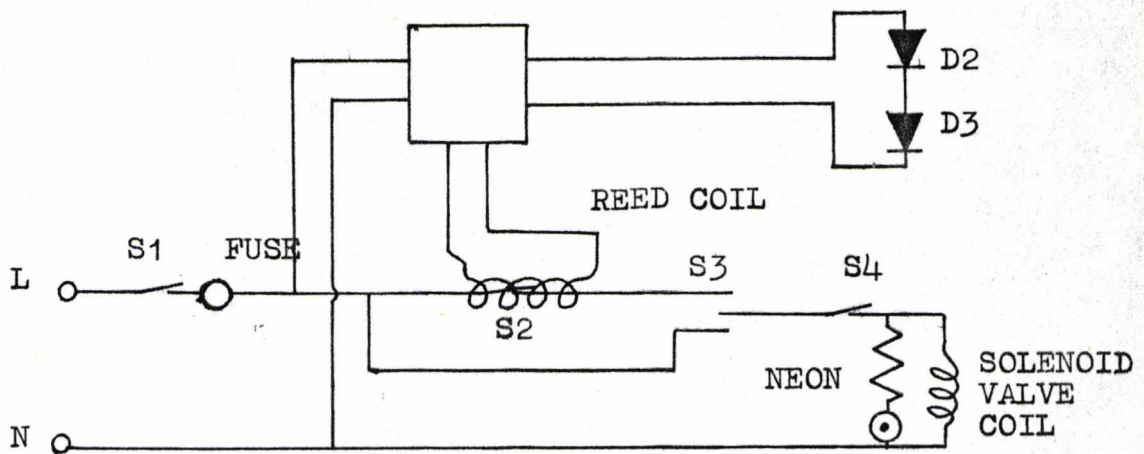
SENSOR WIRING DIAGRAM

high and hence the power dissipation would be negligible.
$(P = V^2/R)$. Since these devices were semiconductors they
had a positive temperature coefficient. At liquid nitrogen
temperatures the combined resistance of D2, D3 and VR1 was
very high, hence the potential at point A was only deter-
mined by TRAN1 and D1. However, when the temperature increased
the sensor's resistance decreased and consequently the
potential at point A increased. As soon as this potential
was greater than the Zener potential of Z2, conduction through
Z2 would be possible. This then allowed the current to
flow through the reed relay which in turn switched on the
solenoid. The whole process was reversed on cooling the
sensor. Variable resistance VR1 effectively altered the
temperature at which the Zener potential of Z2 was exceeded.

The wiring diagram of the whole automatic liquid nitro-
gen filler is shown in figure (4.11). Mains was supplied
to the electronics and solenoid via switch S1; S2 could be
overridden by S3; this then determined whether the system
was under manual or automatic control. For manual operation
switches S3 and S4 were used. The automatic liquid nitrogen
filler used about 0.025 m^3 of liquid nitrogen in 36 hours.

4.10 The roughing line and gas dosing system

To prevent the H.V. line from being contaminated the
cell was always roughed to a vacuum of 1 Pa before opening
the main high vacuum valve. This preliminary evacuation was
carried out by the roughing line shown in figure (4.12).
Apart from evacuating the cell the roughing line was also
used to evacuate the gas dosing system. The liquid nitrogen
cold trap could be isolated and demounted, so that when
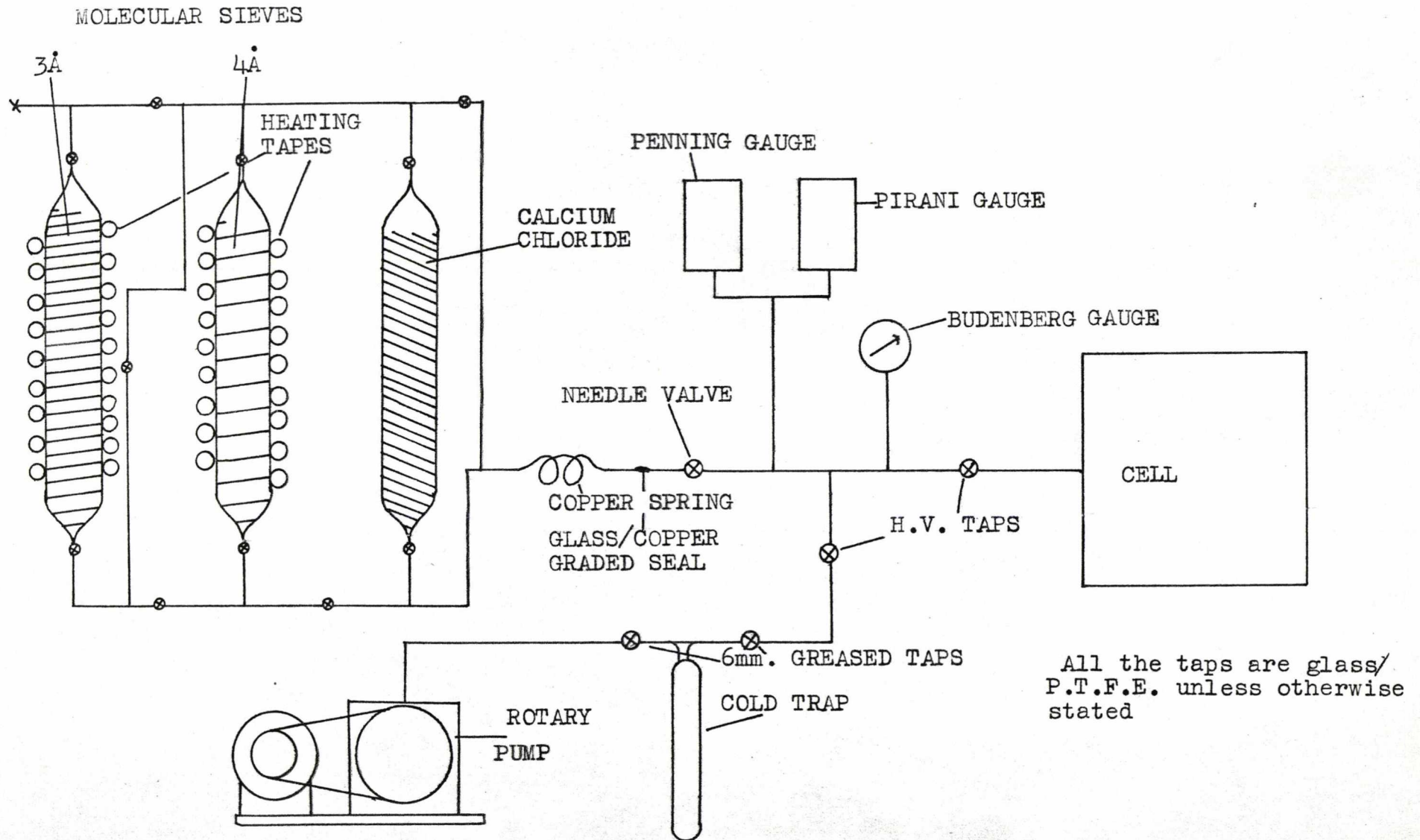toxic gases had been pumped from the cell or gas dosing

FIG: (4.12) ROUGHING LINE AND GAS DOSING SYSTEM

system, the trap could be easily removed to a fume cupboard.

When gases were admitted to the cell they were always thoroughly dried first, either through a molecular sieve or through a calcium chloride column. Before the molecular sieves could be used they had to be heated up to about 400K and pumped for 12 hours, to remove all the adsorbed water vapour and other gases. The gas under study was dried simply by passing it slowly through a drying column; a needle valve then admitted the gas slowly into the cell, the pressure being monitored by one of the pressure indicators. Using this system the cell could be filled with dried gases at accurately known pressures from 1 Pa up to atmospheric pressure.

The gas drying system was constructed in glass. So that the system could be easily demounted for cleaning, ordinary ground glass joints were placed at the top and bottom of each column. Since some of the gases under study are relatively toxic, all the joints were 'black waxed' together. This ensured a very good leak free seal even when the gas pressure was slightly greater than atmospheric. In the interest of safety the whole system was periodically checked for any leaks.

4.11 Pressure measurement

An ionization gauge (Vacuum Generators type VIG 20) was used to monitor the pressure inside the cell for the range of 10^{-4} Pa up to 10^{-1} Pa. The indicated pressure was corrected, using the correction table provided with the gauge, when gases other than nitrogen or air were present inside the cell. The pressure range, 10^{-1} Pa up to 10 Pa, was covered with a Pirani gauge. This instrument was

standardised against a MacLeod vacuum gauge and when gases other than nitrogen or air were present in the cell, a correction was made for the different thermal conductivity of the gas. Finally a Budenberg gauge was used to monitor the pressure from 10^3 Pa up to 10^5 Pa.

4.12 Experimental procedure

Before any crystals were mounted onto the substrate they were optically checked to make sure that they were free from any major defects. Suitable crystals were then washed in a solvent and thoroughly dried. The electrode mounting technique was to attach a very thin copper spring (made from $2 \cdot 5 \times 10^{-2}$mm copper wire) to one end of the crystal, with Acheson DAG 915 high conductivity silver paste. This paste consists of colloidal silver in a mixture of isobutyl methyl ketone and methyl acetate. Once the spring had been firmly attached, the other end of the crystal had a silver electrode painted onto it. After the electrodes had been drying for about ten minutes the crystal and spring were attached to the substrate with more silver paste. When a crystal had been successfully mounted its dimensions were measured using a travelling microscope; the substrate was then mounted onto the block. Detail of a mounted crystal can be seen in figures (4.13) and (4.14).

This type of electrode configuration is commonly referred to as a two electrode system. In some cases a third(earthed)electrode(guard ring) was painted around the centre of the crystal, to eliminate all the surface currents. Due to the sizes of the crystals any other electrode arrangement was impracticable.

FIG: (4·13)
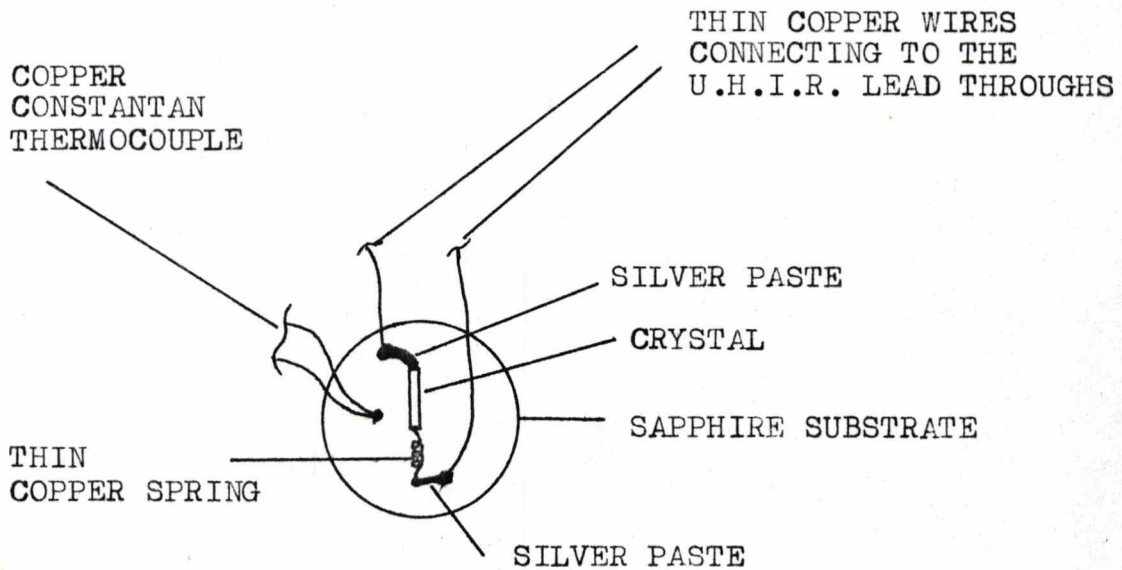
When initial electrical checks had been carried out to verify that Ohmic, non-photovoltaic contacts had been made to the crystal, the flange was bolted into position in the cell. Initial evacuation and heating were then carried out. Each time before a crystal was mounted all the insulators were cleaned with dry alcohol to ensure that the very high insulation resistance would be maintained.

The whole apparatus was kept very compact in order to reduce electrical pick up. It can be seen from figure(4.15) that the apparatus was supported on a 'dexion' frame. The various instruments were ergonomically placed to minimize operator movement and consequent pick up.

Standard measurements were carried out as follows.

Ohmic plot

The dependence of current on the applied voltage was

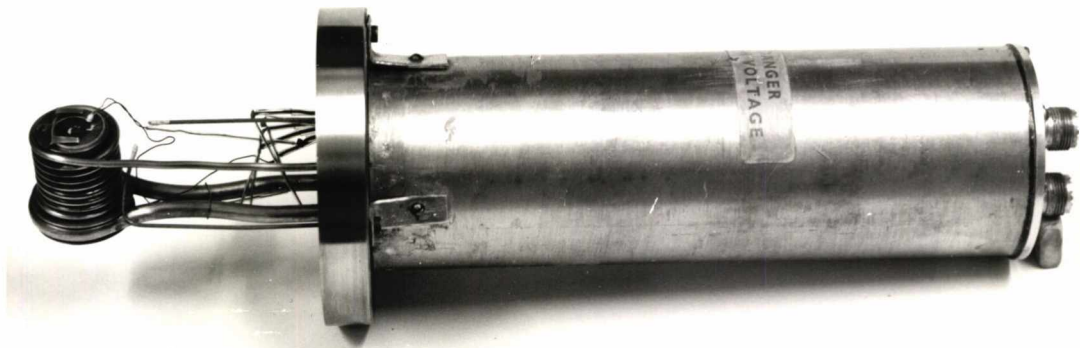FIG: (4·7)   DETAIL OF THE TOP 4½" FLANGE

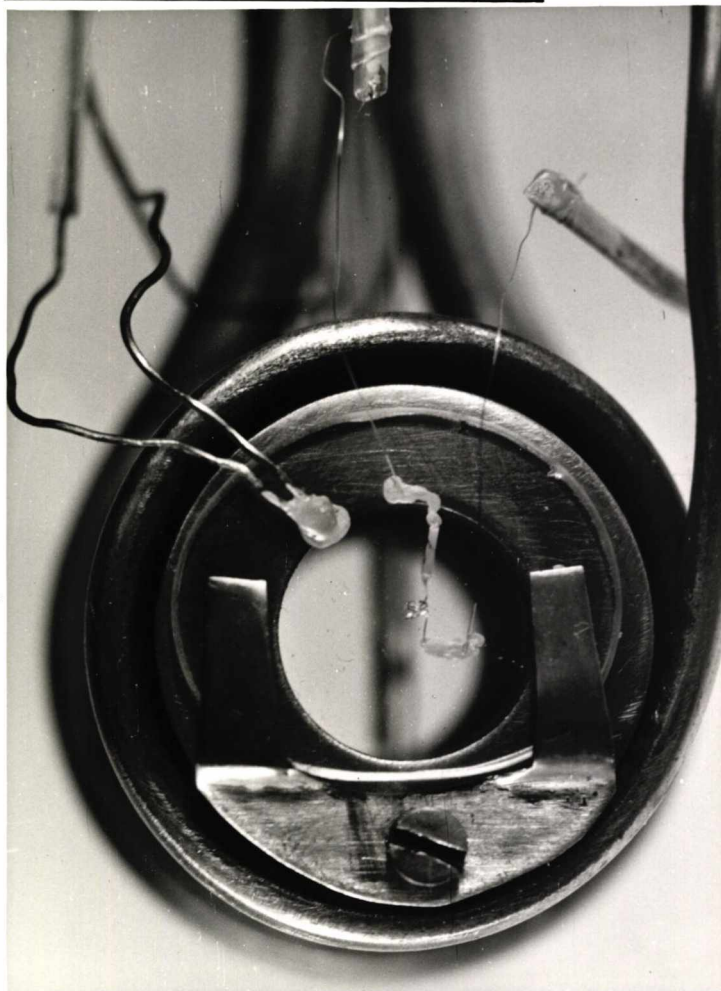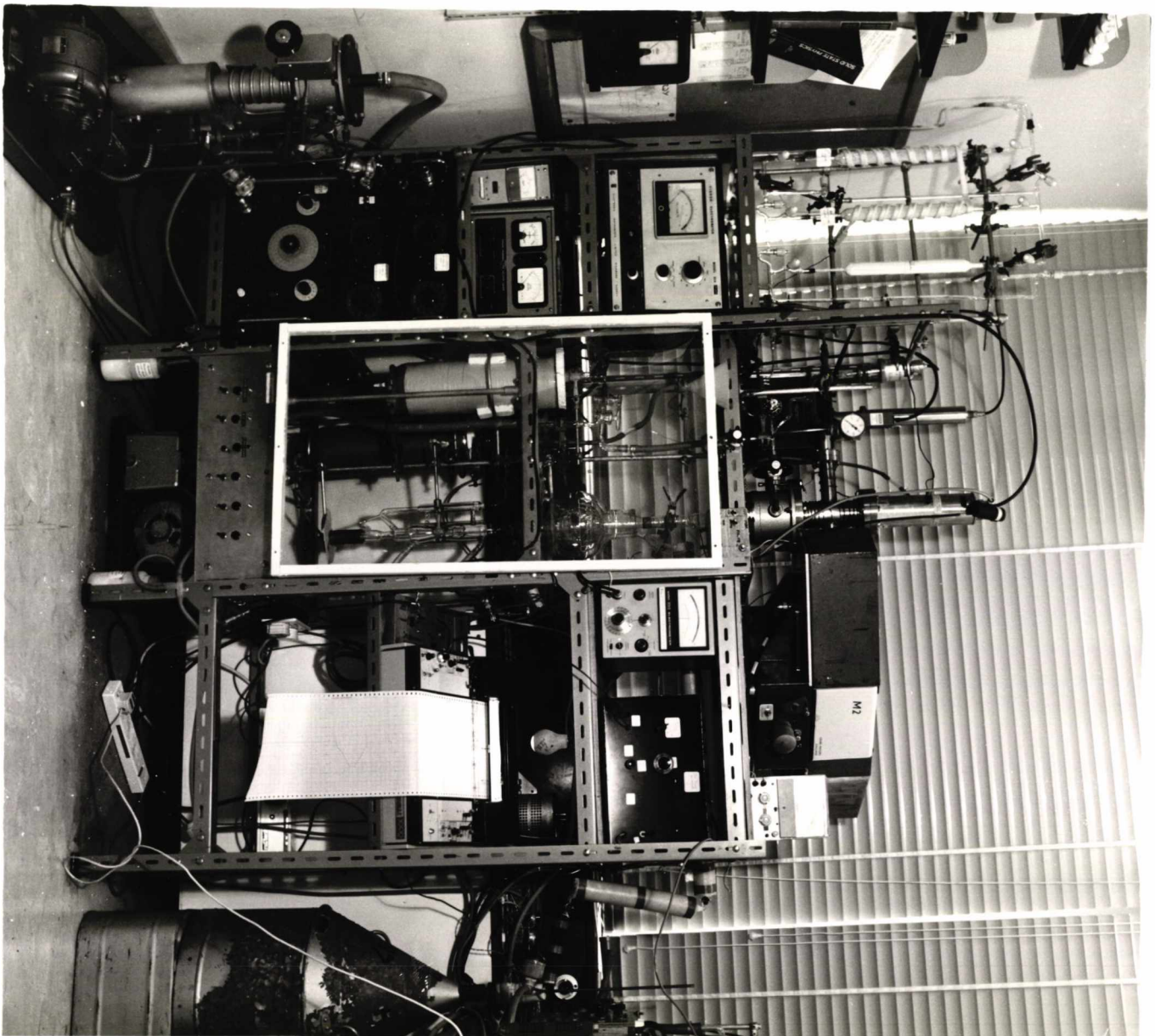FIG: (4·14)   DETAIL OF A MOUNTED CRYSTAL

FIG: (4.15) GENERAL VIEW

noted at fixed intervals and these values were plotted on log-log graph paper. To overcome any hysterisis, due to the current not achieving complete equilibrium, the current was measured for both increasing and decreasing voltage; the current was also monitored on the chart recorder.

Activation energy

The current (at a fixed field gradient) was measured for different equilibrium temperatures. Then, by plotting the data as log(resistivity) versus reciprocal (temperature [K]) the activation energy of the sample could be determined (cf. Chapter 2·6). Calculation of resistivity was carried out using the following formula:

Bulk resistivity:

$$\rho = \frac{RA}{L} = \frac{VA}{IL} \qquad \text{where}$$

A = cross-sectional area for conduction

L = length of crystal

V = applied voltage

I = measured current

Surface resistivity:

$$\rho' = \frac{R\ 2(w+t)}{L} = \frac{V\ 2(w+t)}{IL} \qquad \text{where}$$

w = width of crystal

t = thickness of crystal

To avoid any errors due to measurement of non-equilibrium current the values were noted for both increasing and decreasing temperature. Also, temperature and current were continuously monitored on the chart recorder.

Photo spectra

To enable meaningful comparisons to be made between different crystals the light intensity (about 10^{18}-10^{19} photons m^{-2} s^{-1}) and monochromator slit width were kept constant. The photocurrent (Iph) was measured by noting the difference of the dark current (Id) and the dark + photocurrent (It), i.e.,

$$Iph = It - Id.$$

Both It and Id had to be measured very accurately (to at least 3 significant figures) and this was accomplished by 'backing off' (using the chart recorder's offset control) most of the dark current and using a more sensitive range on the chart recorder. Using the chart recorder it was also possible to make sure that only equilibrium measurements were made. The wavelength intervals were chosen to give reasonably equal energy type (cm^{-1}) intervals.

4·13 Sublimation furnaces

Two nitrogen entrainer sublimation furnaces were designed and built. The resulting system is shown in figure (4·16).
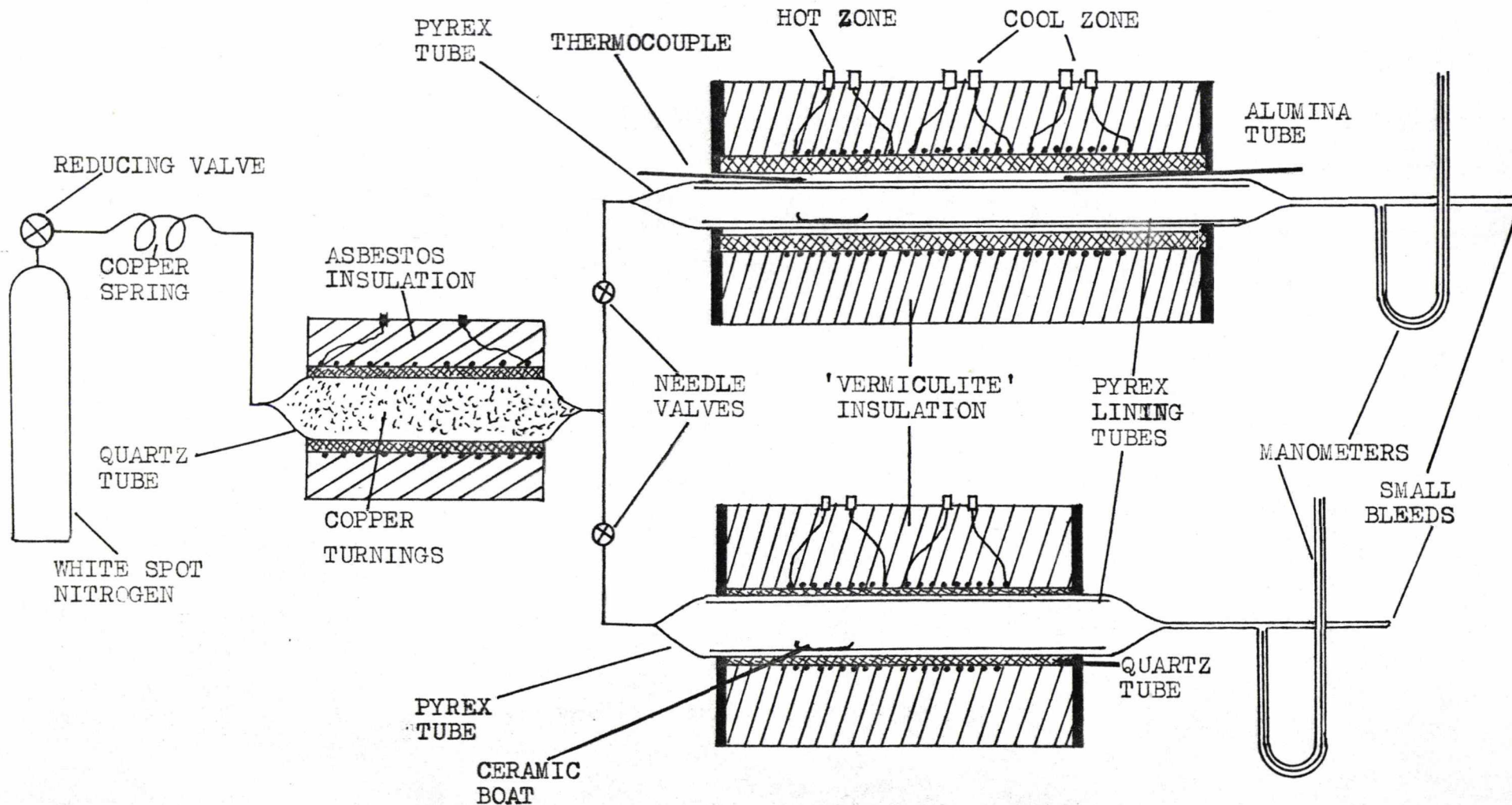
FIG: (4.16)   ENTRAINER SUBLIMATION FURNACES

An entrainer technique operating at atmospheric pressure was employed because of the ease of construction and operation. Also, when used correctly, this technique yields good single crystals of high purity (P. E. Fielding, 1973). The basic principle of this technique is to pass pure nitrogen over the sample being sublimed, at a very slow flow rate (typically a few 100mm^3 per minute). The nitrogen flow preferentially sweeps the subliming compound down the tube to condense out in a cool zone. To prevent any photo initiated reactions taking place, sublimation was carried out in the dark.

The first furnace to be constructed consisted of a quartz tube onto which two heaters were wound. This was then placed inside a steel box filled with 'Vermiculite' to act as thermal insulator. The ends of the box were made out of Syndanyo and were used to support the quartz tube. A close fitting pyrex tube was placed inside the quartz tube and connected up to the nitrogen supply at one end and a manometer and 'bleed' at the other end. Power was supplied to the heaters from the mains via Variacs. The temperatures of the two zones were monitored by using a Comark micro-voltmeter with chromel-alumel thermocouples placed in between the pyrex and quartz tubes. To carry out sublimation the compound was placed in a ceramic boat, which in turn was placed in a pyrex tube. This lining tube fitted very closely inside the main pyrex tube. Great care was taken in cleaning the crucible and lining tube before use; also, before any heating took place the system was flushed with nitrogen for 3 hours.
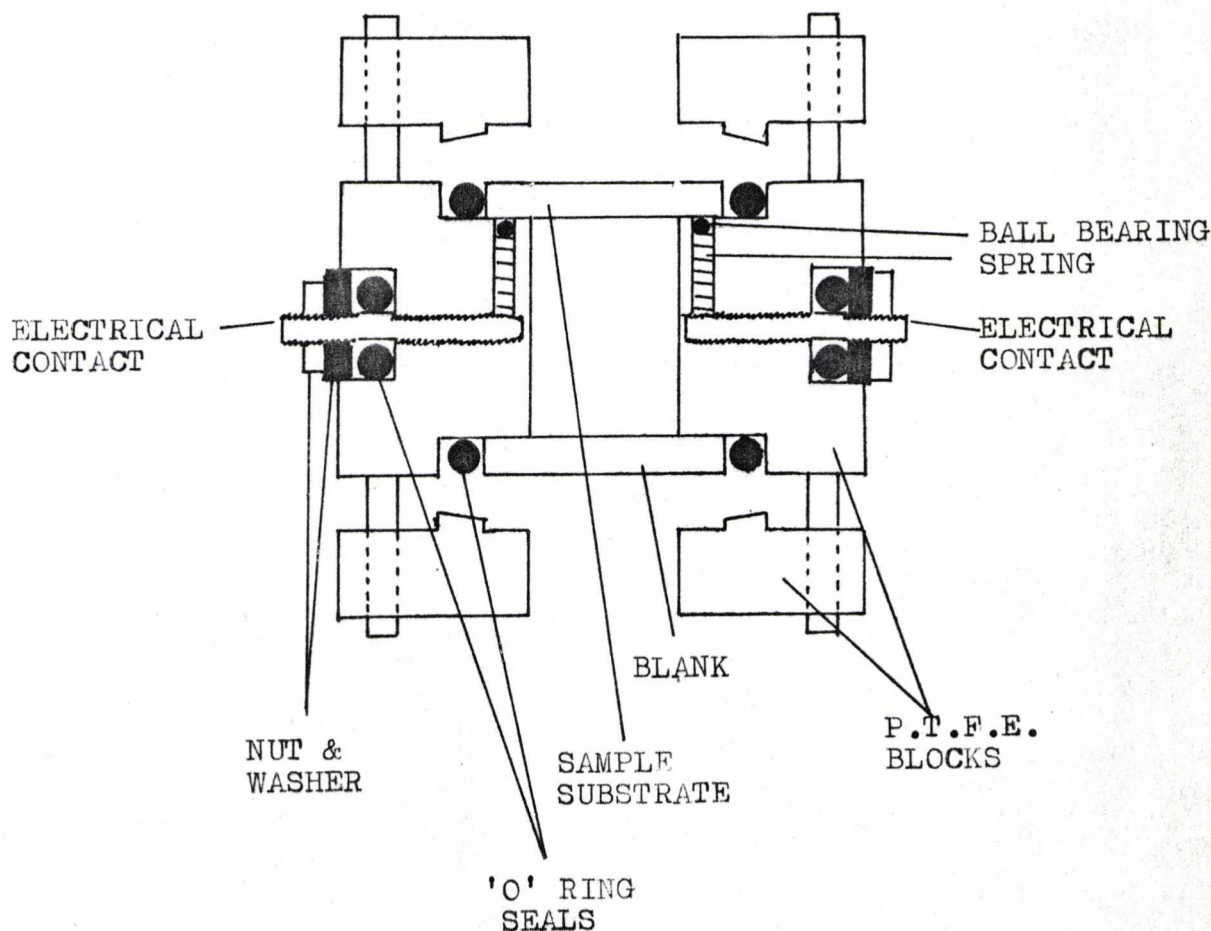
To prevent oxidation of the compound being sublimed,

the entrainer gas must be free of oxygen. It was found that 'B.O.C. white spot' nitrogen contained too much oxygen for this purpose; also, p.v.c. and rubber tubing were porous to oxygen. To overcome the former problem the nitrogen was passed through a hot furnace (950K) containing copper turnings. The latter problem was overcome by using copper tubing.

One of the main problems encountered with the first furnace was that the hot and cool zones were too short. This led to a difficulty in getting sufficient separation between the various sublimed components. The simple solution to this problem was to use a much longer furnace. Also to improve the thermal gradient a third heating zone was wound on. In this case rather than using a quartz tube an alumina tube was used. This material can withstand higher temperatures (1500K) and because of its much higher thermal mass it gave more uniform zones. As with the other furnace the heating tube was placed inside an earthed steel box.

The flow of nitrogen through the two furnaces was controlled by means of a needle valve and a 'pin hole' bleed. Pressures inside the entrainer tubes were monitored by two manometers. Rather than using mercury in the manometers, diethyl phthalate was used. This has a specific gravity of about 1/10 of mercury, and consequently gives rise to a more sensitive manometer; also, it has a very low vapour pressure (S.G. = 1·01 vapour pressure at 295K = 1Pa). Prior to using the 'pin hole' bleeds the flow rate was measured for different pressures. Hence when they were used in the entrainer sublimation furnaces the flow rate could be maintained at the required level by adjusting the pressure, read off the manometers.

FIG: (4·17)   <u>FILM CONDUCTIVITY CELL</u>

BALL BEARING
SPRING

ELECTRICAL
CONTACT

ELECTRICAL
CONTACT

BLANK

NUT &
WASHER

SAMPLE
SUBSTRATE

P.T.F.E.
BLOCKS

'O' RING
SEALS

4·14   Film conductivity cell

The basic design (due to Mr. B. Bott of the Safety in Mines Research Establishment) of the film conductivity cell is shown in figure (4·17). The method of film deposition and thickness measurement is discussed in Chapter (3·8). Resistivity measurements were carried out using a similar procedure as for single crystals.

CHAPTER 5

The Effect of Gases on the Semi- and Photoconduction of
Metal and Metal Free Phthalocyanine Single Crystals and
Lead Phthalocyanine Films

5·1 Introduction

The phthalocyanine single crystals studied in this
work were: manganese, cobalt, nickel, copper, zinc, lead
and metal free. All these compounds were purified by
nitrogen entrainer sublimation before any crystals were
grown (cf. Chapter 3·7). Needle-like crystals were always
obtained with typical dimensions of 5 X 0·5 X 0·01mm; hence
all the electrical measurements were carried out along the
needle axis for ease of electrode mounting. It has been
shown (J.M. Robertson, 1935 and K. Ukei, 1973) that the
phthalocyanine molecules stack along (or nearly along)
the crystal axis.

After mounting a crystal using the 'spring electrode'
technique (cf. Chapter 4·12), preliminary measurements were
carried out to test that a 'good' (Ohmic and non-photo-
voltaic) electrical contact had been made, as described in
Chapter 4·11. If these requirements were not met then the
crystal was abandoned.

Before any gas effects were studied it was important
to establish that the materials were being purified to a
reproducible level. Lead and copper phthalocyanines were
chosen for this study and crystals were grown from 1,2 and 3
fold entrainer sublimed material. The vacuum dark resis-
tivity and activation energy(in the range 290K-470K) were
measured. A field gradient of $3X10^4Vm^{-1}$ was used for these

and all the other phthalocyanine measurements. The results are presented in table (5·1) and figures (5·1) and (5·2).

TABLE (5·1)

phthalocyanine	number of sublimations	electrical characteristics	
		ρ (295K) Ωm	ΔE eV
Lead	1	$2 \cdot 5 \times 10^7$	0·58(3)
	2	$2 \cdot 0 \times 10^8$	0·61(0)
	3	$1 \cdot 2 \times 10^8$	
Copper	1	$4 \cdot 4 \times 10^9$	0·68(0)
	2	$5 \cdot 4 \times 10^{10}$	0·81(0)
	3	$5 \cdot 9 \times 10^{10}$	0·79(5)

It can be seen that there was a slight difference between the 1 and 2 fold sublimed samples and that there was no significant difference between the 2 and 3 fold sublimed samples. Hence the majority of crystals used in this work were prepared from 2 fold sublimed material.

Since the semiconduction and photoconduction of 'clean' metal and metal free phthalocyanines were to be studied, the conditions required to achieve a 'clean' (gas free) surface had to be determined. This was carried out by evacuating a lead phthalocyanine crystal at 520K for 12, 24 and 65 hours. After each period the room temperature resistivity and photospectrum were measured. It was found, in this work, that the photoconduction characteristics were very sensitive to adsorbed gases. Since the spectrum remained the same for different process times it was concluded

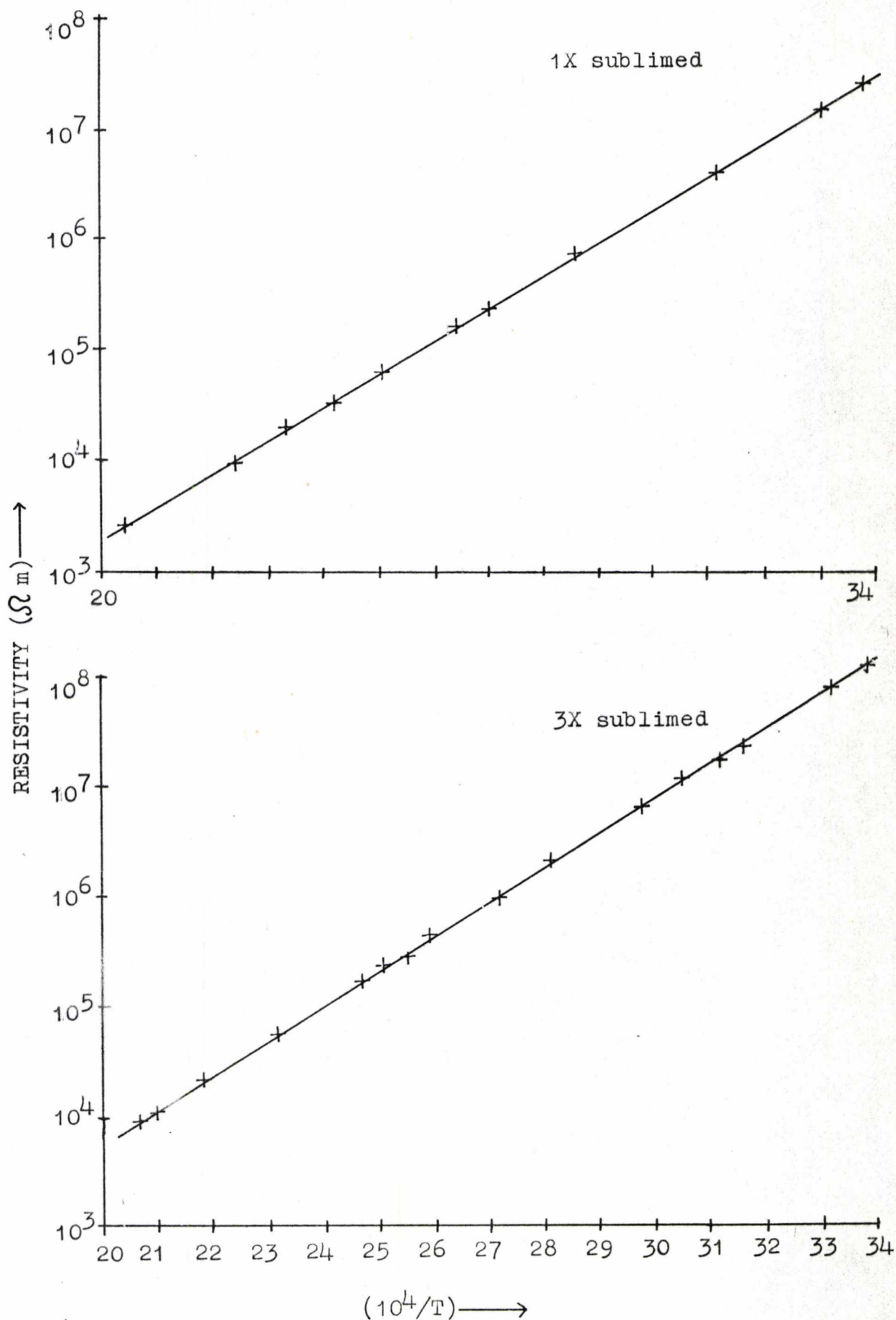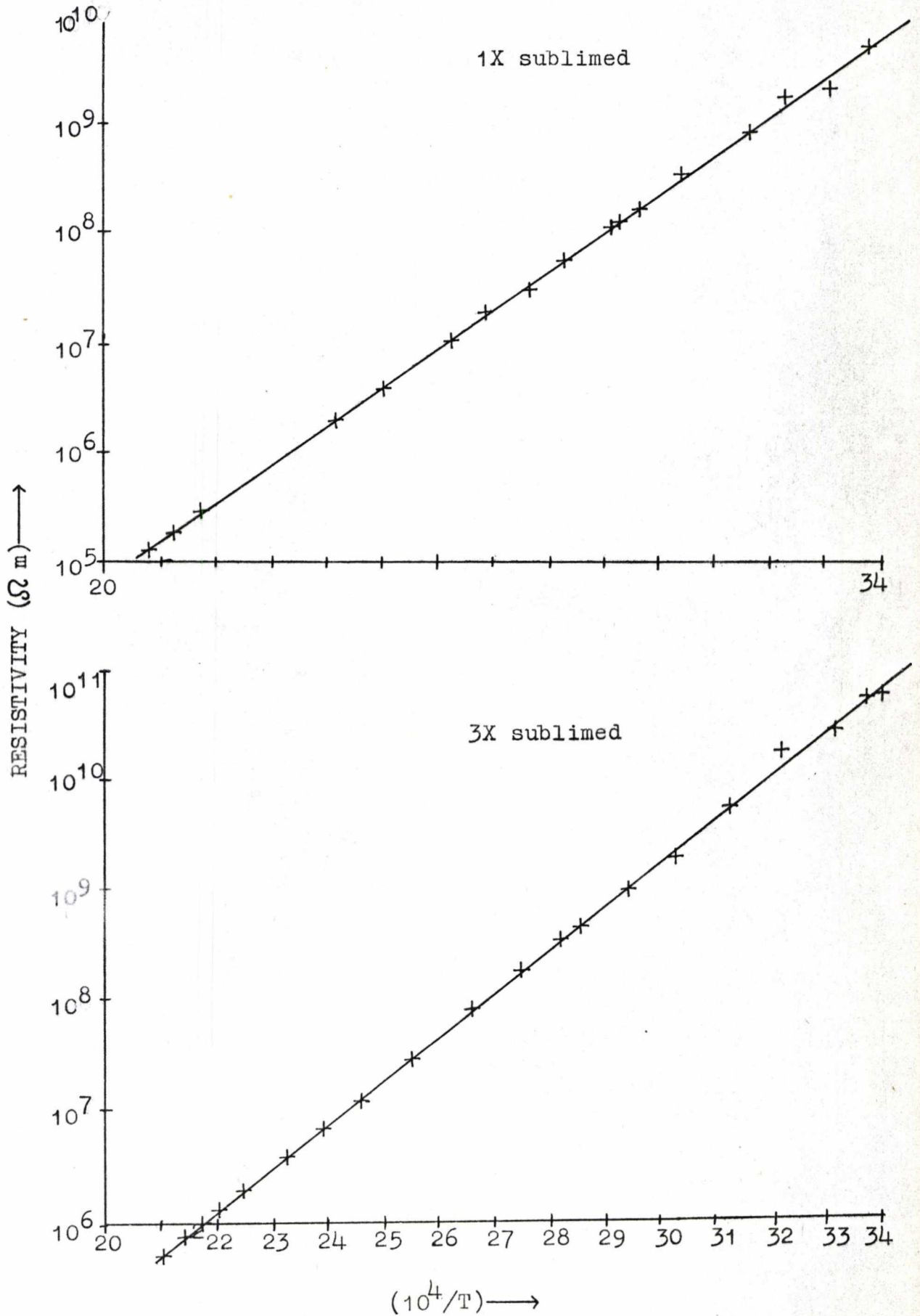FIG: (5·1) EFFECT OF REPEATED SUBLIMATION ON THE ACTIVATION ENERGY OF LEAD PHTHALOCYANINE

FIG: (5·2) <u>EFFECT OF REPEATED SUBLIMATION ON THE ACTIVATION</u>
<u>ENERGY OF COPPER PHTHALOCYANINE</u>

that a 12 hour evacuation period was sufficient to obtain a 'clean' surface (or at least any gases adsorbed were not influencing the photo- or semiconduction properties).

To conclude, all the crystals used in this study were prepared from at least 2 fold sublimed material. Also, before any measurements were carried out, the crystal was cleaned by evacuating it at 10^{-4}Pa and 520K for 12 hours.

5·2 Vacuum measurements - dark

After initial evacuation and heating the resistivities and their temperature dependences were measured in the range of 295K up to 470K (approximately). Then by using equation (2·6) (i.e. $\rho = \rho_o \exp[\Delta E/(kT)]$) the activation energies (ΔE) and pre-exponential factors(ρ_o) were determined. These results are shown in figures (5·3), (5·4), (5·5) and (5·6). The results are also tabulated in table (5·2) together with some literature values for single crystals. In the case of copper and metal free phthalocyanines the low temperature (less than 320K) resistivities were very high and as a consequence the dark currents were very low (about 10^{-15}A). This resulted in reasonably large measurement errors (10-20%) which are demonstrated in figures (5·4) and (5·6) by the scatter in the data points; however, this had little effect on the accuracy of the activation energy determination. The room temperature (295K) resistivities for these two phthalocyanines were measured from the activation energy plots. In all the other cases the dark current could be accurately measured (within 4%) with the result that the activation energy plots were very well defined. The activation energies were determined for at least two crystals,

90

TABLE 5.2

phthalo-cyanine	EXPERIMENTAL RESULTS			LITERATURE VALUES	
	resistivity Ωm (295 K)	activation energy eV	pre-exponential factor Ωm	resistivity Ωm (room temp.)	activation energy eV
Mn	3×10^3	0.37(0)	$1 \cdot 4 \times 10^{-3}$	1.4×10^4 ④ 4×10^4 ⑦	0.35 ④ 0.30 ⑥
Co	2.0×10^9	0.60(8)	$8 \cdot 2 \times 10^{-2}$	6.7×10^{10} ④ 9×10^7 ⑦	0.70 ④ 0.80 ⑤
Ni	7×10^{10}	0.74(3)	$1 \cdot 4 \times 10^{-2}$	1×10^8 ④ 6×10^8 ⑦ 4×10^{11} ②	0.80 ⑤ 0.65 ④ 0.82 ⑤
Cu	6×10^{10}	0.79(5)	$1 \cdot 6 \times 10^{-3}$	1.2×10^8 ④ 6.2×10^{11} ① 2×10^{11} ②	0.58 ④ 0.99 ① 0.82 ⑤
Zn	1×10^9	0.69(0)	$1 \cdot 6 \times 10^{-3}$	1.8×10^{11} ① 3×10^7 ⑦ 6.2×10^{12} ④	0.85 ① 0.90 ④
Pb	3×10^8	0.58(1)	$3 \cdot 5 \times 10^{-2}$	1.2×10^8 ⑧	0.80 ⑧
H_2	1×10^{12}	0.85(2)	$2 \cdot 8 \times 10^{-3}$	5.2×10^{10} ③ 3.1×10^{14} ① 5×10^9 ④	0.85 ⑤ 1.12 ① 0.80 ④

① Y. Aoyagi, K. Masuda, S. Namba, 1971

② P. Day, M.G. Price, 1969

③ G.H. Heilmeier, G. Warfield, 1963

④ K.J. Beales, D.D. Eley, D.J. Hazeldine, T.F. Palmer, 1973

⑤ P.E. Fielding, F. Gutmann, 1957

⑥ P.E. Fielding, H. Struve, 1964

⑦ P. Day, G. Scregg, R.J.P. Williams, 1963

⑧ H. Yasonaga, K. Kojima, H. Yohda, 1974

FIG: (5·4) <u>ACTIVATION ENERGY PLOTS (VACUUM) FOR COPPER</u>
<u>AND NICKEL PHTHALOCYANINES</u>

Copper

Nickel

RESISTIVITY $(\Omega m) \longrightarrow$

$(10^4/T) \longrightarrow$
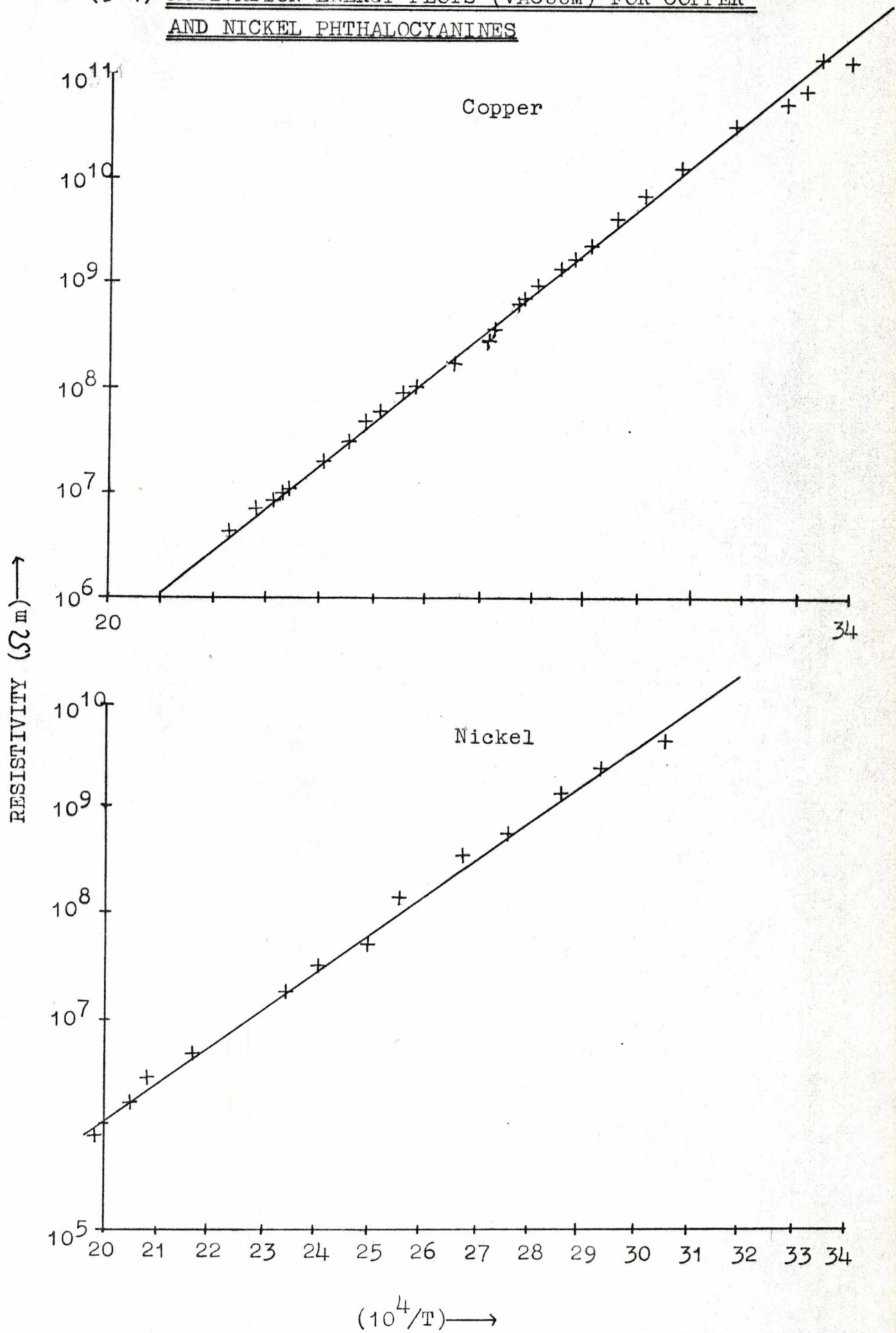
FIG: (5·5) ACTIVATION ENERGY PLOTS (VACUUM) FOR ZINC AND LEAD PHTHALOCYANINES

RESISTIVITY $(\Omega m) \longrightarrow$

$(10^4/T) \longrightarrow$

Zinc

Lead

94
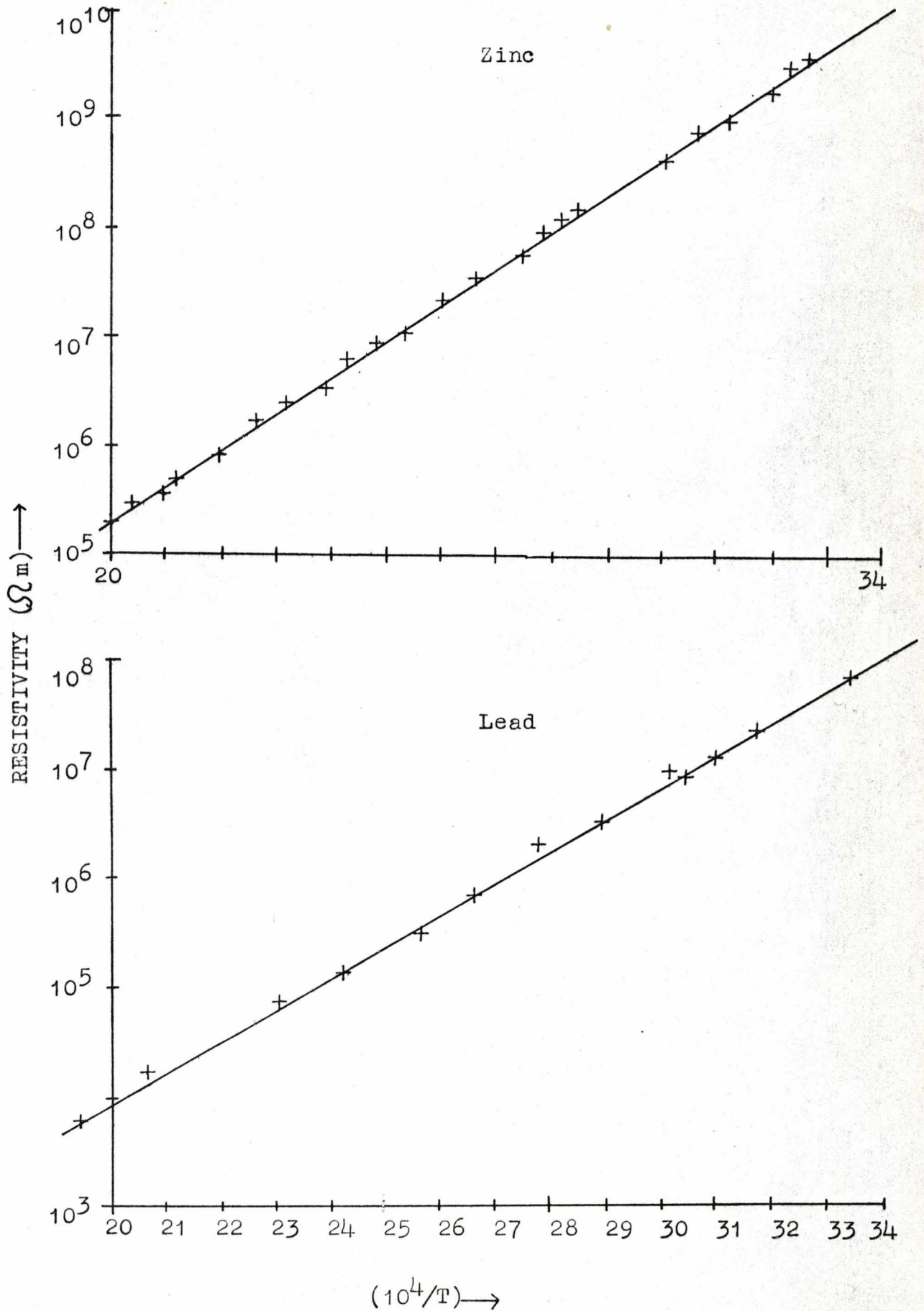
FIG: (5·6) <u>ACTIVATION ENERGY PLOT (VACUUM) FOR METAL FREE PHTHALOCYANINE</u>
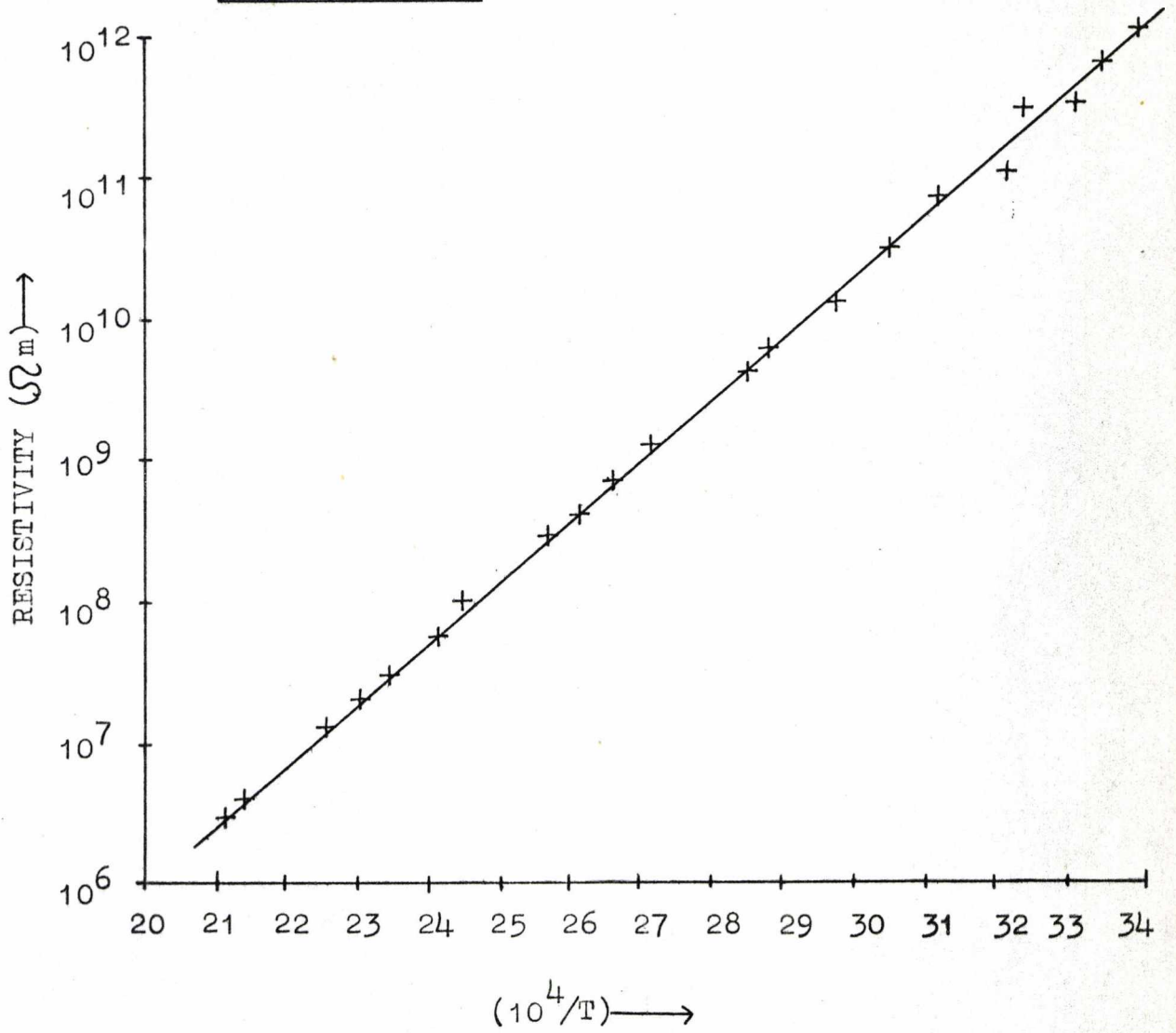
FIG: (5·7) OHMIC PLOTS FOR MANGANESE AND COBALT PHTHALOCYANINES

Manganese
Slope = 0·98
electrode separation
= 3·61mm

Cobalt
Slope = 1·02
electrode separation
= 3·54mm

96
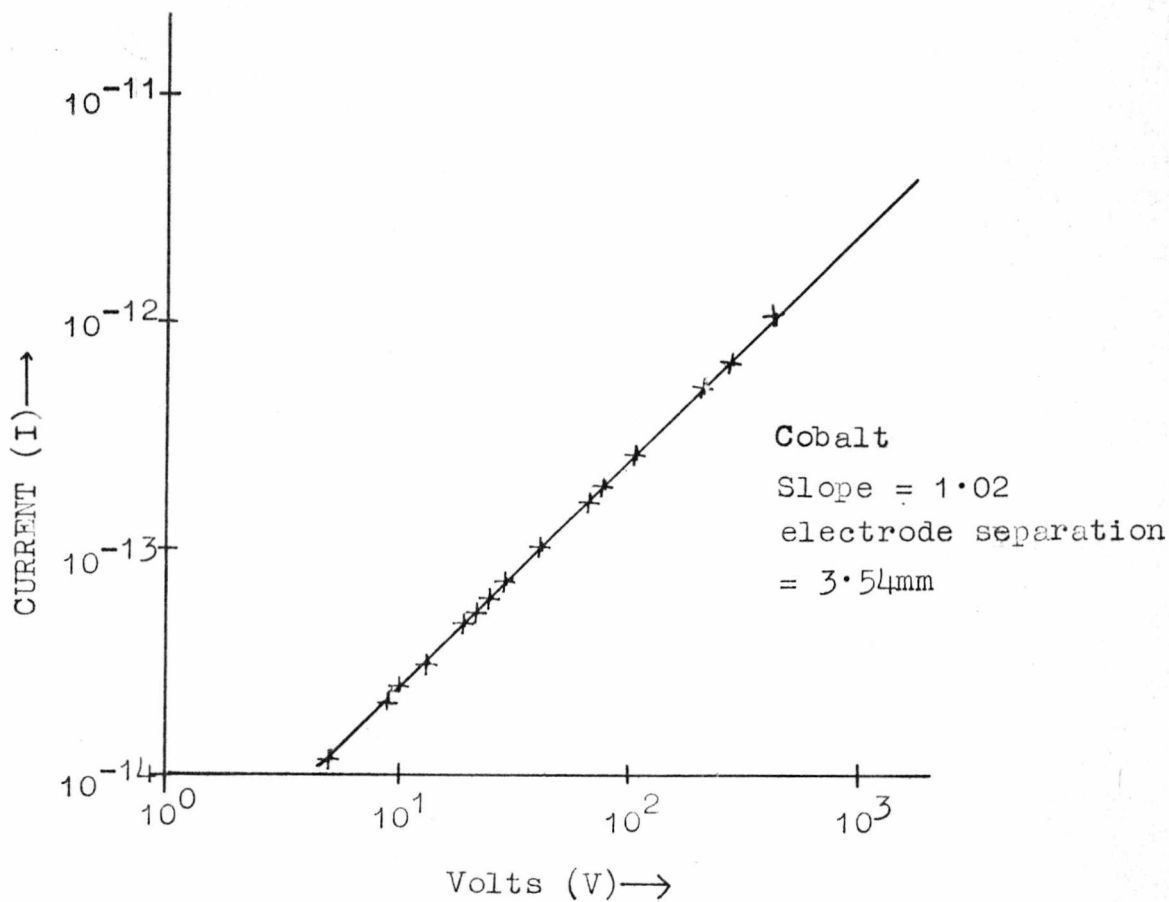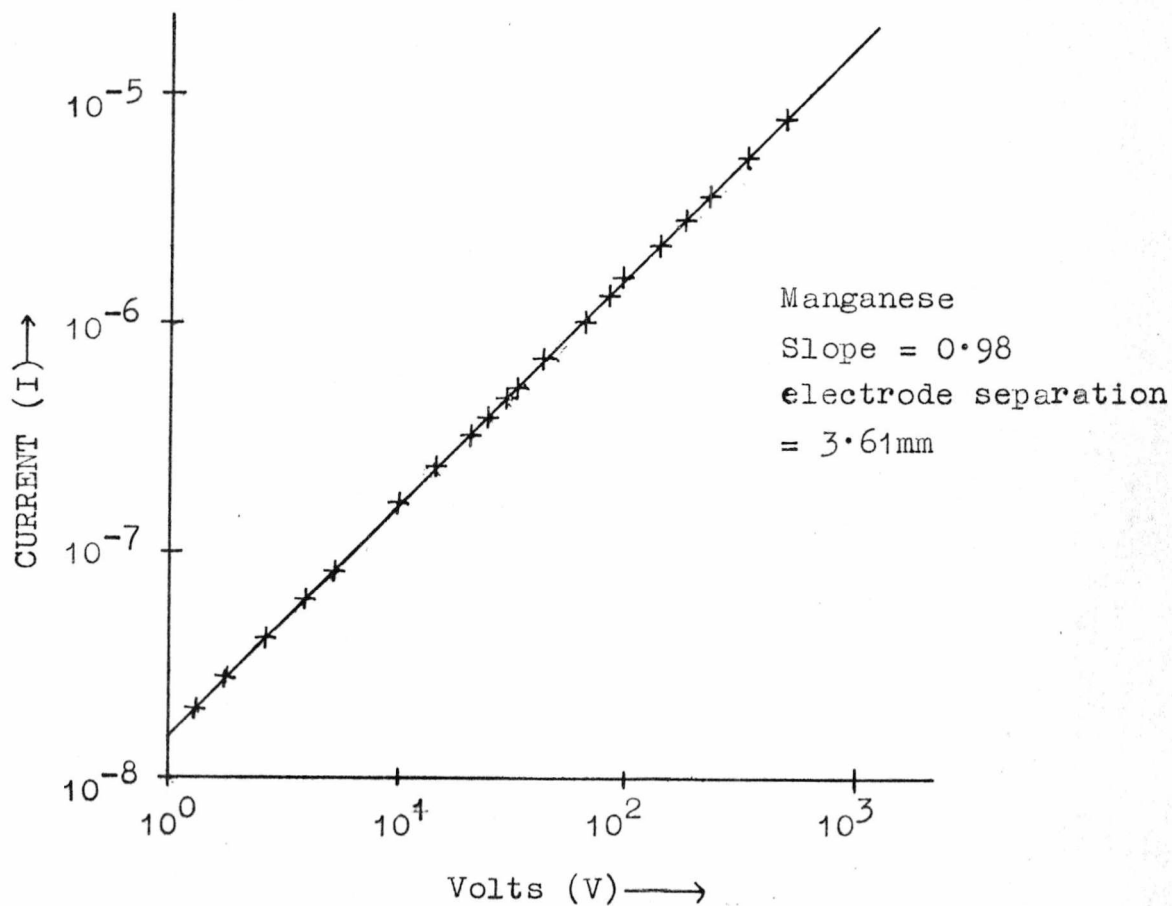
FIG: (5·8) <u>OHMIC PLOTS FOR NICKEL AND COPPER PHTHALOCYANINES</u>

Nickel
Slope = 1·05
electrode separation
= 2·97mm

Copper
Slope = 1·03
electrode separation
= 2·54mm
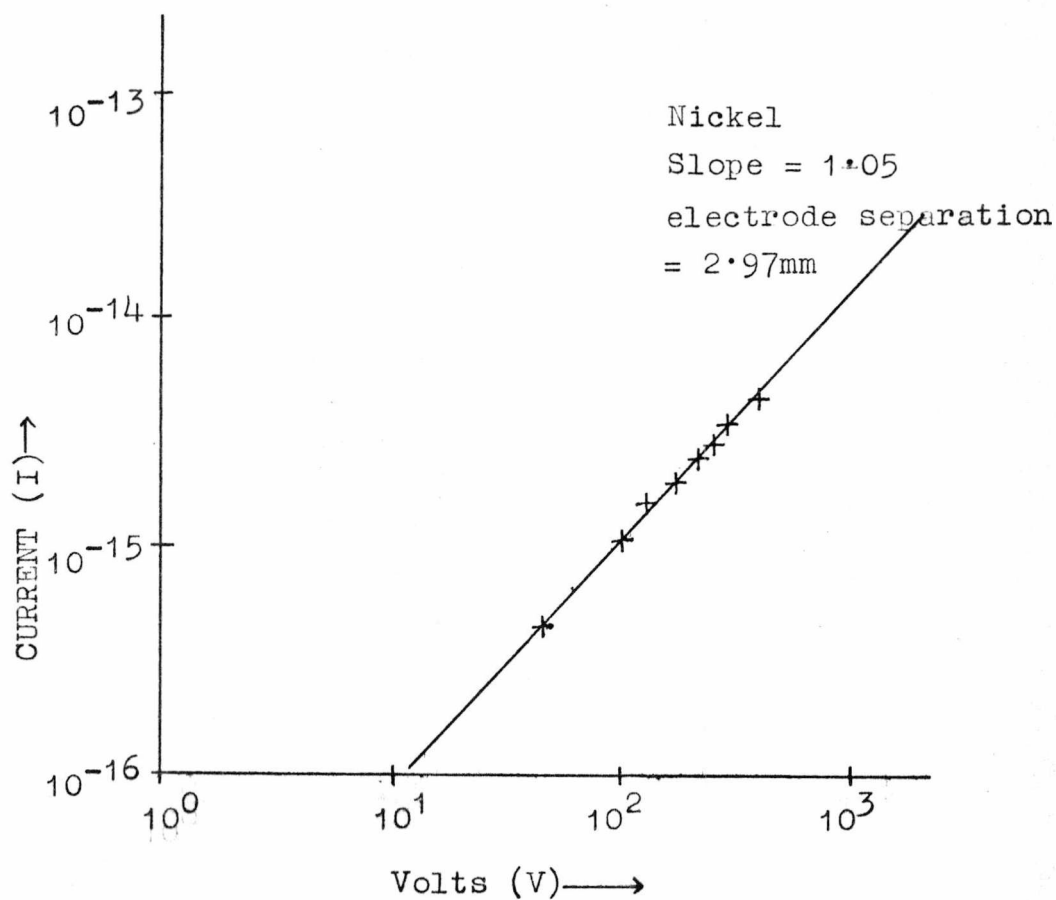
FIG: (5·9) OHMIC PLOTS FOR ZINC AND LEAD PHTHALOCYANINES

Zinc
Slope = 1·0
electrode separation
= 3·23mm

Lead
Slope = 0·98
electrode separation
= 2·83mm

Slope = 0·97
electrode separation
= 3·52mm
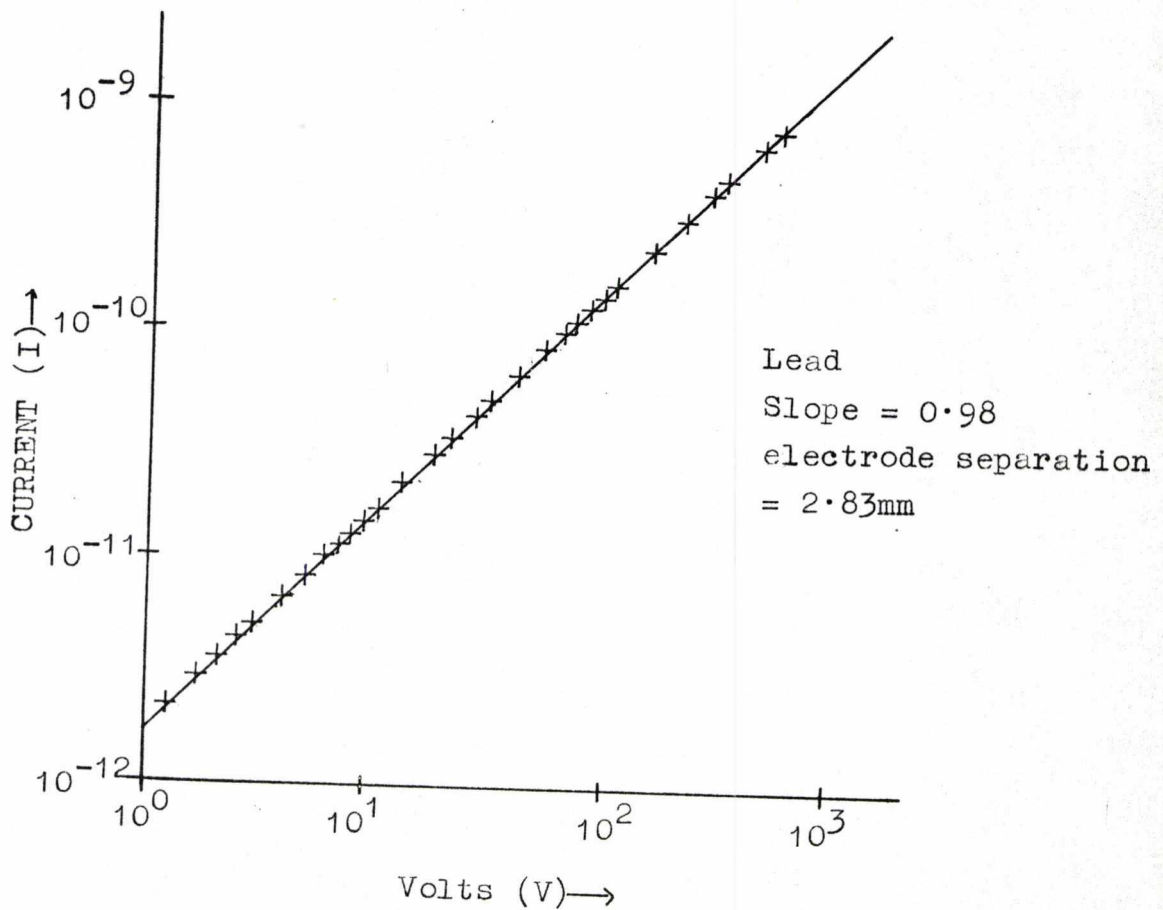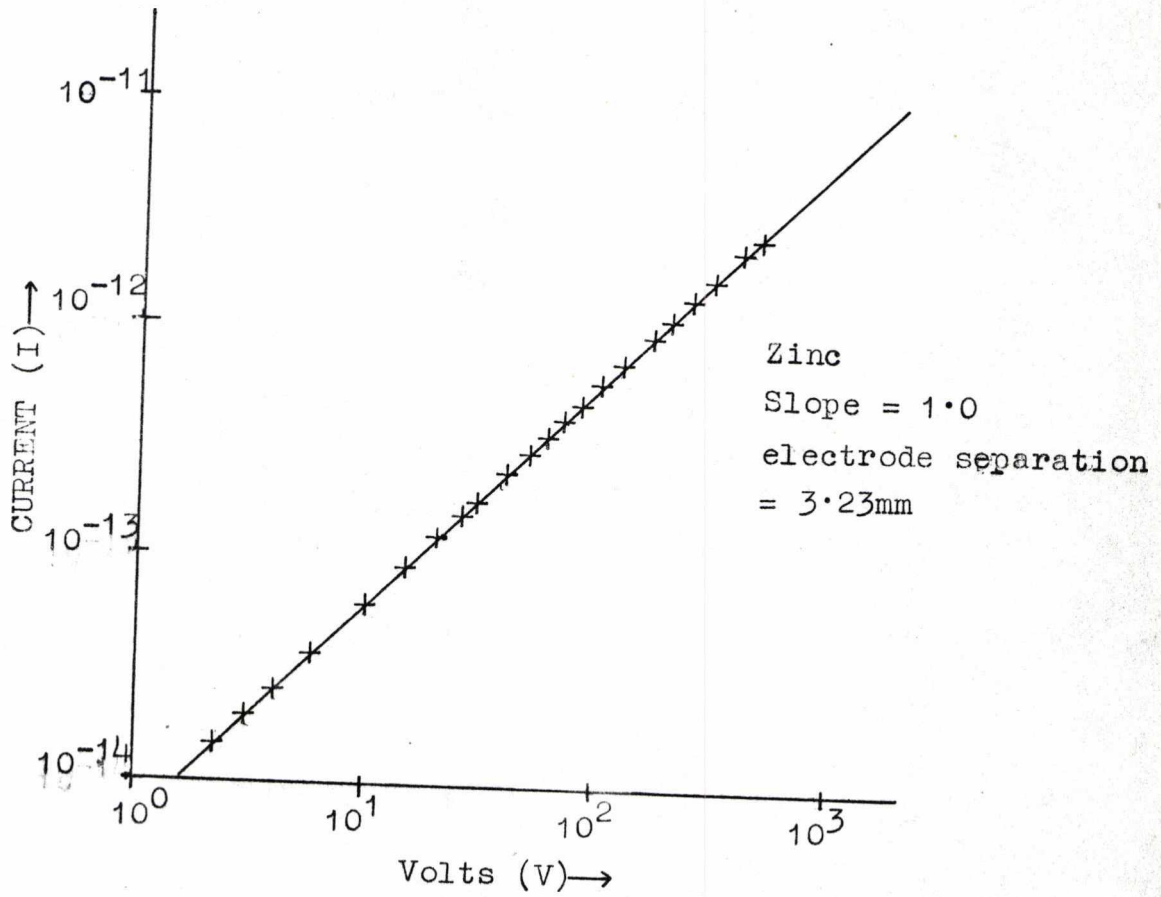
except for metal free phthalocyanine where only one crystal was studied, and the maximum error in the activation energy was found to be $\pm 0 \cdot 05$eV. The estimated error in the pre-exponential factors was about 100% (maximum).

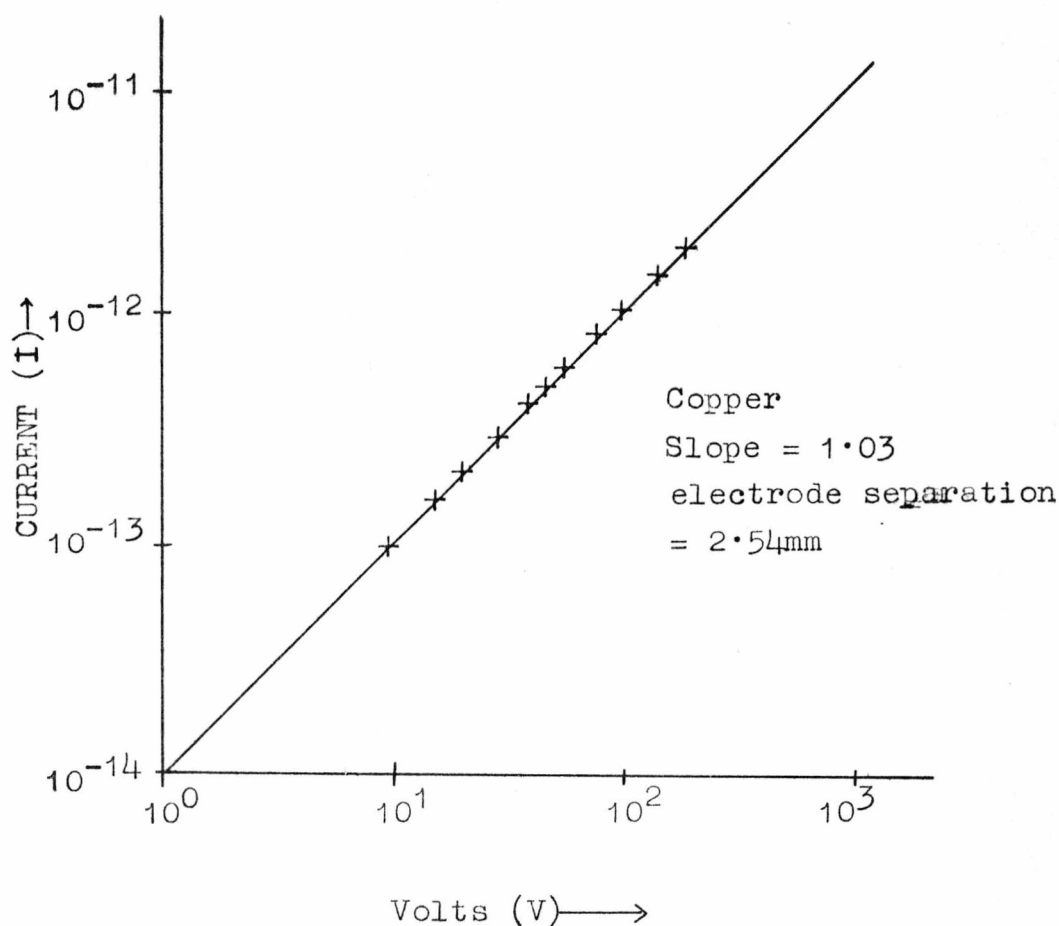These results were calculated in terms of bulk properties which implied that the surface contribution was negligible. To test this a guard ring was used, 'earthing' all of the surface currents. This test was carried out for lead, copper and manganese phthalocyanines; in none of the cases did the introduction of a guard ring have an effect on the measured resistivities. Hence it was concluded that only bulk properties were being measured.

The current-voltage characteristics of each crystal were studied up to a field gradient of about $6 \times 10^4 Vm^{-1}$, and were carried out at 295K and 470K (approximately). In every case the crystals displayed Ohmic (i.e. V = IR) characteristics. For this reason only the low temperature results are shown in figures (5·7), (5·8) and (5·9) with the exception of metal free phthalocyanine, where the high temperature result is shown (figure (5·10)).

By comparison of the number of charge carriers, estimated from the pre-exponential factor, and the density of states, it is possible to estimate if conduction is occurring via an intrinsic or extrinsic mechanism. It has been shown in Chapter (2·2) that the pre-exponential factor is defined as:

$$\rho_o = \frac{1}{\sigma_o} = 1/(ne\mu) \qquad \text{where:}$$

n = number of charge carriers per unit volume

μ = mobility of the charge carriers

e = electronic charge.

Hence the mobility may be estimated from:

$$\mu = \sigma_0 / (ne).$$

For an intrinsic model, n is twice the number of 'molecules' per unit volume (2No). This is true for a narrow band semiconductor (I.G. Austin, 1967). In the case of an extrinsic conductor, n is given by $\frac{1}{2}(NcNo)^{\frac{1}{2}}$ (J.S. Blakemore, 1962 and C. Kittel, 1971), where Nc is the density of impurity states. Hence for the intrinsic model

$$\mu = \sigma_0 / (2No\ e),$$

and for the extrinsic model

$$\mu = \sigma_0 / [\tfrac{1}{2}(NoNc)^{\frac{1}{2}}e].$$
$$(100ppm\ impurity\ for\ Nc)$$

In the case of the phthalocyanines the dimension of the unit cell is typically $1 \cdot 4 \times 10^{-27} m^{-3}$ (J.M. Robertson, 1935). Hence the number of unit cells per unit volume is $\sim 7 \times 10^{26} m^{-3}$. Each unit cell contains two phthalocyanine molecules, hence No = $1 \cdot 4 \times 10^{27} m^{-3}$. With this data together with the pre-exponential factors (cf. table (5·2)) the intrinsic mobilities may be calculated. These results are presented in table (5·3). The measured value for mobility in metal free phthalocyanine is in the range $10^{-4} m^2 V^{-1} s^{-1}$ to $10^{-7} m^2 V^{-1} s^{-1}$ (F. Gutmann and L.E. Lyons, 1967; D.R. Kearns and M. Calvin, 1961; G.H. Heilmeier, G. Warfield and S.E. Harrison, 1962; C.R. Westgate and G. Warfield, 1966). Hence it is difficult to estimate if the extrinsic or the intrinsic model fits, since they both give reasonable values for mobility.

TABLE 5·3

phthalocyanine	pre-exponential factor ρ Ωm	intrinsic mobility $m^2V^{-1}s^{-1}$	extrinsic mobility $m^2V^{-1}s^{-1}$
Manganese	$1·4 \times 10^{-3}$	$1·6 \times 10^{-6}$	3×10^{-4}
Cobalt	$8·2 \times 10^{-2}$	$2·7 \times 10^{-8}$	5×10^{-6}
Nickel	$1·4 \times 10^{-2}$	$1·6 \times 10^{-7}$	3×10^{-5}
Copper	$1·6 \times 10^{-3}$	$1·4 \times 10^{-6}$	$2·5 \times 10^{-4}$
Zinc	$1·6 \times 10^{-3}$	$1·4 \times 10^{-6}$	$2·5 \times 10^{-4}$
Lead	$3·5 \times 10^{-2}$	$6·3 \times 10^{-8}$	$1·0 \times 10^{-5}$
Hydrogen	$2·8 \times 10^{-3}$	8×10^{-7}	$1·4 \times 10^{-4}$

Further evidence for an intrinsic or extrinsic mechanism may be obtained by comparing the measured band gap (E(gap) = 2 X ΔE) with the calculated value. It has been shown (cf. Chapter (2·7)) that the band gap is related to the ionization potential, electron affinity and polarization energies by the following equation:

$$E(gap) = IP - Ea - (P^+ + P^-)$$

or
$$E(gap) = IPx - Ea$$

where IPx = solid state ionization potential.
In the case of phthalocyanines the solid state ionization potential is estimated to be 3·8eV (approximately) (D.D. Eley, D.J. Hazeldine, T.F. Palmer, 1973). The electron affinity of metal free phthalocyanine has been determined, by an electron capture technique, to be 0·68±0·04eV (A. Fulton, L.E. Lyons, G.C. Morris, 1968). Hence the

band gap is calculated to be 3·12eV. Experimentally it was found (cf. table (5·2)) that the band gap was 1·7eV (for metal free, and lower for all the other phthalocyanines).

Comparison of the calculated and observed band gaps indicates that conduction is occurring via an extrinsic mechanism. Furthermore, the activation energies of these impurities are considerably lower than those of the phthalocyanines (which implies that the electron affinity is much higher and/or the ionization potential is lower).

5·3 Vacuum results - photoconductivity

Steady state vacuum photoconduction spectra for the phthalocyanines were measured in the range 400nm to 800nm. It was found that in the cases of copper, cobalt and nickel phthalocyanines the photocurrents were below the detection level of the apparatus ($< 10^{-15}$A) and in the case of manganese phthalocyanine the dark current was very high and 'swamped' the photocurrent. The photoconductive properties of metal free phthalocyanine were not studied in this work. Hence only the vacuum photospectra for lead and zinc phthalocyanines were measured and these results are shown in figures (5·24) and (5·25). These photoconduction spectra were measured at a constant illumination intensity. Also, the photocurrents were corrected to a unit area of illumination. By carrying out the measurements in this manner the photoresponses of different crystals and different phthalocyanines could be quantitatively compared. As may be seen from the two spectra, the general shape is similar, although lead phthalocyanine is a better photoconductor ($\sim$10X), the main

feature being a maximum response at about $20 \times 10^3 cm^{-1}$ (500nm).

The intensity dependence of photoconduction was deter-mined by measuring the photocurrent (Iph) as a function of illumination intensity (L) at a fixed wavelength. These results were plotted on a log-log graph and the resulting slope (m) yielded the intensity dependence, i.e.

$$Iph \propto L^m$$

Table (5·4) lists the results obtained, and these are shown in figures (5·11) and (5·12).

TABLE 5·4

phthalocyanine	wavelength nm.	intensity dependence
Lead	435	0·62
	520	0·57
	640	0·59
Zinc	550	0·55
	620	0·55
	700	0·54

From the theory of intensity dependence, explained in Chapter 2, these results suggest that the photogeneration of charge carriers occurs via a single photon process. Also, recombination is nearly dominated by a bimolecular process. Further evidence for a single photon exciton generation process was obtained by studying the effect of polarized light. It was found that the photocurrent was independent of the direction of polarization. This effect is fully discussed in Chapter 2.

104

FIG: (5·11) <u>PHOTOCURRENT INTENSITY DEPENDENCE PLOTS FOR LEAD PHTHALOCYANINE IN A VACUUM</u>
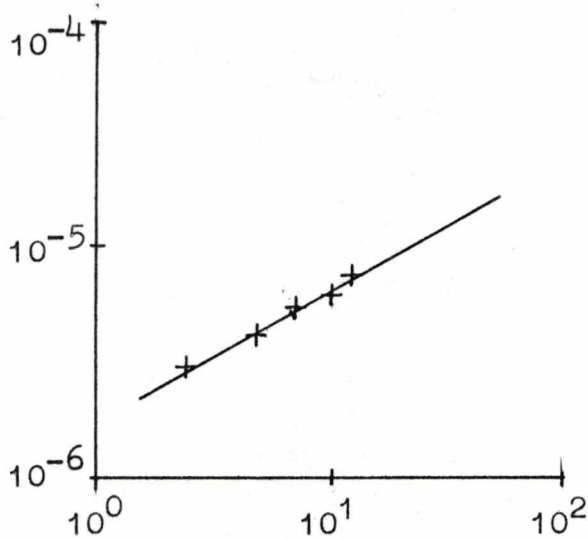
435 nm
(12300 cm^{-1})
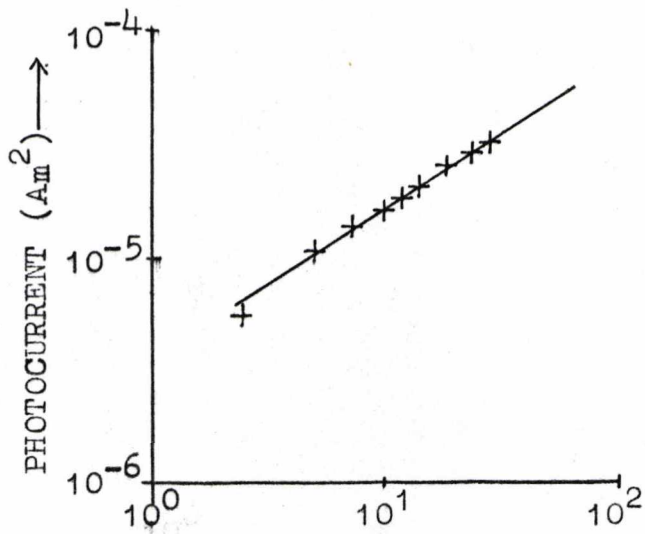
520 nm
(19230 cm^{-1})
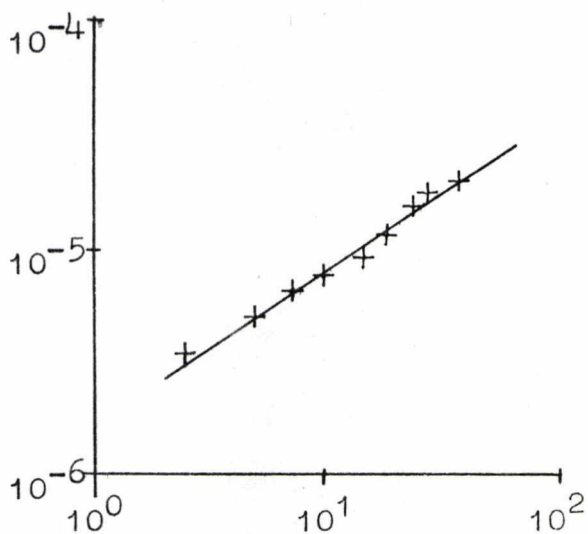
640 nm
(15620 cm^{-1})

THERMOPILE OUTPUT (μV) $\longrightarrow$

105

FIG: (5·12) PHOTOCURRENT INTENSITY DEPENDENCE PLOTS FOR ZINC PHTHALOCYANINE IN A VACUUM

5·4 Reflectance spectra

Measurements of the reflectance spectra were carried out by using a PYE UNICAM SP500 series 2 ultra-violet, visible spectrometer with a diffuse reflectance (type SP540) attachment. Because of their very high absorbances (the extinction coefficient was $\sim 10^5$) the phthalocyanines had to be 'diluted' before any measurements could be carried out. This was achieved by grinding together the purified phthalocyanine and analar potassium bromide (dried) to form a very fine powder. By measuring the difference in the optical density (O.D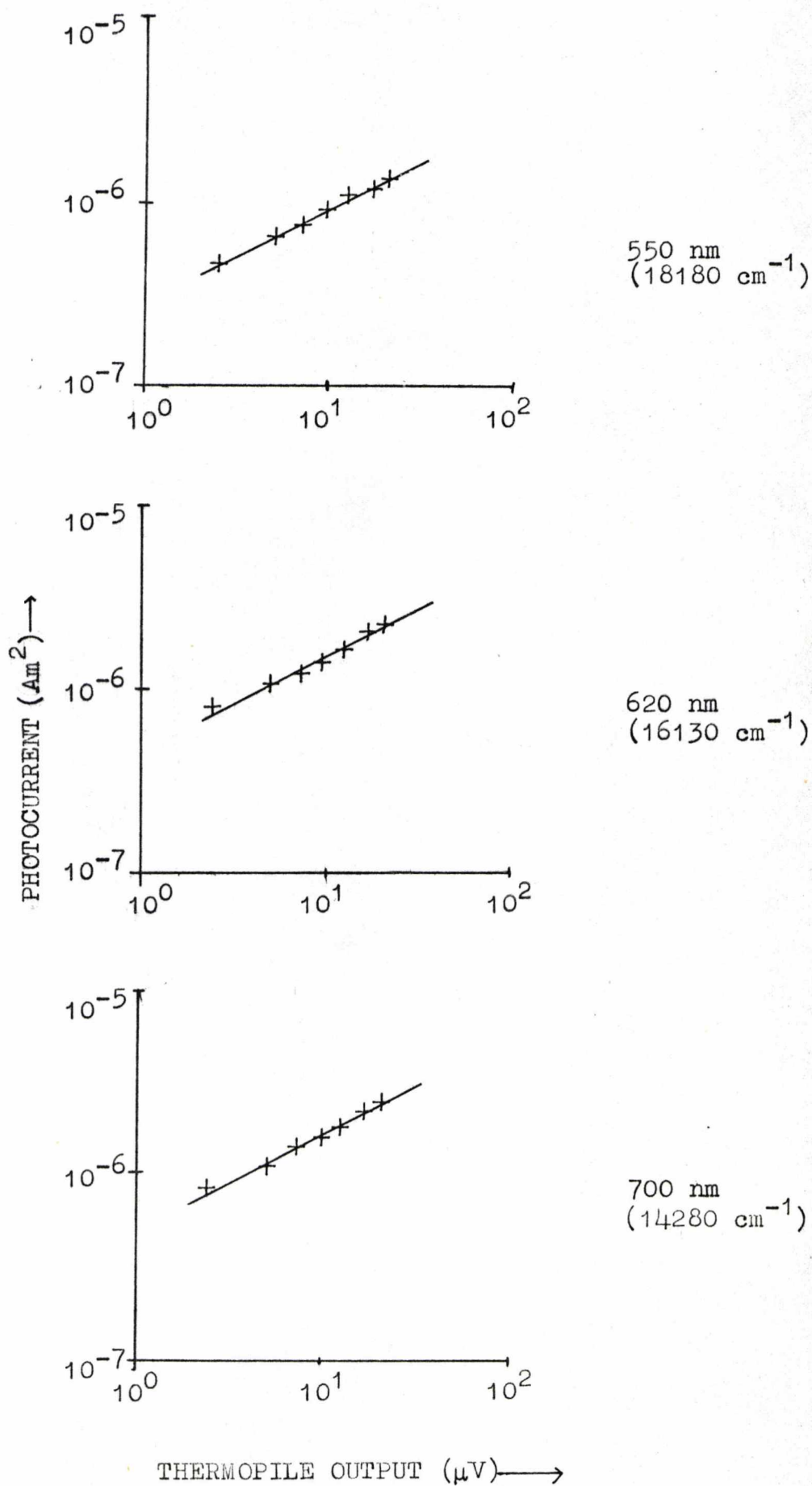.) of the 'diluted' phthalocyanine and a potassium bromide standard at various wavelengths, the reflectance spectrum was determined. The results were plotted using the Kubelka-Munk relation (G.F.A. Kortum, 1969), i.e.

$$K_\infty = \frac{(1-R_\infty)^2}{2R_\infty} \quad \frac{\text{absorption coefficient}}{\text{scattering coefficient}}$$

and

$$\text{O.D.} = \log\left(\frac{1}{R_\infty}\right)$$

where R_∞ = reflectance of an "infinitely thick" sample.

The main assumption made in using the Kubelka-Munk function (K_∞) for plotting reflectance data was that the scattering coefficient (s) was independent of the wavelength. If this assumption were not maintained then the resultant spectrum would not have the same shape as that of the crystal. When the particle size of the powder was kept larger than that of the maximum wavelength (820nm) then the scattering coefficient was independent of wavelength. Using the powder technique the particle sizes were approximately one micron in diameter;

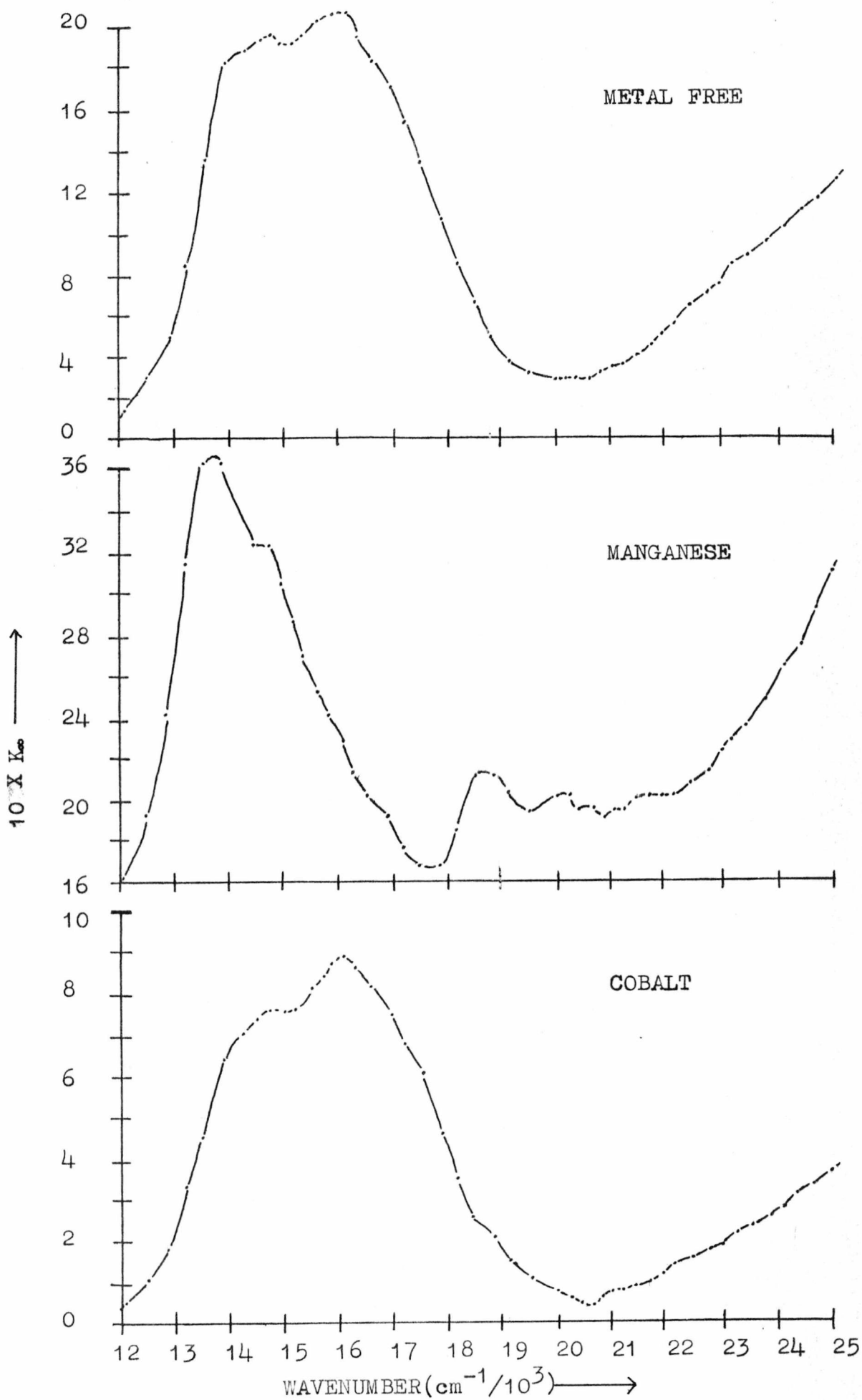FIG: (5·13)   REFLECTANCE SPECTRA FOR VARIOUS PHTHALOCYANINES.

METAL FREE

MANGANESE

COBALT

$10^{-3} \times K_\infty$ ——→

WAVENUMBER$(cm^{-1}/10^3)$——→
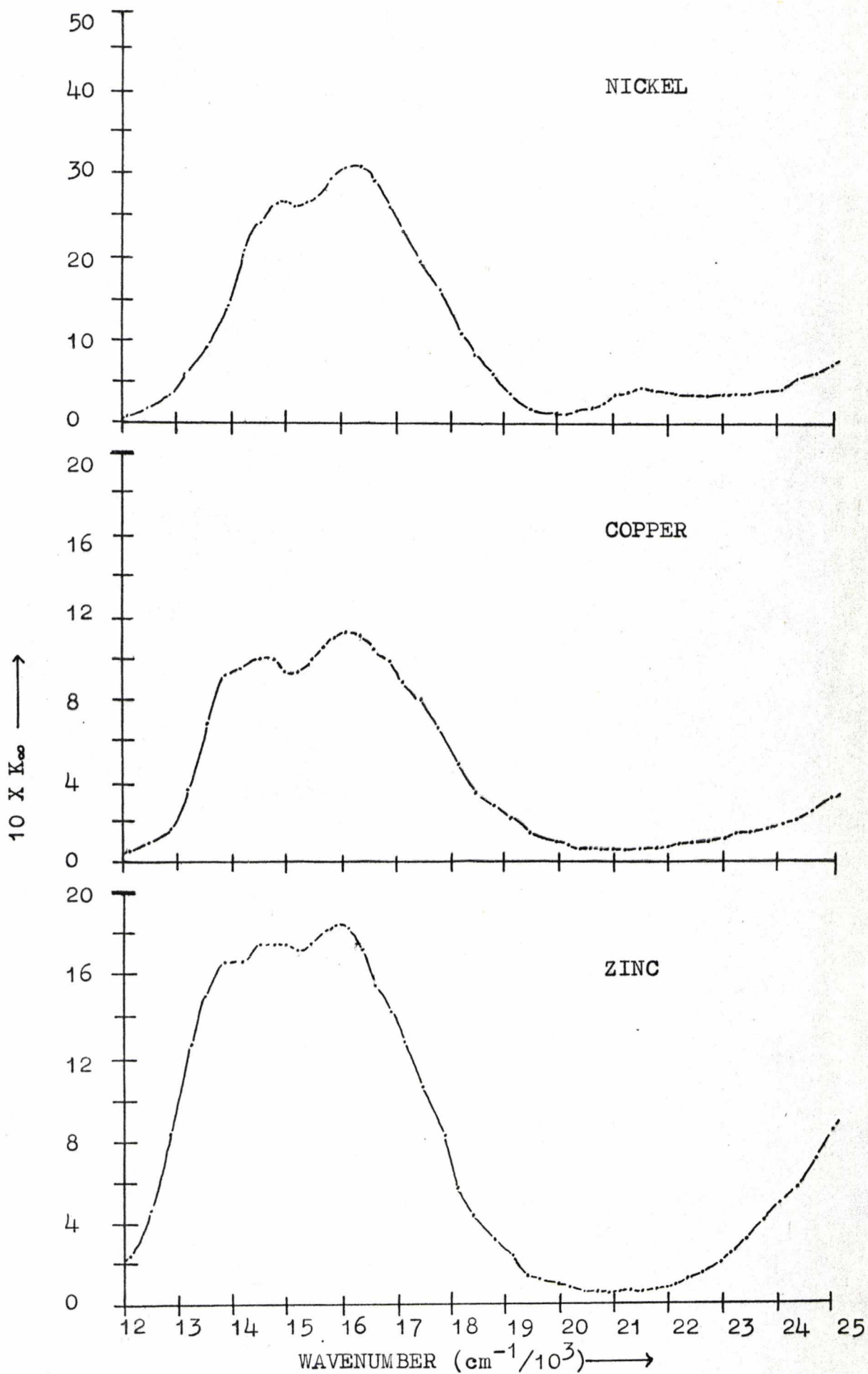
FIG: (5·15)   REFLECTANCE SPECTRUM FOR LEAD PHTHALOCYANINE.
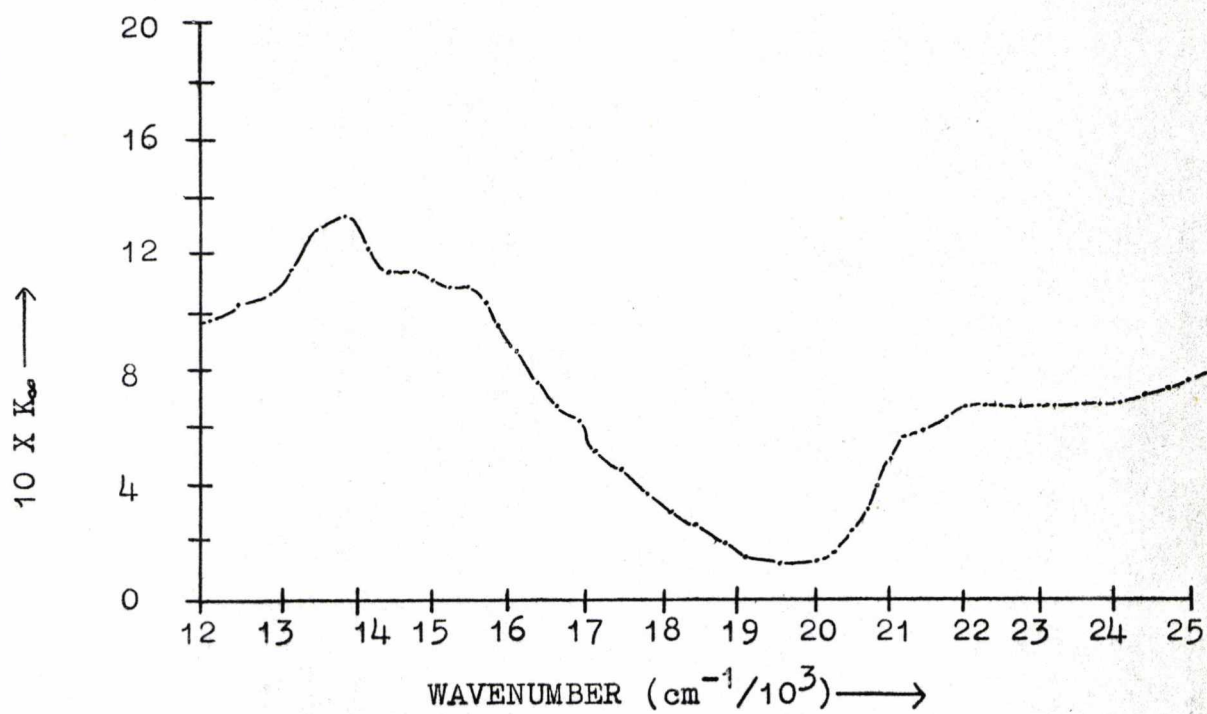
hence the Kubelka-Munk function could be used.

All the spectra were plotted using the Kubelka-Munk function and the results are presented in figures (5·13), (5·14) and (5·15). These spectra, excepting lead and manganese phthalocyanines, have also been recorded by previous workers (P.E. Fielding and F. Gutmann,1957; L.E. Lyons, J.R. Walsh and J.W. White, 1960; P. Day and R.J.P. Williams, 1962; G.H. Heilmeier and G. Warfield, 1963;and S.E. Harrison, 1969) and are in agreement with the results obtained in this work. Furthermore it was concluded by P. Day and R.J.P. Williams, 1962 and 1965, that the main absorption peak (500nm - 800nm approximately) was due to singlet transitions.

Comparison of the reflectance spectra for lead and zinc (figures (5·14) and (5·15)) with the vacuum photoconduction spectra (figures (5·24) and (5·25)) shows that the absorption minimum corresponded to the photoconduction peak. Further comparison of the reflectance spectra, for lead, zinc and copper phthalocyanines (figures (5·14) and (5·15)) with the photoconduction spectra carried out in an oxygen (or any other electron acceptor gas, i.e. N_2O_4 and BF_3) ambient (figures (5·25), (5·26) and (5·37)) shows that the photocurrent minimum corresponded to the absorption minimum. These observations are interpreted as follows. Consider the vacuum photospectrum first. In this case the photoconduction peak occurred at minimum absorption (approximately 500nm), which also corresponded to the maximum penetration depth of photons into the crystal (cf. section (5·5)). This suggested that carrier generation was predominantly a bulk phenomenon since the apparent quantum efficiencies (cf. section (5·14)) became larger as the photon penetration

111

depth was increased. Therefore vacuum photoconduction probed the bulk carrier generation process. This result was first reported by Z.D. Popovic and J.H. Sharp, 1977.

When the crystals were exposed to oxygen, dinitrogen tetroxide or boron trifluoride, the photocurrent was considerably enhanced and the spectral response was altered to give a minimum in photoconduction at minimum absorption. It will be shown in this work (cf. section (5·6) especially) that the gas effect was entirely restricted to the surface of the crystal, except for oxygen where some slight diffusion into the crystal's bulk occurred. Therefore it was concluded that in these cases the surface region became very important in the charge carrier generation mechanism. The increased level of photoconduction with increasing surface impurity centres (due to the adsorbed gases) suggested that carrier generation involved exciton dissociation at these centres. Furthermore, since the surface impurities were all electron traps (i.e. all the gases that enhanced photoconduction were electron acceptors), exciton dissociation would produce 'hole' carriers. The decrease in the quantum yield at minimum absorption was due to the excitons being created further into the bulk of the crystals, due to the greater penetration depth of the photons, and consequently fewer excitons were able to reach the surface impurity sites.

To conclude, the comparison of photoconduction and reflectance spectra suggested that in a vacuum the carrier generation process was predominantly a bulk phenomenon. However, in an electron acceptor gas ambient, exciton dissociation at surface impurities became the main factor influencing the charge carrier generation process.

112

5·5 Penetration depth of photons into crystals

First the extinction coefficient ($\mathcal{E}$) was determined by measuring the absorbance (A), at various wavelengths, of a dilute solution of phthalocyanine in analar αchloro-naphthalene. The extinction coefficient is related to the absorbance by the Beer-Lambert law, i.e.

$$I = Io \, \exp(-\mathcal{E}cx),$$

c = concentration in moles per litre

x = path length (cm)

Io = initial intensity

I = intensity after passing through x cm of solution

$$\therefore \quad \mathcal{E} = -Ln\left(\frac{I}{Io}\right) / (cx).$$

Substituting in the experimental values

$$c \sim 10^{-5} \text{ moles } l^{-1}, \quad x = 1cm, \quad A = 0\cdot 4 \text{ at } 400nm,$$

yields $\mathcal{E} \approx 10^{5}$.

Knowing the density of the phthalocyanine (~ 2 gm cm^{3}) the molarity (M) of the solid may be calculated.

$$M = \rho V/(\text{molecular weight}) \qquad \rho \sim 2 \text{ gm } cm^{-3}$$

$$V = 1l$$

$$\text{mol. wt.} \sim 720$$

$$\therefore \quad M \sim 14 \text{ moles } l^{-1}$$

Then by rearranging the Beer-Lambert law the path length for 99% absorption may be calculated.

$$\frac{I}{Io} = \exp(-\mathcal{E}cx)$$

$$\therefore \quad Ln\left(\frac{I}{Io}\right) = -\mathcal{E}cx$$

$$\therefore \quad x = -Ln\left(\frac{I}{Io}\right)/\mathcal{E}c$$

substituting in the values $\frac{I}{Io} = \frac{1}{100}$, $\mathcal{E} = 10^5$ and $c =$
$c = 14$ moles 1^{-1},

$$x = -Ln(0\cdot99)/10^5 \text{ X } 14$$

$$\approx 330A^\circ = 33nm.$$

By repeating this calculation for various wavelengths and different phthalocyanines, it was found that the minimum penetration was $\sim$5nm and the maximum penetration $\sim$500nm.

5·6 Effect of dinitrogen tetroxide on the dark resistivity

The procedure used to study the effect of dinitrogen tetroxide on the phthalocyanines was to first of all clean the crystal by evacuation and heating. Also, the same field gradient was used for all the crystals thereby preventing any erroneous observations due to voltage dependent effects. The current voltage characteristics of the crystals in an ambient of dinitrogen tetroxide were measured. In every case the results obeyed Ohms law up to the maximum applied voltage (600V). These results are not reproduced in this thesis since they are essentially of the same form as the low temperature vacuum results (cf. section (5·3) and figures (5·7), (5·8), (5·9) and (5·10)). Small amounts of the gas were allowed into

FIG: (5·16)   EFFECT OF DINITROGEN TETROXIDE ON THE DARK
RESISTIVITY OF ZINC AND LEAD PHTHALOCYANINES.
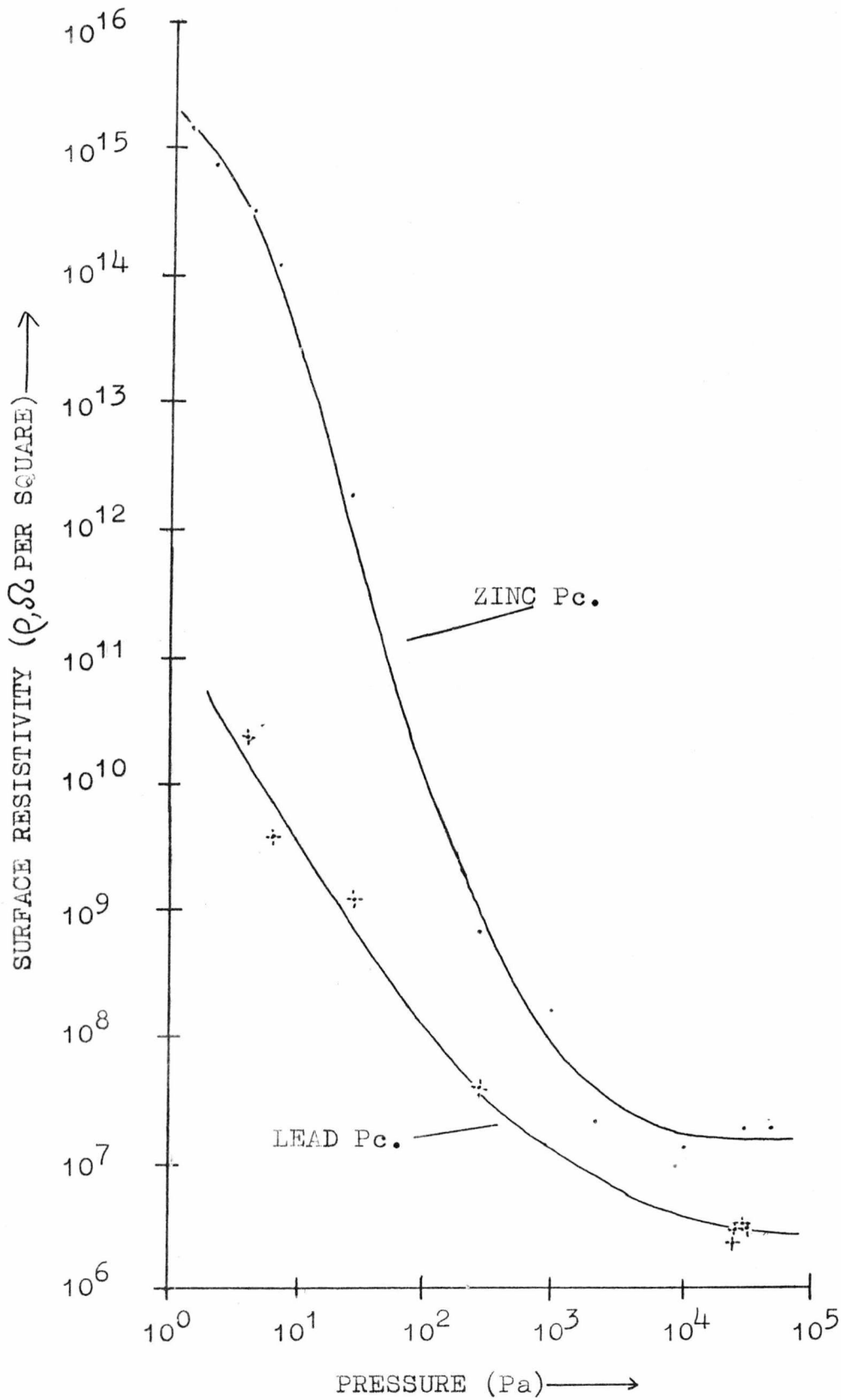
FIG: (5·17) EFFECT OF DINITROGEN TETROXIDE ON THE DARK RESISTIVITY OF NICKEL AND MANGANESE PHTHALOCYANINES.
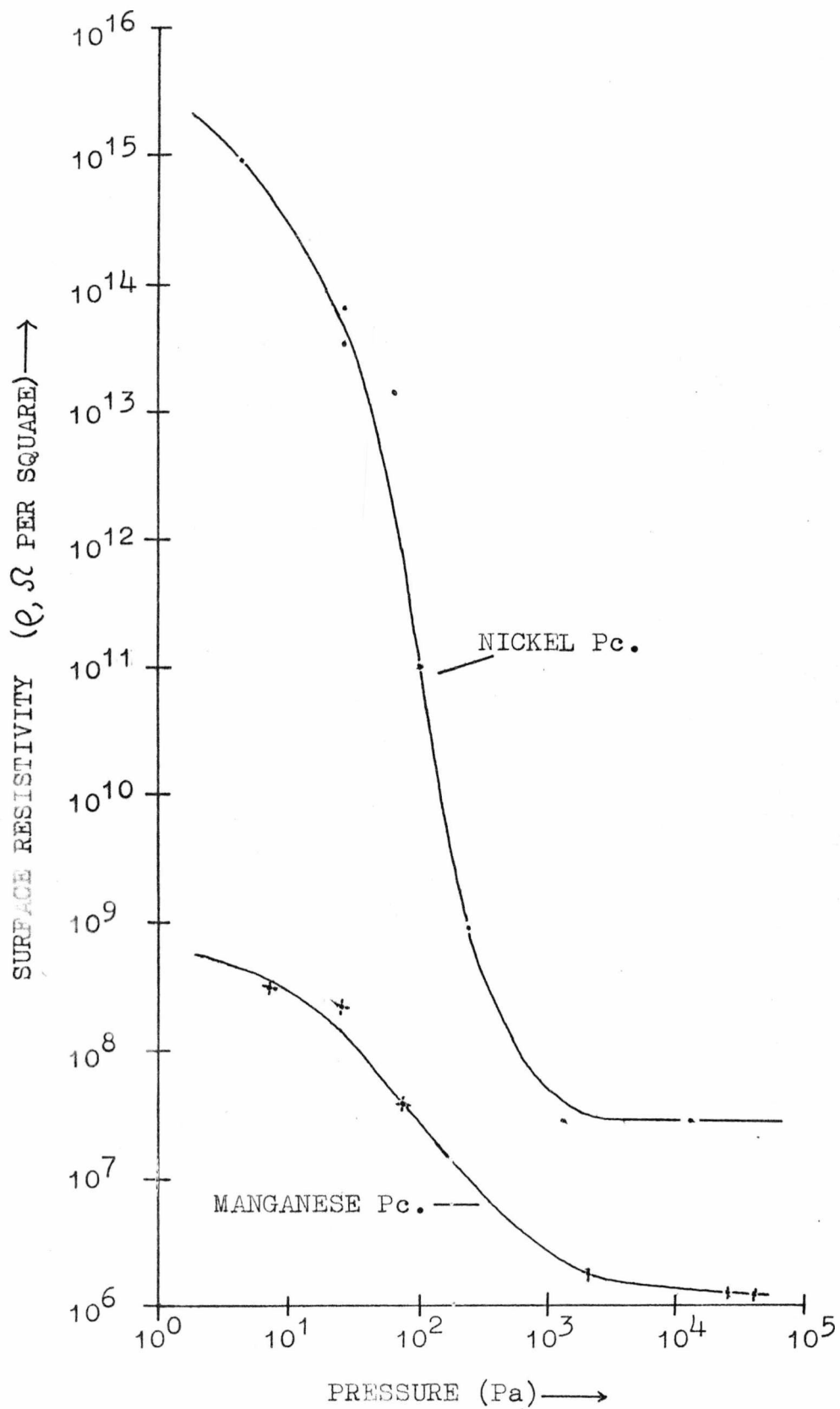
116

FIG: (5·19) EFFECT OF DINITROGEN TETROXIDE ON THE DARK
RESISTIVITY OF COBALT AND METAL FREE
PHTHALOCYANINES.

118
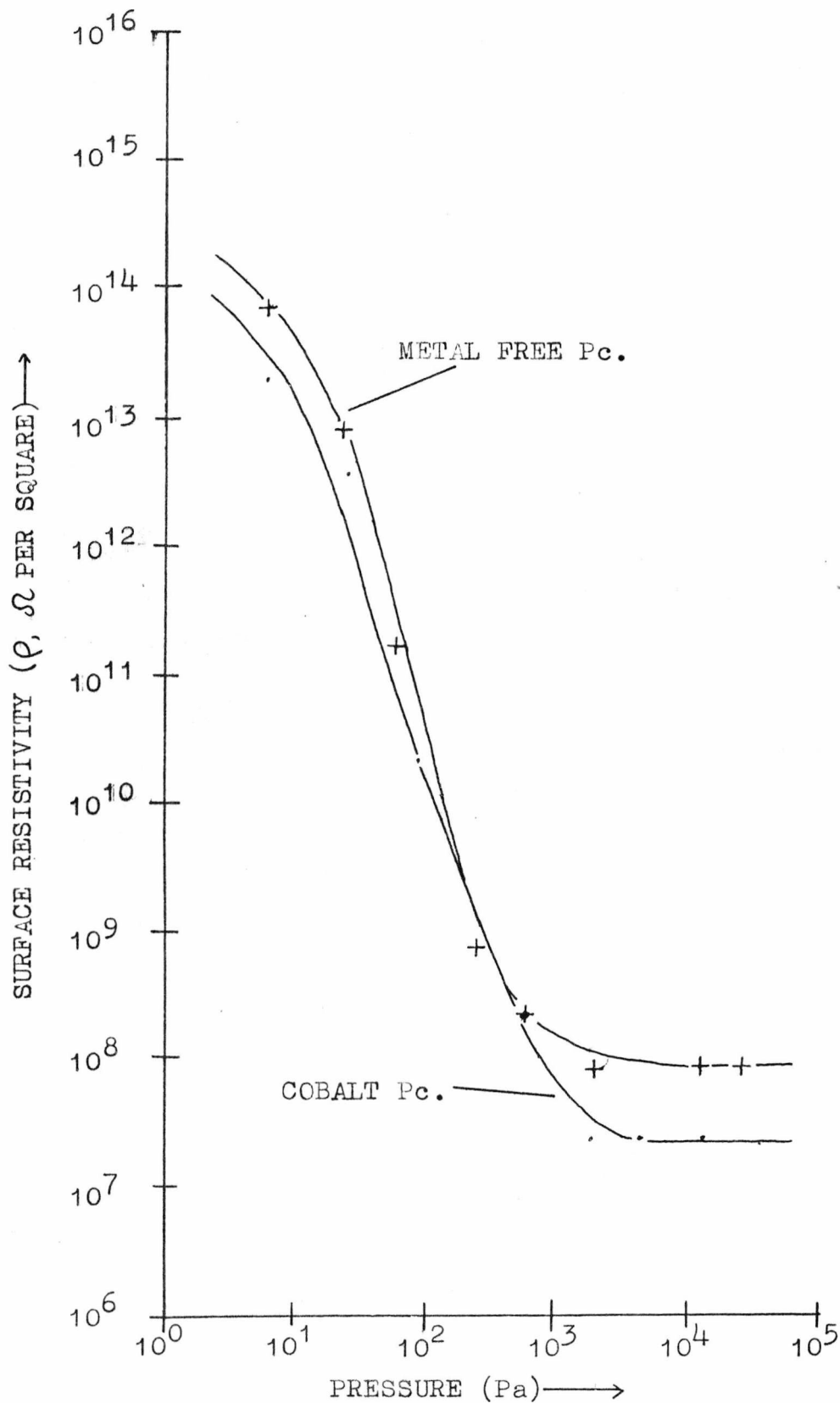
the cell and the decrease in dark resistivity was continuously monitored on the chart recorder. The pressure in the cell was increased by small increments, up to a maximum of 5×10^4 Pa, each time allowing the dark resistivity to equilibrate. These measurements were carried out for all seven phthalocyanines and the results are shown in figures (5·16), (5·17), (5·18) and (5·19). For lead, copper, nickel, zinc and cobalt the results shown in the pressure dependence curves are for two different crystals. As can be seen, very good agreement was obtained. The main feature of these curves is the similarity for all the phthalocyanines, excepting lead and manganese. Since metal free phthalocyanine showed similar results it was concluded that the metal did not influence the sensitivity of the phthalocyanine towards the gas to an observable extent. One important feature was that they all had very similar surface resistivities ($10^7 \Omega$ per square) when exposed to high pressures of the gas (10^4-10^5Pa). It can be seen from these plots that lead and manganese phthalocyanines were different at low pressures. This is explained in terms of the lower vacuum surface resistivities.

As may be seen, the ordinates of these graphs are plotted in terms of surface resistivity since the gas effect was restricted to the surface of the crystal. Proof of this was found from the speed of response, the size of the dinitrogen tetroxide molecule and guard ring experiments. Response of the phthalocyanines to the gas was very fast, from a few seconds to about thirty minutes, hence it was not likely that the gas molecules were diffusing into the bulk of the crystal, especially when the size of a dinitrogen tetroxide molecule is considered. The guard ring experiment was carried out on

119

lead, copper and manganese phthalocyanines. When these crystals, fitted with an earthed guard ring, were exposed to the gas no decrease in the resistivity was observed. This provided conclusive evidence that the interaction between phthalocyanine and dinitrogen tetroxide was entirely restricted to the surface of the crystal. It was also established, that, in a vacuum, bulk conductivity predominated (cf. section(5·2)) by at least a factor of 50 (the detection limit of the apparatus). Hence in the presence of dinitrogen tetroxide the measured resistivity was a combination of bulk and surface. These were separated by considering the currents produced under the same field gradient. The vacuum dark current (Idv) is a bulk property and in the gas the measured current (Id) is due to Idv and a surface current contribution (Idg). Hence

$$Idg = Id - Idv$$

Then the surface resistivity may be calculated from:

$$\rho g = \frac{VA}{(Id - Idv)L}$$

where A = length of electrode contact with the surface

L = length of conduction path

V = applied voltage.

The conduction areas are as follows:

BULK CONDUCTION

$A = (w \times t)$

$A = 2(w+t)$
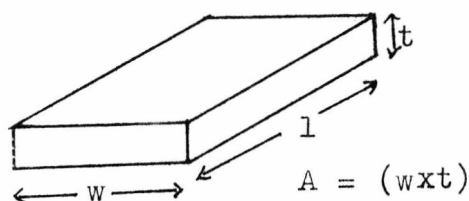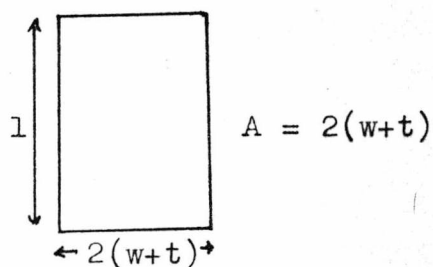
SURFACE CONDUCTION

It should be noted that the surface resistivity expression
(ρ_g) is not entirely correct since it is assumed that in a
vacuum only bulk conduction exists. In this study it has
only been established that the surface conduction contribution
is less than 2% (under vacuum conditions). However, this error
becomes negligible when gases are adsorbed and surface conduc-
tion dominates.

   In the case of copper phthalocyanine a test was carried
out to try and establish if the dinitrogen tetroxide was under-
going chemisorption. For this study the pressure of the gas
was suddenly increased by a factor of 10 (6Pa up to 60Pa).
The time dependence of the surface current increase was then
monitored. This data was then plotted as shown in figure (5·20)
and follows an Elovich type equation (cf. Chapter(2·11)),i.e.

$$\frac{dq}{dt} = a \, \exp(-bq)$$

where q = surface coverage a and b are constants.
It was therefore assumed that the surface resistivity accurately
represented the surface coverage (q). However, in reality
it is probable that the surface sites have a distribution of
energy; consequently the decrease in surface resistivity
is a function of surface coverage and the energy of the sites.
This implies that at high gas pressures only the weakly binding
sites are left. As will become evident later the type of
interaction between the surface and gas is that of a donor-
acceptor. Then, since at high pressures the interaction
becomes less, (i.e. the electron density in the phthalo-
cyanine - gas bond is reduced) the contribution to the enhance-
ment of the surface conduction mechanism is reduced.

In addition to fitting an Elovich type equation to the data
a diffusion type plot was also carried out (as shown in
figure (5·20)); however, this did not give a linear fit and
gives further evidence that only a surface interaction was
taking place.

It can be seen from figure (5·20) that the initial
(the first 100 seconds approximately) rise in the dark
current $(Idg(t) - Idg(0))$ was slow and did not fit on the
Elovich plot. The main cause of this effect was the time
taken for the cell to reach the required pressure. Gas was
admitted into the cell via a small bore tube (a full descrip-
tion of the apparatus is given in Chapter 4). Also, the
volume of the cell was reasonably large (approximately
2×10^{-3} m^3). Hence the time taken to increase the pressure
in the cell from 6Pa to 60Pa (approximately) would not be
negligible. It was found that it took about one minute for
the system to reach a pressure equilibrium.

From the slope and intercept from an Elovich plot it is
possible to determine the initial adsorption velocity (a)
(cf. Chapter (2·11)). However, in this case this was not
possible due to the type of measurements made. It has already
been noted that the decrease in the dark resistivity (or
the increase in the dark conductivity or current) need not
necessarily accurately represent the extent of chemisorption.
In an Elovich plot it is important to know either the surface
coverage or volume adsorbed in a time t. Furthermore, for an
Elovich equation to apply, the number of available sites
must diminish exponentially as the amount adsorbed increases,
implying that the chemisorbed molecules deactivate the sites
in excess of actual occupancy. Hence the plot shown in

122

figure (5·20) is complex since it is dependent on the surface coverage and energy of the sites being filled. Further evidence to show that dinitrogen tetroxide was being chemisorbed onto the phthalocyanines is given in section (5·17).

The ease of desorption of the dinitrogen tetroxide from the crystal's surface was also studied. After exposure to the gas the cell was evacuated and the resistivity of the crystal was monitored. It was found that in the cases of lead, cobalt and manganese, evacuation had little effect, whereas for the other phthalocyanines the resistivity increased by a factor of 50 to 1000. When the crystals were heated (420K) under vacuum the resistivities of copper, zinc, nickel and metal free returned to the vacuum level (prior to N_2O_4 exposure) within a factor of 5. For the other three phthalocyanines a higher temperature was required before any effect was observed. Cobalt and manganese phthalocyanines returned to their vacuum resistivities when heated at 520K under vacuum for about 12 hours, whereas lead phthalocyanine increased its resistivity only by a factor of 100(approximately). These results therefore show that the strength of adsorption is different for the phthalocyanines and the following trend was obtained.

$$Pb > Co > Mn > Cu \approx Ni \approx Zn \approx H_2.$$
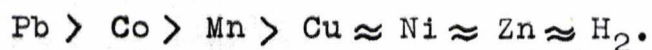
This series can be explained in terms of the ease with which the metal may be oxidised. Lead, cobalt and manganese all have higher oxidation states, whereas the other metals do not. Hence lead, cobalt and manganese are capable of increasing the electron density in the phthalocyanines' delocalized system, when required. Thus when the phthalocyanine
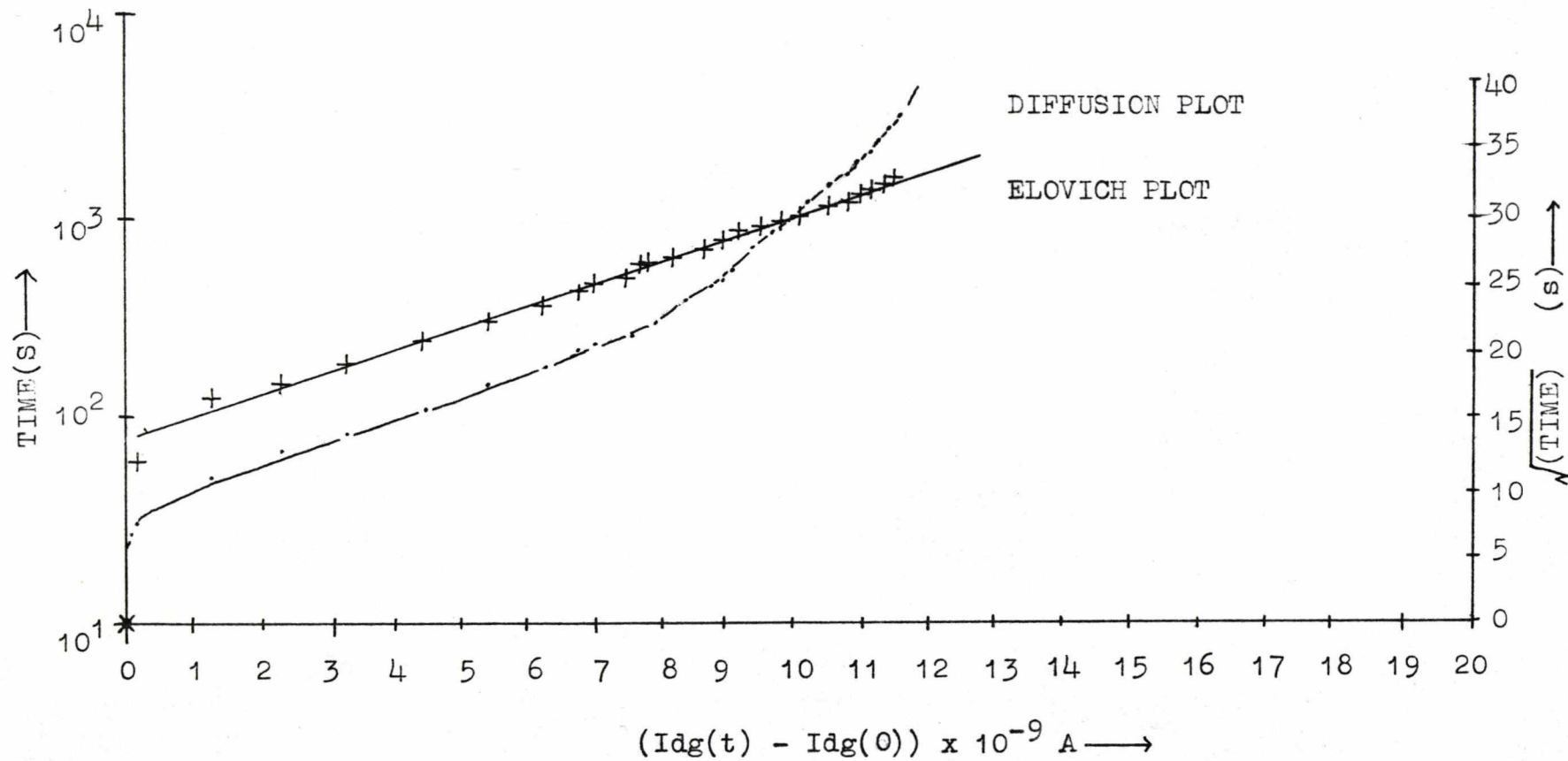
FIG: (5·20) ELOVICH AND DIFFUSION PLOTS FOR N_2O_4 ON COPPER PHTHALOCYANINE

is exposed to dinitrogen tetroxide (an electron acceptor),
lead, cobalt and manganese enhance the chemisorption bond
by partially donating electrons to the phthalocyanine ring,
making it more difficult to remove the gas. Furthermore,
it seems unlikely that the metal is donating directly to the
dinitrogen tetroxide, since metal free phthalocyanine exhibits
a similar effect as the metal phthalocyanines (cf. figure
(5·19)).

5·7 Effect of dinitrogen tetroxide on the activation energy

The activation energies for all the phthalocyanines
were measured in an atmosphere of dinitrogen tetroxide
(5×10^4Pa) and the results are presented in table (5·5) and
shown in figures (5·21), (5·22) and (5·23). One of the
difficulties encountered was to prevent the phthalocyanine
from reacting with the gas. This meant that the temperature
of the crystal had to be kept below 370K (approximately)
and even then some slight reaction occurred, especially in
the case of lead, cobalt and manganese phthalocyanines.
It was found that if the phthalocyanine was heated to a
fairly high temperature in the gas then a slight reaction
would occur and the activation energy would increase, as can
be seen in figures (5·22) and (5·23). The method by which
it was established if a reaction had occurred is discussed
in section(11). Hence the values given in table (5·5) repre-
sent an upper limit. Also, it should be noted that when the
crystal was heated the gas adsorption equilibrium was altered.
Again, this would tend to increase the apparent activation
energy. To try and minimize this effect the measurements
were carried out under a high pressure of dinitrogen tetroxide.

125

FIG: (5·21) ACTIVATION ENERGY PLOTS (N_2O_4) FOR MANGANESE, COBALT AND NICKEL PHTHALOCYANINES
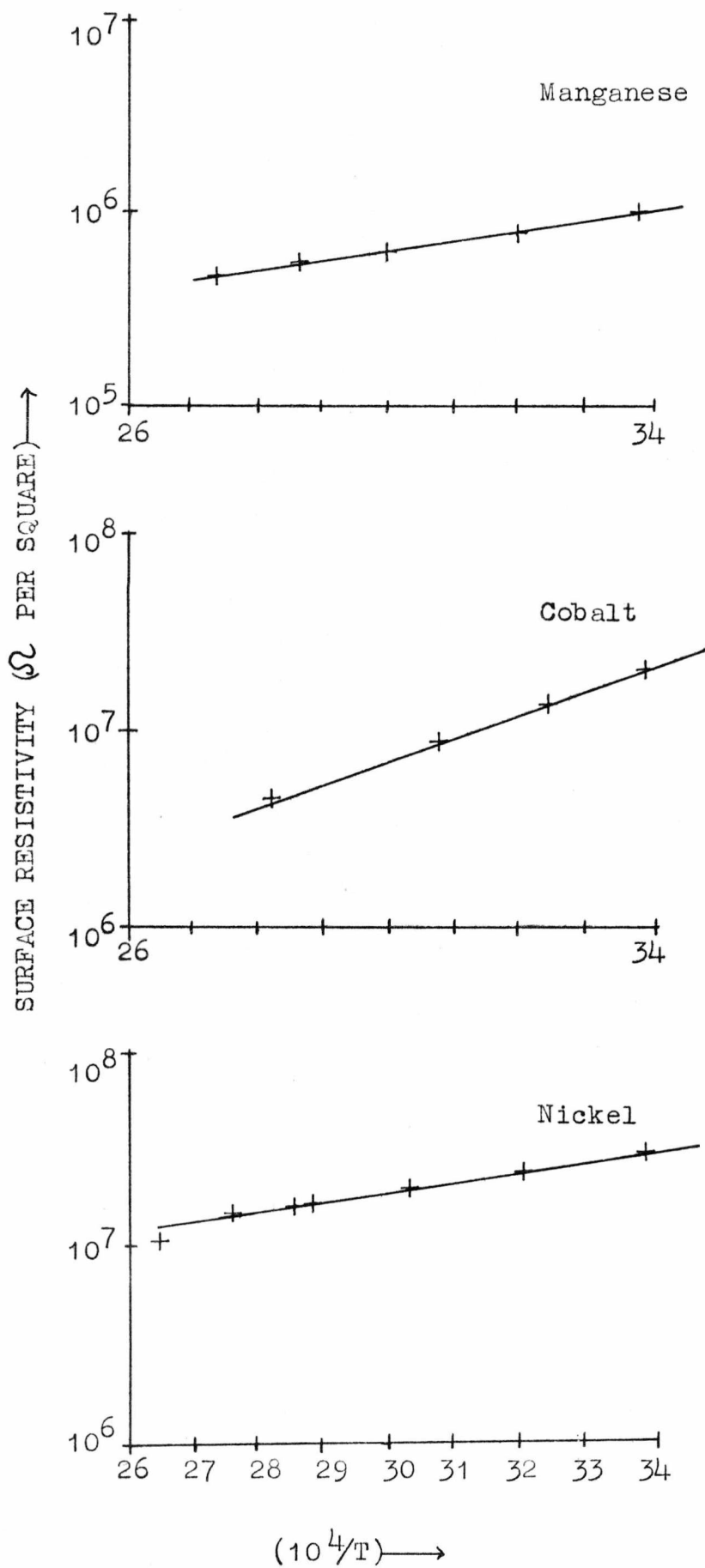
FIG: (5·22) ACTIVATION ENERGY PLOTS (N_2O_4) FOR COPPER, ZINC AND LEAD PHTHALOCYANINES

127
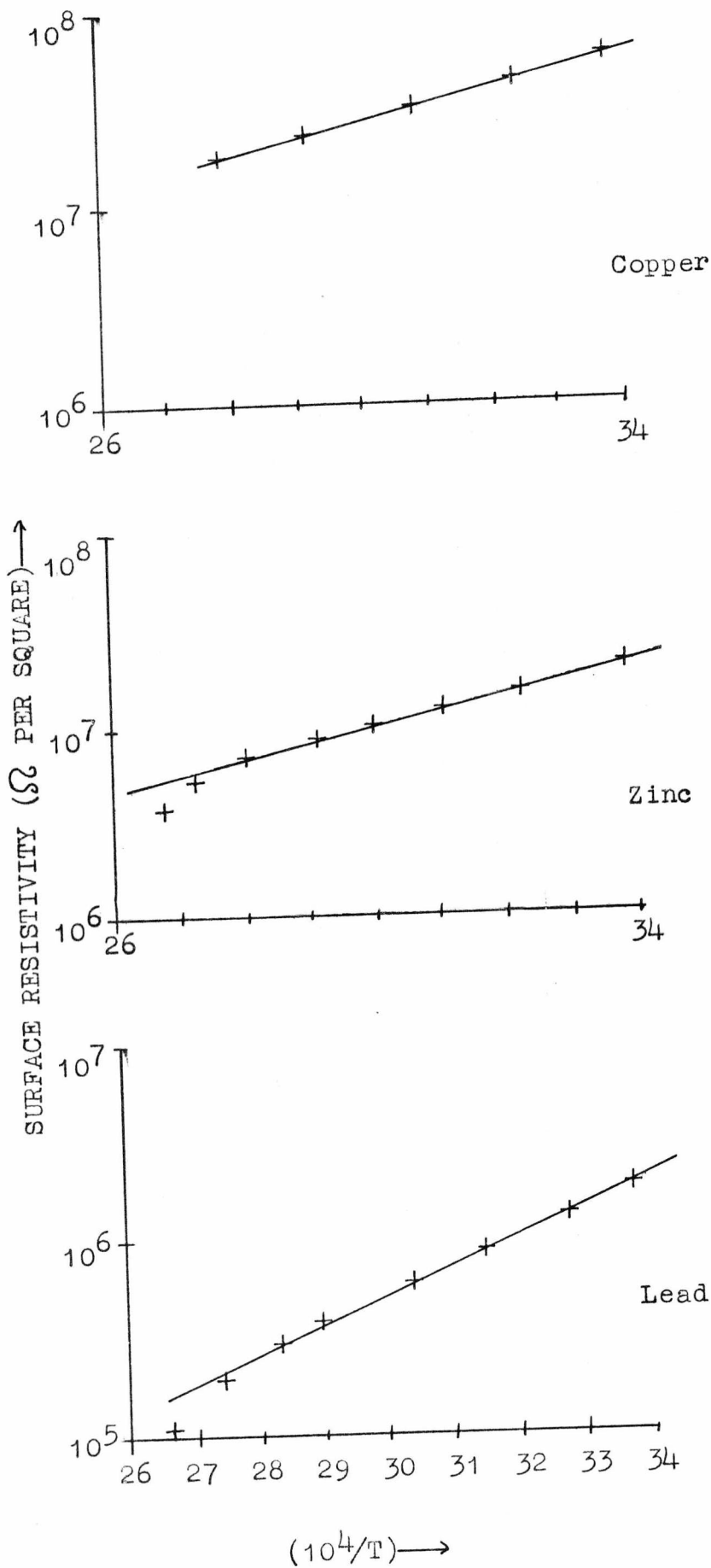
FIG: (5·23) <u>ACTIVATION ENERGY PLOT (N_2O_4) FOR METAL FREE</u>
<u>PHTHALOCYANINE</u>
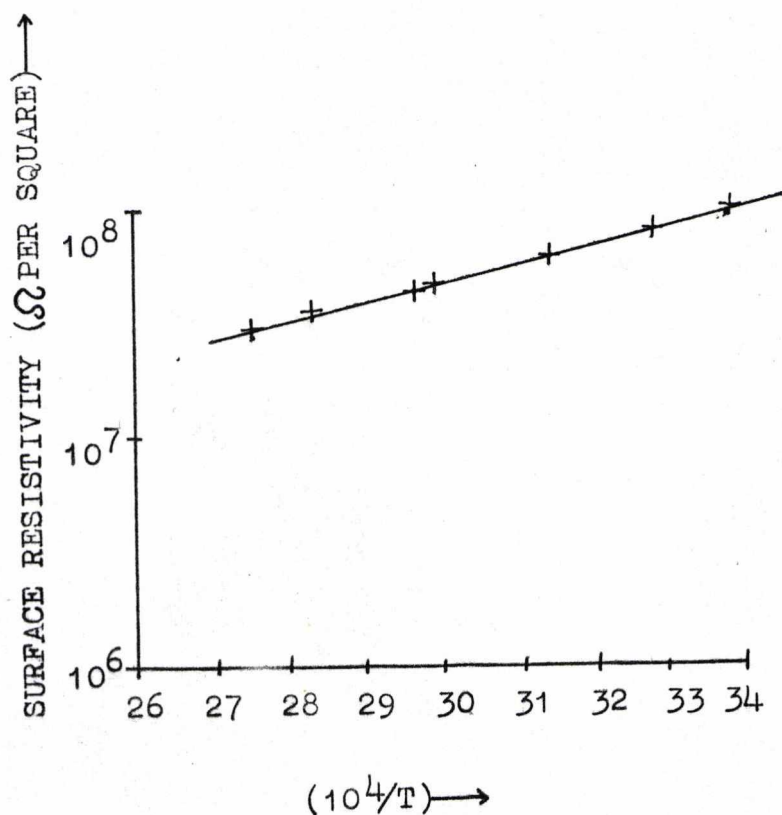
TABLE (5·5)

phthalocyanine	surface resistivity Ω per square (295K)	activation energy eV	pre-exponential factor ρ_0 Ω per square
Manganese	1×10^6	0·10	2×10^4
Cobalt	2×10^7	0·22	$3·5 \times 10^3$
Nickel	3×10^7	0·10	6×10^5
Copper	6×10^7	0·17	$7·5 \times 10^4$
Zinc	2×10^7	C·17	$2·5 \times 10^4$
Lead	2×10^6	C·28	33
Hydrogen	1×10^8	0·15	$2·7 \times 10^5$

NOTE: All measurements made in 5×10^4 Pa, N_2O_4

After these measurements had been carried out it was possible to estimate the surface coverage. This was carried out by using the conductivity equation (cf. Chapter (2·6)) to estimate the number of charge carriers per unit surface area. This value was then compared with the estimated number of adsorption sites.

a) Calculation of the number of carriers per unit surface area.

From the conductivity equation the number of carriers (n) per unit surface area may be calculated, i.e.

$$\sigma = n\mu e \exp\left(\frac{-E(gap)}{kT}\right) \quad \ldots \text{ equation (2·5)}$$

$$n\mu = (\sigma/e) \exp\left(\frac{E(gap)}{kT}\right)$$

where μ = mobility of the carrier

e = electronic charge = $1·602 \times 10^{-19}$ C.

Then by substituting in values for the surface conductivity
$(\sigma = \frac{1}{\rho})$ at the temperature T, a value for $n\mu$ may be obtained.
From literature (C.R. Westgate and G. Warfield, 1967 and
G.A. Cox and P.C. Knight, 1972 and 1974) values for bulk
mobility range from $10^{-4}m^2s^{-1}v^{-1}$ to $10^{-7}m^2s^{-1}v^{-1}$ and these
are typical of organic semiconductors. In this case a value
of $10^{-5}m^2s^{-1}v^{-1}$ was chosen for the surface mobility. Table (5·6)
lists the values obtained.

TABLE (5·6)

phthalocyanine	activation energy eV	$n\mu$	n
Copper	0·17	8×10^{13}	8×10^{18}
Zinc	0·17	2×10^{14}	2×10^{19}
Manganese	0·10	4×10^{15}	4×10^{20}
Lead	0·28	1×10^{14}	1×10^{19}
Nickel	0·10	6×10^{16}	6×10^{21}
Cobalt	0·22	2×10^{14}	2×10^{19}
Metal free	0·15	3×10^{14}	3×10^{19}

b)   Rough estimation of the number of surface sites.

Since the phthalocyanine molecules are stacked along
the needle axis of the crystals, the main faces of the crys-
tals present an edge-on view of the molecules. The area of
the surface occupied by each phthalocyanine molecule is then
approximately the cross section area of the molecule viewed
edge-on, i.e. $0·35 \times 1·5nm = 0·5nm^2$. Hence the number of
phthalocyanine sites per unit area is $\approx 10^{18}$. Very good agree-
ment is achieved between the number of carriers and sites.
This implies that the surface of the crystal is almost
entirely covered with the gas; also, each site is nearly

100% ionized. It should be noted that in this analysis it has been assumed that the surface of the crystal is perfectly smooth. This is not necessarily the case and any surface roughness would increase the number of phthalocyanine sites.

The effect of the gas on the activation energy was found to be reversible for all the phthalocyanines, excepting lead, cobalt and manganese, by evacuation and heating at 520K for 12 hours. In the case of lead, cobalt and manganese phthalocyanines the observed activation energy was dependent on the evacuation and heating times. However, even after a 60 hour period the activation energy was still typically 0·2 to 0·4 eV lower than the vacuum value.

5·8 Effect of dinitrogen tetroxide on the photoconductivity

Photoconduction spectra were measured for copper, zinc and lead phthalocyanines in an ambient of dinitrogen tetroxide (a few Pa) and the results are presented in figures (5·24), (5·25) and (5·26). In the case of cobalt and nickel phtha-locyanines the photocurrent was below the detection limit of the apparatus and in the case of manganese phthalocyanine the photocurrent was rendered unobservable due to the high dark current. From the three spectra (figures (5·24), (5·25) and (5·26)) it can be seen that the photocurrent was greatly enhanced by the presence of a small amount of the gas; further-more, the spectral response was altered (cf. the vacuum spectra in figures (5·24) and (5·25)).

Recently Z.D. Popovic and J.H. Sharp (1977) investigated the spectral response (360-740nm) of 'hole' and electron photoconduction in β-metal free phthalocyanine films, using pulsed photoconduction techniques. With a negative illuminated

131

FIG: (5·24) PHOTOCONDUCTION SPECTRA OF LEAD PHTHALOCYANINE IN VARIOUS AMBIENTS.
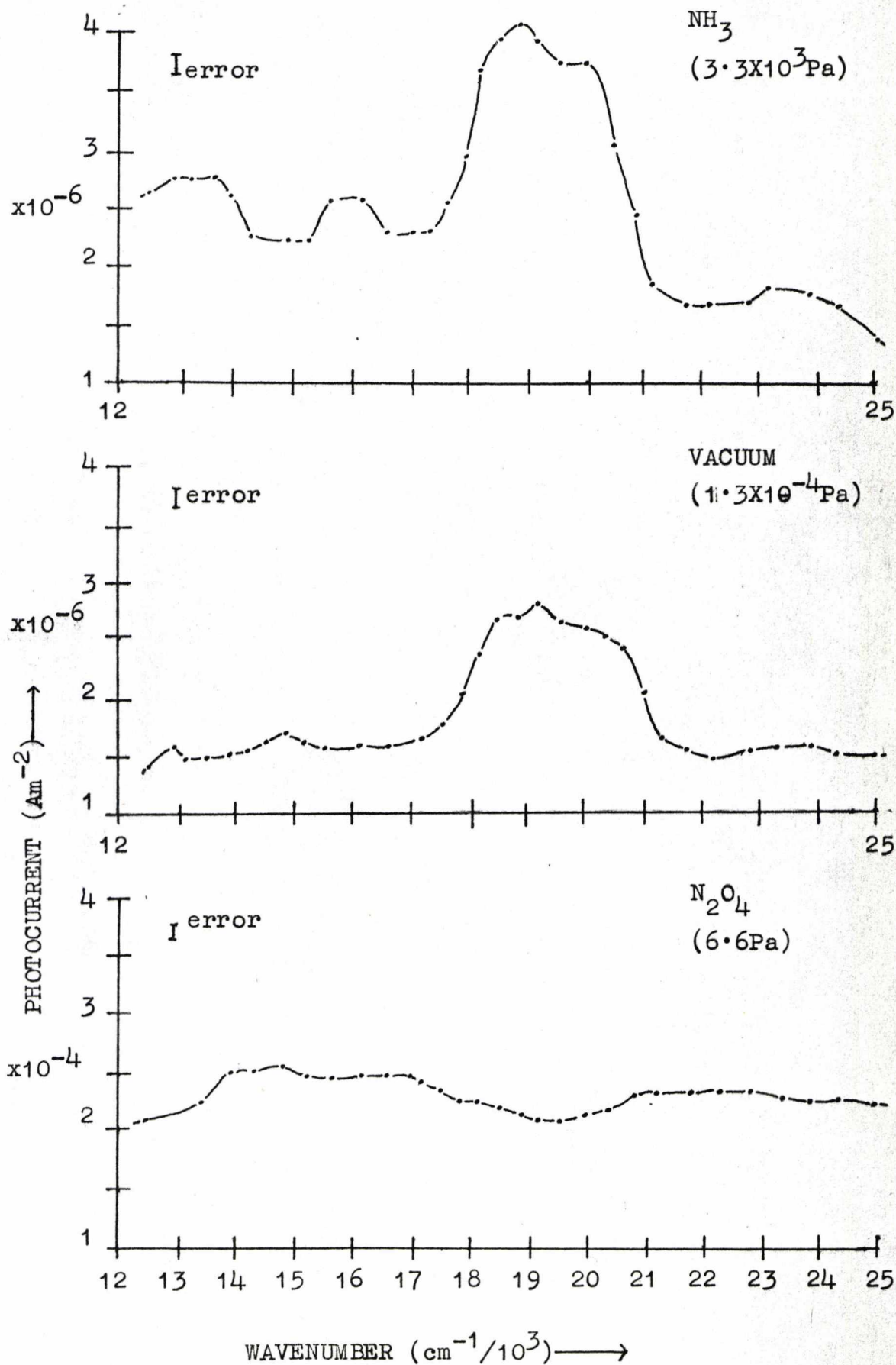
FIG: (5·25) PHOTOCONDUCTION SPECTRA OF ZINC PHTHALOCYANINE IN VARIOUS AMBIENTS.
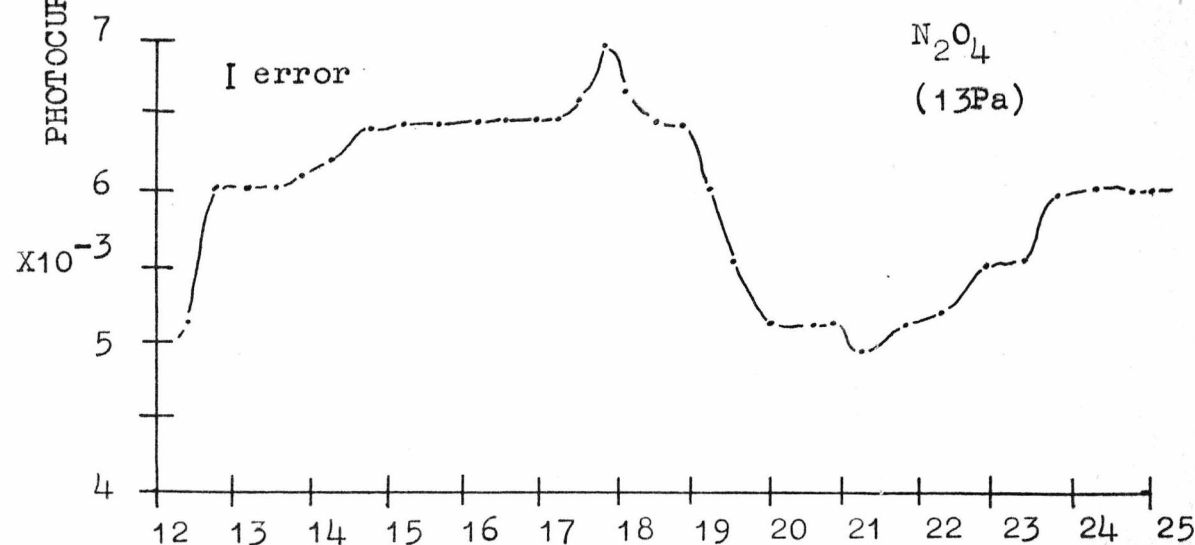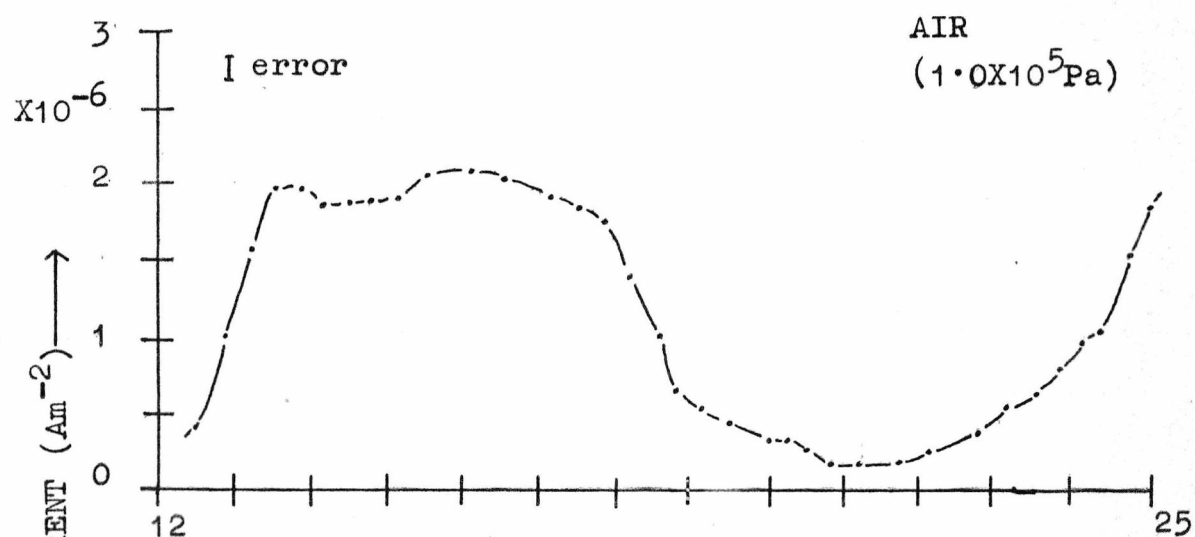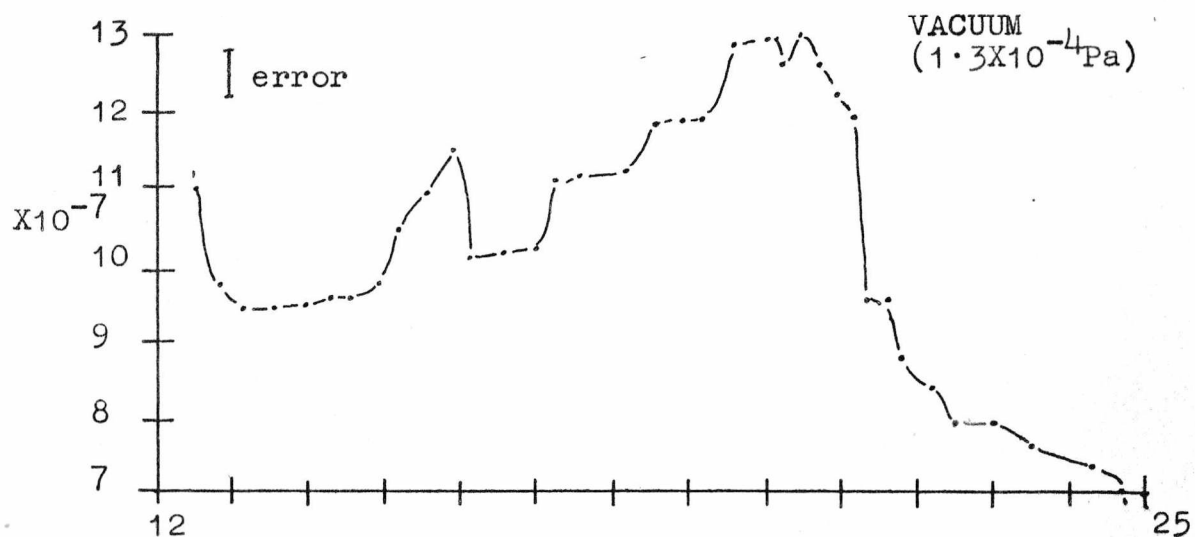
FIG: (5·26) PHOTOCONDUCTION SPECTRA OF COPPER PHTHALOCYANINE IN VARIOUS AMBIENTS.
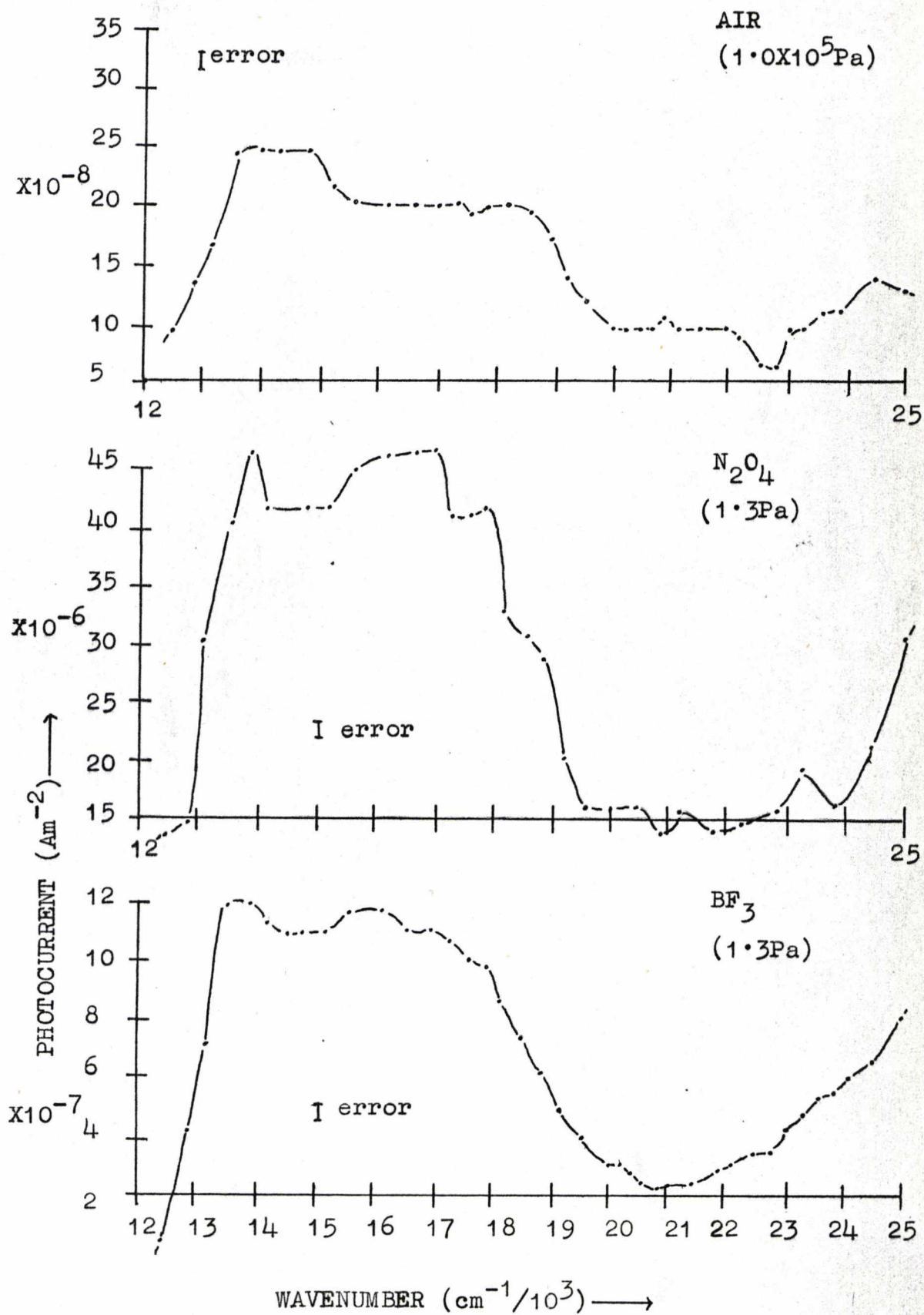
electrode the spectrum obtained had a maximum at 500nm
(approximately) and was similar to the spectra obtained in
a high vacuum in this work. When the illuminated electrode
was positive a minimum in photoconduction was found at about
500nm and the spectrum was similar to that obtained with
copper, zinc and lead phthalocyanines in an ambient of
dinitrogen tetroxide (this work). Furthermore, Popovic and
Sharp found that the photoconduction spectrum was enhanced
by prolonged exposure to oxygen (a weak electron acceptor).
A similar effect was noticed in this work, especially for
lead phthalocyanine (cf. section (5·11)). Hence the photo-
conduction studies for copper, zinc and lead phthalocyanines
suggested that in the presence of dinitrogen tetroxide (or
other electron acceptor gases) a large excess of 'hole'
charge carriers were produced, thereby enhancing photoconduc-
tion and altering the spectral response. This in turn
confirmed that an acceptor (gas) - donor (crystal) type
interaction was occurring.

By evacuation and heating the effect of the gas on the
photoconductivity could be reduced; however, the photocurrent
still remained greatly enhanced (approximately 100 fold)
over the vacuum level and the spectral response remained
much the same (i.e. a minimum at 500nm). As already noted
in section (5·6) the effect of the dinitrogen tetroxide on
the dark resistivity of all the metal phthalocyanines, except
manganese, cobalt and lead, could be removed (to within a
factor of 5 of the vacuum value) by evacuation and heating.
Also, it was concluded from the dark measurements that there
was a distribution in the adsorption energies of the sites,
since some of the gas could be removed by evacuation, more

by evacuation and moderate heating and all of it by evacuation
and heating at 520K. This effect was amplified by the photo-
conduction characteristics since the photocurrent remained
enhanced (10-100 times) and the spectral response remained
unaltered even after a 12 hour evacuation period at 520K.

5·9 Effect of dinitrogen tetroxide on the intensity dependence
of photoconduction

These measurements were carried out at three different
wavelengths for copper, zinc and lead phthalocyanines and the
results are presented in figures (5·27), (5·28) and (5·29)
and are tabulated in table (5·7).

TABLE (5·7)

phthalocyanine	wavelength nm	intensity dependence
Copper	700	0·10
	512	0·15
	450	0·10
Zinc	700	0·09
	600	0·05
	475	0·20
Lead	600	0·26
	500	0·27
	450	0·23

Comparison of these values with those obtained in a vacuum
(cf. table (5·4)) shows that the dependence has been consid-
erably lowered. Furthermore, it can be seen from figure (5·28)
that the intensity dependence tends to zero (i.e. the photo-
current is independent of illumination intensity). In
Chapter (2·10) it was shown that it is possible to have an

136

intensity dependence of 1/3, i.e.

$$Iph \propto L^{1/3} \propto \quad \text{where Iph = photocurrent}$$

$$L \; = \text{illumination intensity.}$$

In the above cases the dependences are well below a third
and the following explanation is offered for this observation.
It has already been suggested (cf. section (5·9)) that when
the phthalocyanine crystal is exposed to dinitrogen tetroxide
a large number of 'hole' carriers are produced; further
evidence for this will be provided in Chapter 6. For each
carrier produced a corresponding electron is trapped.
As previously shown the gas effect is restricted to the
surface of the crystal, hence all of these traps will be on
the surface, as shown in figure (5·30).

FIGURE (5·30)
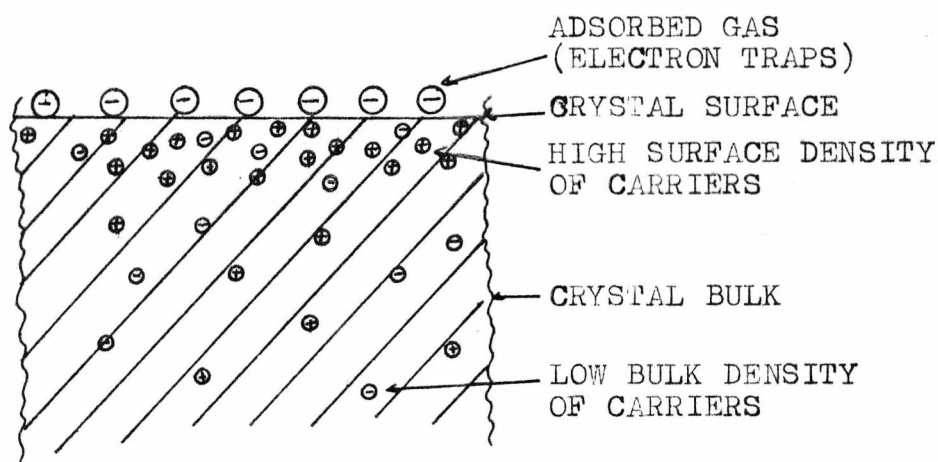
The charge field developed by the surface trapped
electrons decreases the mobility of the 'hole' charge carriers
into the bulk of the crystal. Due to the increased carrier
density, the life time and diffusion length decrease. This
results in an effective desensitisation since the carrier
life time is decreased with respect to the transit time.

FIG: (5·27) PHOTOCURRENT INTENSITY DEPENDENCE PLOTS FOR COPPER PHTHALOCYANINE IN A DINITROGEN TETROXIDE AMBIENT
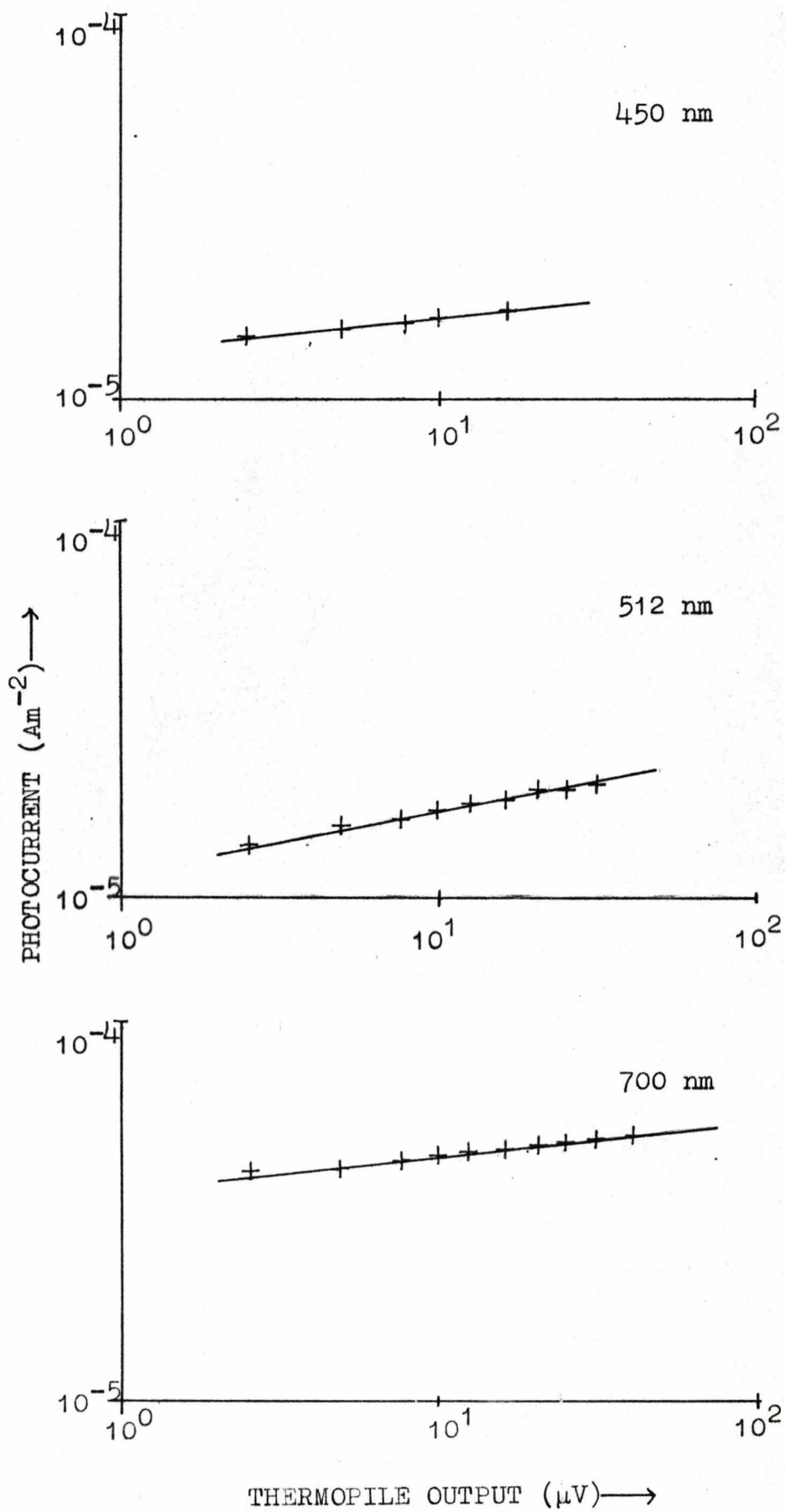
FIG: (5·28) PHOTOCURRENT INTENSITY DEPENDENCE PLOTS FOR ZINC PHTHALOCYANINE IN A DINITROGEN TETROXIDE AMBIENT

450 nm.

500 nm.

600 nm.

PHOTOCURRENT (Am^{-2}) ⟶

THERMOPILE OUTPUT (μV) ⟶
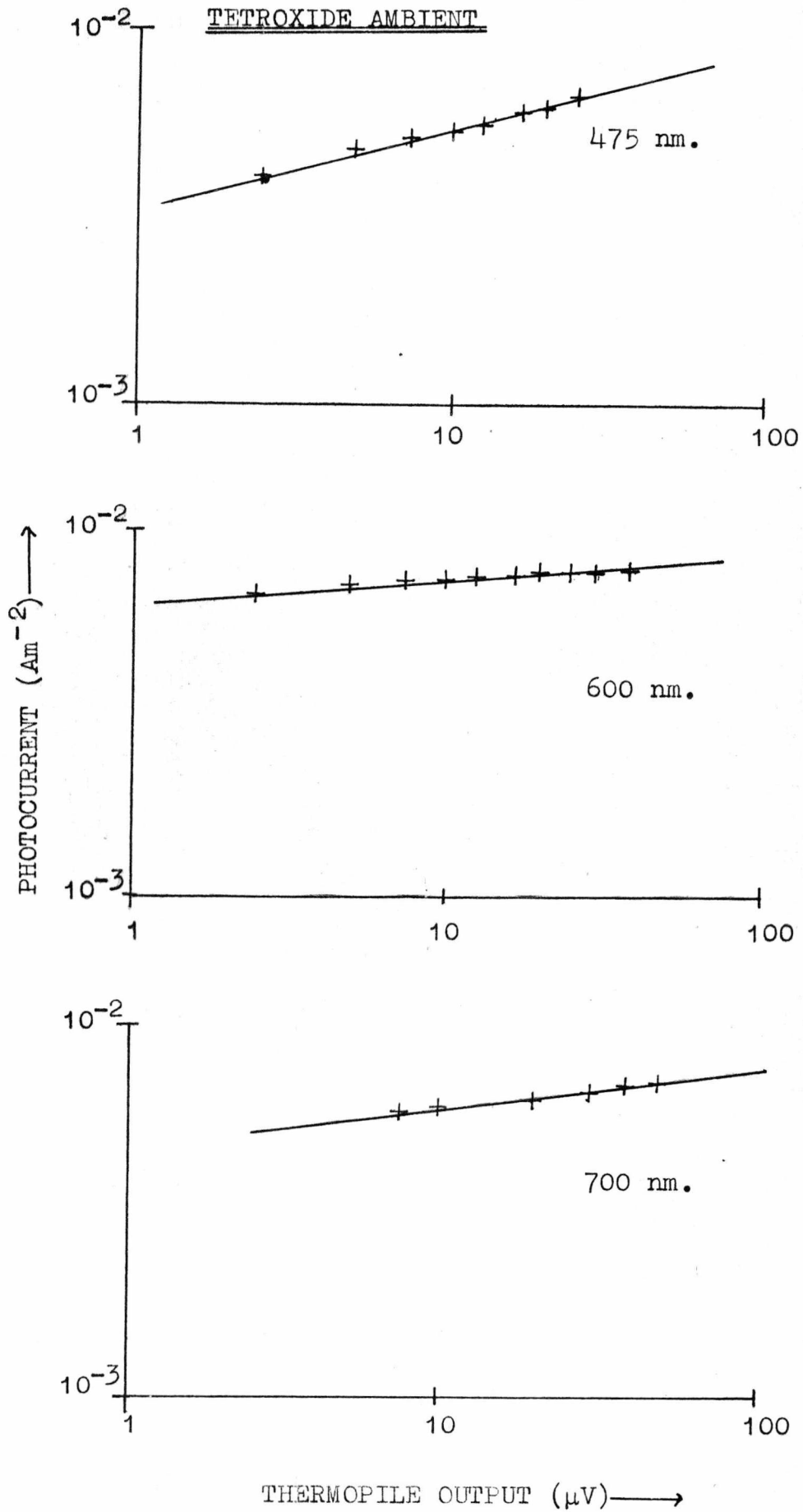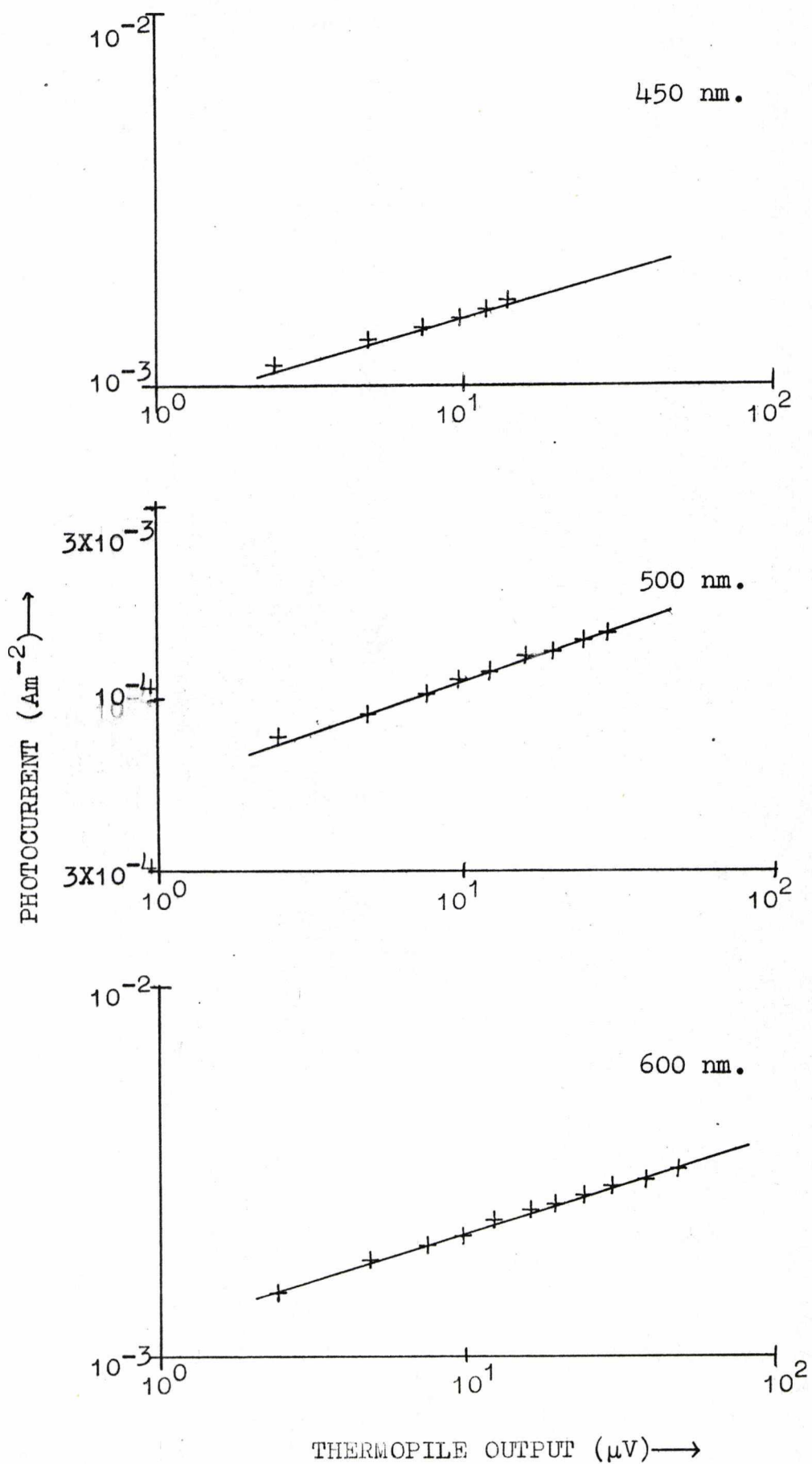
5·10 Effect of ammonia gas on 'clean' crystals

Dried ammonia gas had no effect on the dark resistivity or activation energy of any of the phthalocyanines studied. Since the gas decreased the surface resistivity of the sapphire substrate, as can be seen in Chapter (4·8) and figure (4·8), the pressure of ammonia inside the cell had to be kept low to prevent the substrate interfering with the resistivity measurements. An effect on the photoconduction spectrum was only noted for lead phthalocyanine. By comparison with the vacuum photoconduction spectrum in figure (5·24), it can be seen that this effect was very small and was possibly due to measurement error. Hence it was concluded that ammonia had no effect on the semiconductive and photoconductive properties of the phthalocyanines.

5·11 Effect of ammonia gas on crystals exposed to dinitrogen tetroxide gas

It has been mentioned (cf. sections 6 and 7) that in the case of lead phthalocyanine the dark resistivity and activation energy were irreversibly altered by the effect of dinitrogen tetroxide. Also, all the other phthalocyanines required severe conditions (especially cobalt and manganese), high vacuum and temperatures, to reverse the effect of the gas. The photoconductive properties were irreversibly altered from the vacuum level, even after prolonged evacuation (cf. section 8). It was found that if these crystals were exposed to a small pressure (1 Pa) of dried ammonia gas any residual effects of the dinitrogen tetroxide were removed. This effect was extremely rapid, faster than could be monitored (i.e. less than 10 seconds). The most notable effect was on photoconduction

141

where the spectrum was returned to its vacuum level and shape.

The effect of ammonia on dinitrogen tetroxide exposed crystals was found to be reproducible. Also, the crystals could be cycled ($N_2O_4 \rightarrow NH_3 \rightarrow N_2O_4 \rightarrow$ etc.) without any degradation in the sensitivity towards dinitrogen tetroxide occurring and without altering any of the electrical characteristics. There are two possible explanations for this effect. One is that the ammonia interacts with the dinitrogen tetroxide molecule, breaking the chemisorption bond with the phthalocyanine crystal, leaving an empty site. Or the ammonia interacts in such a manner as to inhibit the dinitrogen tetroxide from affecting the phthalocyanine's photo- and semiconductive properties. The former explanation was found to apply for the following reasons. The crystals could be cycled without affecting the sensitivity towards dinitrogen tetroxide. This would not occur if some of the crystal's surface sites were occupied by inhibited molecules, especially since the most active sites would be occupied. Also, the photospectrum remained unaltered, which would not be expected if some of the sites were being filled irreversibly, since the incident light would be attenuated and this in turn would decrease the level of photoconduction.

In a few cases it was found that the ammonia effect could be removed, to a small degree, by evacuation (i.e. when the ammonia was pumped off, the crystal returned to a decreased resistivity and enhanced photoconduction). However, this only occurred for crystals heated up to reasonably high temperatures (greater than 370K) in dinitrogen tetroxide. It was concluded that in these cases a chemical reaction had occurred between the gas and the crystal. Further evidence was found from the

142

effect of the gas on the activation energies (cf. section 7).
Hence the ammonia effect could be used as a check to see if
an irreversible chemical reaction had occurred between the
crystal and the gas.

5·12 Effect of boron trifluoride on the dark- and photo-properties

It was found that boron trifluoride reacted irreversibly
with the phthalocyanine crystals, decreasing the resistivity
and enhancing the photoconductivity. The pressure dependence
of the response of the crystals is shown in figures (5·31) and
(5·32). It can be seen that the final resistivity was much
higher than that for the dinitrogen tetroxide interaction.
This effect was found to be irreversible with heating and
evacuation. Also, it was found that the effect of ammonia
addition was reversible, on re-evacuation. Hence it was
concluded that a chemical reaction had occurred.

Similarly,the effect on the photoconduction level and
spectral response was irreversible. The magnitude of enhance-
ment was lower by a factor of 10 (approximately) compared
with the effect of dinitrogen tetroxide, as can be seen
in figure (5·26) for copper phthalocyanine. Similar effects,
both in magnitude and spectral response, were found for
zinc and lead phthalocyanines. Figure (5·33) shows the
photoconduction spectrum of lead phthalocyanine after exposure
to boron trifluoride followed by evacuation and heating
(520K) for 12 hours. The spectrum obtained was very similar
to that obtained in boron trifluoride (1·3Pa) initially,
which in turn was very similar to that obtained for copper
phthalocyanine (in 1·3Pa of BF_3) as shown in figure (5·26).

143

FIG: (5·33) <u>PHOTOCONDUCTION SPECTRA OF LEAD PHTHALOCYANINE</u>
<u>IN VARIOUS AMBIENTS.</u>

AIR
$(1 \cdot 0 \times 10^{5} Pa)$

$\times 10^{-6}$

I error

BF_3
(after evacuation
to $1 \cdot 3 \times 10^{-4} Pa$)

I error

PHOTOCURRENT (Am^{-2}) ⟶

$\times 10^{-5}$

WAVENUMBER $(cm^{-1}/10^{3})$ ⟶

144
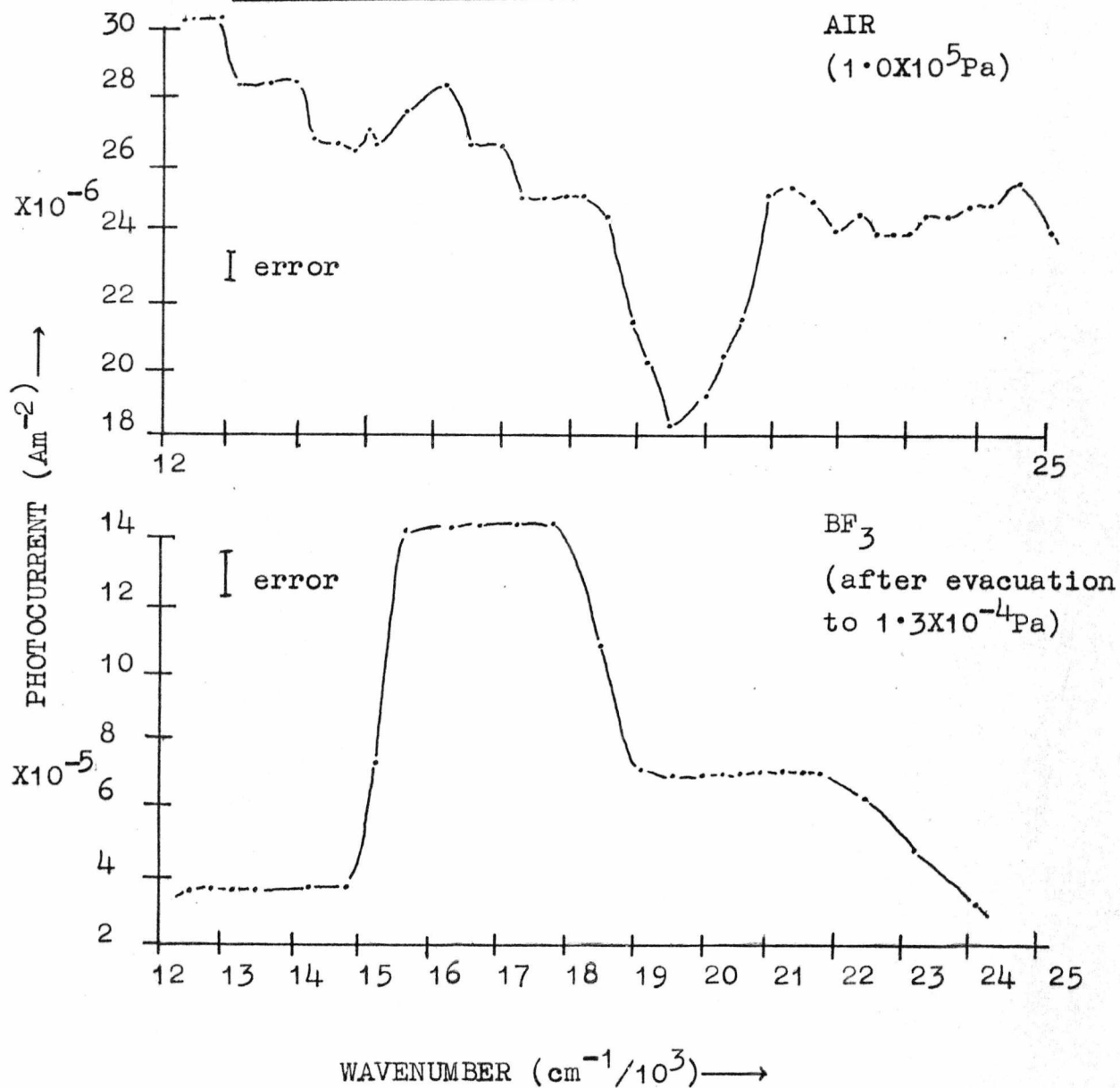
The effect of an ammonia ambient on crystals exposed
to boron trifluoride was to increase the resistivity to
its dark vacuum value. However, on evacuation the resis-
tivity returned to its enhanced level. A similar effect
was found with the photoconduction spectrum. While the
crystal was in an ammonia ambient (10Pa) the photoconduction
spectrum was indistinguishable from that obtained at a high
vacuum; however, on re-evacuation the spectral response
returned to the boron trifluoride level.

It was therefore concluded that boron trifluoride had
an irreversible effect on the dark and photoconduction
properties of all the phthalocyanines studied. This effect
was not predicted with the simple donor-acceptor model for
the gas interaction. Dinitrogen tetroxide has an electron
affinity of $\sim 2\cdot 2$ eV (C. Lifshitz, B.M. Hughes & T.D. Ternan,
1970; J. Berkowitz & W.A. Chupka, 1971) and boron trifluoride
has a value of $0\cdot 65$eV (H.A. Skinner, 1952). Therefore if the
electron affinity was the only crucial factor determining
the bond strength between the crystal and the gas, it would
be predicted that boron trifluoride would be more weakly
bound, which was not found experimentally. Hence there
must be other factors determining the strength of interaction.

The other factor which is of critical importance in
comparing dinitrogen tetroxide and boron trifluoride as
electron acceptors is the nature of the vacant orbital
acting as electron acceptor. Dinitrogen tetroxide forms
a crystalline adduct with 1,4 dioxane, in which the inter-
molecular contact is perpendicular to the N - N bond, sug-
gesting that it is the vacant π^* orbital of N_2O_4 which acts
as the electron acceptor (P. Groth & O. Hassel, 1965).

145

In contrast, boron trifluoride distorts from its original trigonal planar form towards a tetrahedral configuration when it forms complexes with electron donors (J.L. Hoard, S. Geller and T.B. Owen, 1951), and the electron accepting orbital is a non-bonding σ orbital in this electron deficient molecule. Localization of the charge transfer into this specific new σ bond is likely to lead to a stronger bond between phthalocyanine and boron trifluoride than the more diffuse interaction between delocalized π orbitals on phthalocyanine and dinitrogen tetroxide. This strong bond accounts for the irreversibility of the effects of boron trifluoride on electrical properties of phthalocyanines, as well as for the observation that ammonia gas counteracts the electronic effect of boron trifluoride while not releasing the molecules from the crystal surface. Similarly, the lower effect of boron trifluoride on the resistivity of phthalocyanines may be explained, since the positive holes created at the phthalocyanine surface are strongly bound to the negative charges on the associated boron trifluoride molecules, and are therefore less effective as mobile charge carriers. These results, while they represent limitations on the use of phthalocyanines to detect strongly interacting gases, do offer hope for controlling the specificity of gas detectors using molecular crystals.

5·13 Effect of oxygen on the dark- and photo-properties

In an oxygen (dry air) ambient all the phthalocyanines exhibited an enhancement of photoconduction and a decrease in the dark resistivity which was fully reversible on

evacuation and heating. However, this was a very long term effect (in the order of days) and very much smaller than with the other gases (BF_3 and N_2O_4). The photoconduction spectra for copper, zinc and lead phthalocyanines, after exposure to dry air for 28 hours, are shown in figures (5·25), (5·26) and (5·33). By comparison with the spectra obtained in a dinitrogen tetroxide ambient (figures (5·24), (5·25) and (5·26)) it can be seen that the spectrum shape after exposure to oxygen is essentially the same, although the level of enhancement is much lower. The intensity dependences of photoconduction were also lower than in a vacuum, although not as low as in a dinitrogen tetroxide ambient, as can be seen by comparison of the results given in tables (5·8), (5·7) and (5·4) (oxygen, dinitrogen tetroxide and vacuum ambients respectively). The intensity dependence plots are reproduced in figures (5·34), (5·35) and (5·36).

The effect of oxygen on lead phthalocyanine was studied in more detail. In this case the dark resistivity and photoconduction spectra were noted at various times. Figure (5·37) shows the effect on the photoconduction spectrum and the gradual change can be clearly seen. Since the effect of oxygen on the dark resistivity was very slow it was postulated that this was due to oxygen diffusing into the bulk of the crystal. To test this the change in the dark resistivity was monitored as a function of time. A plot of change in dark current v. $\sqrt{time}$ (figure (5·38))was reasonably linear, as expected from Fick's law of diffusion for a process controlled by diffusion rates. It should be noted, as in the case of dinitrogen tetroxide chemisorption studies on copper phthalocyanine, that it has been assumed that the

147

FIG: (5·34) PHOTOCURRENT INTENSITY DEPENDENCE PLOTS FOR COPPER PHTHALOCYANINE IN DRY AIR

450 nm. (22222 cm^{-1})

500 nm. (20000 cm^{-1})

600 nm. (16670 cm^{-1})

THERMOPILE OUTPUT (μV) ⟶

148
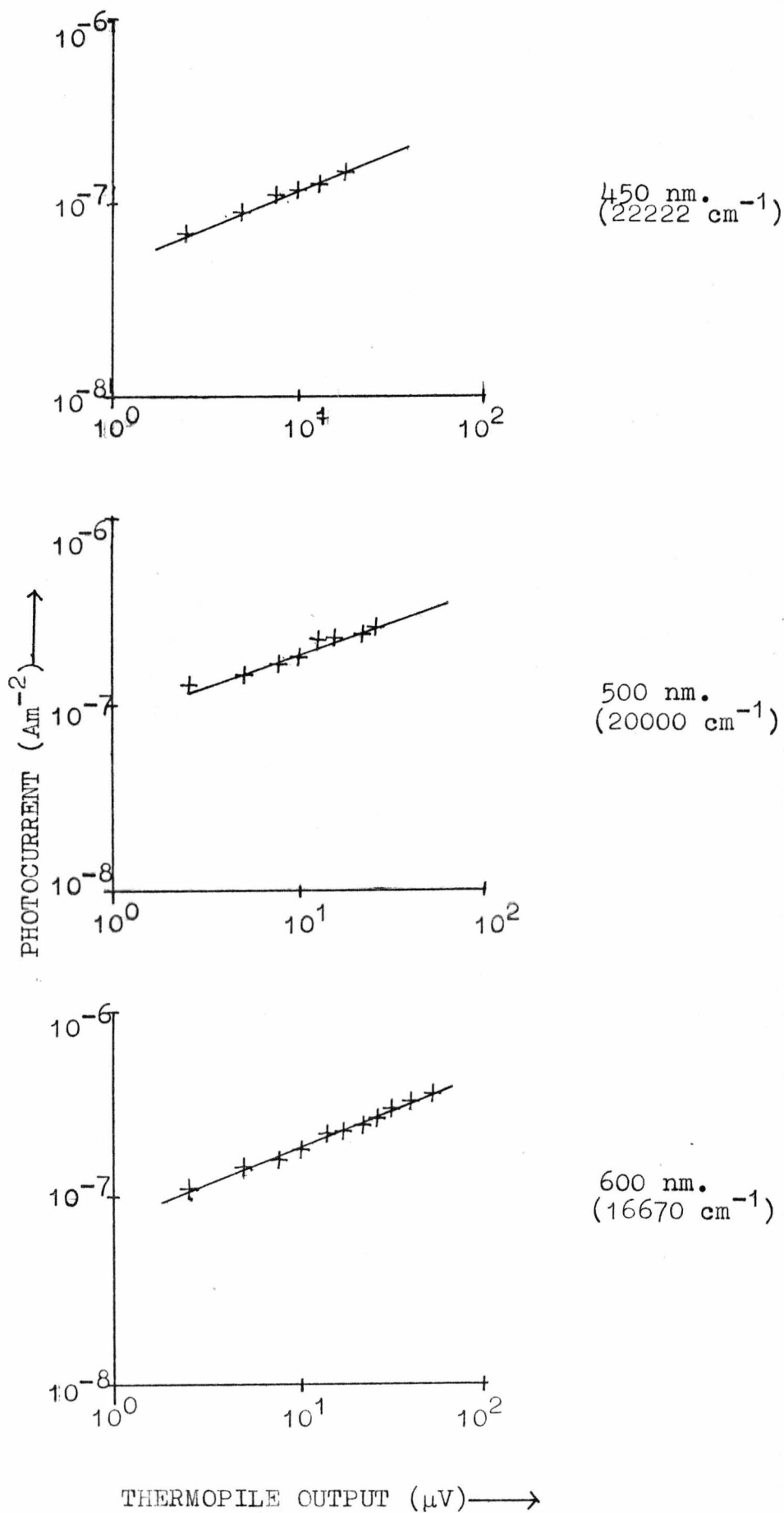
FIG: (5·35) PHOTOCURRENT INTENSITY DEPENDENCE PLOTS FOR LEAD PHTHALOCYANINE IN DRY AIR
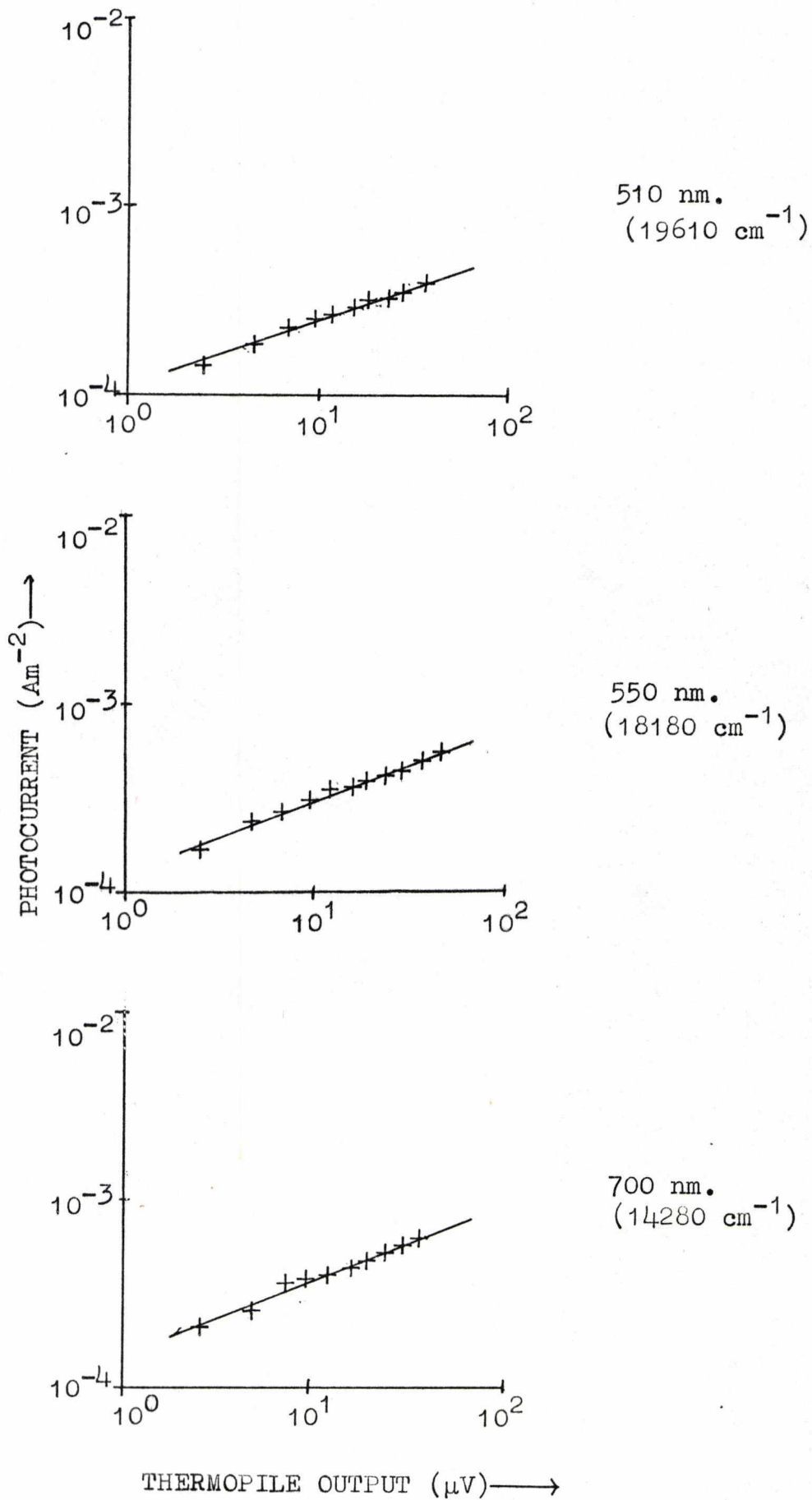
FIG: (5·36) PHOTOCURRENT INTENSITY DEPENDENCE PLOTS FOR ZINC PHTHALOCYANINE IN DRY AIR

475 nm.
(21050 cm^{-1})

520 nm.
(19230 cm^{-1})

700 nm.
(14280 cm^{-1})

PHOTOCURRENT (Am^{-2}) →

THERMOPILE OUTPUT (μV) →

150
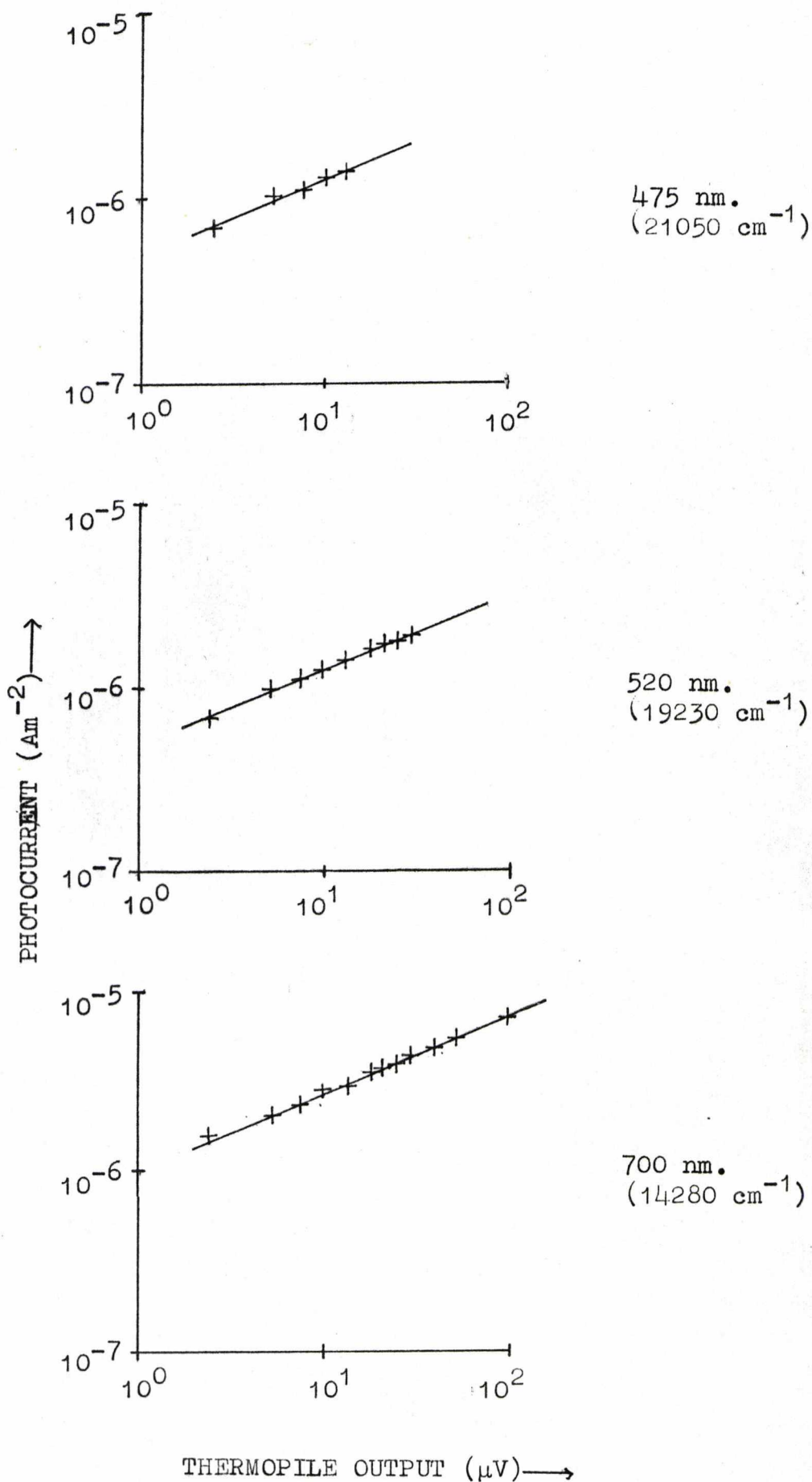
FIG: (5·37) LEAD PHTHALOCYANINE PHOTOCONDUCTION SPECTRA IN AN AIR AMBIENT FOR VARIOUS EXPOSURE TIMES.

EXPOSURE TIMES:

1: 3 hrs
2: 25 hrs
3: 49 hrs
4: 70 hrs
5: 93 hrs
6: 160 hrs
7: 243 hrs after heating to 420K

PHOTOCURRENT ($A\ m^{-2}$) →

WAVENUMBER ($cm^{-1}/10^3$) →

$\sqrt{T}$ x 10^2 (SECONDS)⟶
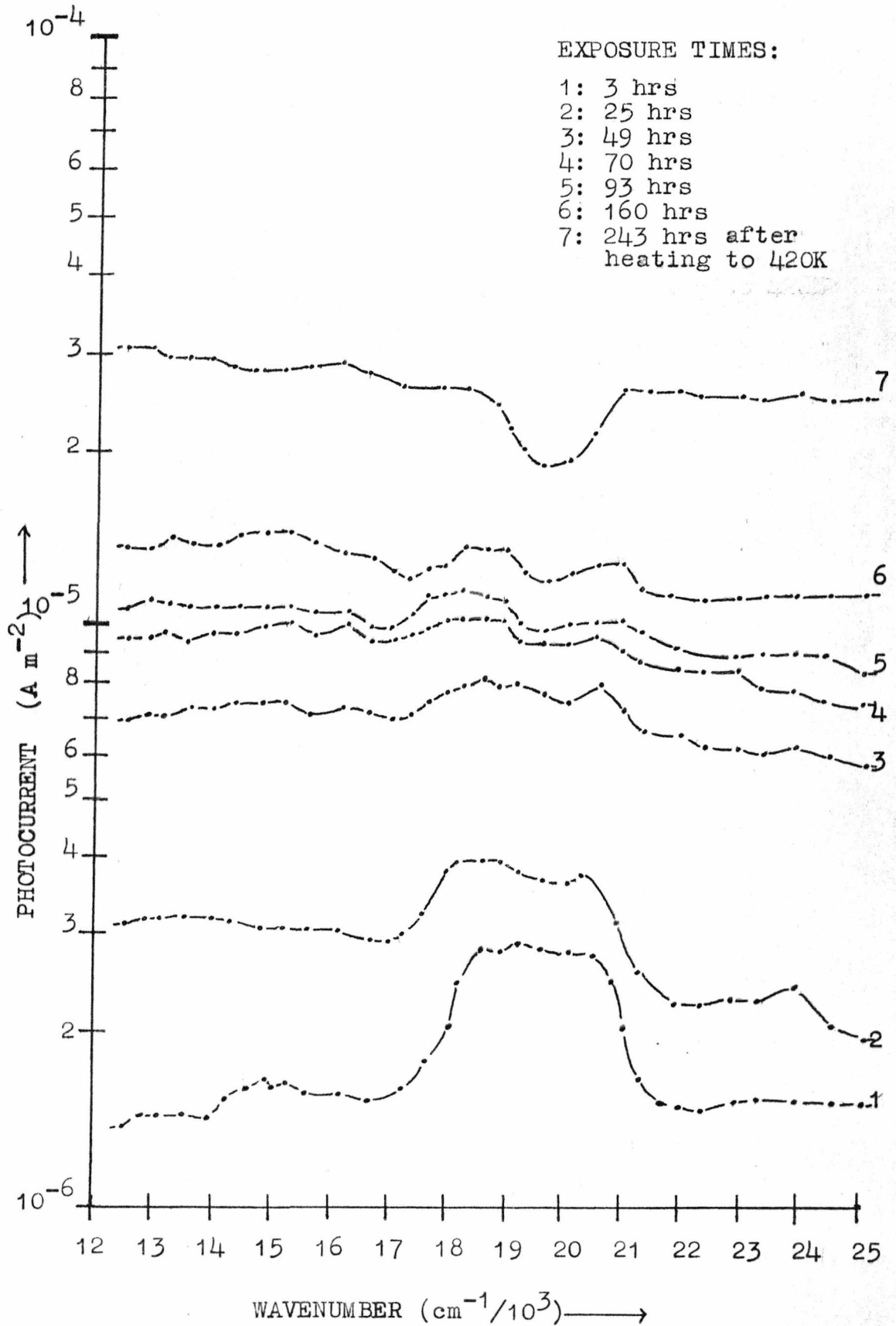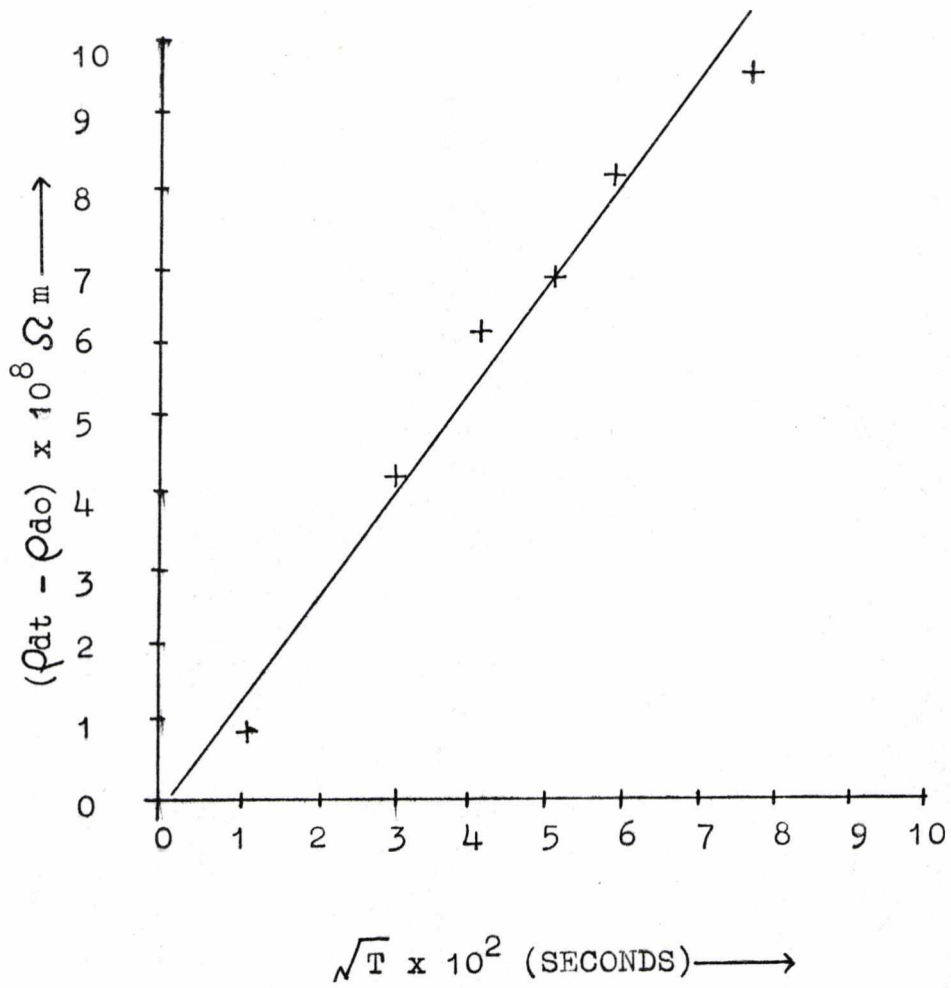
change in resistivity accurately represents the amount of
gas adsorbed. With this in mind figure (5·38) shows that
diffusion of oxygen into the bulk of the lead phthalocyanine
crystal was occurring. More detailed studies of oxygen
diffusion into lead phthalocyanine single crystals have
been made by H. Yasunaga, K. Kojima and H. Yohda (1974).
They found the diffusion process was very slow, even at an
elevated temperature of 515K; the diffusion constant was
found to be $7 \cdot 2 \times 10^{-13} m^2 s^{-1}$ (at 515K) with an activation
energy of $1 \cdot 4eV$. Since the diffusion of oxygen molecules
into the bulk of phthalocyanine crystals is so slow it is
expected that the much larger dinitrogen tetroxide or boron
trifluoride molecules cannot diffuse into the crystal.

TABLE (5·8)

phthalocyanine	wavelength nm	intensity dependence
copper	450	0·35
	500	0·28
	600	0·35
lead	510	0·35
	550	0·38
	700	0·40
zinc	475	0·34
	520	0·38
	700	0·35

5·14 Quantum yield parameters

The quantum yield parameters were calculated using
equation (2·9).

$$Q.Y. = \frac{2 \times Iph}{eLA} \qquad \dots \text{ equation } (2 \cdot 9)$$

where: Iph = photocurrent

e = electronic charge

L = separation between electrodes

A = illumination area.

The full derivation is given in Chapter (2·8). One of the basic assumptions used in the derivation is that recombination loss of the charge carriers is equal to the loss at the electrodes. This assumption is true if the intensity dependence of photoconduction is 0·75 (for a single photon excitation process). In the case of the phthalocyanines the intensity dependence, in a vacuum, was usually nearer 0·5. When the crystals were exposed to dinitrogen tetroxide (or any other electron acceptor gas) the intensity dependence of photoconduction was reduced to below 0·5 (down to 0·1 in the case of zinc phthalocyanine in dinitrogen tetroxide). Hence the assumption that the recombination and electrode loss of charge carriers are equal is invalid; in fact recombination predominates. The effect of the breakdown of this assumption is that the calculated quantum efficiencies are lower than the true value. However, despite this incorrect assumption the quantum yields are listed in table (5·9) and it can be clearly seen that the efficiency of photoconduction was enhanced by electron acceptor gases. In fact the extent of enhancement followed the same trend as that for the dark conductivity (i.e. dinitrogen tetroxide had a much larger effect than oxygen).

Also, by looking at the wavelength dependence of this

TABLE (5·9)

PHTHALOCYANINE	AMBIENT	ILLUMINATION WAVELENGTH λ nm	QUANTUM YIELD PARAMETER
Lead	VACUUM (1×10^{-4} Pa)	700	$2 \cdot 1 \times 10^{-5}$
		512	$5 \cdot 8 \times 10^{-5}$
		450	$3 \cdot 3 \times 10^{-5}$
	AIR ($1 \cdot 03 \times 10^{5}$ Pa)	700	$4 \cdot 0 \times 10^{-4}$
		512	$3 \cdot 7 \times 10^{-4}$
		450	$5 \cdot 3 \times 10^{-4}$
	N_2O_4 (13Pa)	700	$2 \cdot 4 \times 10^{-2}$
		512	$1 \cdot 9 \times 10^{-2}$
		450	$3 \cdot 9 \times 10^{-2}$
Copper	AIR ($1 \cdot 03 \times 10^{5}$ Pa)	700	$3 \cdot 4 \times 10^{-6}$
		512	$2 \cdot 5 \times 10^{-6}$
		450	$1 \cdot 7 \times 10^{-6}$
	N_2O_4 (13Pa)	700	$6 \cdot 1 \times 10^{-4}$
		512	$3 \cdot 3 \times 10^{-4}$
		450	$3 \cdot 1 \times 10^{-4}$
Zinc	VACUUM (1×10^{-4} Pa)	700	$1 \cdot 7 \times 10^{-6}$
		512	$2 \cdot 5 \times 10^{-6}$
		460	$2 \cdot 0 \times 10^{-6}$
	AIR ($1 \cdot 03 \times 10^{5}$ Pa)	700	$2 \cdot 4 \times 10^{-5}$
		512	$1 \cdot 1 \times 10^{-5}$
		460	$7 \cdot 7 \times 10^{-5}$
	N_2O_4 (13Pa)	620	$1 \cdot 0 \times 10^{-1}$
		500	$1 \cdot 0 \times 10^{-1}$
		460	$1 \cdot 1 \times 10^{-1}$

parameter (cf. table (5·9)) it can be seen that, in a vacuum
environment, the quantum yield is greatest at minimum photon
absorption. This effect was discussed in section (5·4),
as was the effect of an electron acceptor gas on the quantum
yield parameter.

5·15 Effect of other gases and vapours

Two other gases were used in this study, namely carbon
monoxide and ethylene. Neither of these had any effect on
the dark or photoconductive properties of lead phthalocyanine.
This is in agreement with the other results since both of
these gases are neutral and hence would not promote a donor-
acceptor type interaction. A series of substituted pyridines
(2,4,6 collidine, 2,6 lutidine and α, β and γ picolines) were
also used in this study. Since these molecules are all
electron donors it was predicted that they would have no
effect and this was found to be the case. Finally lead
phthalocyanine was exposed to tetracyanoethylene vapour
(T.C.N.E. has an electron affinity of 2·8 eV), an electron
acceptor, and it was predicted that there would be an enhance-
ment of conduction. However, none could be found. This was
probably due to the very small amount of vapour present (<1Pa).

5·16 Effect of dinitrogen tetroxide on lead phthalocyanine
films

In a practical device employing an organic semiconductor
for gas detection, a film rather than a single crystal would
be more suitable as the detecting element. A film would be
easier to mass-produce than single crystals as well as giving
larger surface area, better mechanical properties and

permitting the use of interdigitated electrodes which would permit easier electrical measurements . Therefore a study was carried out to see if films behaved in a manner similar to crystals, towards dinitrogen tetroxide gas. This work was carried out at the Safety in Mines Research Establishment (Sheffield) using the conductivity apparatus described in detail in Chapter (4·14). With this apparatus the vacuum properties of the films could not be determined. However, the films were placed in a stream of pure, dry argon for 12 hours before any measurements were made. The results obtained using a 'bulk' electrode arrangement (cf. Chapter (3·7) and figure (3·3)) are shown in table (5·10).

TABLE (5·10)

Lead phthalocyanine film	Bulk resistivity ρ(295K) Ωm
1	$1·7 \times 10^7$
2	$1·1 \times 10^7$

These results are similar to those obtained for single crystals (cf. table (5·2)), especially when allowing for the different ambients.

Other films were prepared using a 'surface' electrode arrangement (cf. Chapter (3·7) and figure (3·3)) and these results are presented in table (5·11).

After these initial measurements had been carried out the film was subjected to a flow of dinitrogen tetroxide in nitrogen (500 ppm.). The change in dark conductivity was continuously monitored. It was found that the resistivity

157

TABLE (5·11)

Lead phthalocyanine film	Surface resistivity ρ(295K) Ω per square
3	$7 \cdot 5 \times 10^{12}$
4	5×10^{12}
5	$5 \cdot 8 \times 10^{13}$

equilibrated after a 2 hour period (approximately). These

final resistivities are tabulated in table (5·12); again,

as with the crystals, the surface resistivity was calcu-

lated. It can be seen that a large decrease in the surface

resistivity was obtained (approximately $10^5 - 10^6$). Further-

more, the final resistivity obtained was similar to that

obtained for crystals (cf. table (5·3)).

TABLE (5·12)

Lead phthalocyanine film	Surface resistivity ρ(295K) Ω per square
1	$8 \cdot 8 \times 10^{7}$
5	$2 \cdot 1 \times 10^{7}$

The reversibility of the dinitrogen tetroxide gas effect

was found to be very poor. When the film was flushed with

argon for 12 hours the resisitvity increased by about a factor

of 2. Hence it was concluded that the gas interaction with

the lead phthalocyanine films was similar to that with

single crystals. Further detailed investigations of the

effects of different gases on the electrical properties

of these films were not undertaken during this project, since

uncertainties concerning degree of crystallinity, crystallite

orientation, effective surface area etc. would prevent detailed analysis of the results along the lines of the foregoing treatment of the single crystal data.

5·17 Fitting an isotherm to the dinitrogen tetroxide pressure dependence results

From the pressure dependence curves (cf. figures (5·16) to (5·19)) for dinitrogen tetroxide adsorption onto phthalocyanine crystals, it can be seen that in the pressure range 5 to 50 Pa the log (ρ) - log (P) plots approximate to straight lines (as shown in figures (5·39), (5·40) and (5·41)). If the assumption is made that the surface resistivity (ρ) is directly proportional to the surface coverage (θ), then these results indicate that a Freundlich isotherm (H. Freundlich, 1962) is applicable. This implies that the gas was being chemisorbed onto the crystal's surface and that the heat of adsorption (q) fell logarithmically with increasing surface coverage (θ).

It can be seen from the results that both at high and at low pressures a linear log (ρ) - log (P) dependence is no longer found. This is because of the following reasons. If the logarithmic dependence were to be maintained then at low pressures (as $\theta \rightarrow 0$) it would imply that the heat of adsorption approaches infinity. Hence the breakdown of the logarithmic dependence means that none of the adsorption sites have an infinite energy. The breakdown of the isotherm at high gas pressures indicates that a saturation state is reached.

From the Freundlich and Elovich (cf. section (5·6)) plots the following conclusions may be drawn.

FIG: (5·39) FREUNDLICH ISOTHERMS FOR NICKEL, COPPER AND MANGANESE PHTHALOCYANINES
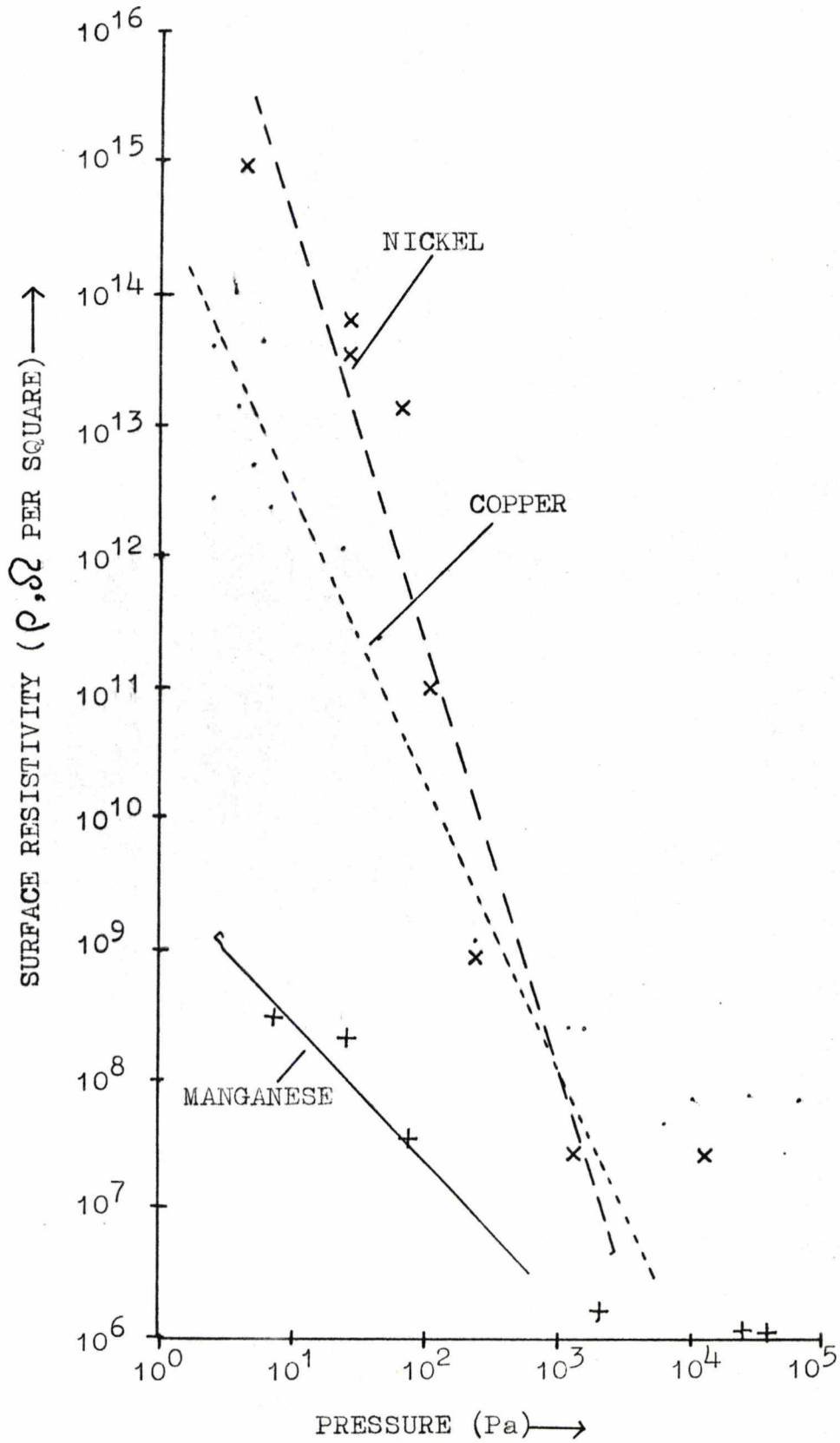
FIG: (5·40)   FREUNDLICH ISOTHERMS FOR METAL FREE AND COBALT PHTHALOCYANINES
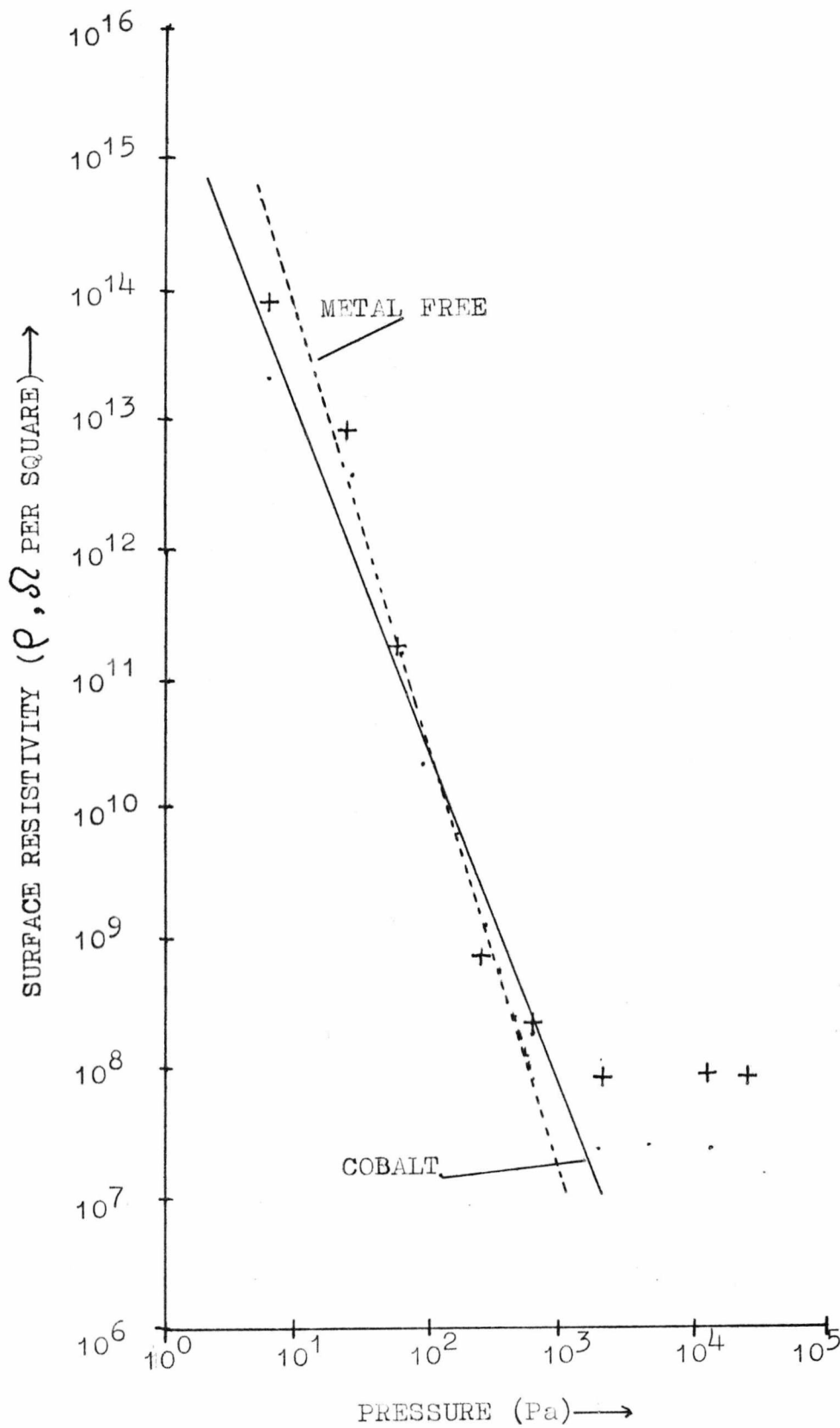
FIG: (5·41) FREUNDLICH ISOTHERMS FOR ZINC AND LEAD
PHTHALOCYANINES
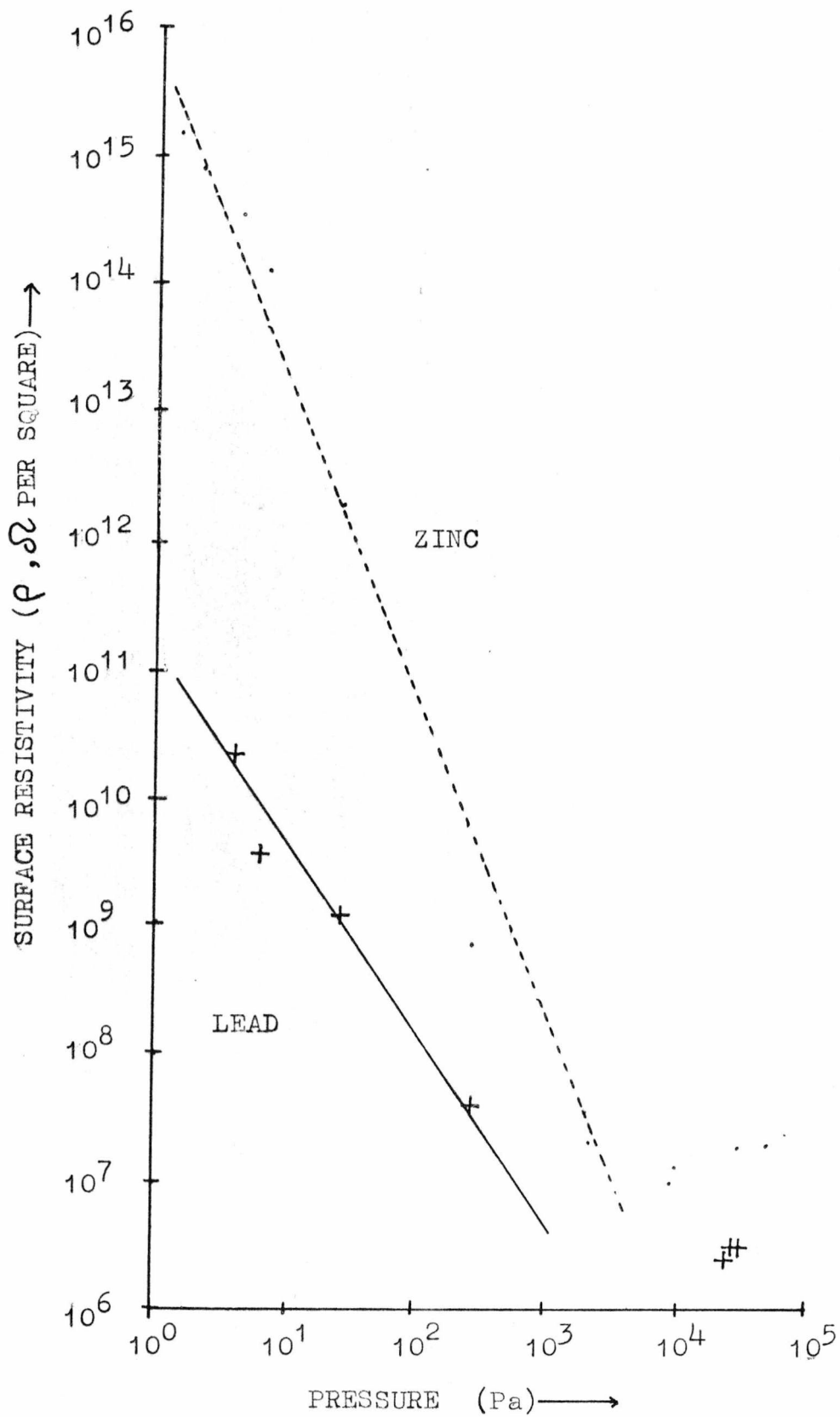
1)   The adsorption of dinitrogen tetroxide onto phthalo-
cyanine crystals is a chemisorption process.

2)   The activation energy (Eg) for the adsorption
process increases linearly with increasing surface coverage.
(i.e. the rate of adsorption follows an Elovich equation).

3)   The heat of adsorption (q) decreases logarithmically
with increasing surface coverage (i.e. the pressure dependence
results could be fitted to a Freundlich isotherm). Figure
(5·42) shows the energy diagram for the chemisorption process.

FIGURE (5·42)
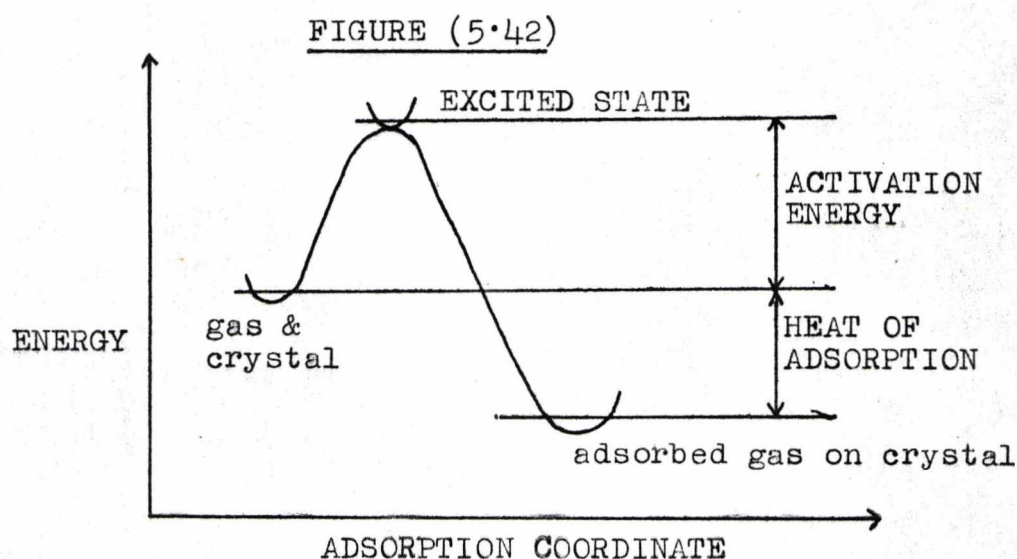
5·18   Comparisons with previous work

Numerous studies on the semiconduction and photoconduc-
tion properties of the phthalocyanines have been carried out
before (e.g. P.E. Fielding and F. Gutmann, 1957; D.R. Kearns,
G. Tollin and L.M. Calvin, 1960; P. Day and R.J.P. Williams,
1962; G.H. Heilmeier and G. Warfield, 1963; P. Day, G. Scregg
and R.J.P. Williams, 1963; J.M. Assour and S.E. Harrison,
1965; K. Gamo, K. Masuda and J. Yamaguch, 1968; F. Gutmann
and L.E. Lyons, 1967). In most of these cases the studies

were carried out under a vacuum or in an inert ambient. The
values obtained in this work for the activation energy and
resistivity are in agreement with the literature values,
as shown in table (5·2). Similarly, the photoconduction
spectra for copper, nickel and metal free phthalocyanines
are in agreement with those recorded by previous workers.
The photoconduction spectrum for lead phthalocyanine
has not been previously recorded.

It was noted in this study that when measurements
were carried out in an oxygen, or air, ambient the dark
resistivity was decreased and the photocurrent was enhanced,
coupled with change in the spectral response. Similar
results have been found previously (e.g. P. Day and
R.J.P. Williams, 1962; J.M. Assour and S.E. Harrison, 1965
and K. Gamo, K. Masuda and J. Yamaguch, 1968). It has
previously been reported (K. Ukei, K. Takamoto and E. Kanda,
1973 and K. Ukei, 1976) that lead phthalocyanine behaves like
a one dimensional conductor; the specific resistivity (295K)
was quoted as being in the region of $10^4 \, \Omega \, m$ with an activation
energy (ΔE) of 0·66 eV. However, in this work no evidence
could be found to support this claim.

Few workers have looked specifically at the effect
of gases on the phthalocyanines. The major studies were
carried out by J. Kaufold and K. Hauffe , 1964 and G.J.
van Oirschot, D. van Leeuwen and J. Medema, 1972. In both
cases sublimed phthalocyanine films were used and conse-
quently an accurate determination of the surface area
(cf. section (5·16)) was impossible. Furthermore, neither
study corrected the results for surface (or bulk) resistivities,

but presented the data in terms of dark current (dependent on the applied voltage and sample geometry).

G.J. van Oirschot et al. only studied metal free phthalocyanine and β carotene. They found, for phthalocyanine, that many gases enhanced the dark conductivity, especially dinitrogen tetroxide and chlorine; a similar effect was noted in this work. However, they also found that ammonia enhanced the conduction, an effect not observed or predicted in this work. Pressure dependence studies for various gases (sulphur dioxide, ammonia, water vapour and 'wet' air) were studied; however, no attempt was made to relate the data to an isotherm.

The photoconductive measurements were limited in that only white light was used. Also, only the effects of ammonia, vacuum and air on the photoresponse were studied. It should also be noted that only one phthalocyanine film was used in the gas effects studies and the contacts to this film were non-Ohmic (i.e. the log (current-voltage) plot had a slope of less than unity).

The second group, J. Kaufhold and J. Hauffe., studied the effects of oxygen, nitrogen oxide, dinitrogen tetroxide, and ammonia on the conductivity of iron, cobalt, nickel, copper and metal free phthalocyanine films. In this case the studies were usually carried out at an elevated temperature and it was found that the conductivity was increased markedly by nitrogen oxide and dinitrogen tetroxide. However, in all the cases this enhancement was found to be irreversible by evacuation. This latter effect was not observed in this work for dinitrogen tetroxide except when lead phthalocyanine crystals were used. Kaufhold and

Hauffe did find that addition of a small amount of ammonia would return the conductivity back down to its previous vacuum level. Some activation energy studies, for the phthalocyanines in gases, were also carried out and these measurements are roughly in agreement with those obtained in this work, as shown in table (5·13).

TABLE (5·13)

Phthalocyanine	Activation energy (ΔE) in N_2O_4 eV	
	This work	Kaufhold & Hauffe
metal free	0·15	0·075
copper	0·17	0·10
zinc	0·17	reaction
cobalt	0·22	–
nickel	0·10	–
lead	0·28	–

The photoconduction studies were measured by illuminating the sample at 650±20nm. The photocurrent was found to be enhanced in an oxygen ambient for copper, zinc and metal free phthalocyanines.

In this work great care has been exercised in obtaining pure single crystals and in thoroughly drying all the gases. Therefore, hopefully, the possibility of the effects of impurities and contaminants was eliminated. The following improvements have been made over previous gas studies.

1) Single crystals were used, thereby eliminating the surface area measurement errors.

2) All the results were corrected for surface (or bulk) geometry. It was therefore possible to compare results easily.

166

3) Results were obtained to confirm the type of adsorption occurring.

4) Information was obtained about the extent of surface coverage.

5) Photoconduction spectra and intensity dependence results were used to obtain further information about the surface conduction mechanism.

6) A whole series of metal phthalocyanines was used so that the effect of altering the metal atom could be studied.

7) Initially, the crystals were evacuated and heated to ensure that the crystals' surfaces were free from gases.

5.19 Conclusions

The main conclusions of the work on phthalocyanine single crystals are listed below.

1) From the vacuum dark measurements it was found that bulk conductivity predominated (by at least a factor of 50). It is also probable that conduction was occurring via an extrinsic mechanism, since the calculated activation energy was very much higher than that found for any of the phthalocyanines. The mobility calculations indicated that either mechanism could be occurring.

2) The photoconductive measurements carried out in a vacuum indicated that the majority carriers were electrons and the excitation process occurred via a single photon.

3) Dinitrogen tetroxide, even at low pressures, was shown to decrease the resistivity and activation energy dramatically. With the guard ring experiments it was shown conclusively that the interaction was entirely restricted

to the surface of the crystal. From the 'surface coverage'
calculation it was found that the crystals were nearly 100%
covered and each site was 100% (approximately) ionized.
Since the response of metal free phthalocyanine was similar
to the other phthalocyanines, it was shown that the metal
had very little effect on the sensitivity. However, an effect
was found on the strength of adsorption (the more oxidizable
metals formed stronger chemisorption bonds with the gas).
Finally, with copper phthalocyanine it was demonstrated that
gas adsorption occurred via a chemisorption process.

4) From the study of the photospectra in dinitrogen
tetroxide ambients it became apparent that a vast majority
of hole carriers were created near the surface, by the gas.
Also, the photoconduction characteristics proved to be
very sensitive to small amounts of gas.

5) None of the donors used had any effect on the
conductive properties of the crystals.

6) Ammonia could be used to reverse the effect of
dinitrogen tetroxide on crystals.

7) From the boron trifluoride gas effect study it
became apparent that the type of orbital involved in the
chemisorption bond was important.

8) Oxygen had a small and easily reversible (evacua-
tion and heating) effect on the crystals. Furthermore, it
was found that the gas diffused into the bulk of lead
phthalocyanine crystals.

9) From the study of lead phthalocyanine films it
became apparent that these behaved in a manner similar to
single crystals towards dinitrogen tetroxide gas.

CHAPTER 6

The Effect of Gases on the Semiconduction and
Photoconduction of Some Molecular Complexes,
Donor and Acceptor Single Crystals

6·1 Introduction

As with the phthalocyanines the single crystals were mounted on the sapphire substrate using the 'spring electrode' technique (cf. Chapter (4·12)). Preliminary measurements were carried out to ensure that the electrical contacts were Ohmic and non-photovoltaic. The materials studied were: anthracene, benzidine-TCNQ, bis [-cis-3,4-bis(trifluoromethyl)-1,2-dithiete] nickel$^\circ$, copper oxinate, palladium oxinate, perylene, perylene-TCNQ, phenanthrene and TCNQ. Purification and crystal growth of these materials are discussed in Chapter 3.

From the study of the gas effects on phthalocyanine crystals it was concluded that the main interaction was that of a donor-acceptor type. The work presented in this chapter supports this conclusion and also gives further insight into other influencing factors.

6·2 Effect of gases on the dark conductivity of perylene crystals

Before the effects of any gases were studied the semiconduction properties were measured under a high vacuum. These measurements were carried out after the crystals had been evacuated at 1·3 X 10^{-4} Pa at 380K for a 12 hour period. (The maximum temperature to which the perylene crystals could be heated was much lower than with the phthalocyanines; this was due to the higher volatility.)

169

After the initial evacuation period, to ensure a 'clean'
surface, the Ohmic characteristics and activation energy
(ΔE) were measured. These two results are shown in figures
(6·1) and (6·2) respectively. It should be noted that these
measurements were carried out for three different crystals;
however, in each case the results were identical (within
experimental error). Hence the results are only shown for
one crystal(perylene 2). The averaged values of the dark
activation energy, pre-exponential factor and the room
temperature bulk resistivity are listed in table (6·1)
together with some literature values for single crystals
and compressed pellets. The estimated error for the acti-
vation energy was $\pm 0 \cdot 05$eV and 100% for the pre-exponential
factor.

After the electrical characteristics had been measured
in a vacuum the crystals were exposed to various gases.

TABLE (6·1)

Activation Energy ΔE eV	Pre-exponential Factor ρ_0 Ω m	Resistivity $\rho(295)$ Ωm	Reference
0·98	$2 \cdot 7 \times 10^{-5}$	$1 \cdot 5 \times 10^{12}$	This work
1·05	$7 \cdot 5 \times 10^{-5}$	$6 \cdot 5 \times 10^{13}$	M. Sano and H. Akamatu, 1961
1·00	$8 \cdot 2 \times 10^{-2}$	$1 \cdot 0 \times 10^{16}$	(compressed pellet) H. Inokuchi, H. Kuroda and H. Akamatu, 1961

FIG: (6·1)   OHMIC PLOT FOR PERYLENE IN A VACUUM AT 295K

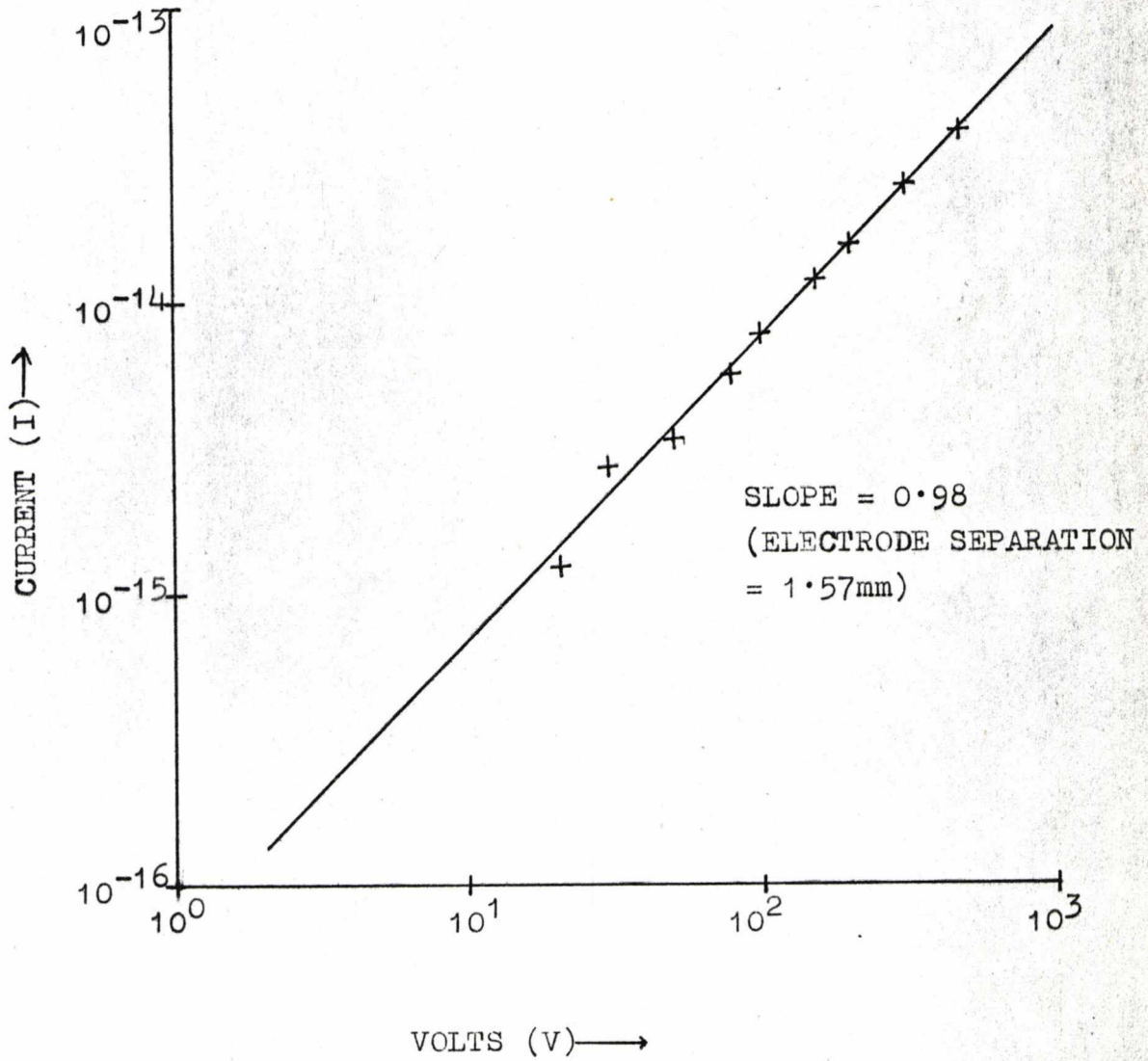SLOPE = 0·98
(ELECTRODE SEPARATION = 1·57mm)

VOLTS (V)⟶

CURRENT (I)⟶
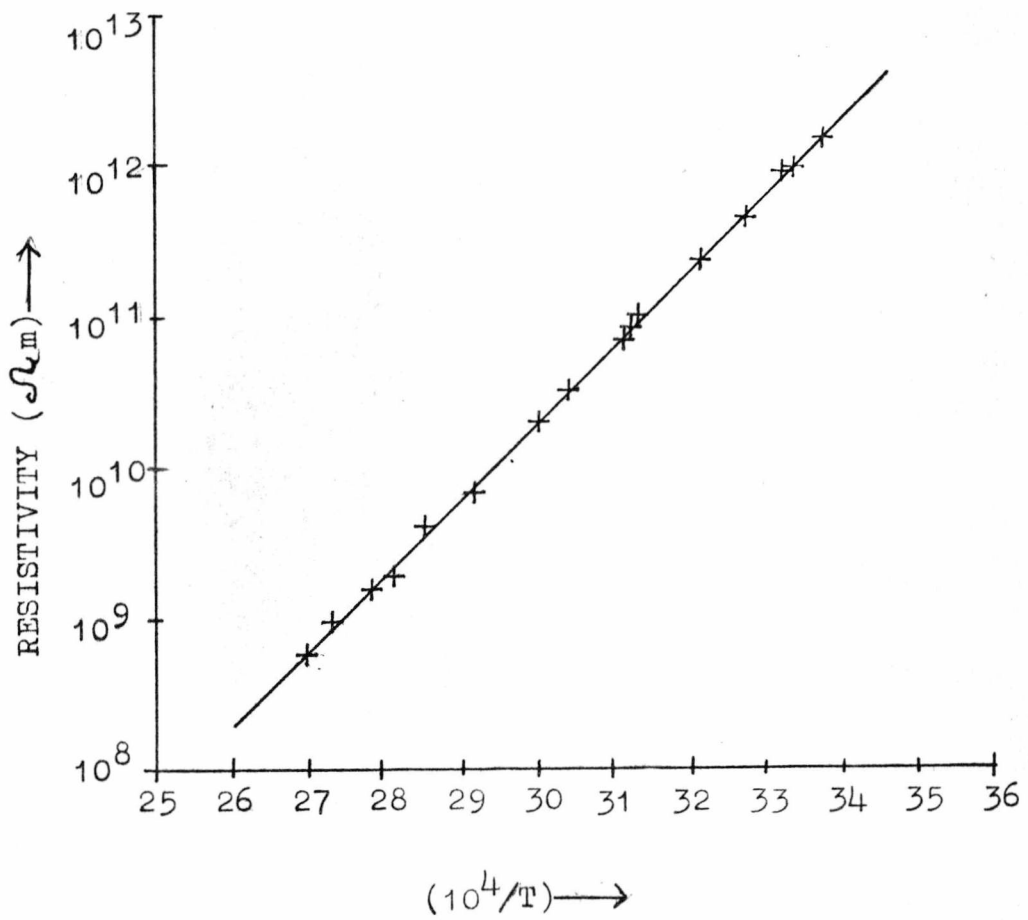
a) Effect of dinitrogen tetroxide

As with the phthalocyanines the amount of gas present in the cell was increased by small amounts from 1 Pa up to a maximum of approximately 5×10^4 Pa. The change in the resistivity of the crystal was continuously monitored and the steady state resistances were noted for fixed gas pressures. The results were then calculated in terms of surface resistivity (cf. Chapter (5·6)). These results (combined for two different crystals) are shown in figure (6·3). It was found that the effect of the gas could be readily removed by evacuation. Also, the response time of the perylene crystals to dinitrogen tetroxide was considerably longer (30 to 45 minutes) than in the case of the phthalocyanines (cf. Chapter (5·6)). Furthermore, the minimum resistivity ($\sim 6 \times 10^{12} \Omega$ per square) was higher than that obtained for the phthalocyanines, under similar conditions ($\sim 10^7 \Omega$ per square). These observations, coupled with the lower sensitivity of perylene to the gas (i.e. the rate of change of surface resistivity with respect to the change in gas pressure was lower; cf. figure (6·3)), suggest that the interaction between the gas and crystal was much weaker than for the phthalocyanines.

b) Effect of boron trifluoride

This study was carried out in a similar manner to that for the dinitrogen tetroxide case (cf. section (6·2a)). For comparison purposes, these results are shown together with the dinitrogen tetroxide effect in figure (6·3). It can be seen that boron trifluoride had a large effect on the surface resistivity of perylene. However, unlike dinitrogen tetroxide, this effect could not be removed by

FIG: (6·3)   EFFECT OF DINITROGEN TETROXIDE AND BORON TRIFLUORIDE ON THE DARK RESISTIVITY OF PERYLENE.

174
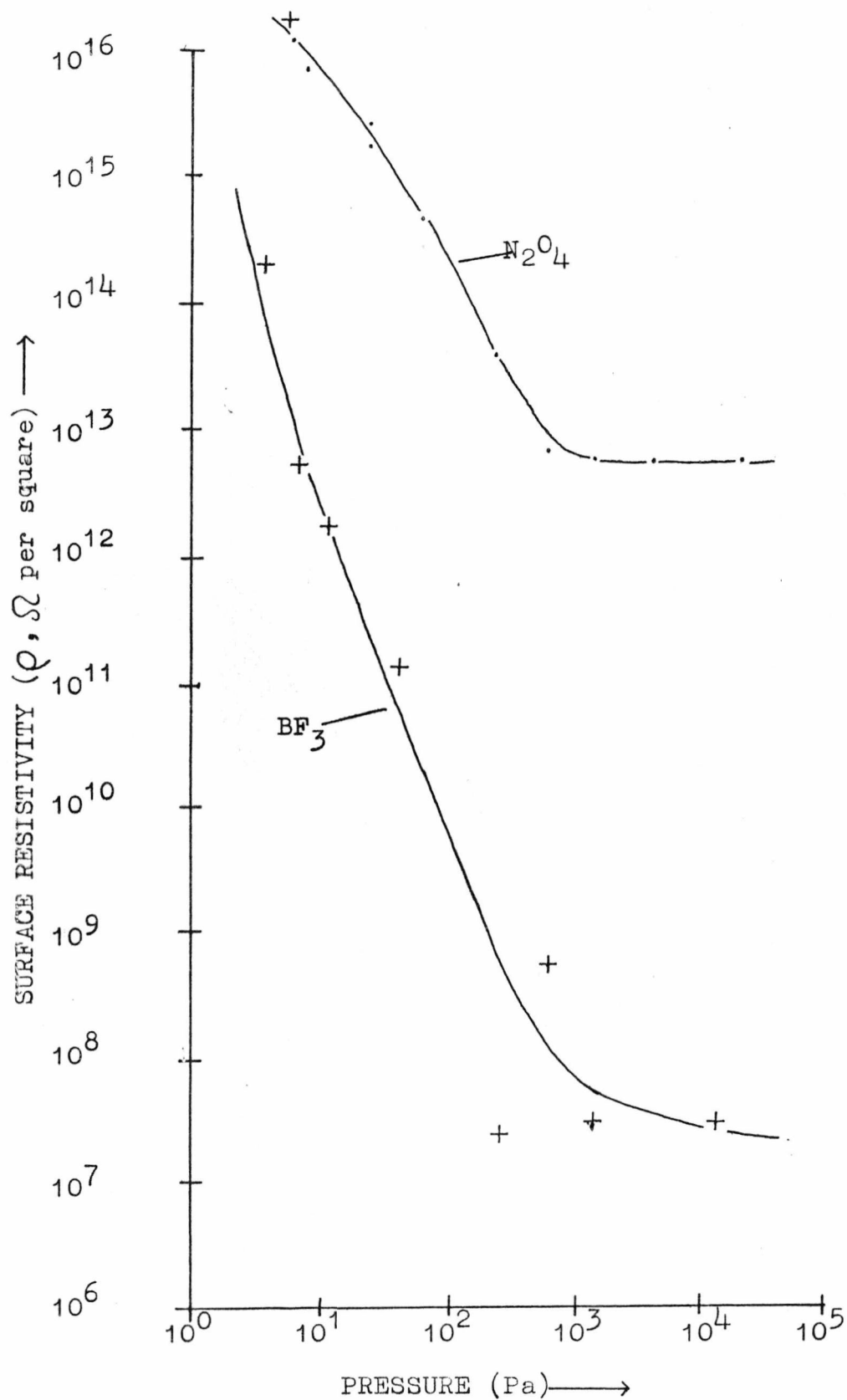
evacuation; even heating up to 380K under a vacuum (1·3 X 10^{-4} Pa) had little effect (the surface resistivity increased by about a factor of 5). The response time of the gas effect was reasonably short (a maximum of 15 minutes). These observations, together with the pressure dependence curve (cf. figure 6·3)), are similar to those obtained for the phthalocyanine/dinitrogen tetroxide systems (cf. figures (5·16), (5·17), (5·18) and (5·19) and Chapter (5·6)). Hence it was concluded that the perylene/boron trifluoride system represented the largest possible gas effect (i.e. ~100% surface coverage with ~100% ionization). The differences between the effects of boron trifluoride on perylene and phthalocyanines will be fully discussed in section (6·14).

c) Effect of oxygen

Dried oxygen was admitted into the cell at a pressure of 1 X 10^5 Pa (atmospheric pressure). No change in the dark resistivity or activation energy was observed (cf. effect of oxygen on the phthalocyanines). This effect is explained in terms of the reduced sensitivity of perylene towards electron acceptor gases (e.g. dinitrogen tetroxide). A more detailed explanation of the change in sensitivity in terms of the surface ionization potential of the crystal is presented in section (6·14).

d) Effect of ammonia

When clean perylene crystals were exposed to dried ammonia no change in the electrical properties could be noted. This was predictable since perylene and ammonia are both electron donors. A similar effect was noted for phthalocyanines.

175

It has been noted that boron trifluoride had an irreversible effect on the surface resistivity of perylene. If these crystals were exposed to ammonia gas (only a small pressure was required, ~10 Pa) then the surface resistivity enhancement due to the boron trifluoride was completely removed (i.e. the crystal exhibited its vacuum characteristics). Furthermore, evacuation of the ammonia had no effect. The crystals could be repeatedly cycled in boron trifluoride and ammonia without any loss in sensitivity. This effect was very similar to that obtained for phthalocyanine cycled in dinitrogen tetroxide and ammonia. It was therefore concluded that when a boron trifluoride contaminated perylene crystal was exposed to ammonia the chemisorption bond between the crystal and the electron acceptor gas was broken.

Throughout the study of the gas effects on perylene the Ohmic characteristics were frequently measured. In each case the crystals exhibited Ohmic behaviour. Hence these current-voltage plots are not reproduced since they were essentially of the same form as the vacuum result (cf. figure (6·1)).

6·3 Effect of gases on the photoconductivity of perylene crystals.

As with the dark conductivity measurements the photoconductive properties were first of all measured in a high vacuum (1 X 10^{-4} Pa). The results obtained were similar for all three crystals and typical results for the spectrum and intensity dependences are shown in figures (6·4) and (6·5). The photoconduction spectrum obtained was similar to that

176

FIG: (6·4) PHOTOCONDUCTION SPECTRA FOR PERYLENE IN VARIOUS AMBIENTS
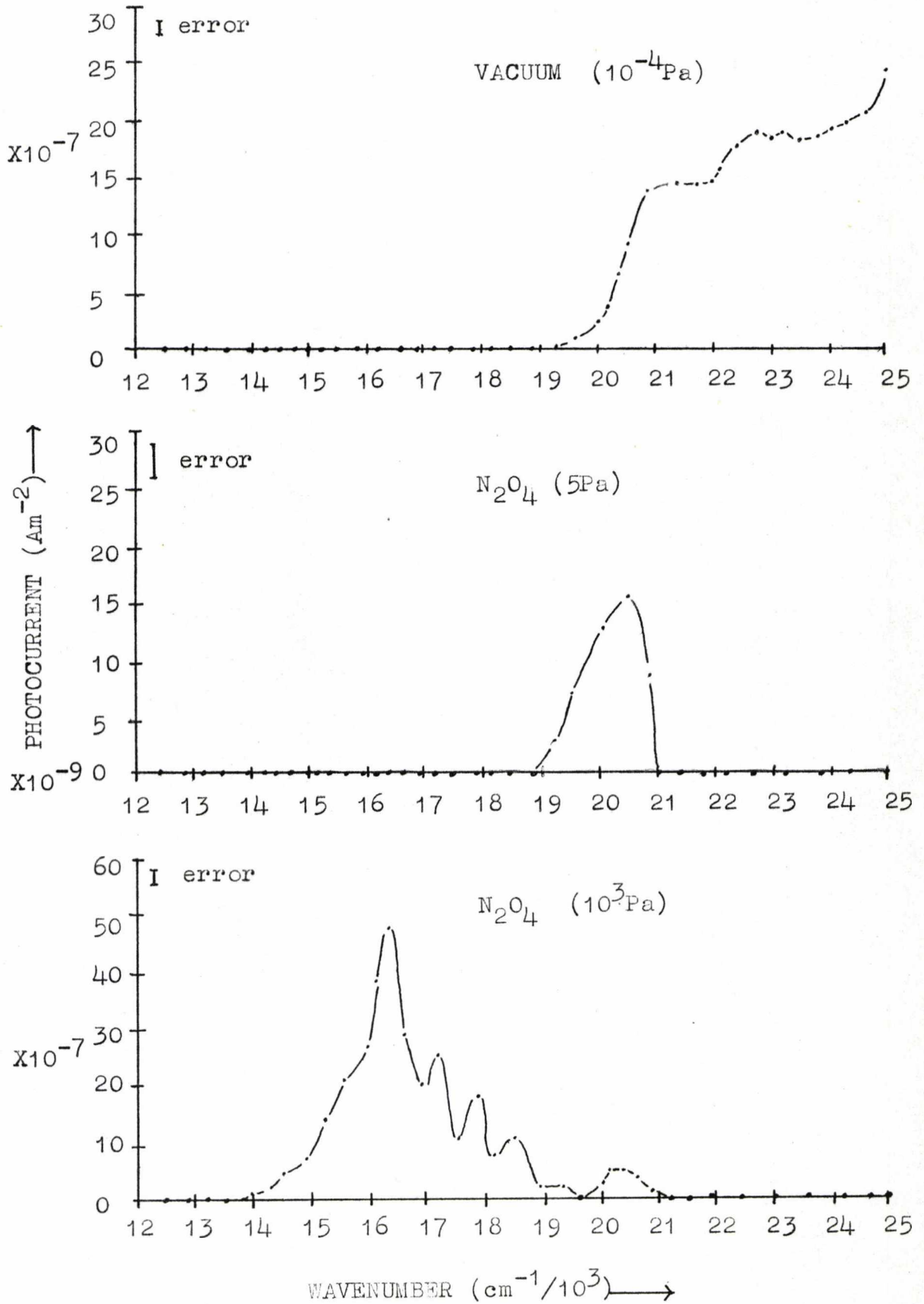
FIG: (6·5) PHOTOCURRENT INTENSITY DEPENDENCE PLOTS FOR
PERYLENE IN A VACUUM
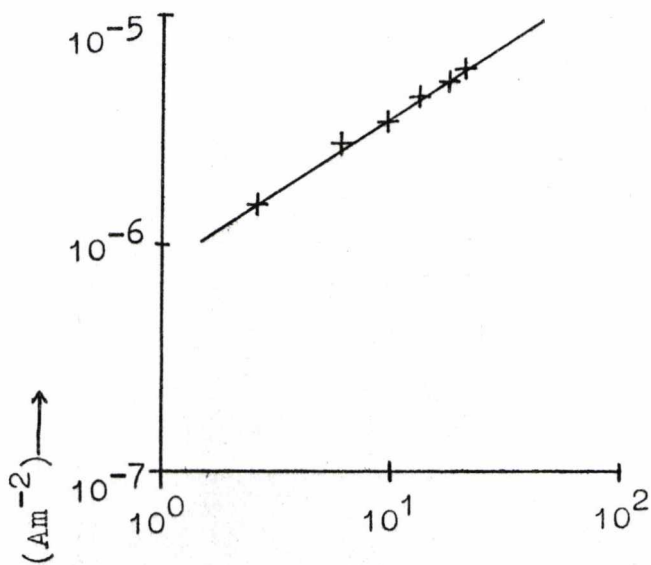
450nm
SLOPE = 0·65
(22220cm^{-1})
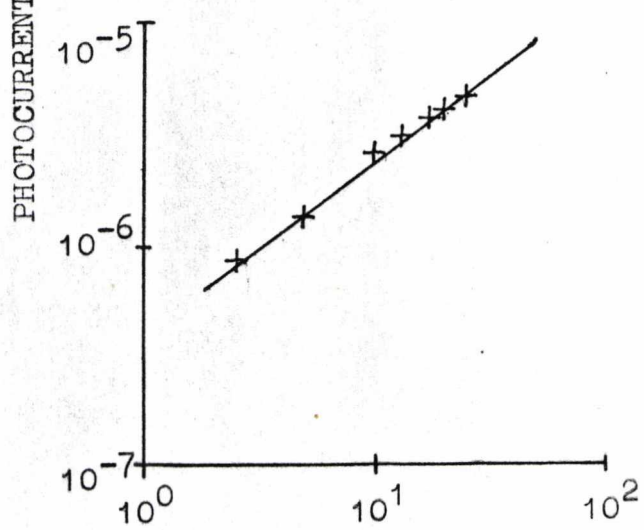
480nm
SLOPE = 0·80
(20830cm^{-1})

obtained by M. Sano and H. Akamatu, 1962. It can be seen
that the main photoconduction peak occurred at 20,000 to
25,000 cm^{-1} (500-400 nm). From the intensity dependence of
photoconduction results (cf. figure (6·5)) it is probable
that the photogeneration of charge carriers occurred via a
single photon process. Furthermore, recombination was almost
entirely dominated by a bimolecular process. After the
vacuum photospectrum had been recorded the crystal was
exposed to various gases.

a) Effect of dinitrogen tetroxide

When the crystals (two crystals were studied) were
exposed to a low pressure (approximately 5 Pa) the main
photoconduction peak at 20,000-25,000 cm^{-1} was rendered
unobservable. The photoconduction spectrum obtained
was similar for both crystals; a typical result is shown
in figure (6·4). Furthermore, it was found that evacuation
and heating (380K) had no effect at all on the photoconduction
spectrum (after N$_2$O$_4$ exposure). Also, it was found (cf.
section (6·3d)) that ammonia had no effect. Therefore it
was concluded that dinitrogen tetroxide had an irreversible
effect on the photoconduction spectrum. If this result
is compared with that obtained for the dark conductivity
measurements it becomes evident that these two measurements
are not similar. It was therefore concluded that the photo-
conduction effect was far more sensitive to adsorbed gases.

Increasing the pressure of dinitrogen tetroxide present
in the cell had an unexpected effect. The photoconduction
spectrum obtained at moderate to high pressures (10^2-10^5 Pa)
is shown in figure (6·4). It can be seen, by comparison
with the other spectra, that perylene became a reasonable

photoconductor (although in a different region than in a vacuum). Furthermore, it was found that this effect could be reduced to its initial level (1 Pa of N_2O_4) by evacuation. One of the main features of the spectrum in high pressures of dinitrogen tetroxide was the small peaks on the high energy shoulder of the main peak ($\sim 16,000$ cm^{-1} = 625 nm). These small peaks were found to be reproducible for all of the crystals. The spacing between these small peaks was found to be approximately constant (about 700 cm^{-1}). An explanation for this effect is proposed in section (6·7a).

b) Effect of boron trifluoride

The effect of this gas was identical (within measurement errors) to that obtained with dinitrogen tetroxide at low pressures. Increasing the pressure of the boron trifluoride present had no effect on the spectrum, the shape being similar to that shown in figure (6·4) for dinitrogen tetroxide at low pressures (5 Pa). Evacuation and heating and ammonia (cf. section (6·3d)) again had no effect on the photoconduction spectrum.

Hence it was concluded that boron trifluoride, as with dinitrogen tetroxide, had an irreversible (even after evacuation and exposure to ammonia) effect on the photoconductive properties of perylene crystals (cf. the fact that dark conductivity was found to have a reversible effect by exposure to ammonia, section (6·2b)).

c) Effect of oxygen

It was found that dried oxygen gas had no effect (at high or low pressures) on the photoconductive properties of perylene. The spectrum shape and level remained the same

180

as that shown in figure (6·4) for a vacuum.

d) Effect of ammonia

As predicted, dried ammonia had no effect on the photo-conductivity of 'clean' (after initial evacuation and heating) perylene crystals (cf. effect on phthalocyanine crystals, Chapter (5·10)). However, it was also found that ammonia had no effect on crystals that had been previously exposed to an electron acceptor gas (boron trifluoride and dinitrogen tetroxide). This result indicates that an irreversible reaction had taken place on the surface of the perylene crystals. Furthermore, when the results from the dark conductivity measurements (cf. sections (6·2a) and (6·2b)) are taken into account, it would seem that the sites active in photoconduction do not contribute to the dark conductivity mechanism. This is concluded because the effect of boron trifluoride and dinitrogen tetroxide on the dark conductivity was found to be fully reversible by treatment with NH_3, whereas the effect on the photoconductivity was irreversible even after exposure of the sample to NH_3.

6·4 Effect of gases on the dark conductivity of perylene-TCNQ crystals

The room temperature resistivity and an Ohmic plot were measured after the crystal had been evacuated (1 X 10^{-4} Pa) and heated (300K) for a 12 hour period. For comparison purposes, the room temperature resistivity is listed in table (6·2) together with some literature values. The result of the Ohmic plot is shown in figure (6·6) where it can be seen that the crystal was Ohmic for fields up to approximately $10^5 Vm^{-1}$. After these initial vacuum measurements

FIG: (6·6) OHMIC PLOT FOR PERYLENE-TCNQ IN A VACUUM AT 295K

SLOPE = 0·98
(ELECTRODE SEPARATION
= 3·60mm)
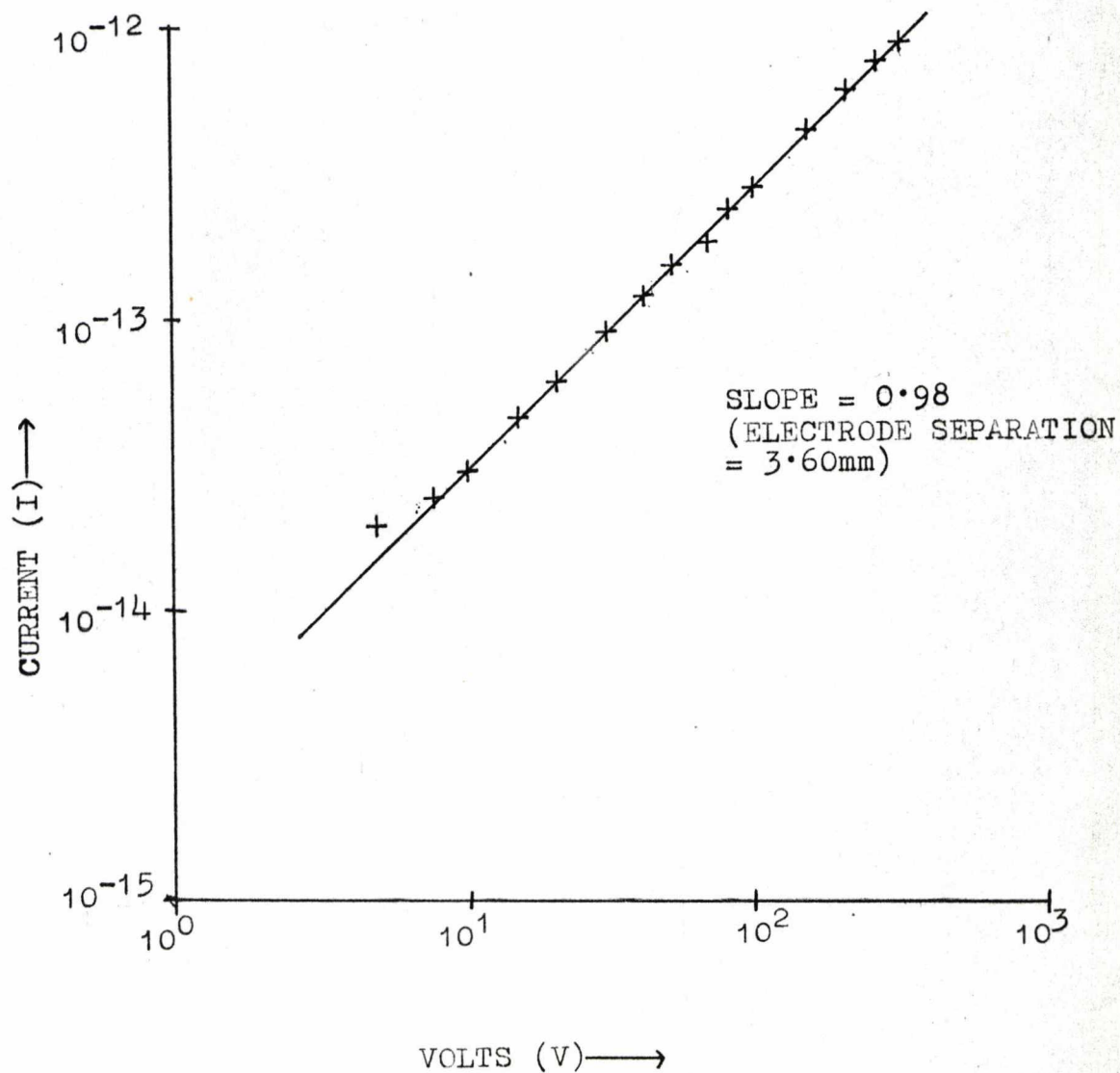
had been made, the crystal was exposed to various gases.

TABLE 6·2

Activation energy ΔE eV	Resistivity (295K) Ωm	Reference
not measured	$1 \cdot 5 \times 10^{10}$	this work
0·46	$0 \cdot 35 - 6 \cdot 4 \times 10^{9}$	V.M. Vincent and J.D. Wright, 1974
0·57	$5 \cdot 3 \times 10^{8}$	P.J. Munnoch and J.D. Wright, 1976

a) Effect of dinitrogen tetroxide

The technique employed in studying the gas effect was identical to that employed for the phthalocyanines and perylene (cf. Chapter (5·6) and section (6·2a) respectively). The results were calculated in terms of surface resistivity and the resultant pressure dependence curve is presented in figure (6·7). This curve shows that perylene-TCNQ was not particularly sensitive towards dinitrogen tetroxide, indicating that only a weak bond was formed between the gas and the crystal. Further evidence for this was found from the ease of removing the gas from the crystal. Only a moderate vacuum (10^{-1} Pa) was needed to return the perylene-TCNQ crystal to its vacuum dark resistivity.

An interesting feature of the pressure dependence curve is the initial increase in surface resistivity (a maximum at about 10 Pa pressure). This observation was found to be

reproducible and can be explained as follows. First it must be assumed that the majority carriers, on the surface of the crystal, are electrons. This is reasonable since the Seebeck coefficient for perylene-TCNQ is negative (V.M. Vincent and J.D. Wright, 1974). It has already been stated (cf. Chapter (5·8)) that the effect of the chemisorbed dinitrogen tetroxide was to produce hole carriers. Therefore in the case of perylene-TCNQ, the initial effect of creating hole carriers in the surface region (by dinitrogen tetroxide adsorption) is to increase the recombination rate of the surface electrons. Hence the number of charge carriers available for conduction is reduced and the resistivity is increased. However, the situation is soon reached (when $P > 10$ Pa in this case) when the holes become the majority carriers and therefore the surface resistivity decreases with increasing gas pressure.

b) Effect of oxygen

Oxygen had no effect on the dark conductivity of perylene-TCNQ.

c) Effect of ammonia

In all of the compounds so far studied ammonia had no effect on the dark conductivity of 'clean' crystals. The crystals were all donors and therefore it was not expected that an interaction would occur. However, perylene-TCNQ is a donor-acceptor complex and therefore it was predicted that it should exhibit both donor and acceptor properties. It has already been shown that it acts like a donor in an acceptor gas (dinitrogen tetroxide effect, cf. section (6·4a)). Therefore it should also give a similar effect in a

donor type-gas ambient, thereby exhibiting an acceptor type
of behaviour. This was found to be the case and the resultant
pressure dependence curve is presented in figure (6·7), where
it can be seen that the effect is similar to that obtained
for dinitrogen tetroxide, except that there is no initial
decrease in conduction since in this case the donor gas is
producing negative charge carriers. The effect of ammonia
on the dark surface resistivity could be removed (to within
a factor of 5 of the initial surface resistivity in a vacuum)
by evacuation (1 X 10^{-4} Pa) and heating (300K) for an
18 hour period.

Again, as with perylene crystals, the current-voltage
dependence of perylene-TCNQ was studied in the different
gas environments. However, since the compound always exhibited
an Ohmic dependence, these results are not reproduced since
they were similar (in shape but not magnitude) to the vacuum
plot (cf. figure (6·6)).

6·5 Effect of gases on the photoconductivity of perylene-
TCNQ crystals

The photoconduction spectrum was initially measured
in a high vacuum and after heating under a high vacuum for
12 hours. It is reproduced in figure (6·8). It can be seen
that the main feature is a photoconduction peak at $\sim$18,000 cm^{-1}
($\simeq$550 nm). The intensity dependence of photoconduction was
also measured. The plots are shown in figure (6·9) and the
results are listed in table (6·3). These results suggest
that the photogeneration of charge carriers occurred via
a single photon process and that recombination was almost
entirely dominated by a bimolecular process. Previous

185

FIG: (6·7) EFFECT OF DINITROGEN TETROXIDE AND AMMONIA ON THE DARK RESISTIVITY OF PERYLENE-TCNQ.

186
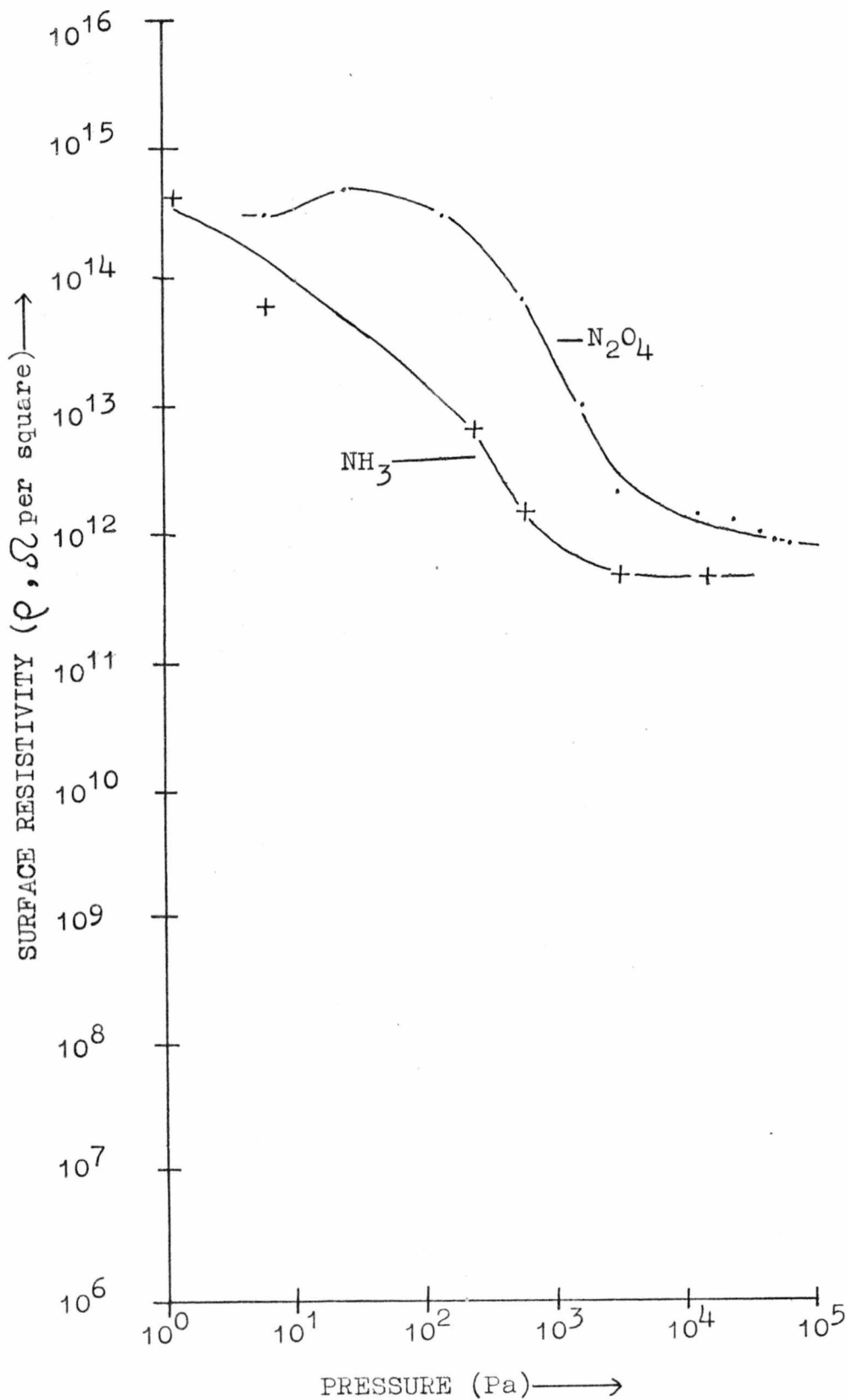
FIG: (6·8)   PHOTOCONDUCTION SPECTRA OF PERYLENE T.C.N.Q. IN VARIOUS AMBIENTS.
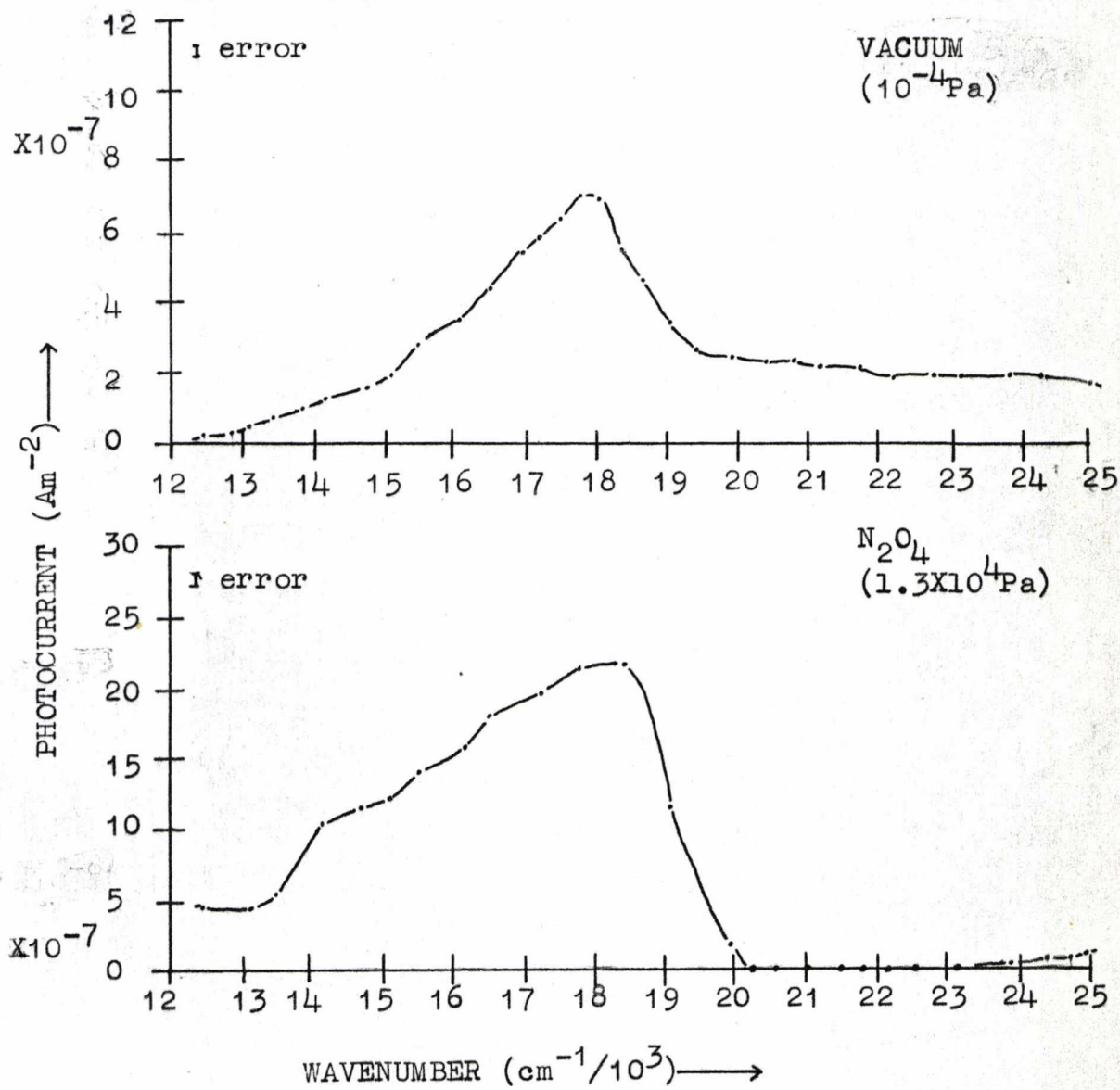
FIG: (6·9) PHOTOCURRENT INTENSITY DEPENDENCE PLOTS FOR
PERYLENE-TCNQ IN A VACUUM

475nm
SLOPE = 0·64
(21050cm^{-1})

550nm
SLOPE = 0·59
(18180cm^{-1})

700nm
SLOPE = 0·50
(14280cm^{-1})

PHOTOCURRENT (Am^{-2}) ⟶

THERMOPILE OUTPUT (μV) ⟶
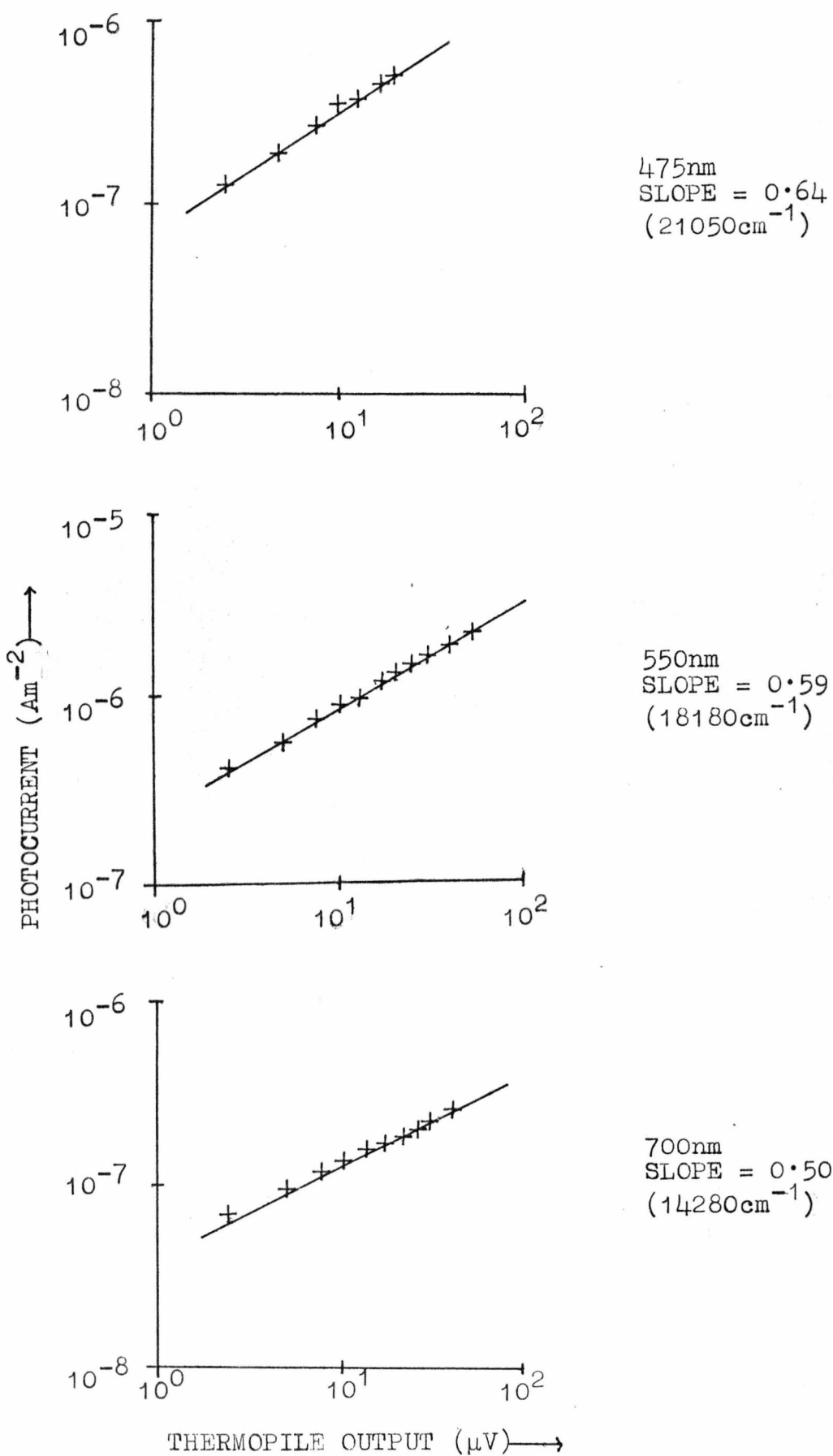
work (V.M. Vincent, 1972 and P.J. Munnoch, 1974) found similar spectra and intensity dependences.

It was found that exposing perylene-TCNQ to electron acceptor or donor gases had no effect on the photoconduction magnitude or the spectral response. On exposure to air the photoconduction spectrum remained identical with that obtained in a high vacuum (figure (6.8)). Furthermore, exposure to dinitrogen tetroxide had very little effect (an enhancement of ~2 fold was observed) on the photoconduction spectrum (figure (6.8)). Therefore it was concluded that the photogeneration of carriers was not influenced (within experimental errors) by electron donor or acceptor type gases.

TABLE 6.3

Wavelength nm	Intensity dependence
475	0.64
550	0.59
700	0.50

6.6 Effect of gases on the dark conductivity of TCNQ crystals

Results for the Ohmic dependence and activation energy plots are presented in figures (6.10) and (6.11) respectively. These measurements were carried out under a high vacuum for two crystals. Since the results obtained were identical (within experimental errors) only one set of results is reproduced (TCNQ crystal 1) and averaged values for the activation energy, pre-exponential factor and resistivity are presented in table (6.4) together with some literature

SLOPE = 1·01
(ELECTRODE
SEPARATION
= 2·74mm)

CURRENT (I)→

VOLTS (V)→
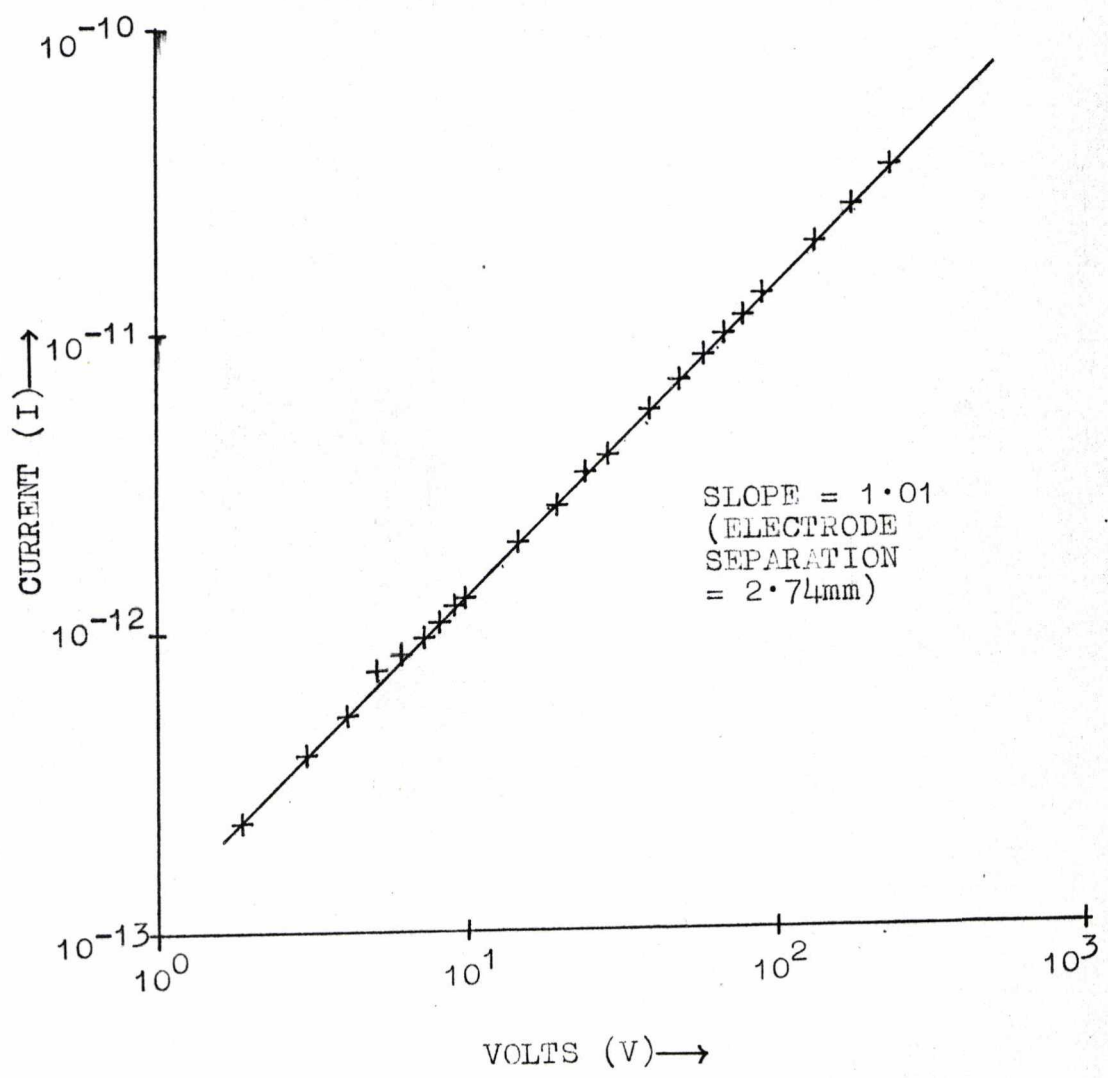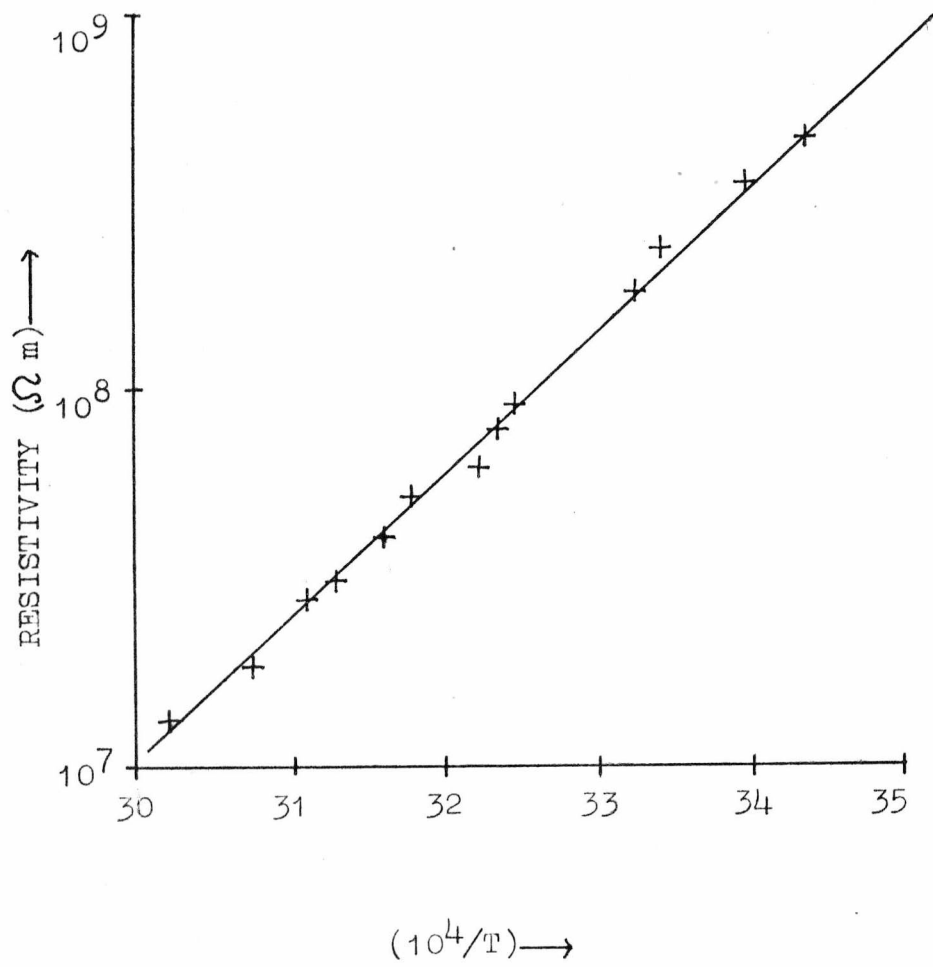
values for comparison purposes.

<div align="center">TABLE 6·4</div>

ACTIVATION ENERGY ΔE eV	PRE-EXPONENTIAL FACTOR ρ_o Ω m	RESISTIVITY (295K) Ω m	PURITY	REFERENCE
0·79	$1·5 \times 10^{-5}$	$4·6 \times 10^{8}$		this work
		$7·5 \times 10^{8}$	high	R.J. Hurditch, V.M. Vincent & J.D. Wright, 1972
		$1·8 \times 10^{9}$	high	
		$1·7 \times 10^{7}$	low	
		$1·5 \times 10^{7}$	low	

By comparison of the semiconduction characteristics obtained in this work with those obtained by R.J. Hurditch, V.M. Vincent and J.D. Wright (1972) for a series of crystals of different purity levels it can be seen that the crystals used in this work contained a significant amount of surface impurity (probably of the type Na^{+} $TCNQ^{-}$).

a) Effect of dinitrogen tetroxide

The effect of this gas was studied in a similar manner as before (cf. sections (6·2a) and (6·4a)). The results for the pressure dependence are shown in figure (6·12). It can be seen that TCNQ only showed an enhancement of dark conductivity at relatively high pressures ($\sim 10^{4}$ Pa) of gas. Also, this effect only occurred for one of the three TCNQ crystals

FIG: (6·12) EFFECT OF DINITROGEN TETROXIDE AND AMMONIA ON THE DARK RESISTIVITY OF TCNQ
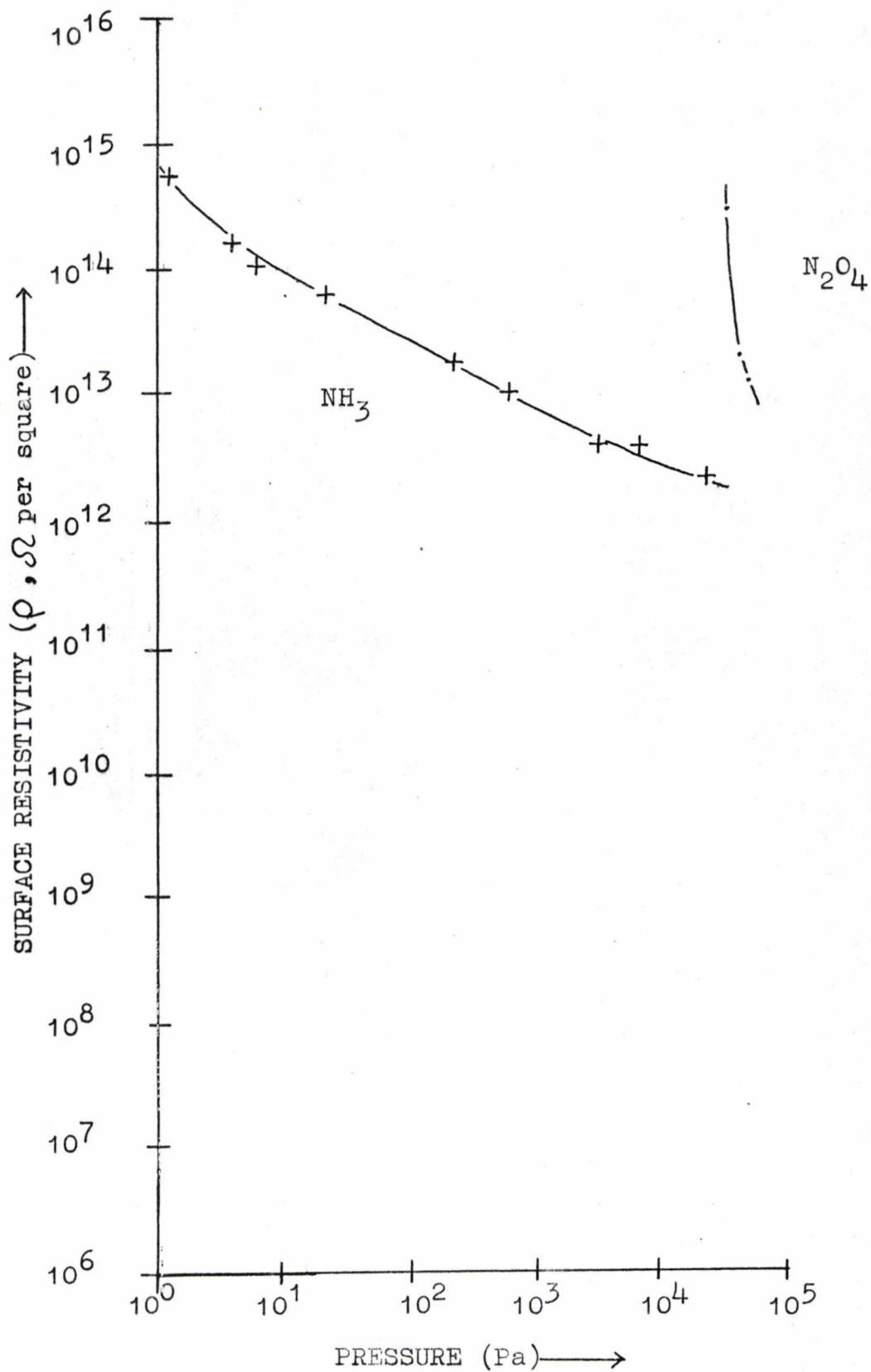
studied. Furthermore, it was found that this enhancement was irreversible. Therefore it was concluded that in this case the dinitrogen tetroxide was contaminated and therefore reacted with the TCNQ crystal. Hence these results show that TCNQ is not affected by dinitrogen tetroxide. This result was expected since both crystal and gas are electron acceptors and consequently an interaction was unlikely.

b) Effect of boron trifluoride

No effect was observed with any of the crystals, again indicating that electron acceptor gases do not undergo chemisorption with electron acceptor crystals.

c) Effect of oxygen

Again, as expected, no effect was observed.

d) Effect of ammonia

The expectation was that ammonia should enhance the conductivity of TCNQ. From the pressure dependence curve shown in figure (6·12) it can be seen that there was a reasonable effect. Furthermore, it was found that most of this effect could be reversed by evacuating and heating the crystal; the final resistivity fell to within a factor of 50 of the initial vacuum value. Therefore this effect is similar to that obtained for the phthalocyanine-dinitrogen tetroxide system (cf. Chapter 5), although the decrease in resistivity was by no means so large. With the phthalocyanine system it was found in some cases (lead, cobalt and manganese especially) that evacuation could not remove the effect of the gas. However, when the crystals were exposed to an electron donor gas (ammonia) the dark resistivity fell rapidly

to the vacuum level. A similar effect was found for the TCNQ-ammonia system on exposure to an electron acceptor gas (dinitrogen tetroxide).

6·7 Effect of gases on the photoconductivity of TCNQ crystals

Photoconduction spectra and intensity dependence plots were initially measured in a high vacuum after ensuring clean crystal surfaces by heating under a high vacuum for 12 hours. The spectra obtained (two crystals were studied) were identical, hence only one of the spectra is reproduced in figure (6·13) (for TCNQ crystal 2). Also, the intensity dependences were similar for both crystals and consequently only one set of results is reproduced in figure (6·14); the results are listed in table (6·5). As with perylene and perylene-TCNQ crystals the intensity dependences of photoconduction indicate that the photogeneration of charge carriers occurred via a single photon process and that recombination was dominated by a bimolecular process.

TABLE 6·5

Wavelength nm	Intensity dependence
450	0·55
490	0·61
550	0·59

It should be noted that a two photon excitation process with bimolecular recombination and concentration dependent mobility terms (cf. Chapter 5·9)) (R.J. Hurditch, V.M. Vincent and J.D. Wright, 1972) will also give rise to a similar intensity dependence. The results obtained for the shape of the

FIG: (6·13) PHOTOCONDUCTION SPECTRA OF T.C.N.Q. IN VARIOUS AMBIENTS.

196
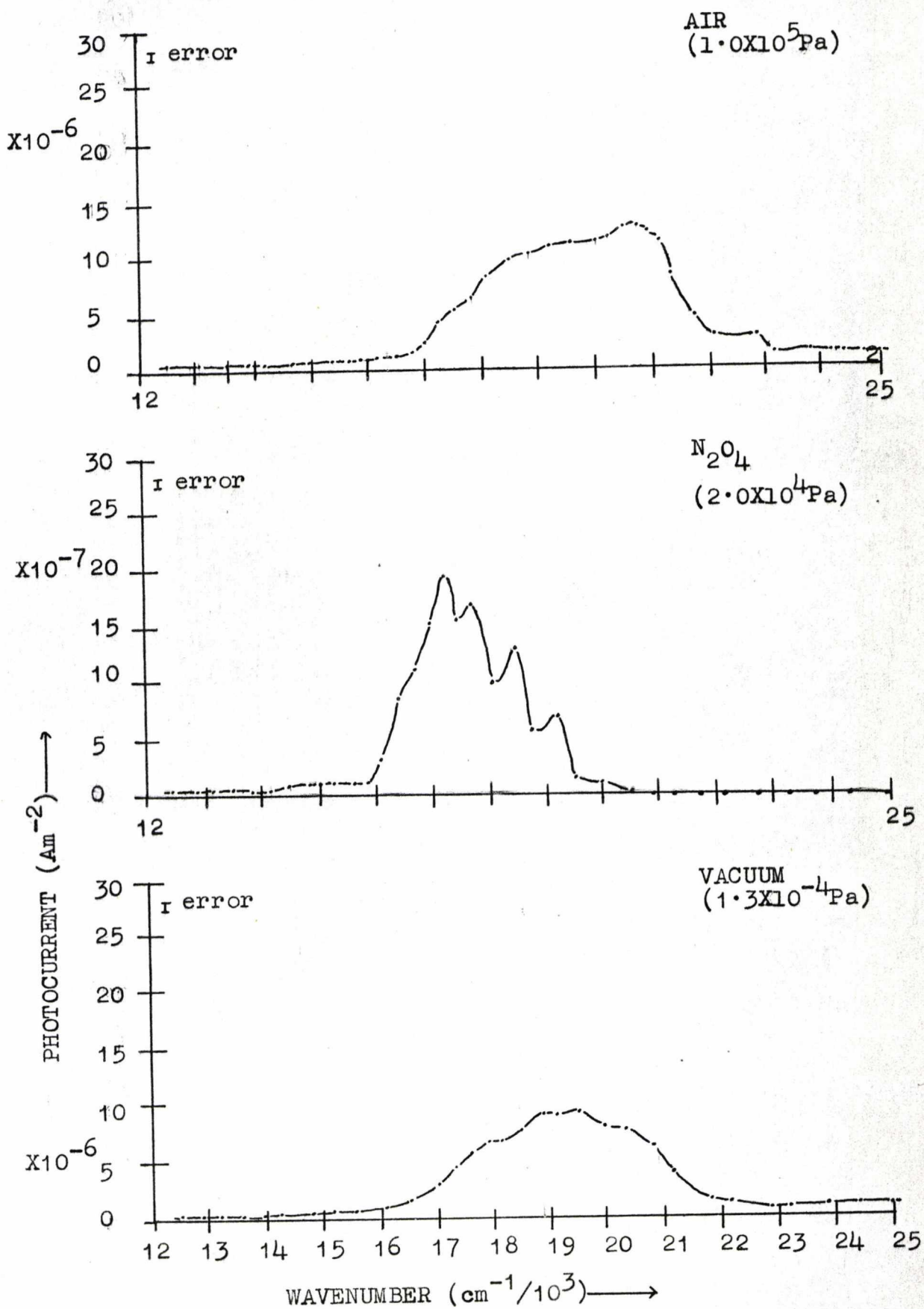
FIG: (6·14) PHOTOCURRENT INTENSITY DEPENDENCE PLOTS FOR TCNQ IN A VACUUM

450nm
SLOPE = 0·55
($22220cm^{-1}$)

490nm
SLOPE = 0·61
($20410cm^{-1}$)

550nm
SLOPE = 0·59
($18180cm^{-1}$)

PHOTOCURRENT (Am^{-2}) ⟶

THERMOPILE OUTPUT (μV) ⟶

197
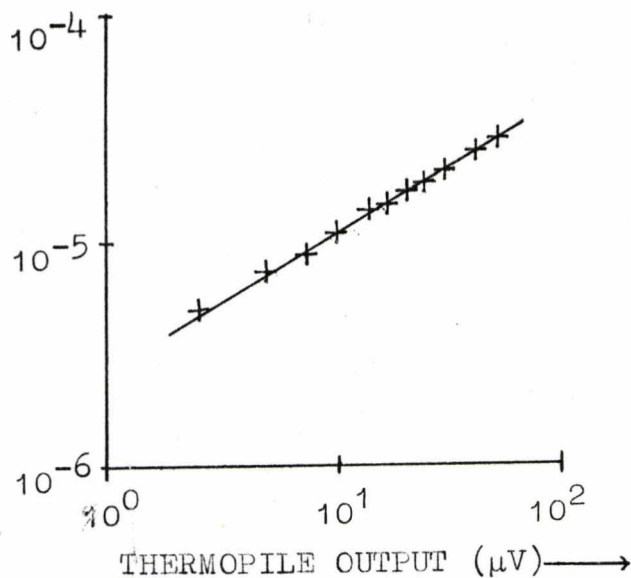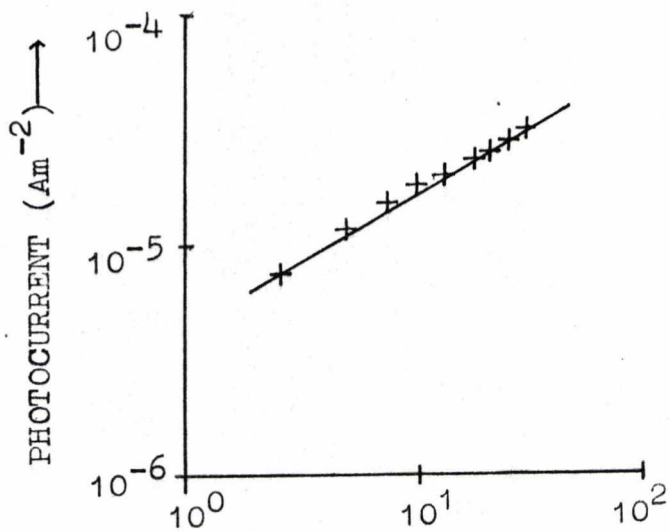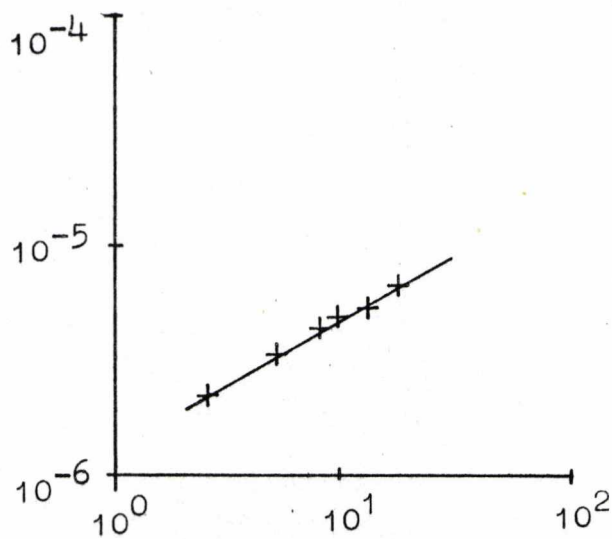
photoconduction spectrum and intensity dependence agree with those obtained by previous workers (R.J. Hurditch, V.M. Vincent and J.D. Wright, 1972) for TCNQ crystals with surface impurities of the type Na^+ $TCNQ^-$.

a) Effect of dinitrogen tetroxide

When relatively high pressures (10^2-10^5 Pa) of dinitrogen tetroxide were present in the cell the photocurrent was depressed by approximately a factor of 10. Furthermore, the spectral response was completely altered. The photoconduction spectrum in an ambient of dinitrogen tetroxide (10^4 Pa pressure) is presented in figure (6·13). Both of the TCNQ crystals exhibited the same effect within the experimental errors. The main feature of this spectrum is the reproducible peaks on the high energy side of the main peak (17,250 cm^{-1} $\simeq$580 nm).

This type of spectrum is similar to that obtained for the perylene crystals (cf. figure (6·4)). However, in this case the peaks occur at slightly higher energies (for perylene the main peak occurred at $\sim$16,000 cm^{-1}). Also, the spacing between adjacent peaks is not the same, whereas in the perylene case the spacing was found to be approximately constant ($\sim$700 cm^{-1}). The photospectrum could be returned to its original vacuum shape and magnitude by evacuation. Hence the interaction between crystal and gas was weak.

The following explanation is offered for these observations. From work previously carried out in this laboratory (R.J. Hurditch, V.M. Vincent and J.D. Wright, 1972) it was reported that the photogeneration of carriers more likely involved singlet excited states than triplets since the large

198

photoconduction peak was in the region of strong singlet absorption. Therefore the vacuum photoconduction spectrum is dominated by photogeneration of singlet excitons. Furthermore, due to the high absorption, this is mainly a surface effect. It is observed that the presence of dinitrogen tetroxide on the surface of the crystal inhibits photoconduction. This implies that photogeneration produces electron charge carriers; these would be readily trapped by the adsorbed gas molecules. However, this effect is restricted to the surface of the crystal and consequently bulk photoconduction is still possible. For bulk photoconduction to occur the photons must be weakly absorbed, thereby allowing penetration into the crystal. Absorption corresponding to production of excited triplet states would be multiplicity forbidden (i.e. singlets have zero net electron spin momentum whereas triplets have a positive value) and would therefore be weak. Therefore it is concluded that the photoconduction spectrum in an ambient of dinitrogen tetroxide is probably due to triplet excitons (i.e. bulk photoconduction).

b) Effect of boron trifluoride

The photoconductive properties remained the same as their vacuum values when crystals were exposed to the gas. It has already been noted (cf. Chapter (5·12)) that although boron trifluoride is an electron acceptor it behaves differently than dinitrogen tetroxide. This effect was explained in terms of the different orbitals used for accepting electrons. Hence it is concluded that the surface photocurrent (produced by singlet excitons) is not inhibited by σ type electron

accepting orbitals but is inhibited by π^* orbitals (as is the case with dinitrogen tetroxide). This supplies further evidence for the argument that the chemisorption of gases is not only affected by the donor or acceptor properties of the gases but also by the type of orbital involved in the possible bonding.

c) Effect of oxygen

It was found that dried oxygen enhanced the photocurrent very slightly and the spectrum is shown in figure (6·13). A similar observation was recorded by R.J. Hurditch, V.M. Vincent and J.D. Wright, 1972. Again, this indicates that factors other than the electron affinity are involved in the interaction between gas and crystal.

d) Effect of ammonia

Although ammonia enhanced the dark conductivity of TCNQ, it had no measurable effect on the photoconductivity. The photoconduction spectrum obtained in vacuum (figure (6·13)) corresponds to results obtained by R.J. Hurditch, V.M. Vincent and J.D. Wright, 1972, for TCNQ crystals with high surface impurity concentrations, the most likely impurity being $Na^+ TCNQ^-$. It was suggested that these impurities affect the photoconduction spectral response by influencing the charge carrier recombination rate; a similar effect was observed in the phthalocyanine-dinitrogen tetroxide case (cf. Chapter (5·9)). Although ammonia tends to donate electrons to TCNQ, as shown by its effect on the dark conduction, the influence of this on the photoconduction may be small if the surface already contains a high proportion of impurity species (i.e. $Na^+ TCNQ^-$) to dominate the recombination

200

process for the charge carriers. The photoconduction spectrum of TCNQ is sensitive to impurities (R.J. Hurditch, V.M. Vincent and J.D. Wright, 1972), and it is likely that TCNQ crystals of higher purity would show a change in spectral response when exposed to ammonia.

6·8 Effect of gases on the semiconductive and photoconductive properties of anthracene

The dark resistivity, photoconduction spectrum and Ohmic character were measured in a vacuum and the results are given in table (6·6) and in figures (6·15) and (6·16) for the Ohmic plot and the photoconduction spectrum respectively. Literature values for resistivity and activation energy are also included in table (6·6).

TABLE 6·6

Activation energy ΔE eV	Resistivity ρ (295K) Ω m	Reference
not measured	10^{12}	this work
0·75	10^{12}	N. Riehl, 1957
0·85	10^{14}	K. Hasegawa, 1964

The main feature of the photoconduction spectrum is the peak at 24,000 cm^{-1} (approximately). Similar spectra have been observed by various other workers (J.W. Steketee and J. de Jonge, 1962; D.M.J. Compton and T.C. Waddington, 1956). It was also found that the photoconductivity was slightly (approximately a factor of 2) enhanced when the crystals (two were used in this study) were exposed to oxygen.

SLOPE = 1·04
(ELECTRODE SEPARATION = 3·90mm)
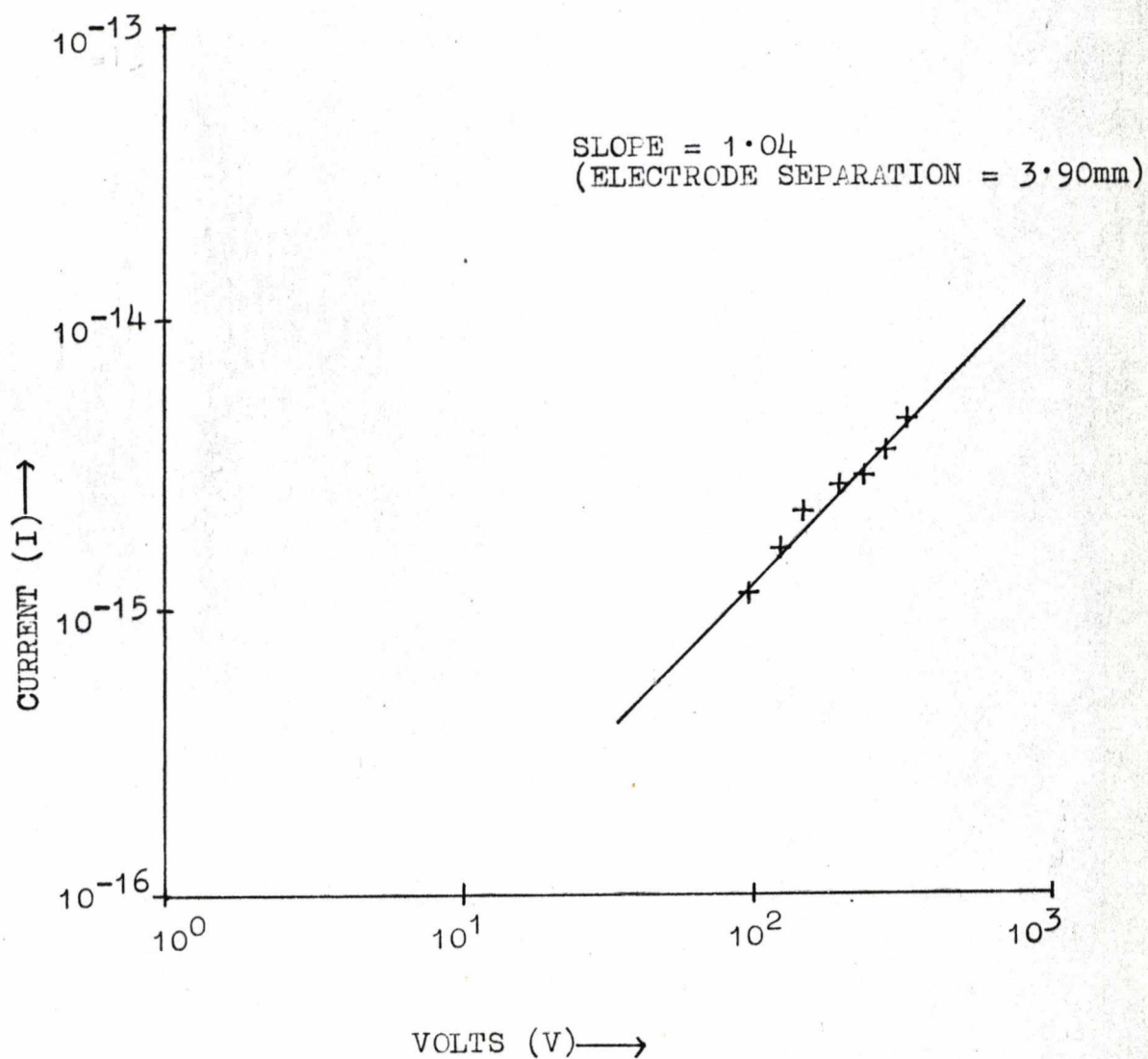
FIG: (6·16) PHOTOCONDUCTION SPECTRA FOR ANTHRACENE IN
VACUO AND IN DINITROGEN TETROXIDE

203
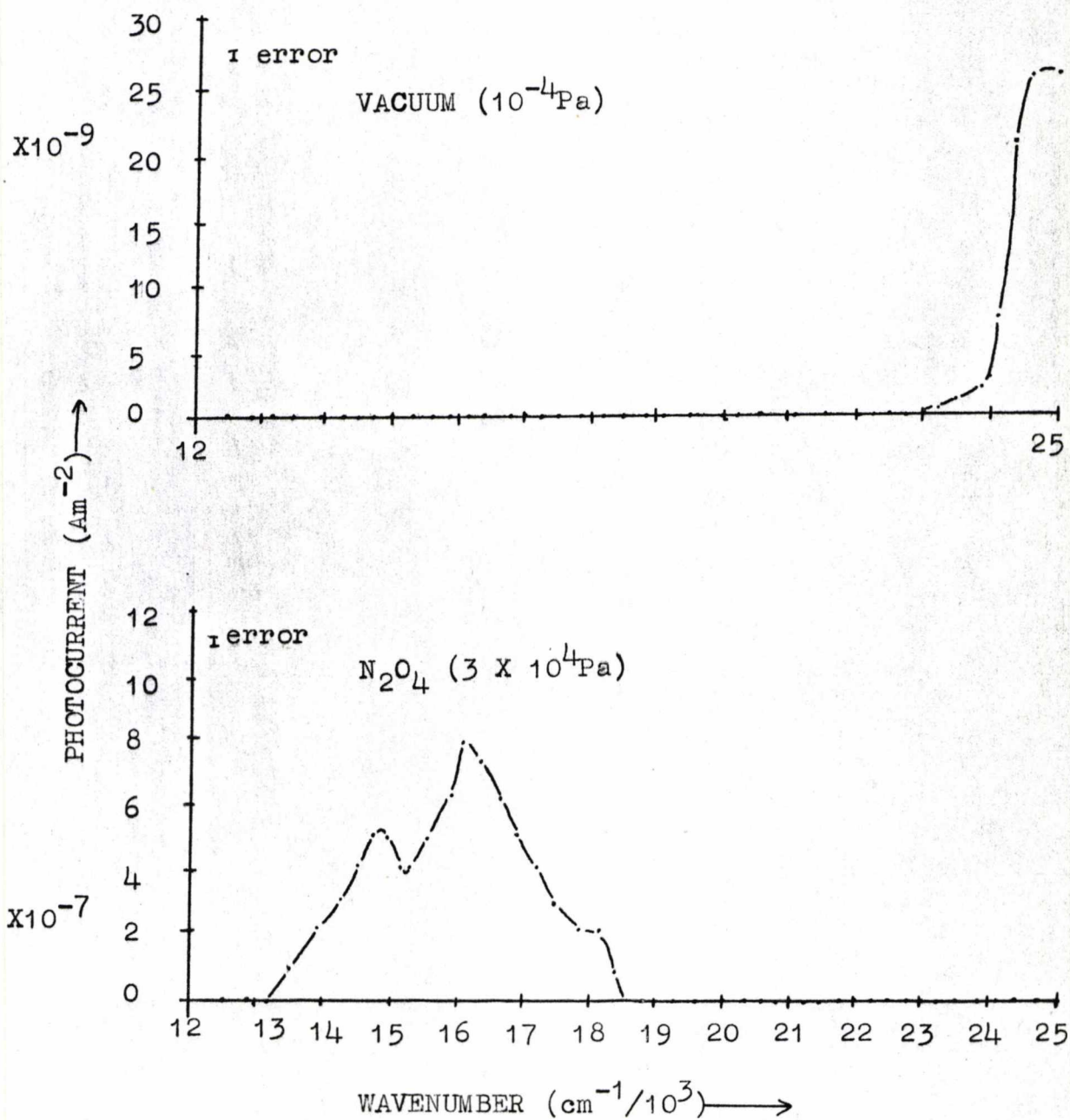
This effect has also been noted by W.G. Schneider and
T.C. Waddington, 1956 and D.M.J. Compton and T.C. Waddington,
1956.

When the anthracene crystals were exposed to dinitrogen
tetroxide the dark conductivity was enhanced; the pressure
dependence curve is reproduced in figure (6·17). It can be
seen, by comparison with the results obtained for the phtha-
locyanines (cf. figures (5·16) to (5·19)) that anthracene
was less sensitive to dinitrogen tetroxide. However, unlike
the phthalocyanines the effect could not be reversed by
evacuation plus heating or by the addition of ammonia. It
was therefore concluded that irreversible chemisorption had
occurred. Further evidence for an irreversible effect was
found by studying the effect of gas on the photoconduction
spectrum. As with the dark current an irreversible change
took place when the crystals were exposed to dinitrogen
tetroxide. The photocurrent was enhanced and the spectral
response was altered, as can be seen in figure (6·15).
Similar results were observed by W.G. Schneider and T.C.
Waddington, 1956; D.M.J. Compton and T.C. Waddington, 1956
and W.G. Schneider and T.C. Waddington, 1958. Also, after
exposure to dinitrogen tetroxide the crystals' colour
changed from white to yellow.

A similar irreversible change in the dark conductivity
and photoconductivity occurred when anthracene was exposed
to boron trifluoride. Due to the apparent chemical reactions
between the crystals and electron acceptor gases the dark
and photocarrier generation processes will not be discussed
in detail here.

FIG: (6·17) EFFECT OF DINITROGEN TETROXIDE ON THE DARK
RESISTIVITY OF ANTHRACENE AND PHENANTHRENE
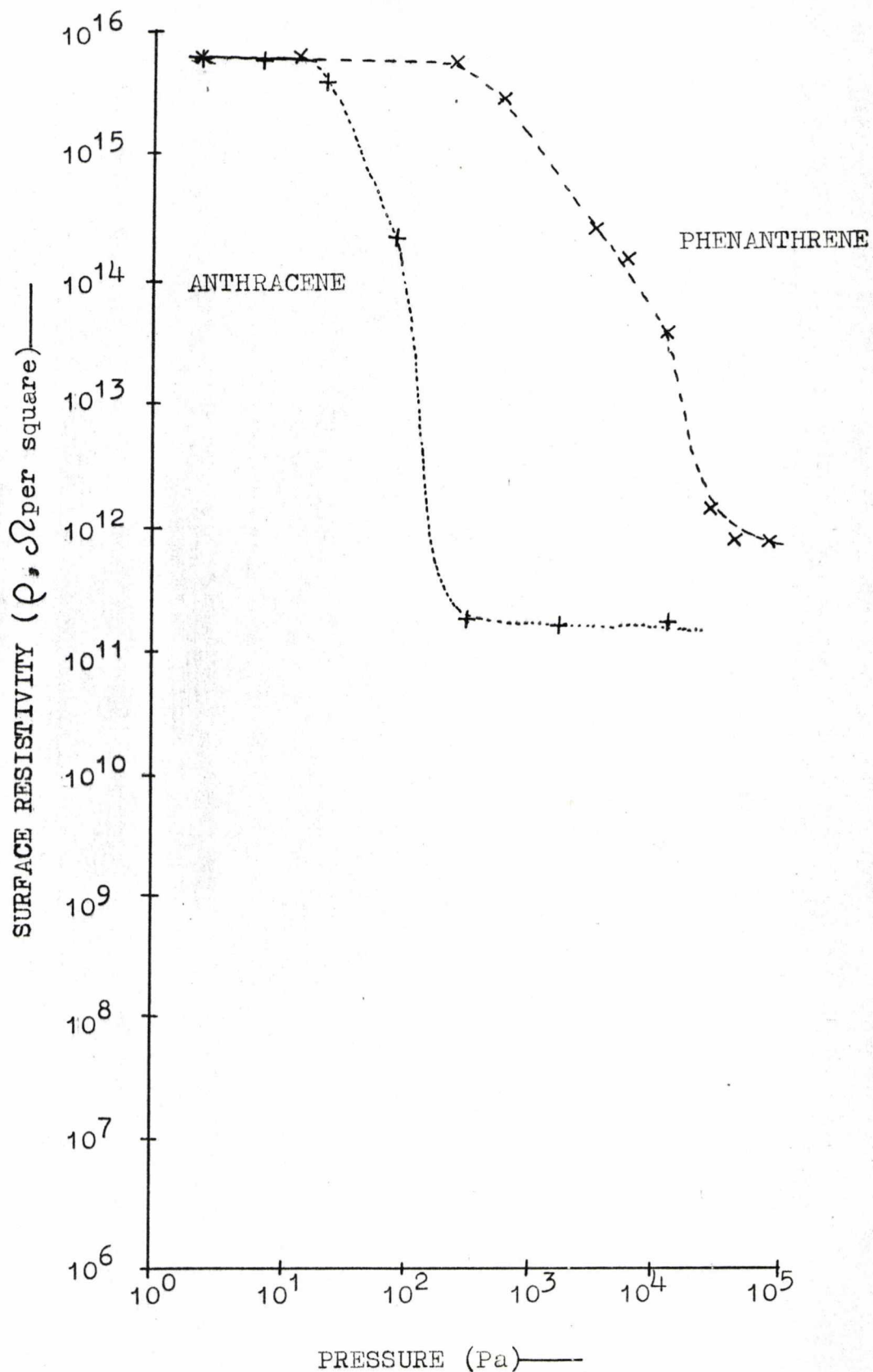
6·9 Effect of gases on the semiconductive and photoconductive properties of phenanthrene

In this case the photoconductive properties were not measured since they were below the detection level of the apparatus. However, the dark resistivity and Ohmic character (figure (6·18)) were measured in a vacuum. The resistivity was found to be $6·0 \times 10^{11}$ Ωm at 295K. As with anthracene the effect of dinitrogen tetroxide was found to be irreversible. The pressure dependence curve is reproduced in figure (6·17) together with the results for anthracene. Also, as in the case of anthracene the crystal changed colour from white to yellow.

6·10 Effect of occluded solvents in benzidine-TCNQ crystals

It has been reported (M. Ohmasa, M. Kinoshita, M. Sano and H. Akamatu, 1968; M. Ohmasa, M. Kinoshita and H. Akamatu, 1971; I. Ikemoto, K. Chikaishi, K. Yakushi and H. Kuroda, 1972 and N. Takahashi, K. Yakushi, K. Ishii and H. Kuroda, 1976) that the benzidine-TCNQ system forms two types of charge-transfer complexes; one contains solvent molecules, while the other does not. The aim of this study was to remove the solvent molecules from the complex containing solvent molecules, and leave an 'open' crystal lattice whereby gas molecules could easily diffuse into the bulk. This would greatly increase the effective area for gas adsorption which in turn would increase the sensitivity of the crystal towards gases. Hence initial measurements were concerned with removing solvent molecules from the bulk of solvent occluded crystals.

Two types of crystals were studied, one containing

SLOPE = 0·98
(ELECTRODE SEPARATION
= 1·88mm)

CURRENT (I) ⟶

VOLTS (V) ⟶
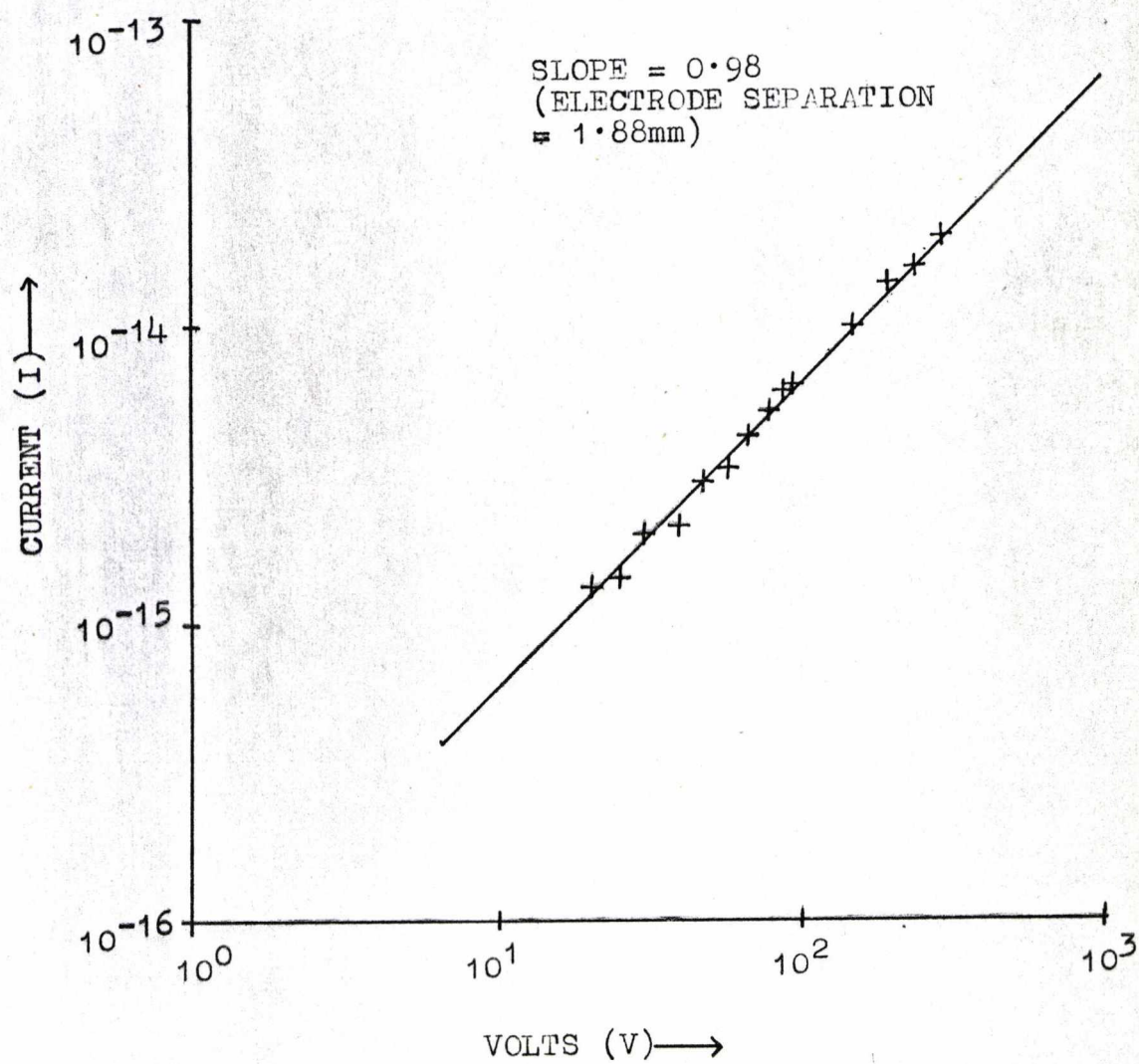
dichloromethane solvent molecules and the other free from
solvent molecules.

a) Solvent free benzidine-TCNQ crystals

Three crystals were used in this study and it was found
that in each case the current-voltage dependence was Ohmic.
Hence only one of the plots is presented in figure (6·19).
The activation energy and room temperature resistivity were
also studied, under a dry nitrogen atmosphere, and again
these results were the same for each crystal (within experi-
mental errors, i.e. $\pm0\cdot05$eV for the activation energy and
$\pm50\%$ for the resistivity). A typical activation energy
plot is shown in figure (6·20) and the results are listed
in table (6·7) together with some literature values. The
maximum temperature used in the activation energy plots
was 390K. It was found that evacuation had no effect on the
electrical properties. Photoconduction studies were attempted;
however, the photocurrent was below the detection level of
the apparatus.

<div align="center">TABLE 6·7</div>

Activation energy ΔE eV	Resistivity ρ (295K) Ωm	Pre-exponential factor Ωm	Reference
0·48	9·0 X 10^4	5·7 X 10^{-4}	This work
0·34	2·0 X 10^7	31	M. Ohmasa, M. Kinoshita and H. Akamatu, 1971

It should be noted that the measurements made by M. Ohmasa
et al. were on compressed pellets.

FIG: (6·19)   OHMIC PLOT FOR SOLVENT FREE BENZIDINE-TCNQ
              IN DRY NITROGEN

Slope = 0·97
(electrode separation
= 1·20 mm)
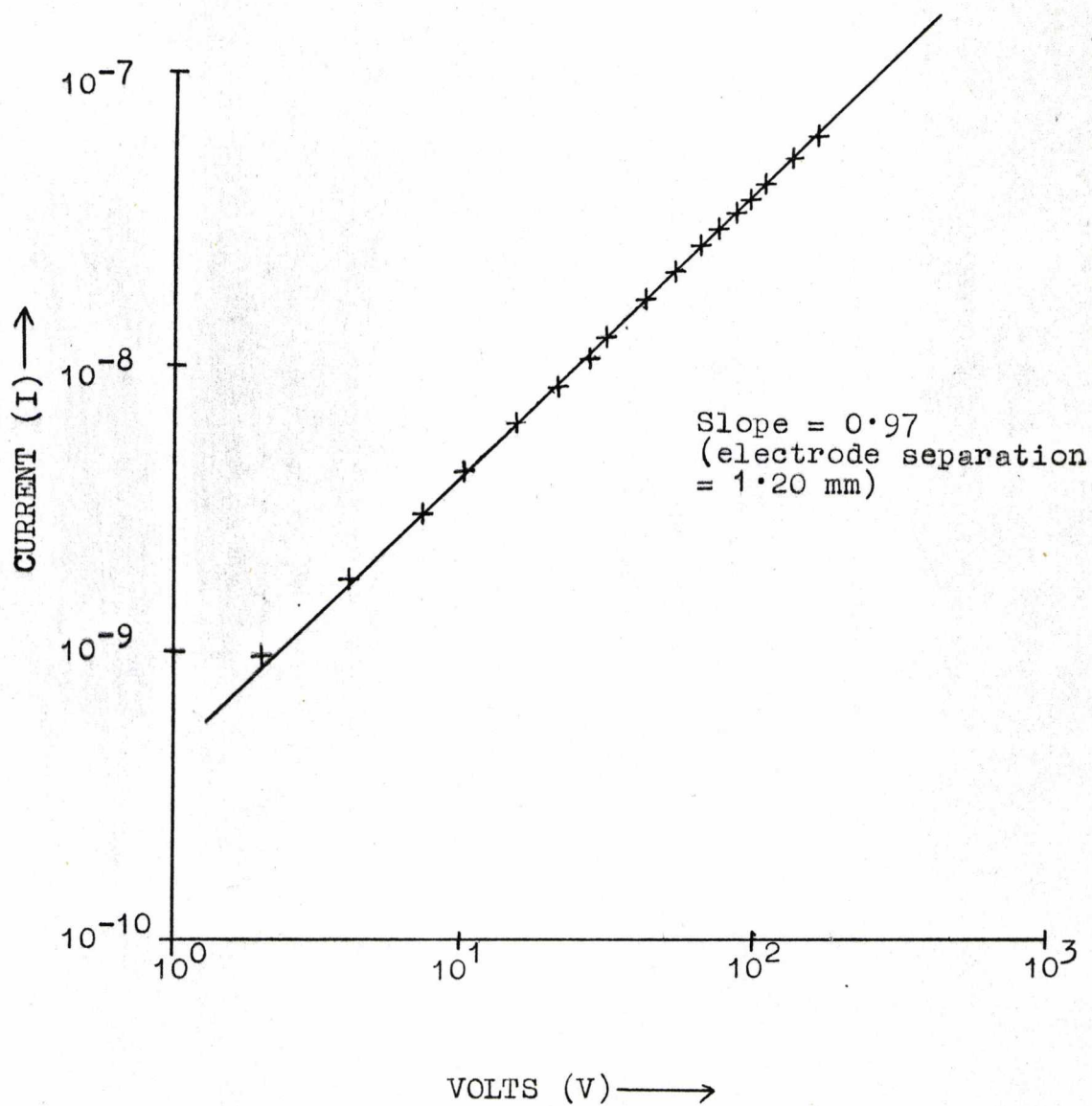
FIG: (6·20) ACTIVATION ENERGY PLOT FOR SOLVENT FREE
BENZIDINE-TCNQ IN DRY NITROGEN
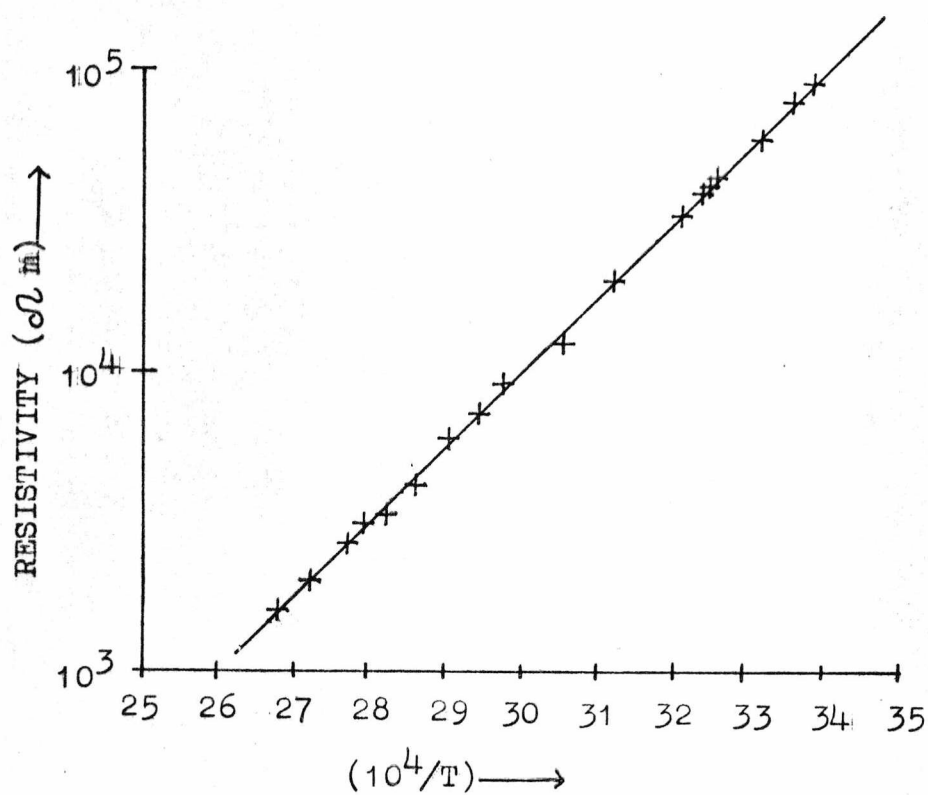
b) Solvent containing benzidine-TCNQ crystals

These crystals (ten were used in this study) were found to be Ohmic and a typical plot is shown in figure (6·21). The activation energy and room temperature resistivity were again measured under a dry nitrogen atmosphere. However, in this case before measuring the activation energy the crystals were heated up to a temperature T. This temperature was maintained until the resistivity reached a steady value. The activation energy was then measured, keeping the maximum temperature below the temperature T. This was repeated for various, increasing values of T. The results obtained for a typical crystal are shown in figure (6·22) and are listed in table (6·8). Similar results were obtained for the other crystals. It was found that these crystals were very weak and were easily broken if they were heated too fast.

TABLE 6·8
(results for crystal 4)

Maximum temperature T (K)	Activation energy ΔE eV	Pre-exponential factor ρ_o Ωm	Resistivity ρ (295) Ωm
315	0·04	2·7	$1·3 \times 10^1$
350	0·09	1·1	$3·9 \times 10^1$
373	0·13	4·8	$8·0 \times 10^2$
390	0·37	$2·0 \times 10^{-3}$	$4·3 \times 10^3$

A similar effect was found by N. Takahashi, K. Yakushi, K. Ishii and H. Kuroda, 1976.

The above results suggest that the solvent may be removed, to an unknown extent, by heating. Since the maximum temperature used was low (390K), to prevent excessive

211

FIG: (6·21) OHMIC PLOT FOR SOLVENT OCCLUDED BENZIDINE-
TCNQ IN DRY NITROGEN

Slope = 0·98
(Electrode separation
= 2·36 mm)
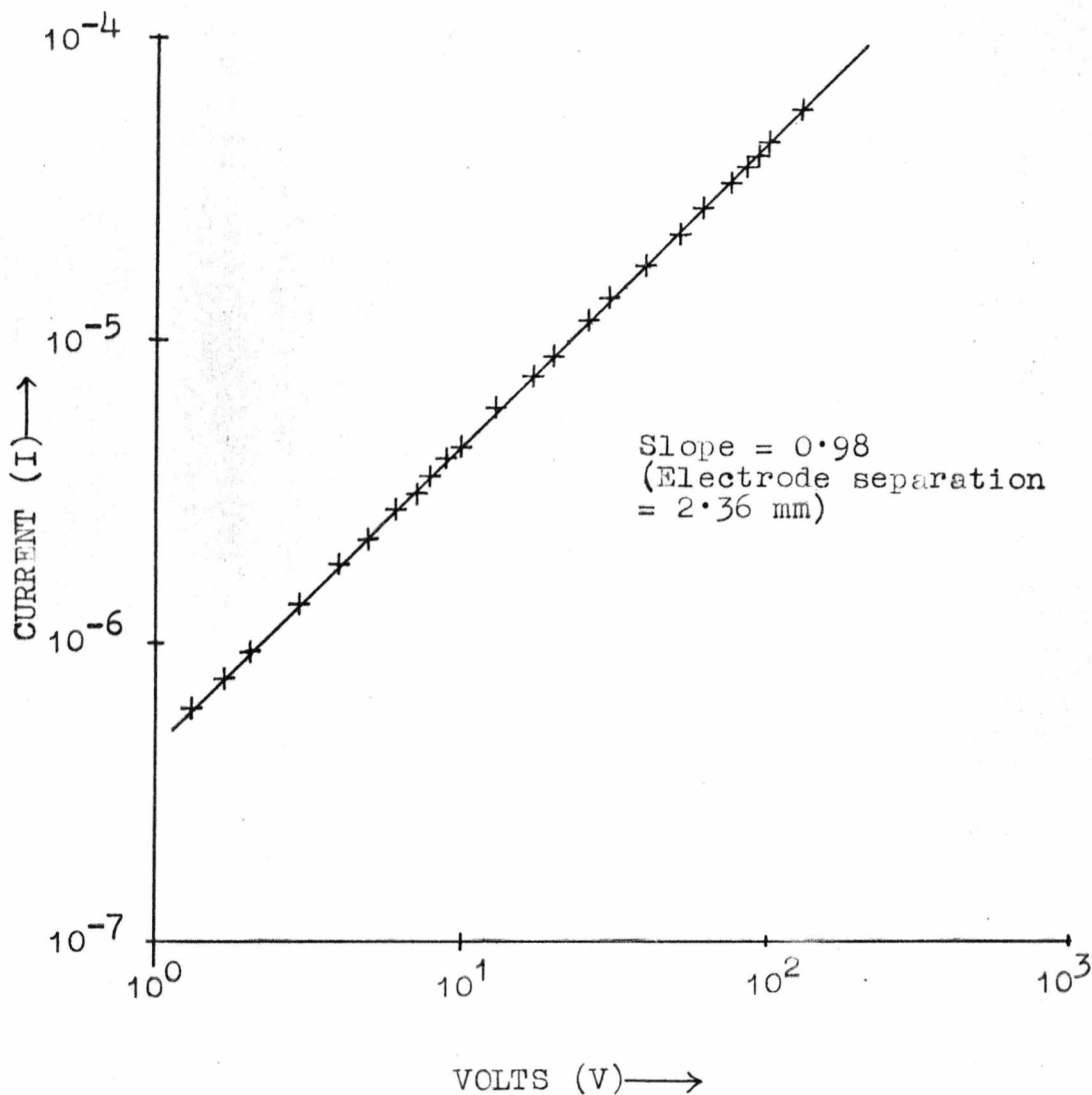
FIG: (6·22)   ACTIVATION ENERGY PLOTS FOR SOLVENT OCCLUDED BENZIDINE-TCNQ IN DRY NITROGEN
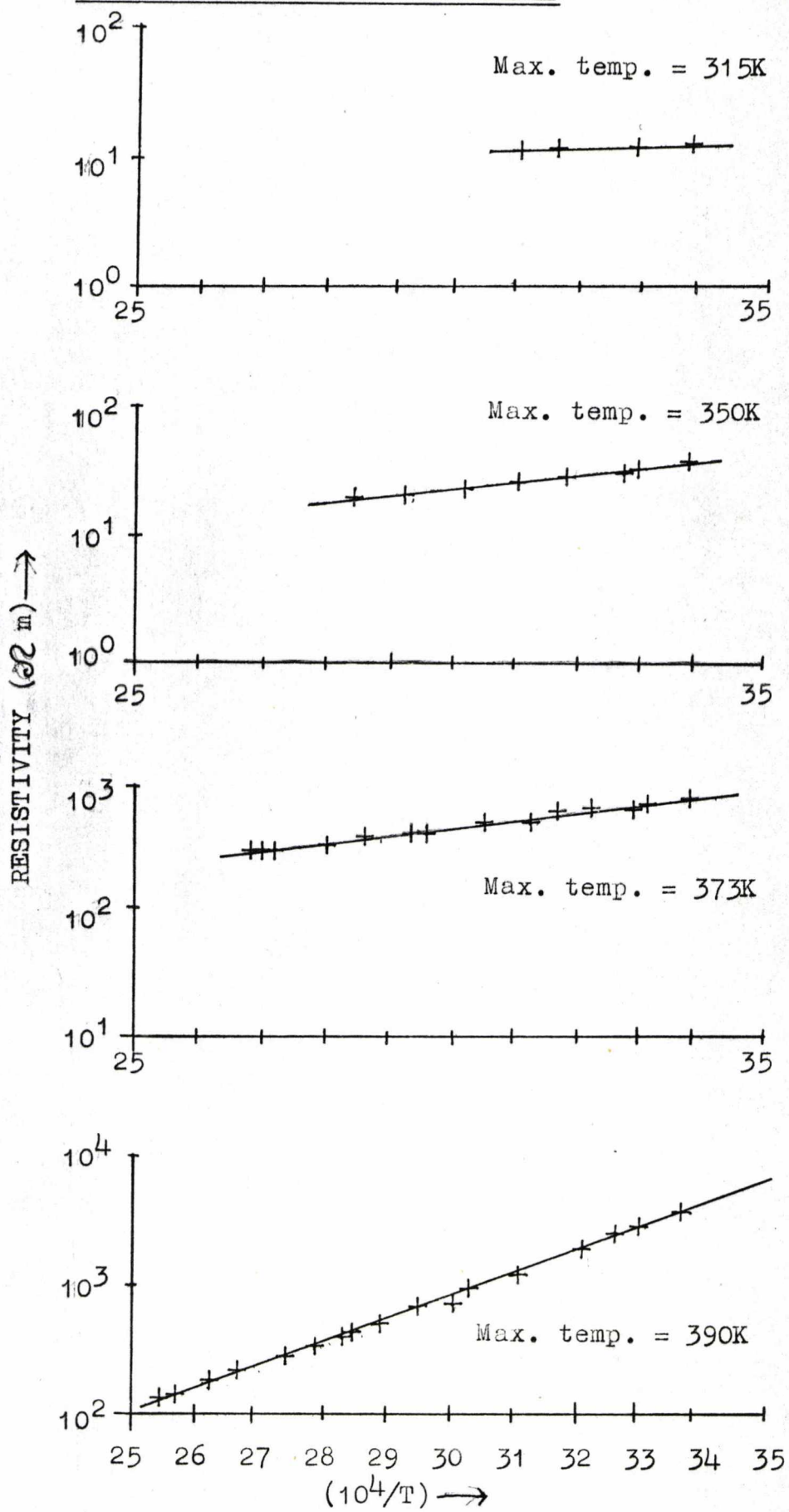
sublimation, the solvent molecules were not held very strongly. Therefore three of the crystals were placed in a vacuum to see if the solvent could be removed. However, since these crystals were very weak, it was found that they disintegrated on evacuation.

One of the main difficulties in studying benzidine-TCNQ crystals, with or without included solvent molecules, was that they easily fractured. This gave rise to erratic results due to broken crystals. Therefore the effect of gases on these crystals was not studied. The pronounced effect of solvent on these compounds is thought to arise because the donor molecule (benzidine) has a low ionization potential and the complex is close to the borderline between molecular complexes and charge transfer salts. Variations in polarization energy terms, such as may be produced by incorporating solvent molecules, may induce ionic character in the ground electronic state of the complex. If it had been possible to remove the solvent and introduce gases without disintegration of the crystal, significant gas effects on conduction may therefore have occurred, depending on polarizability of the gas molecules as well as on electron donor or acceptor character.

6·11 Electrical measurements of bis[cis-3,4-bis(trifluoromethyl)-1,2-dithiete]nickel$^{\circ}$

Mounting these crystals was found to be very difficult since the compound was very soluble in the silver paste solvent (isobutyl methyl ketone). However, two crystals were successfully mounted and initial Ohmic plots were carried out under an inert atmosphere (dry nitrogen).

These plots are shown in figure (6·23) where it can be seen
that at high voltage (V > 100V) the slope becomes steeper.
The activation energy was measured, keeping the maximum
temperature low (350K) to prevent excessive sublimation.
However, due to the very high volatility of the nickel complex
it was found that even at this low temperature sublimation
occurred at the electrode regions, causing excessive noise.
The two activation energy plots are shown in figure (6·24)
and the results are tabulated in table (6·9).

TABLE 6·9

Crystal	Activation energy ΔE eV	Pre-exponential factor ρ_0 Ωm	Resistivity $\rho(295K)$ Ωm
1	0·57	$3·3 \times 10^{-5}$	$1·8 \times 10^{5}$
2	0·63	$7·6 \times 10^{-5}$	$4·4 \times 10^{6}$

Vacuum measurements could not be carried out due to
the high sublimation rate. Photoconduction studies were
attempted; however, the photocurrent was too small to be
measured. To try and overcome the problem of the crystals'
solubility in the silver paste solvent, some films were
evaporated in a similar manner as for lead phthalocyanine
(cf. Chapter (5·16)). Preparation of good uniform films
proved to be impossible with the apparatus available, due
to the high volatility of the nickel complex. Resistivity
measurements on these films (four were prepared) gave
surface resistivity values of $2 \times 10^{8}\Omega$ per square (approxi-
mately). However, it should be noted that these measurements
are very inaccurate (> 100% error) due to the very low
signal to noise ratio.

FIG: (6·23)   OHMIC PLOTS FOR BIS[CIS-3,4-BIS(TRIFLUOROMETHYL)-1,2-DITHIETE]NICKEL° IN DRY NITROGEN

Slope = 0·94
(Electrode separation
= 2·49 mm)

Slope = 1·07
(Electrode separation
= 3·12 mm)

CURRENT (I) ⟶

VOLTS (V) ⟶

216
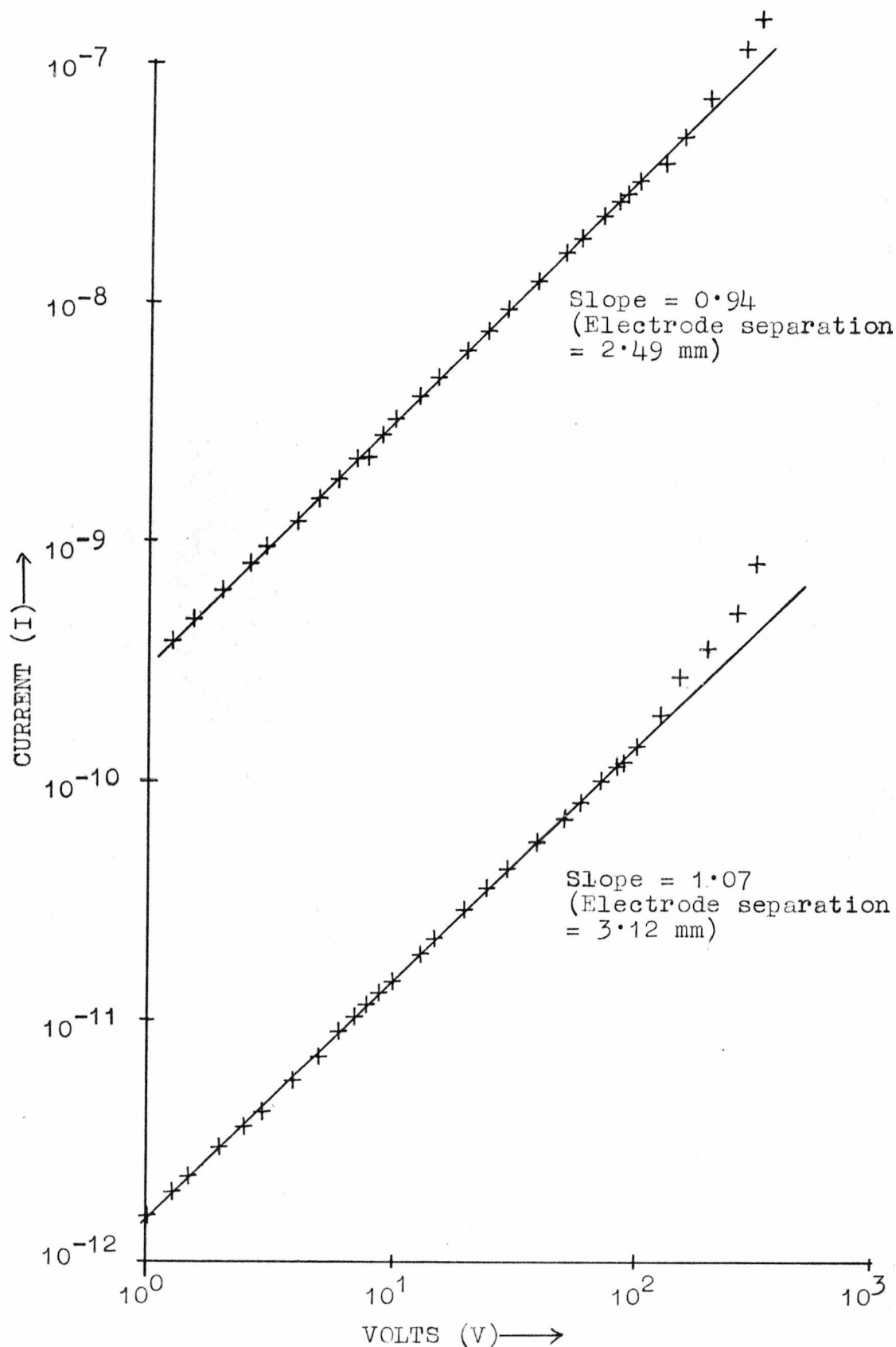
FIG: (6·24)   ACTIVATION ENERGY PLOTS FOR BIS[CIS-3,4-
BIS(TRIFLUOROMETHYL)-1,2-DITHIETE]NICKEL°
IN DRY NITROGEN
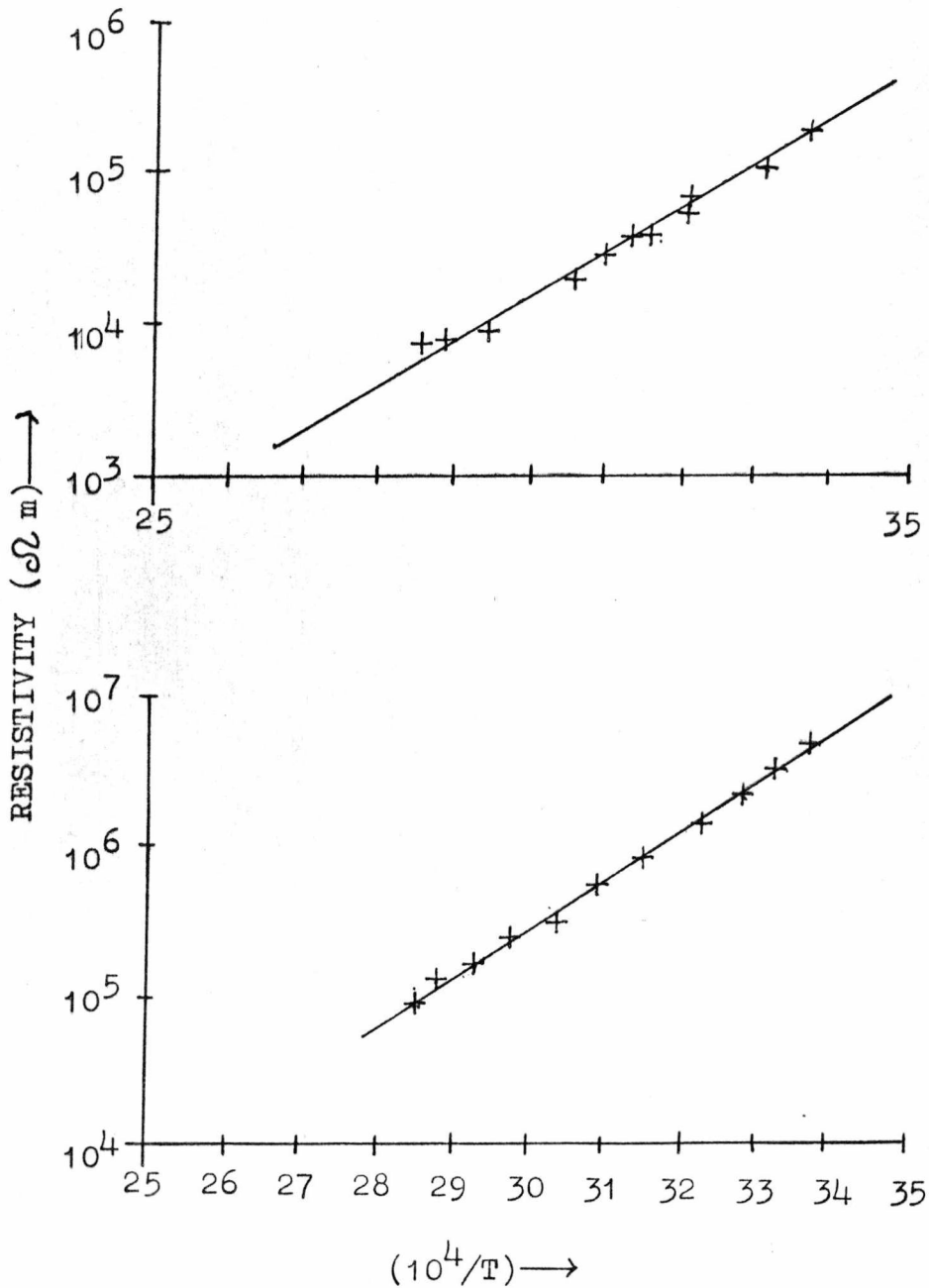
To conclude, the single crystal measurements indicated that the resistivity of bis[cis-3,4-bis(trifluoromethyl)-1,2-dithiete]nickel$^{\circ}$ was in the region of $5 \times 10^5 \, \Omega$ m with an activation energy of $0 \cdot 55$ eV ($\pm 0 \cdot 06$ eV).

6·12 Effect of gases on copper oxinate and palladium oxinate single crystals

After mounting the crystals and degassing the surfaces by evacuation ($\sim 10^{-4}$ Pa) and heating (~ 400K) the current-voltage characteristics were studied. In each case the crystals (two crystals of each compound were studied) exhibited Ohmic characteristics, hence only one Ohmic plot is shown for each compound (figures (6·25) and (6·26)). The activation energies were also measured under a high vacuum, and these results are shown in figures (6·27) and (6·28), and in table (6·10). The measurement errors were $\pm 0 \cdot 03$ eV for the activation energy and 80% for the pre-exponential factor.

TABLE 6·10

Oxinate	Activation energy ΔE eV	Pre-exponential factor ρ_0 Ω m	Resistivity ρ (295K) Ω m
Copper	$1 \cdot 27$	$1 \cdot 6 \times 10^{-7}$	$8 \cdot 0 \times 10^{14}$
Palladium	$0 \cdot 78$	$1 \cdot 6$	$3 \cdot 5 \times 10^{13}$

a) Effect of dinitrogen tetroxide

It was found that this gas had very little effect on the resistivity of both oxinates. The resistivity was decreased by a maximum factor of 2 when the pressure of gas present in the cell was approximately 5×10^4 Pa. The

FIG: (6·25) OHMIC PLOT FOR COPPER OXINATE IN A
DRY NITROGEN AMBIENT AT 328K

Slope = 1·06
(Electrode separation
= 1·73 mm)

CURRENT (I) ⟶

VOLTS (V) ⟶

219
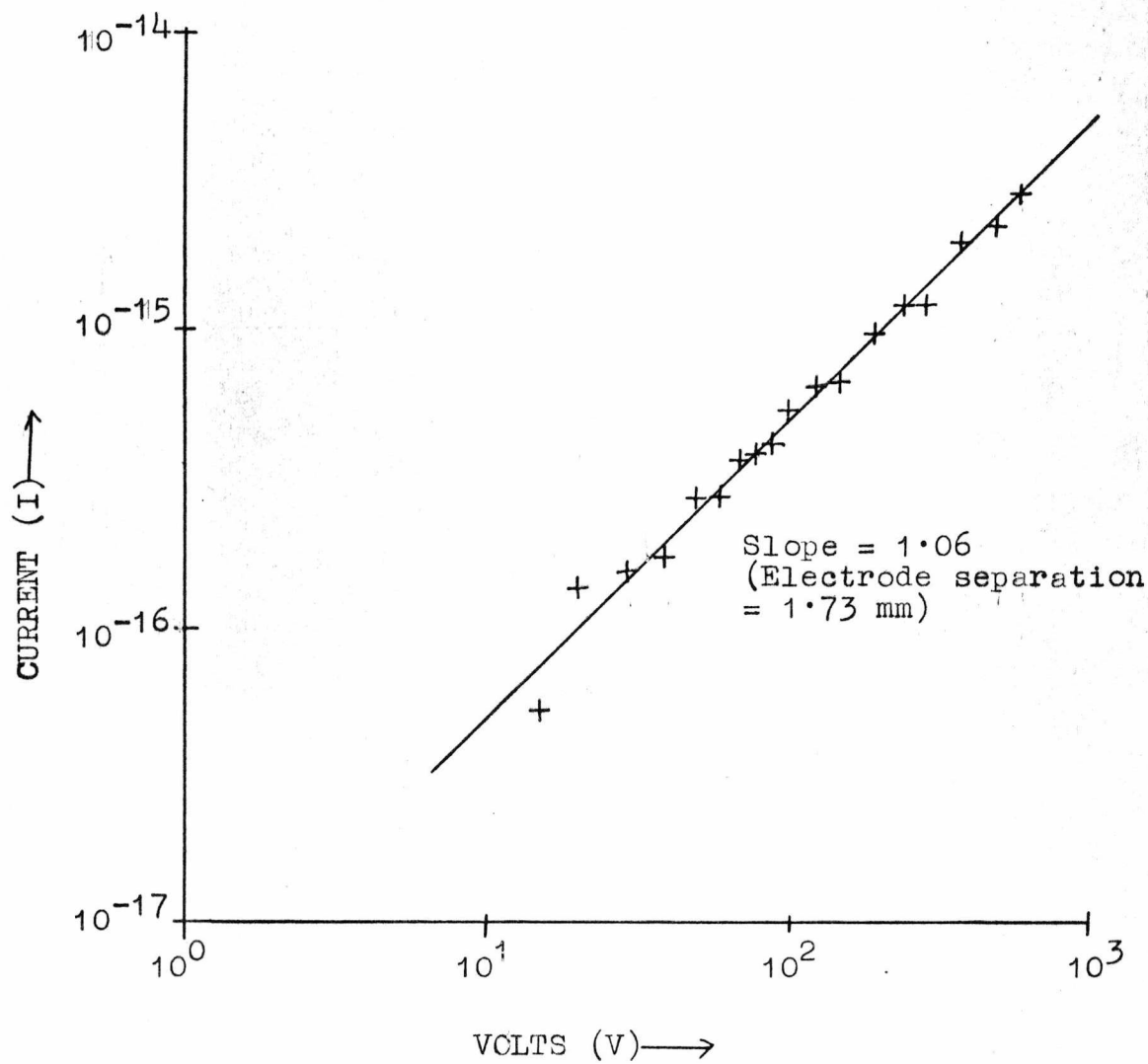
FIG: (6·26)   OHMIC PLOT FOR PALLADIUM OXINATE IN A
DRY NITROGEN AMBIENT AT 335K

Slope = 1·03
(electrode separation
= 2·32 mm)
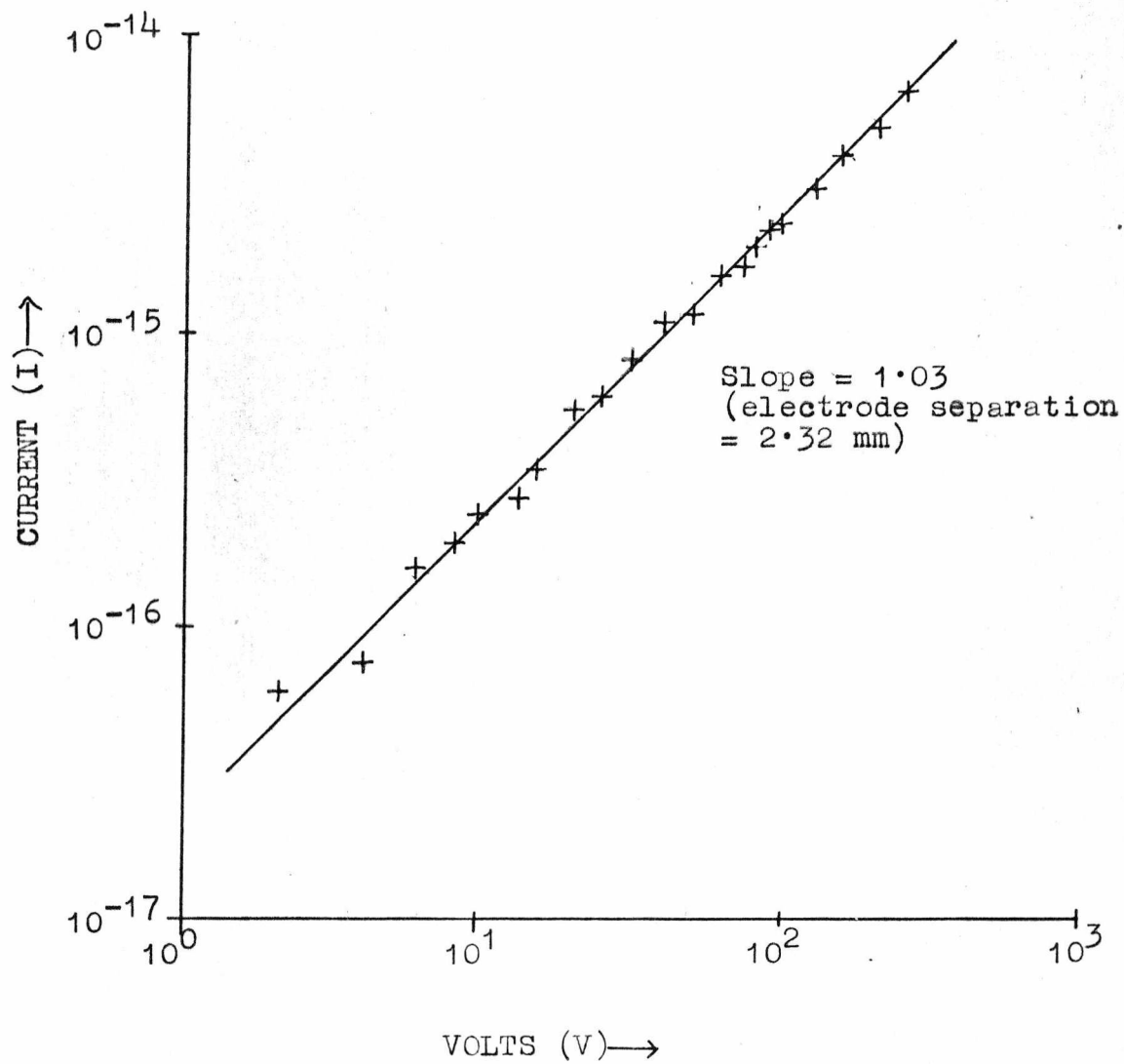
FIG: (6.27) ACTIVATION ENERGY PLOT FOR COPPER OXINATE IN A HIGH VACUUM

221
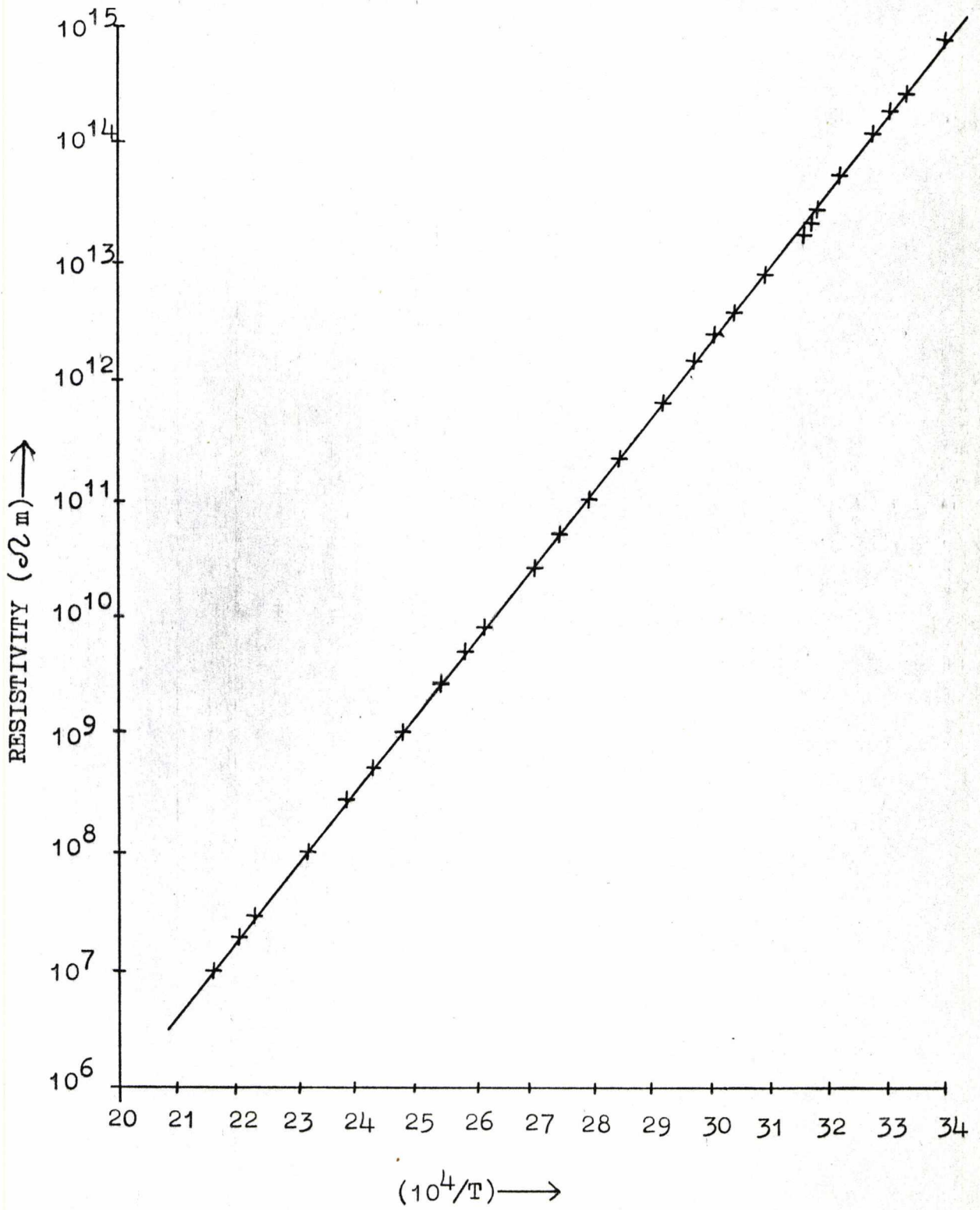
FIG: (6·28) ACTIVATION ENERGY PLOT FOR PALLADIUM OXINATE IN A HIGH VACUUM

222
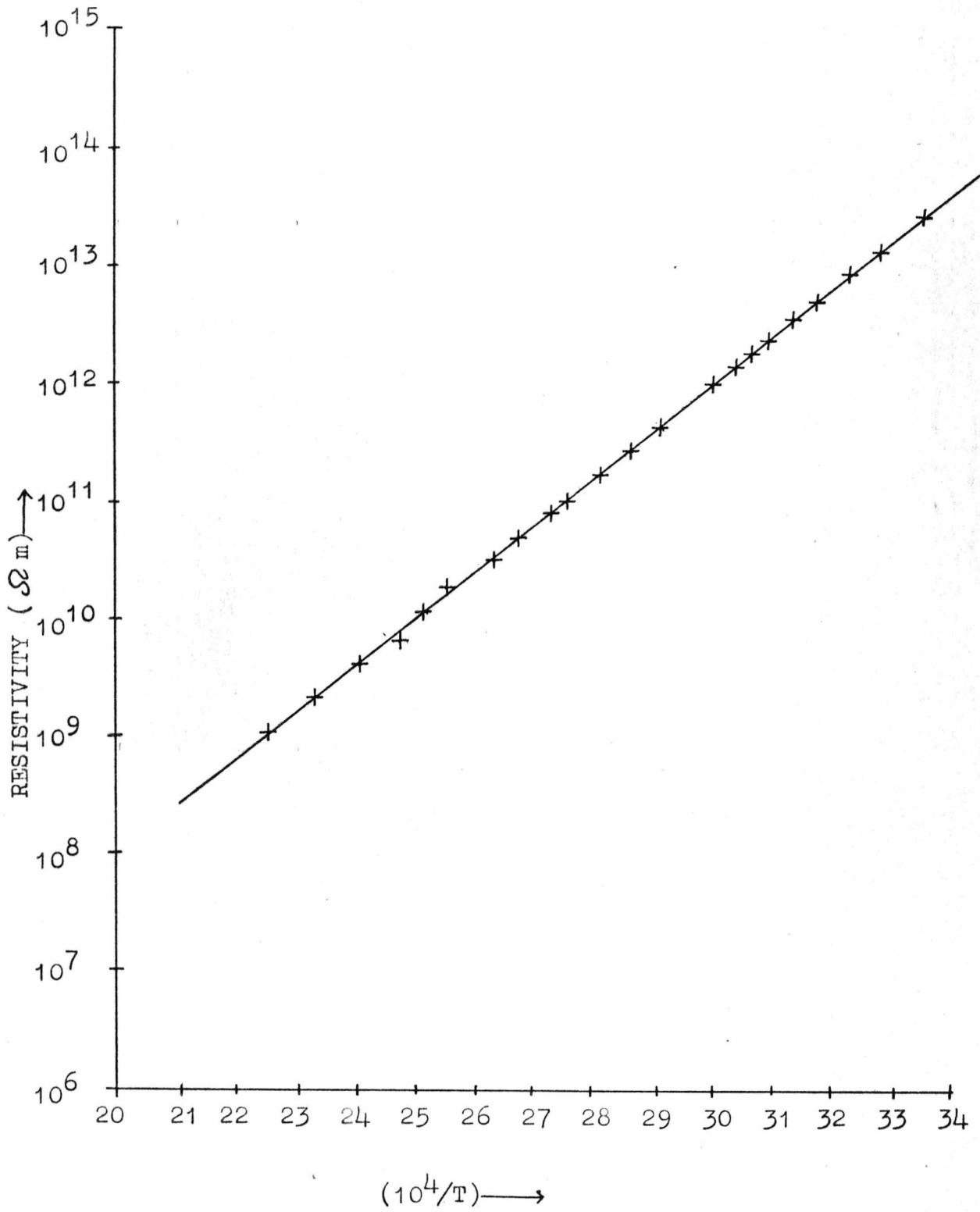
activation energies of the oxinates in an ambient of approximately 10^4 Pa of dinitrogen tetroxide were measured. Figures (6·29) and (6·30) show the results obtained; they are also presented in table (6·11). These results indicated that dinitrogen tetroxide had very little, if any, effect on the conduction mechanism of the two oxinates.

TABLE 6·11

Oxinate	Activation energy ΔE eV	Pre-exponential factor ρ_o Ω m	Resistivity $\rho(295K)\Omega$ m
Copper	1·25	$5 \cdot 3 \times 10^{-9}$	$1 \cdot 2 \times 10^{13}$
Palladium	0·78	2·8	$6 \cdot 0 \times 10^{13}$

b) Effect of boron trifluoride

Again it was observed that the resistivity and activation energy remained unaltered by the gas.

c) Effect of other gases

Ammonia and oxygen were also found to have no effect on the conduction mechanism of the oxinates.

Photoconduction studies in a vacuum or different gas environment were not carried out since the photocurrent was below the detection limits of the apparatus. Hence it was concluded that electron acceptor and donor gases had no effect on the conduction mechanism. This implies either that the gases do not adsorb significantly onto the compounds or that they react to form a compound of high resistivity.

223

FIG: (6·29) ACTIVATION ENERGY PLOT FOR COPPER OXINATE IN AN AMBIENT OF DINITROGEN TETROXIDE (10^4 Pa)

224
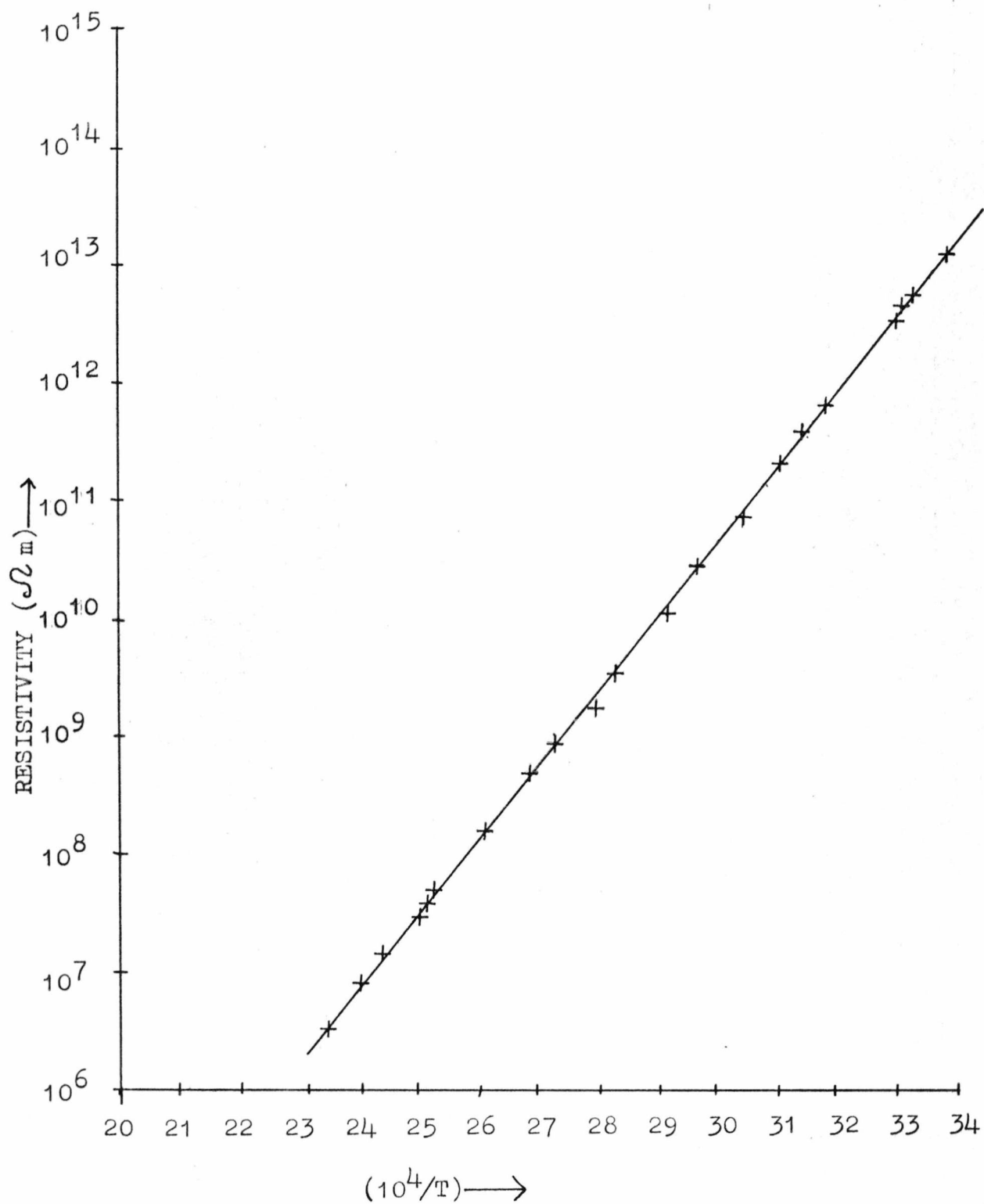
FIG: (6·30) ACTIVATION ENERGY PLOT FOR PALLADIUM OXINATE
IN AN AMBIENT OF DINITROGEN TETROXIDE (10^{4}Pa)
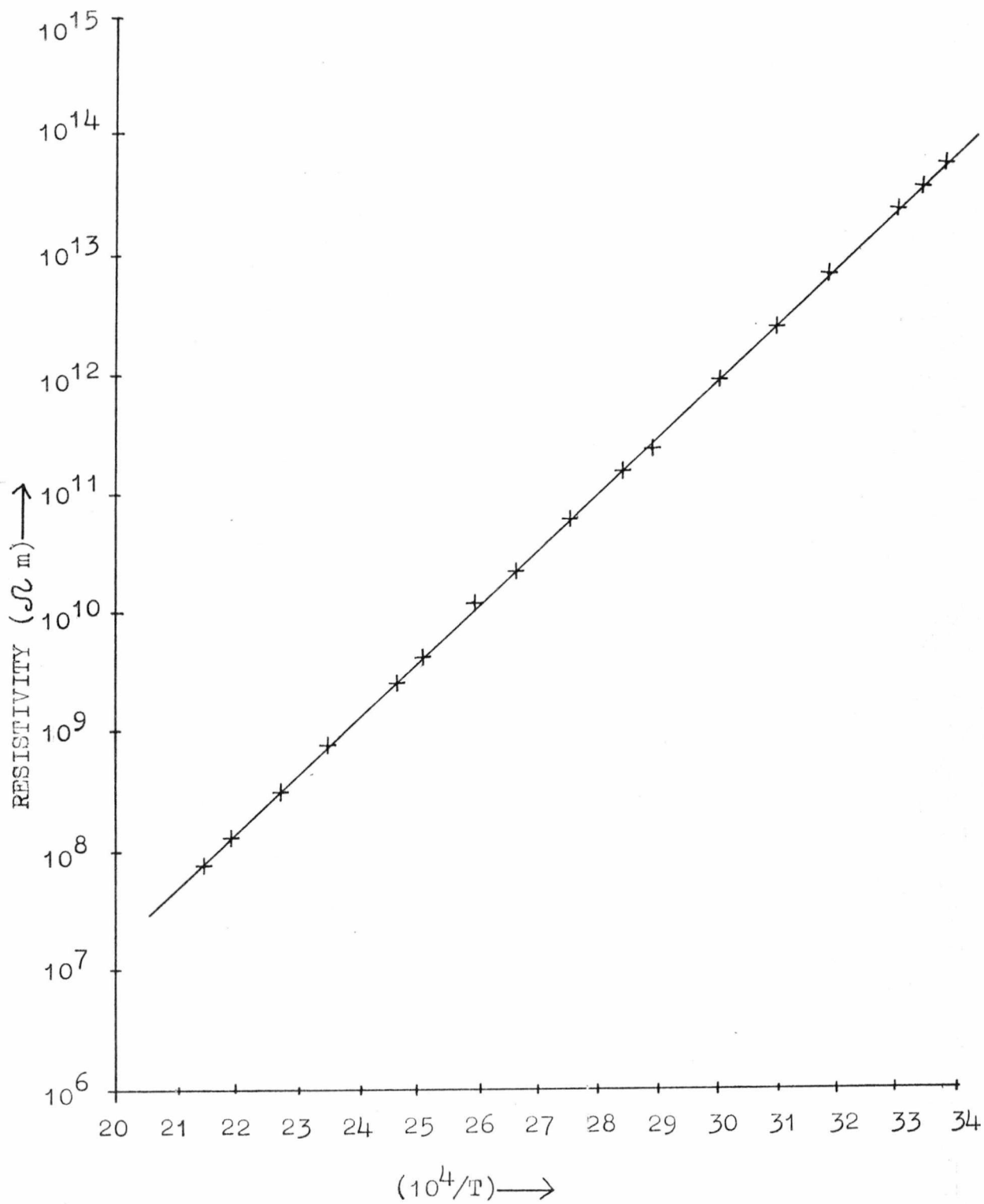
6·13   Discussion 1: Type of interaction between gas and crystal

From the study of gas effects on phthalocyanine single crystals (cf. Chapter 5), it was concluded that the main interaction was a donor-acceptor type. Further confirmation for this conclusion was found by studying the effect of systematically altering the chemical nature of the crystals. If electron donor crystals only interact strongly with acceptor gases then the converse should also be true (i.e. electron acceptor crystals only interact strongly with donor gases). Furthermore, if a crystal can exhibit both donor and acceptor properties then it should interact with both acceptor and donor gases. With this in mind the following series of crystals was studied: perylene, perylene-TCNQ and TCNQ, which are donor, donor-acceptor and acceptor type crystals.

The results of the study of gas effects on these crystals have already been presented (cf. sections (6·2) to (6·7) inclusive). A summary of the results is given in table (6·12), and clearly demonstrates that the above predictions were valid.

TABLE 6·12

Crystal	Chemical character	Gas effect	
		dinitrogen tetroxide	ammonia
perylene	donor	conductivity enhanced	no effect
perylene-TCNQ	donor-acceptor complex	conductivity enhanced	conductivity enhanced
TCNQ	acceptor	no effect	conductivity enhanced

6·14 Discussion 2: Effect of altering the surface ionization potential

For this study the following compounds were used: metal-free phthalocyanine, perylene, anthracene and phenanthrene. The effect of dinitrogen tetroxide on each of these electron donors was studied and the results have been presented in this chapter and in Chapter 5. A brief summary of the results is given in table (6·13). It was found that in the cases of anthracene and phenanthrene a chemical reaction took place. This was deduced from the irreversible effect of the gas and the colour change of the crystals. C. Dufraisse, J. Rigaudy and K. Vang Thang (1963) also found that anthracene, suspended in benzene, reacted with dinitrogen tetroxide under mild conditions (283–288K).

REACTION

$$N_2O_4 + \quad \xrightarrow{(283-288K)} \quad$$
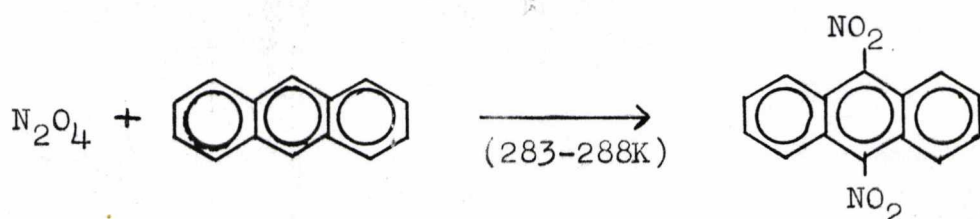
Since phenanthrene has a similar structure it should also undergo a similar addition reaction. For perylene and the phthalocyanines this type of reaction is sterically hindered.

Therefore only the results for metal-free phthalocyanine and perylene can be considered. It can be seen that perylene has a higher surface ionization potential and is less sensitive towards dinitrogen tetroxide. This is predicted because a higher ionization potential implies that the donor-acceptor interaction is weaker, resulting in a smaller gas effect. However, these two results are hardly conclusive. Further

Donor	Ionization potential eV		Surface resistivity Ω per square		
	Gaseous	Surface	H.V.	100 Pa N_2O_4	10^4 Pa N_2O_4
metal-free phthalocyanine	7·36	5·20	6×10^{14}	2×10^{11}	1×10^8
perylene	7·22	5·39	2×10^{16}	6×10^{13}	8×10^{12}
anthracene	7·40	5·65	7×10^{16}	7×10^{13}	2×10^{11}
phenanthrene	7·85	6·45	8×10^{15}	5×10^{15}	4×10^{13}

TABLE 6·13

evidence for a decrease in the gas effect with increasing surface
ionization potential may be found by looking at the gas
effects on the phthalocyanines in more detail. Table (6·14)
lists the minimum surface resistivities and surface ioniza-
tion potentials. It can be seen that there is an increase
of the minimum surface resistivity with respect to increasing
surface ionization potential.

TABLE 6·14

Phthalocyanine	Surface ionization potential eV	minimum surface resistivity Ω per square
metal-free	5·20	1×10^8
copper	5·00	7×10^7
nickel	4·95	2×10^7

To conclude, the variation in the surface ionization
potential seems to be reflected in the effect of gases on
the crystals. Also, in some cases chemical reactions may
occur which result in irreversible gas effects.

6·15 Conclusions

The main conclusions of the work presented in this
chapter are listed below.

1) From the study of gas effects on perylene, perylene-
TCNQ and TCNQ it is evident that the main interaction is
of a donor-acceptor type. This is in agreement with the
conclusion in Chapter 5.

2) Crystals with both electron donor and acceptor
molecules (complex crystals) exhibit both donor and acceptor

229

properties in gas adsorption. Furthermore, the sensitivity
is not drastically altered, as may be seen by comparing the
dinitrogen tetroxide effect on perylene and on perylene-
TCNQ (figures (6·3) and (6·7) respectively).

3) The type of orbital accepting electrons is important
in determining the extent of interaction. σ type orbitals
were much more effective at accepting electrons than π type
orbitals (cf. N_2O_4 and BF_3 effects).

4) Adsorption of gas onto the surface of the crystal
can inhibit the surface photoconduction mechanism, thereby
allowing the bulk photoconduction mechanism to be studied
(cf. N_2O_4 on TCNQ and on perylene-TCNQ).

5) Both anthracene and phenanthrene undergo chemical
reactions with dinitrogen tetroxide and boron trifluoride.

6) Solvents included in the benzidine-TCNQ crystal may
be removed, to some extent, by heating. However, this
results in a very weak crystal which readily disintegrates.

7) Neither copper oxinate nor palladium oxinate showed
any effect with either dinitrogen tetroxide or boron tri-
fluoride. This indicates that there are other important
factors determining the extent of gas interaction (i.e.
polarizability and steric factors).

Chapter 7 - Conclusions

7·1 Results of the present study

The main objective of the work presented in this thesis was to determine the type of chemical properties dominating the adsorption of gases onto the surface of organic crystals. The phenomena investigated fall into three main categories:

1) High vacuum semiconduction parameter (activation energy, resistivity, and pre-exponential factors).

2) High vacuum photoconduction parameter (spectral response, magnitude and dependence on light intensity).

3) Effect of adsorbed gases on both semiconduction and photoconduction parameters.

Where possible the results have been correlated with those obtained in previous studies. Furthermore, to obtain reproducible gas effects it was found necessary to admit the gas into the conductivity cell under controlled conditions (temperature, purity and rate of increase of gas pressure).

Two distinct series of studies were carried out:

1) where the chemical nature of the crystals was altered very slightly.

2) where the chemical nature of the crystals was grossly altered.

In the first case the metal phthalocyanine series was used; only very minor changes in the surface ionization potential occurred when the central metal atom was changed. For the second series crystals with donor, acceptor and both donor and acceptor characteristics were chosen. From the study of the effect of gases on the phthalocyanine series several conclusions were made. These were further tested in the second series of compounds. The main conclusions of this

work are listed below.

1) The type of gas adsorption producing electrical conductivity changes is predominantly chemisorption.

2) The main interaction between gas molecules and the crystal responsible for the chemisorption is of an electron donor-acceptor type.

3) Gas adsorption is restricted to the surface of the crystals, except in the case of small gas molecules such as oxygen, where there is evidence of slow diffusion into the bulk of several phthalocyanine crystals.

4) The type of orbital involved in donating or accepting electrons is important in determining the strength of the adsorption and the resulting electrical conductivity changes. Where electron transfer is between delocalized π orbitals of molecules of the crystal and adsorbed gas (e.g. phthalocyanines with N_2O_4) the adsorbed molecules may be removed either by heating in vacuo or, more easily, by treatment with a gas of opposite donor or acceptor character to the adsorbed gas (e.g. treatment of phthalocyanine covered with the electron acceptor N_2O_4 with the electron donor gas NH_3). In such cases the increase in electrical conductivity is consistent with nearly complete surface coverage by adsorbed gas at pressures above approximately 10^3 Pa, with each gas molecule producing one surface charge carrier. Where electron transfer is between more localized orbitals (e.g. with the σ-bonded electron acceptor BF_3) the adsorption is stronger and less easily reversible.

5) Different metal phthalocyanines show similar behaviour towards gases, and small effects of changing the metal atom on the magnitude and reversibility of the gas effects

232

correlate with the redox properties of the metal ions.

6) Unexpectedly small changes in electrical properties of some aromatic hydrocarbons (e.g. anthracene) on treatment with N_2O_4 are ascribed to irreversible chemical reaction following the initial electron donor-acceptor interaction.

7) Crystals of electron donor-acceptor complexes show small increases in conductivity with both donor and acceptor gases.

8) The semiconduction activation energy in the presence of gases which enhance conductivity is much lower than the value for clean crystals in vacuo, and comparable to the values typically obtained from temperature dependence of photoconduction. Thus, the chemical formation of ionized surface states by interaction of gases with the crystal surface may be compared to the optical production of ionized states in photoconduction.

9) Although very small amounts of adsorbed gases produce a more readily observable effect on photoconduction than on semiconduction, at higher surface coverages the enhanced semiconduction obscures the smaller photocurrent.

10) The increased surface ionized state density, due to gas adsorption, was found to decrease the dependence of the photocurrent on the incident light intensity to levels below 1/3 (usually in the range 0·3 to 0·1).

7·2 Design criteria for an organic semiconductor gas detector (olfactometer)

From the results obtained in this study it is possible to formulate several design criteria for a gas detector based on an organic semiconductor. The criteria are listed below.

1) Chemical nature

If electron accepting gases are to be detected (e.g. N_2O_4, BF_3, Cl_2, O_2, etc.) then the organic semiconductor should be an electron donor. Furthermore, there will be an ideal combination of electron affinity (gas) and surface ionization potential (semiconductor) which will result in high surface coverage (and consequently a large change in electrical resistivity) and easy reversibility. If the difference between the electron affinity and the ionization potential is too high then irreversible gas adsorption will occur. To detect electron donor gases the semiconductor would obviously have to be an electron acceptor. However, it is possible to detect both types of gases by using a charge transfer complex semiconductor (donor-acceptor crystals). This will result in loss of sensitivity.

2) Surface effect

Except for the cases where the gas molecules are small enough to diffuse into the bulk of the crystal, gas adsorption is entirely restricted to the surface of the semiconductor. Consequently, for maximum gas sensitivity the semiconductor sensing element should have the largest possible surface area (e.g. films). Ideally the lattice structure of a crystal should be sufficiently porous to allow gases to easily diffuse into the bulk of the crystal. However, in this study it was found that removal of solvent from channels in benzidine-TCNQ crystals drastically reduced the mechanical strength of the crystals, suggesting that

234

porosity and mechanical strength may be incompatible in molecular crystals.

3) Resistivity

The adsorption of a gas onto the surface of an organic semiconductor results in an increase in the number of charge carriers in the material. This is observed as a decrease in the resistivity. Therefore for maximum sensitivity the semiconductor should have a very high intrinsic resistivity (i.e. very few free charge carriers m^{-3}). However, there will be a limiting value beyond which the increased resistivity cannot be measured. With the apparatus used in this study an ideal resistivity was in the order of $10^8 - 10^{10} \Omega$ m.

4) Electrode contact

To be able to make use of an organic semiconductor as a sensing element it must be possible to attach Ohmic contacts. If paste electrodes are used then the crystals must be relatively insoluble in the solvents used in the paste.

5) Specificity

By choosing suitable materials as organic semiconductors it should be possible to obtain sensing elements that are specific to certain gases. For example, in the present work it was found that the relative sensitivities of phthalocyanines, aromatic hydrocarbons and tetracyanoquinodimethane to N_2O_4, BF_3, O_2 and NH_3 were different. Selectivity may be enhanced by varying the temperature of the sample, utilising differences

235

in the strength of adsorption as well as differences
in the effects of gases on the activation energy for
conduction.

7·3 Relation to other types of gas detectors

Present systems for monitoring toxic gases include:
chemical means (Dräger tubes), mass spectrometry, infra-red
adsorption, chromatography and catalytic bead detectors. The
latter are only useful for detecting combustible gases since
their operation relies on the evolution of heat during
combustion. Mass spectrometry, chromatography and infra-
red adsorption are relatively expensive and not easily
portable; furthermore they require experienced operators.
Chemical detection can be made continuous using a moving paper
tape system, but accurate readout of the colour change
produced by the gas to be detected requires additional optics
and electronic detectors of the reflected light.

It is envisaged that the use of an organic semiconductor
gas detection element could result in overcoming all the
drawbacks of the above instruments. It could be designed
to be sensitive (down to at least 1 ppm), continuous in
operation, easy to use, low cost and robust. The basic need
is to monitor the change in resistivity of the sensing
element. Using a bridge circuit and an operational amplifier
the resistivity change could be very accurately and easily
monitored. Considerable selectivity may be achieved by
combining several different organic semiconductor sensing
elements, and a device using this principle in conjunction
with simple logic circuitry to provide specific alarm
indications for a variety of gases has been described

236

(R.H. Wright and J.E. Cumming, Canadian Patent 915458, 1972).

7·4 Suggestions for further work

In order to study the gas adsorption process on organic crystals, further and different studies will need to be carried out. The types of investigations which would yield valuable information about the adsorption process are listed below.

1) Adsorption isotherms

These would provide information about the type of adsorption occurring. However, the main experimental difficulty is the very small surface areas of the crystals commonly encountered. Powdered samples could be used; however, the characteristics of the surface of a powdered sample may not correspond with those of a single crystal. Nevertheless adsorption isotherm studies on a series of compounds could indicate general trends.

2) Charge carrier studies

Mobility studies, although difficult to perform, would give valuable information about any change in the conduction mechanism due to gas adsorption. It should be noted that adsorption is restricted to the surface, whereas mobility measurements usually refer to bulk properties. However, with the large changes in resistivity encountered in this study any changes in the mobility of the carriers should be fairly easily observed.

3) Majority carrier determination

It has been suggested in this study that the adsorption of gases will determine which type of majority carrier is present (i.e. electron acceptor gases would create 'hole' charge carriers). By measuring the Hall effect or the

thermoelectric emf it will be possible to determine the majority carrier.

4) Adsorption

Further information about the nature of the bond formed between the gas and the crystal surface is required before models for the adsorption process can be postulated. Measurement of the change in the crystal reflectance spectrum could provide information about the bonding and the type of adsorbed gas molecule.

5) Different materials

There is still a wide variety of materials that have not been studied. By looking at different materials other factors influencing gas adsorption may be noted. Two groups of materials that might be worth studying in some detail are polymers and dyes.

To conclude, very few measurements have been made that relate specifically to gas adsorption on organic semiconductors. Apart from possible uses as gas sensors, this type of study can also provide useful information about the dark and photo-conduction mechanisms.

7·5 Conclusion

The present work has shown that both the dark and photo-conductivity of organic semiconductors can be greatly enhanced by gases. This effect is selective. Furthermore, the adsorption process is fast and easily reversible. However, it is interesting to note that the human olfactory system is capable of detecting extremely low concentrations of gases. This process is both very rapid and selective. Comparison with the results obtained in this thesis show that there is still considerable scope for improvement for a gas detector based on an organic semiconductor.

APPENDIX

A1   Copper constantan thermocouple programme

The first stage in writing a programme to relate the thermal emf to temperature was to fit a curve to standard thermocouple data. This was carried out by using a standard curve fitting programme (PLOFIT) on the university's Eliot 4130 computer. It was found that a polynomial of degree 5 gave a satisfactory fit. This equation was then used in the BASIC programme shown below (programme 1). First an approximate temperature was guessed by solving a quadratic equation; further refinement was then carried out using a Newton Raphson itterative process.

Programme 1

```
1        DIM M(10),O(10)
5        REM ***** COPPER-CONSTANTAN THERMOCOUPLE PROGRAMME.
10       PRINT "NUMBER OF RESULTS=";
11       INPUT N
20       LET A = -6:28615
30       LET B = 4:37824?-3
40       LET C = 8:19781?-5
50       LET D = -5:50951?-8
60       LET E = 1:7483?-11
70       PRINT
100      FOR I = 1 TO N
110       PRINT "MV.=";
111       INPUT M(I)
120       LET F = A-M(I)
130       LET G = B↑2-(4+F+C)
140       LET T = (-B+SQR(G))/(2*C)
150      PRINT "FIRST APPROX.=";T;"K"
160       LET R = 0
200       LET R = R+1
210       LET H = F+B*T*C*T↑2*D*T↑3+E*T↑4
220       LET K = B+2*C*T+3*D*T↑2+4*E*T↑3
230       LET L = H/K
240       LET O(I) = T-L
250       IF R = 20 THEN 350
260       IF ABS(L) < 1?-7 THEN 300
270       LET T = O(I)
280       GOTO 200
300       PRINT "+++ TEMP=";O(I);" K AFTER";R;" ITERATIONS."
310       GOTO 400
350       PRINT "***********SERIES HAS NOT CONVERGED***********"
360       PRINT "TEMP AFTER 20  ITERATIONS IS";O(I);" K."
```

```
400     NEXT I
490     PRINT
491     PRINT
492     PRINT
500     PRINT "                   TEMP.","10↑3/T","MV."
501     PRINT "DEG.C","K"
510     PRINT "_ _ _ _ _ _ _ _ _ _ _ _ _ _ _ _ _ _ _ _ _"
520     FOR I = 1 TO N
530       PRINT O(I)-273.13,O(I),10↑3/(O(I)-273.13),M(I)
540     NEXT I
550     PRINT "_ _ _ _ _ _ _ _ _ _ _ _ _ _ _ _ _ _ _ _ _"
600     END
```

A2 Platinum resistance thermometer programme

PLOFIT was used to fit a curve to the experimental data. The resulting equation (a polynomial of degree 5) was used in the BASIC programme shown below (programme 2), to construct a table of output voltage versus temperature.

Programme 2

```
10      REM ***** PLATINUM RESISTANCE THERMOMETER PROGRAMME.
20      PRINT "  OUTPUT","       TEMPERATURE    ","10↑3/T"
30      PRINT "  VOLTS","    C","    K"
40      PRINT "========================================="
50      FOR X = 0 TO 500 STEP 0·5
60        LET Y = 0·10602+1·6041?-2*X-1·936?-5*X↑2
70        LET Y1 = -2·6739?-8*X↑3+9·703?-11*X↑4
80        PRINT Y+Y1,X,X+273,10↑3/(X+273)
90      NEXT X
95      PRINT "========================================="
100     END
```

A3   Line fitting programme

The BASIC programme shown below (programme 3) was used
to fit the thermal activation energy and Ohmic data to
straight lines. The functions for 'X' and 'Y' could be
defined at the beginning of the programme (i.e. log, recip-
rocal and linear). Also this programme was written to allow
data points to be deleted or altered.

Programme 3

```
90       REM ***** MIN. SUM SQS. LINE FITTING PROGRAMME.
100      PRINT "EXPONENT FOR THE X AXIS=";
110      INPUT E1
120      PRINT "EXPONENT FOR THE Y AXIS=";
130      INPUT E2
140      LET N = 0
150      INPUT X,Y
160      IF X = 99999 THEN 210
170      LET N = N+1
180      LET G(N) = FNA(X)
190      LET F(N) = FNB(Y)
200      GOTO 150
210      PRINT
220      PRINT
290      LET D = 0
300      LET X1,X2,Y1,Y2,Z,L = 0
310      FOR I = 1 TO N
320       FOR J = 1 TO D
330        IF C(J) = I THEN 400
340       NEXT J
350       LET X1 = X1+G(I)
360       LET X2 = X2+G(I)*G(I)
370       LET Y1 = Y1+F(I)
380       LET Y2 = Y2+F(I)*F(I)
390       LET Z = Z+G(I)*F(I)
400      NEXT I
500      LET X3 = X1/(N-D)
510      LET Y3 = Y1/(N-D)
520      LET S1 = X2-X1*X3
530      LET S2 = Y2-Y1*Y3
540      LET S = Z-X1*Y3
550      LET B = S/S1
560      LET B1 = Y3-B*X3
570      LET S3 = S2-B*S
580      LET S4 = S3/(N-D-2)
590      REM ***** DATA OUTPUT.
591      PRINT
592      PRINT
600      PRINT "NUMBER OF DATA SETS READ=";N;" AND NUMBER
USED IN CALC=";N-D
610      PRINT "***SLOPE=";B,"INTERCEPT=";B1
620      PRINT "***MEAN X=";X3," AND MEAN Y=";Y3
```

```
630        PRINT
640        PRINT "STANDARD DEVIATIONS."
650        PRINT "   X";SQR(S1/(N-1-D))
660        PRINT "  Y";SQR(S2/(N-1-D))
670        PRINT "   SLOPE";SQR(S4/S1)
680        PRINT "    INTER.";SQR(S4*(1/(N-D)*X3*X3/S1))
690        PRINT
691        IF L = 1 THEN 699
695        PRINT "DO YOU WANT THE DATA OUTPUT?";
697        INPUT Q
698        IF Q = 0 THEN 830
699        PRINT
700        PRINT "  X","  Y","   DEV. Y","   INDEX NO."
701        PRINT "_ _ _ _ _ _ _ _ _ _ _ _ _ _ _ _ _ _ _ _ _"
710        FOR I = 1 TO N
720         LET Y5 = B*G(I)+B1
730         LET F = F(I)-Y5
740         PRINT G(I),F(I),F,I;
750         FOR J = 1 TO D
760          IF C(J) = I THEN 800
770         NEXT J
780         PRINT
790         GOTO 810
800         PRINT "***"
810        NEXT I
820        PRINT "_ _ _ _ _ _ _ _ _ _ _ _ _ _ _ _ _ _ _ _ _"
825        REM ***** ANY DATA POINTS TO BE DELETED.
830        PRINT
831        IF L = 1 THEN 1005
840        IF D = 0 THEN 900
850        PRINT "DO YOU WANT TO KEEP THE DELETED POINT(S)
DELETED?";
860        INPUT Q
870        IF Q = 1 THEN 900
880        FOR J = 1 TO D
890         LET C(J) = 0
895        NEXT J
896        LET D = 0
900        PRINT "NO. OF POINTS TO BE DELETED=";
910        INPUT P
920        IF P = 0 THEN 970
925        PRINT "INDEX NO. OF THE DATA SET=";
930        FOR J = D+1 TO D+P
950         INPUT C(J)
960        NEXT J
965        PRINT
966        PRINT
968        LET D = D+P
969        REM ***** ANY DATA POINTS TO BE ALTERED.
970        PRINT "DO YOU WANT TO ALTER ANY OF THE DATA POINTS?";
971        INPUT Q
972        IF Q+P = 0 THEN 1000
973        IF Q = 0 THEN 300
980        PRINT "NO. OF DATA SETS TO BE ALTERED=";
981        INPUT K
982        FOR J = 1 TO K
983         PRINT "INDEX NO. OF THE DATA SET TO BE ALTERED=";
984         INPUT A
985         PRINT "X(";A;")=";
```

```
986     INPUT A1
987     PRINT "Y(";A;")=";
988     INPUT A2
989     LET G(A) = FNA(A1)
990     LET F(A) = FNB(A2)
991    NEXT J
995    GOTO 300
996    REM ***** DATA OUTPUT TO DISC.
1000   PRINT "DO YOU WANT THE TABULATED DATA RUN TO DISC?";
1001   INPUT L
1002   IF L = 0 THEN 1005
1003   REM DRSPEC GOES HERE
1004   GOTO 591
1005   REM ANOTHER DRSPEC GOES HERE
1010   PRINT N,B,SQR(S4/S1),B1,SQR(S4*(1/(N-D)+X3*X3/S1)),D
1020   FOR I = 1 TO N
1030    FOR J = 1 TO D
1040     IF C(J) = I THEN 1070
1050    NEXT J
1060    PRINT G(I),F(I)
1070   NEXT I
2000   END
```

References

Chapter 1

J.A. Bomman, J. Chem. Phys. 27, 604

A. Bree, D.J. Carswell and L.E. Lyons, J. Chem. Soc.
1729, 1735

A. Bree and L.E. Lyons, J. Chem. Phys. 25, 1284 (1956)

A. Bree and L.E. Lyons, J. Chem. Soc. 5179 (1960)

M.H. Briggs and R.B. Duncan, Nature 191, 1310

R.J. Cherry and D. Chapman, Nature 215, 956

A.G. Chynoweth, J. Chem. Phys. 22, 1029

D.M.J. Compton and T.C. Waddington, J.Chem. Phys.
25, 1075

F. Gutmann and L.E. Lyons, "Organic Semiconductors"
p. 147-224, New York, Wiley (1967)

J. Kaufhold and K. Hauffe, Ber. Bunsenges. Physik. Chem.
69, 168

N.A. Milas, W.M. Bostman and R. Heggie, J. Am. Chem. Soc.
61, 1929

T.N. Mistra, B. Rosenberg and R. Switzer, J. Chem. Phys.
48, 2096

C.J. van Oirschot, D. van Leeuwen and J. Medema,
J. Electroanal. Chem. 37, 373

B. Rosenberg, J. Chem. Phys. 34, 812

B. Rosenberg, T.N. Mistra and R. Switzer, Nature 217,423

A.T. Vartanyan, Zhur. Fiz. Khim 22,769 (1948)

A.T. Vartanyan, Doklady Akad. Nauk SSSR 71, 641 (1950)

T.C. Waddington and W.G. Schneider, J. Chem. Phys.
25, 358 (1956)

T.C. Waddington and W.G. Schneider, Can. J. Chem. 36,
789 (1958)

Chapter 2

F. Bloch, Z. Physick, 52, 555

D.D. Eley and G.D. Parfitt, Trans. Far. Soc. 51, 1529

D.D. Eley, G.D. Parfitt, M.J. Perry and D.H. Taysum, Trans. Far. Soc. 49, 79

D.D. Eley and D.J. Spivey, Trans. Far. Soc. 58, 411

S. Yu Elovich and G.M. Zhabrova, Zhur. Fiz. Khim 13, 1761

F. Gutmann and L.E. Lyons, "Organic Semiconductors" New York, Wiley (1967)

G.H. Heilmeier and S.E. Harrison, J. Chem. Phys. 34, 2732

T. Holstein, Am. Phys. 8, 343

A.F. Ioffé, Sov. Phys. Solid State 1, 139

G.R. Johnston, Disc. Far. Soc. 51, 221

N. Karl, Advan. Solid State Phys. 14, 261

J.L. Katz, J. Jortner, S.I. Choi and S.A. Rice, J. Chem. Phys. 39, 1683

C. Kittel, "Introduction to Solid State Physics" New York, Wiley (1971)

J.L. Lippert, M.W. Hanna and P.J. Trotter, J.A.C.S. 91, 4035

F.J. Martin, Phys. Rev. 93, 1195

W. Mey and A.M. Hermann, Phys. Rev. B. 7, 1652

R.W. Munn and W. Siebrand, Chem. Phys. Lett. 3, 655 (1969)

R.W. Munn and W. Siebrand, J. Chem. Phys. 52, 6391 (1970)

L.B. Schein, Chem. Phys. Lett. 48, 571 (1977)

L.B. Schein, Phys. Rev. B. 15, 1024 (1977)

R. Silbey, J. Jortner, S.A. Rice and M.T. Vala, J. Chem. Phys. 43, 2925

V.M. Vincent, Ph.D. thesis, University of Kent, (1972)

Chapter 3

J. Briegleb, Elektronen-Donator-Acceptor-Komplexe, Springer-Verlag, Berlin (1961)

J. Briegleb and J. Czekalla, Z. Elektrochem. 63, 6

M. Calvin and D.R. Kearns, J. Chem. Phys. 34, 2026

A. Davison, N. Edelstein, R.H. Holm and A.H. Maki, Inorg. Chem. 2, 1227

A. Davison and R.H. Holm, Inorg. Syn. 10, 8

.D.D. Eley, D.J. Hazeldine and T.F. Palmer, J. Chem. Soc. Farad. Trans. II 69, 1808

P.E. Fielding, Energy and charge transfer in organic semiconductors, Proc. U.S.-Japan Seminar (1973)

P. King and L.E. Lyons, unpublished work

C.G. Krespan, J. Am. Chem. Soc. 83, 3434

H. Kusakawa and S. Nishizaki, Bull Chem. Soc. Jpn. 38, 783

R.P. Linstead, P.A. Barrett and D.A. Frye, J. Chem. Soc. 1157 (1938)

L.E. Lyons and G.C. Morris, J. Chem. Soc. 5192 (1960)

L.E. Lyons and L.D. Palmer, Aust. J. Chem. 29, 1919

M. Pope, Chem. Phys. Lett. 2810 (1962)

G. Roberts, V.K. Molecular Crystals Discussion Group Meeting, Manchester (1977)

M. Voler, Ann. Phys. 40, 775

Chapter 4

P.E. Fielding, Energy charge transfer organic semiconductors, Proc. U.S.-Japan Seminar (1973)

G.J. van Oirschot, D. van Leeuwen and J. Medema, J. Electroanal. Chem. 37, 373

Chapter 5

Y. Aoyagi, K. Masuda and S. Namba, J. Phys. Soc. Jpn. 31(1), 164

J.M. Assour and S.E. Harrison, J. Chem. Phys. 26(3), 670

I.G. Austin, Proc. Phys. Soc. 90, 172

K.J. Beales, D.D. Eley, D.J. Hazeldine and T.F. Palmer, Katalyse an Phthalocyaninen Symposium (Hamburg, May, 1972) ed. H. Kropf and F. Steinbach (Georg Thieme Verlag, Stuttgart, 1973)

J. Berkowitz and W.A. Chupka, J. Chem. Phys. 55(6), 2733

J.S. Blakemore, "Semiconductor Statistics" Pergamon Press (1962)

G.A. Cox and P.C. Knight, Phys. Stat. Sol. (b), 50, K135 (1972)

G.A. Cox and P.C. Knight, J. Phys. C. 7, 146 (1974)

P. Day and M.G. Price, J. Chem. Soc. (A), 236 (1969)

P. Day, G. Scregg and R.J.P. Williams, Nature 197, 589

P. Day and R.J.P. Williams, J. Chem. Phys. 37, 567 (1962)

P. Day and R.J.P. Williams, J. Chem. Phys. 42, 4049 (1965)

D.D. Eley, D.J. Hazeldine and T.F. Palmer, Trans. Farad. Soc. 69, 1808

P.E. Fielding and F. Gutmann, J. Chem. Phys. 26, 411

P.E. Fielding and H. Struve, unpublished data (1964)

H. Freundlich, "Colloid and Capillary Chemistry", London, Methuen (1962)

A. Fulton, L.E. Lyons and G.C. Morris, Aust. J. Chem. 21, 2853

K. Gamo, K. Masuda and J. Yamaguch, J. Phys. Soc. Jpn. 25(2), 431

P. Groth and O. Hassel

F. Gutmann and L.E. Lyons, "Organic Semiconductors" p. 717 New York, Wiley (1967)

S.E. Harrison, J. Chem. Phys. 50, 4739

G.H. Heilmeier and G. Warfield, J. Chem. Phys. 38(1), 163 (1963)

G.H. Heilmeier and G. Warfield, J. Chem. Phys. 38, 897 (1963)

G.H. Heilmeier, G. Warfield and S.E. Harrison, Phys. Rev. Lett. 8, 309

J.L. Hoard, S. Geller and T.B. Owen, Acta Cryst. 4, 405

J. Kaufhold and K. Hauffe, Berichte der Bunsengesellschaft 168 (1964)

D.R. Kearns and M. Calvin, J. Chem. Phys. 34, 2022

D.R. Kearns, G. Tollin and M. Calvin, J. Chem. Phys. 32, 1013

C. Kittel, "Introduction to Solid State Physics" New York, Wiley (1971)

G.F.A. Kortum, "Reflectance Spectroscopy: Principles, Methods, Applications" Springer, Berlin (1969)

C. Lifshitz, B.M. Hughes and T.D. Ternan, Chem. Phys. Lett. 7(4), 469

L.E. Lyons, J.R. Walsh and J.W. White, Aust. J. Chem. 167 (1960)

G.J. van Oirschot, D. van Leeuwen and J. Medema, Electro-analytical Chem. and Interfacial Electrochemistry 37, 373

Z.D. Popovic and J.H. Sharp, J. Chem. Phys. 66(11), 5076

J.M. Robertson, J. Chem. Soc. 615 (1935)

H.A. Skinner, Proc. Conf. Univ. Coll. North Staffordshire 28-38 (1952)

K. Ukei, Acta Cryst. B29, 2790 (1973)

K. Ukei, J. Phys. Soc. Jpn. 40, 140 (1976)

K. Ukei, K. Takamoto and E. Kanda, Phys. Lett. A, 45(4), 345

C.R. Westgate and G. Warfield, J. Chem. Phys. 46, 94

H. Yasunaga, K. Kojima and H. Yohda, J. Phys. Soc. Jpn. 37(4), 1024

Chapter 6

D.M.J. Compton and T.C. Waddington, J. Chem. Phys. 25, 1075

C. Dufraisse, J. Rigaudy and K. Vang Thang, Compt. Rend. 256, 548

R.J. Hurditch, V.M. Vincent and J.D. Wright, J. Chem. Soc. Farad. Trans. I 68, 465

I. Ikemoto, K. Chikaishi, K. Yakushi and H. Kuroda, Acta Cryst. B28, 3502

H. Inokuchi, H. Kuroda and H. Akamatu, Bull. Chem. Soc. Jpn. 34, 749

P.J. Munnoch, Ph.D. thesis, University of Kent (1974)

P.J. Munnoch and J.D. Wright, J.C.S. Faraday II, 72, 1981

M. Ohmasa, M. Kinoshita and H. Akamatu, Bull. Chem. Soc. Jpn. 44, 395

M. Ohmasa, M. Kinoshita, M. Sano and H. Akamatu, Bull. Chem. Soc. Jpn. 41, 1998

M. Sano and H. Akamatu, Bull. Chem. Soc. Jpn. 34, 1509 (1961)

M. Sano and H. Akamatu, Bull. Chem. Soc. Jpn. 35(4), 587 (1962)

W.G. Schneider and T.C. Waddington, J. Chem. Phys. 25, 358 (1956)

W.G. Schneider and T.C. Waddington, Can. J. Chem. 36, 789 (1958)

J.W. Steketee and J. de Jonge, Philips Res. Repts. 17, 363

N. Takahashi, K. Yukushi, K. Ishii and H. Kuroda, Bull. Chem. Soc. Jpn. 49, 182

V.M. Vincent, Ph.D. thesis, University of Kent (1972)

V.M. Vincent and J.D. Wright, J.C.S. Faraday II 70, 58

Chapter 7

R.H. Wright and J.E. Cumming, Canadian Patent 915458, 1972